Sara Pascual Sevilla

Operational optimization of Calcium Looping-based thermal energy storage system in concentrated solar power plants

Director/es

Romeo Giménez, Luis Miguel
Lisbona Martín, María Pilar

Universidad Zaragoza
1542

Tesis Doctoral

OPERATIONAL OPTIMIZATION OF CALCIUM LOOPING-BASED THERMAL ENERGY STORAGE SYSTEM IN CONCENTRATED SOLAR POWER PLANTS

Autor

Sara Pascual Sevilla

Director/es

Romeo Giménez, Luis Miguel
Lisbona Martín, María Pilar

UNIVERSIDAD DE ZARAGOZA
Escuela de Doctorado

Programa de Doctorado en Energías Renovables y Eficiencia Energética

2023

Universidad Zaragoza

1542

TESIS DOCTORAL

Operational optimization of a Calcium Looping-based thermal storage system in concentrated solar power plants

Memoria presentada por Sara Pascual Sevilla a la Universidad de Zaragoza para la obtención del título de Doctora con Mención de Doctorado Internacional

Director/es

Romeo Giménez, Luis Miguel

Lisbona Martín, Mª Pilar

ESCUELA DOCTORADO UNIVERSIDAD DE ZARAGOZA

Programa de Doctorado en Energías Renovables y Eficiencia Energética

Zaragoza, Mayo de 2023

A mi familia y Jesús G.

Compendio de publicaciones

La presente tesis ha sido elaborada como compendio de las siguientes publicaciones:

i) Bailera M, Pascual S, Lisbona P, Romeo LM. *Modelling Calcium Looping at industrial scale for energy storage in concentrating solar power plants*. Energy (2021), 225, 120306.

ii) Pascual S, Lisbona P, Bailera M, Romeo LM. *Design and operational performance maps of Calcium Looping thermochemical energy storage for concentrating solar power plants*. Energy (2021), 220, 119715.

iii) Pascual S, Lisbona P, Romeo LM. *Operation maps in Calcium Looping thermochemical energy storage for concentrating solar power plants*. Journal of Energy Storage (2022), 55, 105771.

iv) Pascual S, Di Lauro F, Lisbona P, Romeo LM, Tregambi C, Montagnaro F, Solimene R, Salatino P. *Improvement of performance of fluidized bed Calcium Looping for thermochemical solar energy storage: Modelling and experiments*. Proceedings of 10th European Combustion Meeting (2021).

v) Tregambi C, Di Lauro F, Pascual S, Lisbona P, Romeo LM, Solimene R, Salatino P, Montagnaro F. *Solar-driven Calcium Looping in fluidized beds for thermochemical energy storage*. Chemical Engineering Journal (2023), 466, 142708.

vi) Pascual S, Lisbona P, Romeo LM. *Optimized Ca-looping thermochemical energy storage under dynamic operation for concentrated solar power*. Journal of Energy Storage (2023). Accepted for publication.

vii) Pascual S, Lisbona P, Romeo LM. *Thermal energy storage in concentrating solar power plants: A review of European and North American R&D projects*. Energies (2022), 15, 8570.

Agradecimientos

En primer lugar, especial mención a mis directores de tesis, Luis M. Romeo y Mª Pilar Lisbona, por su dedicación y apoyo prestado durante mi tesis doctoral. La oportunidad de comenzar la presente etapa investigadora tras finalizar los estudios de Máster se lo agradezco enormemente a Luis M. Romeo. Mientras que Pilar Lisbona ha sido mi guía desde el inicio de los estudios predoctorales, animándome siempre a continuar con la carrera investigadora dentro de la universidad. Gracias a ambos por ayudarme y enseñarme, a través de vuestra experiencia, a sobrellevar la dedicación que supone la realización de una tesis doctoral, incluyendo buenos y malos momentos.

Dentro de la etapa desarrollada durante la tesis a nivel internacional, me gustaría destacar a mis compañeros y tutores de mi estancia en Nápoles. Gracias por dedicar parte de vuestro tiempo en mi formación y permitir la utilización vuestras instalaciones para realizar una campaña experimental, la cuál ha sido esencial para el desarrollo de esta tesis.

No podría olvidarme de mencionar a mis compañeros de despacho en la Universidad de Zaragoza, con los que he compartido vivencias de la etapa de doctorado. De entre todos, me gustaría destacar a Ana Iris Escudero y Manuel Bailera. La primera por aconsejarme y mostrarme siempre la visión más optimista en este camino. A Manuel por transmitirme sus conocimientos y apoyarme durante el inicio de la tesis doctoral.

En el ámbito más personal, me gustaría destacar a mis padres, Germán y Mª Carmen, y a mi hermana Blanca, por su apoyo incondicional durante mi formación universitaria. No quiero olvidarme de mis abuelos, José y Victorina. Gracias al amor por el conocimiento y el saber que me inculcaron, he podido llegar hasta aquí. Por último, y no menos importante, agradecer a Jesús su paciencia, comprensión y ánimo en todos estos años. Sin él los baches encontrados en el camino andado hubiesen sido más difíciles de sortear.

Abstract

The International Energy Agency (IEA) recommends that the establishment of a low-carbon economy supported by renewable energy sources as the necessary path to reach the scenario of net zero emissions by 2050. Energy storage will be key for the massive deployment of renewable energy sources, contributing decisively to the mitigation of climate change. The use of solar resource will become one of the most widespread technologies/renewable sources, given its wide availability and cost reduction in the last decade. Energy storage is essential to improve dispatchability in concentrated solar power (CSP) plants. The first and second generation of CSP plants already apply thermal storage in the form of sensible heat mainly through the use of molten salts. Prospects for the next generation of CSP plants indicate an increase in the implementation of high-temperature thermal energy storage to integrate highly efficient power cycles. The state of the art and future research lines of the thermal energy storage technologies integrated into the CSP plants have been summarized in the following review:

- Pascual S, Lisbona P, Romeo LM. *Thermal energy storage in concentrating solar power plants: A review of European and North American R&D projects*. Energies 2022, 15, 8570.

The most promising thermal energy storage technology for the third generation of CSP plants is the gas-solid based thermochemical energy storage (TCES) systems. The Calcium Looping (CaL) process based on a carbonation-calcination gas-solid reaction is one of the potential TCES systems to be integrated into CSP plants, given its high storage capacity and high operating temperature. This PhD Thesis presents innovative technical solutions to improve the energy efficiency of calcium cycles such as TCES systems. Specifically, an innovative option for the improvement of energy efficiency related to the circulation of non-reactive solids in the CaL process is proposed for the very first time and thoroughly assessed. Moreover, the real dynamic operation of the CaL TCES is addressed, comprising the variability of energy demand and solar resource.

The research included in this PhD Thesis was developed in the *Mechanical Engineering Department* of the *School of Engineering and Architecture* of the *Universidad de Zaragoza*, within the *Program of Renewable Energy and Energy Efficiency*. This PhD Thesis has been fully funded by the *Programa de Formación de Profesorado Universitario* (FPU) of the Spanish *Ministry of Science, Innovation and Universities*, from October 2018 to March 2023.

This PhD Thesis addresses the improvement of energy efficiency in the CaL process operating as a TCES, influenced by the circulation of non-reactive material. Up to now, research in literature was focused on the assessment of conventional CaL TCES configurations, where partially carbonated solids are circulated throughout the whole system. The dynamic operation of the conventional system is analyzed based on solar resource availability without accounting for energy demand. Under the present work a step further is taken, energy efficiency is enhanced by means of a novel management of unreacted solids and a systematic methodology to define the dynamic

operating pattern of the CaL TCES system considering the solar resource availability and the electricity price market is established.

As a starting point, the energy requirements of the conventional CaL TCES system proposed in the literature are assessed. Solids circulate within the system and are stored or retrieved from silos depending on the availability of solar resource and the energy demand. The objective of this first stage was to lay the foundations of this PhD Thesis, analyzing the energy efficiency when storing and retrieving gas and solid materials to and from the storage tanks. As a result of this work, the following paper was published:

- Bailera M, Pascual S, Lisbona P, Romeo LM. *Modelling Calcium Looping at industrial scale for energy storage in concentrating solar power plants*. Energy 2021, 225, 120306.

After analyzing the energy requirements of the conventional CaL TCES system, a novel CaL TCES configuration is proposed within the next step of the PhD Thesis. The energy efficiency is enhanced through the recirculation of unreacted CaO into the carbonator. A solid-solid classifier based on density difference is included in the CaL TCES scheme to ideally and completely separate the unreacted CaO particles from partially carbonated ones. Additionally, the energy efficiency and plant equipment size are compared under both CaL TCES configurations (conventional and novel) under the same operating conditions and plant equipment assumptions. The second objective is to assess the effect of the carbonated solids separation on the plant size and energy savings, setting up those operating maps which maximize energy efficiency of the CaL TCES system. The published papers related to this second stage of the PhD Thesis are:

- Pascual S, Lisbona P, Bailera M, Romeo LM. *Design and operational performance maps of Calcium Looping thermochemical energy storage for concentrating solar power plants*. Energy 2021, 220, 119715.

- Pascual S, Lisbona P, Romeo LM. *Operation maps in Calcium Looping thermochemical energy storage for concentrating solar power plants*. Journal of Energy Storage 2022, 55, 105771.

The simulation results of the CaL TCES system were supported by an experimental stage. The objective of the experimental campaign was to determine the sorbent carbonation degree under real operating conditions of the CaL TCES system and to assess the technical feasibility of the carbonated solids separation. The sorbent behaviour was analyzed under CaL TCES conditions (850 °C for carbonation and 950 °C for calcination, both under pure CO_2 atmosphere) in lab scale facilities based on fluidized bed reactors, assuming operating behaviour close to large scale. Moreover, the bulk density and the minimum fluidization velocity were measured for calcined and carbonated particles to assess the potential separation of unreacted CaO and partially carbonated material by density difference. Additionally, a new methodology and an empirical equation to estimate sorbent conversion based on experimental bulk density were developed and validated. This experimental stage was carried out during an international research stay at the *Università degli Studi di Napoli Federico II* (UNINA) and the *Institute for Research on Combustion* (IRC-CNR) of Italy, giving rise to two following papers, one presented at an international conference and one published in a scientific journal:

- Pascual S, Di Lauro F, Lisbona P, Romeo LM, Tregambi C, Montagnaro F, Solimene R, Salatino P. *Improvement of performance of fluidized bed Calcium Looping for thermochemical solar energy storage: Modelling and experiments*. Proceedings of 10th European Combustion Meeting 2021.

- Tregambi C, Di Lauro F, Pascual S, Lisbona P, Romeo LM, Solimene R, Salatino P, Montagnaro F. *Solar-driven Calcium Looping in fluidized beds for thermochemical energy storage*. Chemical Engineering Journal 2023, 466, 142708.

The last stage of the present PhD Thesis focuses on the dynamic operation of the CaL TCES system along the day and year. The objective was to establish the methodology to define the system operation which maximizes the daily incomes of the CSP plant considering the variability of solar supply and energy demand. The real operating pattern and the size required for the plant equipment are the result of applying the operating methodology based on solar resource availability and electricity price market. Higher revenue for the CSP plant could come from a CaL TCES system which minimizes the non-reactive solids convey within the system. The last stage of the present PhD Thesis has led to the publication of one more research paper:

- Pascual S, Lisbona P, Romeo LM. *Optimized Ca-looping thermochemical energy storage under dynamic operation for concentrated solar power*. Journal of Energy Storage 2023. Accepted for publication.

Resumen

La Agencia Internacional de la Energía (IEA) señala la necesidad de establecer una economía basada en bajas emisiones de carbono y utilización de recursos renovables, con el fin de alcanzar el escenario de cero emisiones netas para el año 2050. Por tanto, el almacenamiento de energía será clave para el despliegue masivo de energías renovables, contribuyendo de forma decisiva a la mitigación del cambio climático. El aprovechamiento de los recursos solares a través de tecnología de energía solar de concentración será una de las fuentes renovables más extendidas, dada su amplia disponibilidad y reducción de costes en la última década. La mejora de la capacidad de despacho en las plantas de energía solar de concentración (CSP) está supeditada al almacenamiento de energía. La primera y segunda generación de centrales CSP ya utilizan almacenamiento térmico en forma de calor sensible, principalmente sales fundidas. Las perspectivas para la próxima generación de plantas de CSP indican un aumento en la implementación de almacenamiento de energía térmica a alta temperatura, integrando ciclos de energía altamente eficientes. El estado del arte y futuras líneas de investigación de las tecnologías de almacenamiento de energía térmica integradas en las plantas CSP se han recogido y publicado en la siguiente revisión:

- Pascual S, Lisbona P, Romeo LM. *Thermal energy storage in concentrating solar power plants: A review of European and North American R&D projects*. Energies 2022, 15, 8570.

La tecnología de almacenamiento de energía térmica más prometedora para la tercera generación de plantas de CSP se basa en sistemas gas-sólido de almacenamiento de energía termoquímica (TCES). El ciclo de calcio (*Calcium Looping* - CaL) basado en la reacción gas-sólido de carbonatación-calcinación es uno de los potenciales sistemas TCES a integrar en plantas CSP, dada su alta capacidad de almacenamiento y alta temperatura de operación. Esta Tesis Doctoral presenta soluciones técnicas novedosas con el objetivo de mejorar la eficiencia energética de ciclos de calcio como sistemas TCES. En concreto, se propone y se analiza por primera vez una opción innovadora para la mejora de la eficiencia energética basada en la gestión dela circulación de sólidos no reactivos en el proceso CaL. Además, se aborda el funcionamiento dinámico del sistema CaL TCES bajo condiciones reales de operación, considerando la variabilidad de la demanda energética y del recurso solar.

La presente Tesis Doctoral aborda la mejora de la eficiencia energética del proceso CaL operando como sistema TCES mediante una gestión mejorada dela circulación de material no reactivo. Hasta ahora, la investigación realizada en este ámbito se ha centrado en la evaluación de configuraciones convencionales del sistema CaL TCES, en las cuales los sólidos parcialmente carbonatados circulan por todo el sistema. Por otra parte, el funcionamiento dinámico del sistema convencional se ha analizado únicamente en función de la disponibilidad del recurso solar sin tener en cuenta la demanda de energía. En el presente trabajo se da un paso más, (i) mejorando la eficiencia energética mediante un novedoso manejo de sólidos sin reaccionar y (ii) definiendo el patrón dinámico de operación del sistema CaL TCES, considerando la disponibilidad del recurso solar y el precio de la electricidad en el mercado.

Como punto de partida, se evalúan los requerimientos energéticos del sistema CaL TCES convencional propuesto en bibliografía. Los sólidos circulan dentro del sistema y se almacenan o recuperan de los silos según la disponibilidad del recurso solar y la demanda de energía. El objetivo de este primer paso es sentar las bases de la Tesis Doctoral, analizando la eficiencia energética en función de la gestión de las sustancias almacenadas (gas y materiales sólidos) hacia y desde los tanques de almacenamiento. Como resultado de este trabajo, se publicó el siguiente artículo:

- Bailera M, Pascual S, Lisbona P, Romeo LM. *Modelling Calcium Looping at industrial scale for energy storage in concentrating solar power plants*. Energy 2021, 225, 120306.

Tras analizar las necesidades energéticas del sistema CaL TCES convencional, se propone una novedosa configuración en el siguiente bloque de esta Tesis Doctoral. La eficiencia energética se mejora a través de la recirculación al carbonatador del CaO que no ha reaccionado. Se incluye un clasificador sólido-sólido basado en la diferencia de densidades, con el fin de separar las partículas de CaO sin reaccionar de las parcialmente carbonatadas. Además, se comparan la eficiencia energética y el tamaño de los equipos de la planta entre ambas configuraciones CaL TCES (convencional y nueva propuesta) bajo las mismas condiciones de operación de los equipos de la planta. El segundo objetivo es evaluar el efecto de la separación de sólidos carbonatados sobre el tamaño de la planta y el ahorro energético, estableciendo aquellos mapas operativos que maximicen la eficiencia energética del sistema CaL TCES. Los trabajos publicados relacionados con esta segunda etapa de la Tesis Doctoral son:

- Pascual S, Lisbona P, Bailera M, Romeo LM. *Design and operational performance maps of Calcium Looping thermochemical energy storage for concentrating solar power plants*. Energy 2021, 220, 119715.

- Pascual S, Lisbona P, Romeo LM. *Operation maps in Calcium Looping thermochemical energy storage for concentrating solar power plants*. Journal of Energy Storage 2022, 55, 105771.

Los resultados de la simulación del sistema CaL TCES han sido complementados por una campaña experimental. Los objetivos de la etapa experimental son (i) determinar el grado de carbonatación del sorbente en condiciones reales de funcionamiento del sistema CaL TCES y (ii) evaluar la viabilidad técnica de la separación de sólidos carbonatados. El comportamiento del sorbente se analizó bajo condiciones CaL como sistema TCES (850 °C carbonatación y 950 °C calcinación, en atmósfera de CO_2 puro) en reactores de lecho fluidizado escala laboratorio, asumiendo un comportamiento operativo escalable a gran escala. Además, se midieron tanto la densidad aparente como la velocidad mínima de fluidización de partículas calcinadas y carbonatadas para evaluar el potencial de separación del CaO parcialmente carbonatado con diferente contenido de $CaCO_3$ por diferencia de densidad. Adicionalmente, se desarrolló y validó una nueva ecuación empírica para estimar la conversión del sorbente en función de la densidad

aparente experimental. Esta etapa experimental se llevó a cabo durante una estancia de investigación internacional en la *Università degli Studi di Napoli Federico II* (UNINA) y el *Institute for Research on Combustion* (IRC-CNR) de Italia, dando lugar los siguientes trabajos, uno presentado en conferencia internacional y otro publicado en revista científica:

- Pascual S, Di Lauro F, Lisbona P, Romeo LM, Tregambi C, Montagnaro F, Solimene R, Salatino P. *Improvement of performance of fluidized bed Calcium Looping for thermochemical solar energy storage: Modelling and experiments*. Proceedings of 10th European Combustion Meeting 2021.

- Tregambi C, Di Lauro F, Pascual S, Lisbona P, Romeo LM, Solimene R, Salatino P, Montagnaro F. *Solar-driven Calcium Looping in fluidized beds for thermochemical energy storage*. Chemical Engineering Journal 2023, 466, 142708.

El último bloque de la presente Tesis Doctoral se centra en el funcionamiento dinámico del sistema CaL TCES a lo largo del día y del año. El objetivo es establecer una metodología que establezca la operación del sistema maximizando los ingresos diarios de la planta CSP teniendo en cuenta la variabilidad del suministro solar y la demanda de energía. Como resultado de la aplicación de la metodología desarrollada, se obtiene el patrón de operación real y el tamaño requerido para los equipos de la planta en base a la disponibilidad del recurso solar y el precio del mercado eléctrico. Los mayores ingresos para la planta de CSP provendrán de un sistema CaL TCES que minimiza el transporte de sólidos no reactivos dentro del sistema. Este último bloque de la Tesis Doctoral ha dado lugar a la publicación de un artículo científico más:

- Pascual S, Lisbona P, Romeo LM. *Optimized Ca-looping thermochemical energy storage under dynamic operation for concentrated solar power*. Journal of Energy Storage 2023. Aceptado para publicación.

Conclusions

The main aim of this PhD Thesis is the improvement of the energy efficiency of the Calcium Looping (CaL) process as thermochemical energy storage (TCES) system and the in-depth study of its operation in transient mode. The research has been focused on the effect of (i) non-reactive solids management on energy efficiency, (ii) the solids and gas flows management between reactors and storage on the setting up of operating maps which maximize energy efficiency and (iii) the variability of solar resource and electricity prices on the system operation which maximizes revenues. Moreover, real conditions of solar energy availability and daily electricity price evolution are used to determine the operational behaviour of a CaL TCES system which optimizes the economic feasibility of the system.

The efficiency improvement of the CaL TCES system is obtained through an enhanced solids management after carbonation step. Partial carbonation degree, which depends on the sorption activity of the sorbent, generates a mixed stream of reacted/unreacted sorbent after carbonation step. Sorbents are gradually deactivated and the sorption activity is reduced with the number of carbonation/calcination cycles. The experimental tests showed an average sorption activity of 25% after 20 cycles in an electrically heated fluidized bed using only limestone as bed inventory. CaL TCES conditions were set during the experimental tests: 850 ºC during carbonation and 950 ºC during calcination under pure CO_2 atmosphere. The circulation of the unreacted material to the calciner and limestone storage tank increases energy losses in the CaL TCES system. Thus, the inclusion of a novel solid-solid classifier after carbonation reactor is a promising alternative to separate carbonated material, recirculating the not-carbonated material into the carbonator. The ideal full separation of unreacted and carbonated material assumed in the calculations yielded positive results, reducing the size of the plant equipment by up to 74% and generating significant energy savings. The efficiency is 11 and 28 average points higher for energy storage and energy availability respectively, compared to the conventional CaL TCES configuration proposed in literature. The technical feasibility of the solid-solid separation unit was experimentally assessed, given the positive effects on energy cost of the CaL TCES system. The difference between the experimental minimum fluidization velocity of carbonated and unreacted particles could promote their separation in a solid-solid fluidized bed classifier, partially separating by density difference the more carbonated particles from the less carbonated ones. The solid-solid fluidized bed classifier could be the suitable technology to partially separate carbonated granular solids by density difference, given the significant difference between the minimum fluidization velocity of both carbonated and calcined material.

The influence of the solids and gas management to/from storage tanks on the CaL TCES system efficiency has been assessed under different combinations of solar resource availability and energy demand. Besides the energy savings generated by reducing the convey of unreacted solids, an exhaustive analysis was performed to set up the operation map which maximizes the

energy performance of the CaL TCES system. A large number of different operating points may lead to the same amount of stored and retrieved energy for each pair of reactor loads (calciner and carbonator). The operating points considered to define the operation maps meet technical and design criteria defined in the framework of the PhD Thesis. The technical and design criteria are related to the plant equipment of the CaL TCES system and include (i) the control of the direction of the heat flows, (ii) the limitation of their minimum load to encourage proper system operation or reduction of excessive energy consumption and (iii) the management of the gas and solids from and to the storage tanks. Then, the amount of stored energy was quantified for the operational points analyzed within the energy storage operation mode. The thermal energy availability was estimated for all the possible operating points within the energy retrieval operation mode. The selected operating map maximizes the energy storage efficiency under energy storage operation mode and the thermal energy availability efficiency under energy retrieval operation mode.

Once the optimized operational maps were established, a novel methodology to determine the most profitable dynamic operation of the CaL TCES system was created and applied to a specific case study. The daily income was maximized, taking into account (i) the maximum energy efficiencies for the operating points, (ii) the conservation of stored energy from one day to the following one and (iii) the influence of the hourly variability of solar resource and electricity prices. More energy is retrieved when demand is larger, achieving greater stability in operation with uniform electricity price profiles and greater availability of solar resources. Energy retrieval is concentrated at the beginning and end of the day under sharply price profiles, increasing the number of hours under full energy storage mode without operating the carbonator or energy retrieval operation mode. The obtained daily operating pattern which maximizes the daily income included a limited number of operation points which only correspond to threshold points within the defined operation map. Most of carbonator/calciner loads combinations are not included in the optimized daily pattern of operation points. Only those situations in which one of the reactors is completely off are considered in the optimized pattern. The highest efficiencies are not found at these extreme operating points. However, the present PhD Thesis assesses how to operate the CaL TCES system to obtain the maximum energy efficiency under those extreme points belonging to full operation modes: storage and retrieval. The full storage operation mode takes place when carbonator is shut down, while the full energy retrieval operation mode comprises operating points without solar resource availability. The real incomes obtained by the CaL TCES system could vary between the revenues from the conventional and the novel configurations analysed in the present PhD Thesis.

The present PhD Thesis has contributed to discover how to enhance the energy efficiency of the CaL TCES system under the assessment of the dynamic operation based on the instability of the solar resource and the electricity market. The CaL process is a promising mid-term candidate to store thermal energy in CSP plants. Undoubtedly, the proposal for partial separation of carbonated solids still requires to be addressed from the design and economic point of view. However, the assessment of the novel CaL TCES configuration points out the potential energy savings achievable by the CSP plants coupled with CaL TCES system. Moreover, the novel operating methodology enables approaching the operation of CaL TCES systems close to reality, contributing to the development of CaL technology as thermal energy storage in large-scale CSP plants.

Conclusiones

Los principales objetivos de la Tesis Doctoral son (i) la mejora de la eficiencia energética del ciclo de calcio (*Calcium Looping* - CaL) como sistema de almacenamiento termoquímico de energía (TCES) y (ii) el estudio en profundidad de su funcionamiento en régimen transitorio. La investigación se ha centrado en el efecto de (i) una gestión diferente de los sólidos no reactivos sobre la eficiencia energética, (ii) la gestión de los flujos de sólidos y gases entre reactores y almacenamiento en el establecimiento de mapas operativos que maximicen la eficiencia energética y (iii) la variabilidad del recurso solar y los precios de la electricidad en la operación del sistema, maximizando los ingresos. Adicionalmente, las condiciones realistas de disponibilidad de energía solar y la evolución diaria del precio de la electricidad podrían permitir la definición del comportamiento operativo de un sistema CaL TCES que optimice la viabilidad económica del sistema.

La mejora de la eficiencia energética del sistema CaL TCES se ha centrado en la gestión de sólidos tras la reacción de carbonatación. La carbonatación parcial, que depende de la actividad de sorción del sorbente, produce una corriente de mezcla de sorbente carbonatado y no carbonatado tras la etapa de carbonatación. Los sorbentes se desactivan gradualmente y la actividad de sorción se reduce con el número de ciclos de carbonatación/calcinación. Los resultados experimentales de la Tesis mostraron una actividad de sorción promedio del 25% tras 20 ciclos en un lecho fluidizado calentado eléctricamente, empleando únicamente caliza como material de lecho. En el transcurso de las pruebas experimentales se establecieron las siguientes condiciones: 850 °C durante la carbonatación y 950 °C durante la calcinación, bajo atmósfera de CO_2. La circulación del material que no reacciona en la carbonatación hacia el calcinador y el tanque de almacenamiento de piedra caliza aumenta las pérdidas de energía en el sistema CaL TCES. La inclusión de un novedoso clasificador sólido-sólido después del reactor de carbonatación es una propuesta prometedora para separar el material tras la carbonatación, recirculando el material no carbonatado al carbonatador. La separación completa de CaO no carbonatado y material parcialmente carbonatado arrojó resultados positivos, reduciendo el tamaño del equipo de la planta hasta en un 74% y generando importantes ahorros de energía. En comparación con la configuración CaL TCES convencional propuesta en literatura, la eficiencia de almacenamiento energético y la eficiencia de disponibilidad energética son 11 y 28 puntos promedio superiores, respectivamente. Considerando los efectos positivos en el coste energético del sistema CaL TCES, se evaluó experimentalmente la viabilidad técnica de la unidad de separación sólido-sólido. La diferencia entre la velocidad mínima experimental de fluidización de partículas carbonatadas y no carbonatadas podría promover su separación en un clasificador de lecho fluidizado sólido-sólido, separando parcialmente por diferencia de densidad las partículas más carbonatadas de las menos carbonatadas. El clasificador de lecho fluidizado sólido-sólido podría representar una tecnología adecuada para separar parcialmente los sólidos granulares carbonatados por diferencia de

densidad, dada la diferencia significativa entre la velocidad mínima de fluidización del material carbonatado y calcinado.

Se ha evaluado la influencia de la gestión de sólidos y gases hacia y desde los tanques de almacenamiento en la eficiencia del sistema CaL TCES bajo diferentes combinaciones de disponibilidad de recurso solar y demanda energética. Además del ahorro energético generado por la reducción de la cantidad de sólidos inertes transportados, se realizó un análisis exhaustivo para establecer el mapa de operación que maximizase el rendimiento energético del sistema CaL TCES. Un gran número de puntos de operación diferentes conducen a la misma cantidad de energía almacenada y recuperada para cada par de cargas en los reactores (calcinador y carbonatador). Los puntos de operación considerados para definir los mapas de operación cumplen criterios técnicos y de diseño. Los criterios técnicos y de diseño que se han fijado sobre los equipos de planta del sistema CaL TCES implican (i) controlar su comportamiento, (ii) limitar su carga para favorecer el correcto funcionamiento del sistema o reducir el consumo excesivo de energía y (iii) gestionar los gases y sólidos desde y hacia los tanques de almacenaje. La cantidad de energía almacenada se cuantificó para los puntos operativos analizados dentro del modo de operación de almacenamiento de energía. La disponibilidad de energía térmica se estimó para todos los posibles puntos de operación dentro del modo de operación de recuperación de energía. El mapa operativo definido maximiza la eficiencia de almacenamiento de energía en el modo de operación de almacenamiento de energía y la eficiencia de disponibilidad de energía térmica en el modo de operación de recuperación de energía.

Una vez establecidos los mapas operativos optimizados, se creó una nueva metodología para determinar la operación dinámica del sistema CaL TCES más rentable, aplicándose posteriormente a un caso de estudio específico. El ingreso diario se maximizó teniendo en cuenta (i) las máximas eficiencias energéticas para los puntos de operación, (ii) la conservación de la energía almacenada de un día al siguiente y (iii) la influencia de la variabilidad horaria del recurso solar y precios de la electricidad. La recuperación de energía es superior a mayor incremento de demanda, logrando una mayor estabilidad en la operación con perfil uniforme de precios de electricidad y una mayor disponibilidad de recurso solar. La recuperación de energía se concentra al principio y al final del día bajo perfiles de precios variables y picos máximos y mínimos marcados, lo que aumenta la cantidad de horas en modo de almacenamiento de energía total o en modo de operación de recuperación de energía. El patrón de operación diario demuestra la operatividad del sistema CaL TCES a través de puntos extremos dentro del mapa de operación definido que maximiza la eficiencia del sistema. Las eficiencias más elevadas no se encuentran en estos puntos de operación extremos. Sin embargo, la presente Tesis Doctoral evalúa cómo operar el sistema CaL TCES para obtener la máxima eficiencia energética en aquellos puntos extremos pertenecientes a los modos de almacenamiento y recuperación totales. El modo de operación de almacenamiento total tiene lugar cuando se apaga el carbonatador, mientras que el modo de operación de recuperación de energía total comprende puntos de operación sin disponibilidad de recurso solar. Los ingresos reales obtenidos por el sistema CaL TCES podrían variar entre los ingresos generados en las configuraciones convencional y novedosa analizadas en la Tesis Doctoral.

La presente Tesis Doctoral ha contribuido a descubrir cómo mejorar la eficiencia energética del sistema CaL TCES mediante una evaluación del funcionamiento dinámico basada en la inestabilidad del recurso solar y el mercado eléctrico. El proceso CaL es un candidato prometedor a medio plazo para almacenar energía térmica en plantas CSP. Sin duda, la propuesta de separación parcial de sólidos carbonatados aún requiere ser abordada desde el punto de vista de diseño y económico. Sin embargo, la evaluación de la nueva configuración CaL TCES propuesta señala los posibles ahorros de energía que pueden lograr las plantas CSP junto con el sistema CaL

TCES. Además, la nueva metodología operativa permite acercar la operación de los sistemas CaL TCES a la realidad, contribuyendo al desarrollo de la tecnología CaL como almacenamiento de energía térmica en plantas CSP a gran escala.

Contents

1. General introduction

The Intergovernmental Panel on Climate Change (IPCC) highlights the importance of mitigating greenhouse gases (GHG) emissions through the higher penetration of renewable energy sources (RES) in the energy mix [1]. RES, excluding hydropower, only contributed by 13.17% to global electricity production in 2021 [2], estimating an increased share of 20% by 2023 in 50 world regions [3]. The global renewable power capacity must increase threefold to achieve the carbon neutrality scenario by 2050 [4]. The International Energy Agency (IEA) roadmap to reach net zero emissions by 2050 includes targets related to (i) the extension of energy storage to support power network/grid and (ii) the implementation of a low-carbon economy [5]. Aligned with these targets, the European Commission (EC) promotes policies for decarbonization of energy sectors such as (i) minimizing GHG emission by at least 55% up to year 2030 and (ii) raising the share of RES in the energy mix [6]. Meeting both objectives is essential in the fight against climate change, as well as in the improvement of Europe's energy autonomy even more in the current era of energy crisis.

Within RES, solar power will play a significant role in the future economy, given its worldwide availability. Moreover, the solar-based RES have a promising future due to the exponential growth of the global concentrating solar power (CSP) plants [7] caused by the drop of their average investment/capital costs by 70% in the last decade [4]. However, the intermittence in the electrical supply is the major issue to be solved to massively deploy solar energy. The energy storage was already proposed in 2017 by the EC as a solution for variability in renewable energy production [8]. Thermal energy storage (TES) integrated into CSP plants allows for (i) better load/discharge efficiencies and lower capital cost than mechanical or chemical storage systems [9] and (ii) lower annual price variability than fossil fuels [10]. The TES CSP plants consist of a solar field, a heat transfer fluid (HTF), a storage system and a power block [11]. The solar radiation is concentrated onto a receiver to heat up the HTF at high temperature. The hot transport fluid transfers thermal energy to a TES system and/or to a thermodynamic cycle for electrical generation [12]. The stored energy is retrieved when electricity production is required and solar resource is total or partially unavailable, enhancing the dispatchability of the CSP plants [13]. The amount of thermal energy stored is subjected to the thermophysical properties of the storage medium (i.e. specific heat, temperature range, amount of stored energy) [14]. The TES systems are classified according to the load/discharge physical phenomena in sensible heat storage (SHS), latent heat storage (LHS) and thermochemical energy storage (TCES).

SHS materials store/retrieve the thermal energy by heating/cooling their mass, given their high specific heat (131-4187 J/kg·K). Most of the SHS systems are commercial and low cost, being molten salts the most widespread medium. Moreover, molten salts can be used as HTF and TES to enhance the dispatchability of CSP plants. Their major drawback is the narrow operating temperature range (290-565 °C) to prevent material solidification and degradation [15].

Secondly, LHS materials store/retrieve the thermal energy during phase change given their high latent heat (112-260 kJ/kg), minimizing oscillations in energy production [16]. Organic, inorganic or eutectic Phase Change Materials (PCMs) with volume variations from solid to liquid phase transition below 10% are used as LHS [17]. However, their low thermal conductivity and instability at high temperatures are their major drawbacks [18,19] Heat transfer structures such as shell and tubes enhance the heat exchange [20,21].

Lastly, TCES systems store/retrieve thermal energy through a cyclic process based on reversible chemical reactions, working at high temperatures up to 1300 ºC. The energy density of TCES (about 240-1090 kWh/t [22]) is almost 10 times higher than energy density of SHS (1001-4453 kJ/m³·K [16]) and 5 times higher than that of LHS (50 to 150 kWh/t [17,23]), providing long-term storage with minimal heat losses. However, technical aspects of TCES systems such as reactors design, reaction control and process integration must be still addressed to be more efficient. The CSP plants will require TCES systems in which heat and mass transfer are enhanced. The improvement in the stability of the cycles in the reversible reactions and the reduction in the cost of TCES materials will play a crucial role in the development of CSP plants, whose production depends on the variability of solar resource [22]. The transient state of TCES process must be assessed to simulate the real operation of the CSP plants with TES systems.

1.1. State of the art of thermal energy storage in concentrating solar power plants

The state of the art of the integration of thermal energy storage in solar power plants was thoroughly reviewed to settle the existing knowledge on the topic. The status of TES in the main CSP plants and its prospects have been reviewed and carefully presented. The information was gathered from (i) the current worldwide commercial CSP plants [24] and (ii) the main worldwide TES CSP research and development (R&D) projects located in Europe and North America [25,26]. These regions present a greater development in the field of CSP technology, contributing to almost two thirds of the total installed CSP power [24]. The results of this status and future prospective of thermal energy storage in concentrated solar power plants was gathered and published in the review paper *"Thermal energy storage in concentrating solar power plants: A review of European and North American R&D projects"* 2022, Energies, 15, 8570 [27].

TES has been proposed as a solution for the intermittency in power production of CSP plants. More than half of the ongoing worldwide CSP facilities integrate TES systems to manage power generation [9]. SHS, LHS and TCES are the most analyzed and developed TES systems to date with different pathways of integration with CSP plants. The main features of previous and future generation of CSP facilities have been reviewed, including (i) the implemented concentrating solar power technology in the solar field, (ii) the integrated TES medium to store/release thermal energy (SHS, LHS or TCES), (iii) the connection through the HTF between the solar field and the TES system, highlighting if the HTF is used as a means of heat transport and energy storage, (iv) the performed configuration to integrate the TES system into the CSP plant, according to the natural state of the storage medium: fluid (active storage) or solid (passive storage) and (v) the coupled power cycle to the CSP plant to produce electricity maximizing thermal to electrical performance. Table 1 shows the most widespread elements of the current state and the future directions of these TES systems for first/second and third generation of CSP plants, respectively.

Table 1. Characteristics of the current and the future third generation of CSP plants.

Elements	State of the art	Prospective
CSP technology	• Parabolic through collectors	• Parabolic through collectors • Solar power tower
TES medium	• SHS: conventional molten salts, water	• SHS: rocks, solid particles, liquid metals, new molten salts • LHS: PCMs • TCES: redox, hydroxide, carbonate
HTF	• Thermal oil ($\neq$TES)* • Water (=TES)§	• Air, CO_2 ($\neq$TES)* • Molten salts, solid particles, TCES systems (=TES)§
TES CSP integration	• 2-tank active indirect • Steam accumulator	• Single-tank thermocline & passive storage • Passive storage
Power block	• Steam Rankine	• CO_2 Brayton or supercritical

* Same substance used as storage medium (TES) and heat transfer medium (HTF).
§ The TES medium and the HTF are different substances.

The current commercial facilities are part of the first and second generation of CSP plants, including large molten salt-based TES [28] or water as TES and HTF to direct steam generation in the receiver [15]. Molten salts are currently integrated in a 2-tank indirect active storage format, implementing a steam Rankine based power cycle and a solar field with parabolic through collectors as CSP technology, which are connected by thermal oil as HTF [24]. The 2-tank format includes separated hot and cold tanks, being the hot tank charged with thermal energy while the cold tank contains the discharged molten salt [29,30]. Water is the second most used SHS medium as steam accumulator format to provide a direct steam generation [24]. Limitations related to properties (i.e. high freezing point of common molten salts, low thermal conductivity of water) and high cost associated to conventional molten salts and pressurized storage tanks for water led research efforts to develop new TES materials for the next generation of CSP plants [29,30].

Low-cost materials (i.e. natural rocks [16,31], solid particles [32,33], liquid metals [34]) and new high-temperature resistance molten salts up to 740 ºC will be the future options for SHS media in CSP plants [35,36], being able to save 35% of the cost using single-tank format. The stored heat is stratified in the single tank creating a thermal gradient [29,30]. Improved heat transfer ratio and lower storage cost would be achieved using high-temperature PCMs as LHS [37]. The storage size and associated costs for the next third generation of CSP facilities could be minimized through a new configuration coupling passive storage and single-tank thermocline systems using molten salts as SHS and HTF and PCMs as LHS. The passive storage consists of a simple and compact storage unit which is charged and discharged by circulating the HTF [29,30]. The use of air, CO_2 or even TES as HTF could minimize the cost of electricity production. Moreover, the thermophysical properties of PCMs will be enhanced embedding nanoparticles in their structure [38]. However, the emerging set of TES technologies with the greatest future potential is the TCES system as passive storage configuration. Advantageous characteristics of the TCES systems make them the most investigated ones during the last decade, such as low-cost storage media, high working temperatures, high energy density, seasonal storage with minimal energy losses [29,30]. As the development of reaction control involving TCES systems progresses, lower storage cost is expected compared to SHS and LHS materials [39]. Moreover, high-efficient power blocks (i.e. Brayton or supercritical CO_2 cycles) could be coupled to CSP facilities with TCES integration, enhancing the overall plant efficiency.

The future third generation of CSP plants will focus on the inclusion of (i) non-corrosive, high operational durability and high energy density TES materials, (ii) HTFs with high working

temperature and low operational degradability and (iii) more efficient thermodynamic cycles such as Brayton or supercritical [40]. Thus, the ongoing TES CSP R&D projects could lead the projection of future CSP plants, including high operating temperature (i) CSP technologies (i.e. solar power tower or parabolic through collectors), (ii) TCES systems (i.e. hydroxide, carbonate and redox) and (iii) power blocks such as supercritical CO_2.

TCES is the most preferred option as TES for the next generation of CSP plants, working above 800 °C [16,41] and enhancing the CSP conversion efficiency [42]. Among the TCES systems, gas-solid reactions are the most promising given their high reaction enthalpy and their simplicity in storage and transport as the products can be easily separated. Within gas-solid based TCES systems, one of the main challenges is the energy performance of the associated CSP plants.

The present PhD Thesis addresses the main issues of TCES systems based on reversible gas-solid reactions, specifically the Calcium Looping (CaL) process. The cyclic degradability of the CaL sorption material determines the amount of inert material circulating in the system which negatively influences the energy efficiency of the system. A new and optimized strategy for solids management can enhance the energy efficiency in the CSP plant. Thus, the influence of the solar resource variability and the circulation of inert material within the CaL TCES system are assessed to enhance the efficiency of the CSP plants.

1.2. Calcium Looping as thermochemical energy storage

The present PhD Thesis addresses those issues related to the dynamic operation and energy improvement of TCES systems (i.e. degradability, stability and lifetime of reversible reaction cycles) are addressed through the application of CaL technology.

The CaL gas-solid reaction has been extensively investigated in the last decade for its application as post combustion carbon capture integrated in the energy sector (i.e. fossil-fuel based power plants [43] or cement plants [44]). The technical feasibility of CaL process as carbon capture system in coal-fired power plants has been assessed in literature through process simulation, showing lower efficiency penalties (between 6 and 7% points) than other CO_2 capture systems [45]. The net efficiency penalty associated to CO_2 capture can be minimal (2.4% points) [46], providing calcination thermal energy requirements from a combustor [47]. Additionally, recent literature shows the potential of CaL technology for carbon dioxide (CO_2) capture to achieve zero or negative emissions bioenergy systems from wastes [48] or biomass [49] energy transformation.

Despite CaL system as a TCES was first proposed in 1974 by Barker [50], the greatest research interest emerged in recent years in support of solar-based RES as CSP. The CaL reaction (Equation (1)) may be the basis of a TCES system which easily integrates thermal energy in CSP plants, given its high reaction enthalpy and associated energy density between 390 and 490 kWh/t [22,51,52]. Another great advantage of CaL as TCES is the use of limestone as sorbent rich in calcium carbonate ($CaCO_3$), which is non-toxic, cheap (< 10 €/t $CaCO_3$) and abundant [53]. Thus, the CaL technology could play a key role in both (i) the decarbonization of energy-intensive sectors and (ii) enhancing the dispatch capacity of CSP plants.

$$CaCO_{3\,(s)} \leftrightarrows CaO_{(s)} + CO_{2\,(g)} \qquad \Delta H_R^\circ = +178\ kJ/mol \qquad (1)$$

4
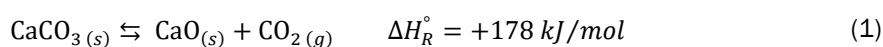
The CaL process as TCES is based on the reversible cyclic calcination-carbonation reaction. Calcination reaction of limestone (Equation (1)) occurs at 920-950 °C forming calcium oxide (CaO) and CO_2. The required heat is supplied by solar energy in the CSP plant when available [54]. The solar energy invested in the endothermic calcination process must be stored and later retrieved in the carbonator step. Thus, calcination products, CaO and CO_2, are fully or partially stored in separated tanks, diverting the rest to the carbonator to release thermal energy. The stored energy is recovered when electricity is required under total or partial solar resource unavailability. A minimum operating load could be maintained to avoid costly power plant shutdowns. The energy storage density defined as the chemical and sensible energy stored per unit mass CaO can reach 1419 MJ/m^3, being almost 2 times higher typical molten salts [55]. The thermal energy is retrieved in the carbonator reactor to provide thermal energy to an associated power cycle which supplies the electricity demand. The carbonation process takes place when CaO partially reacts with CO_2 to form $CaCO_3$ at 600 – 850 °C (reverse Equation (1)), releasing high temperature heat [56]. A conceptual diagram of the CaL TCES system is shown in Figure 1.
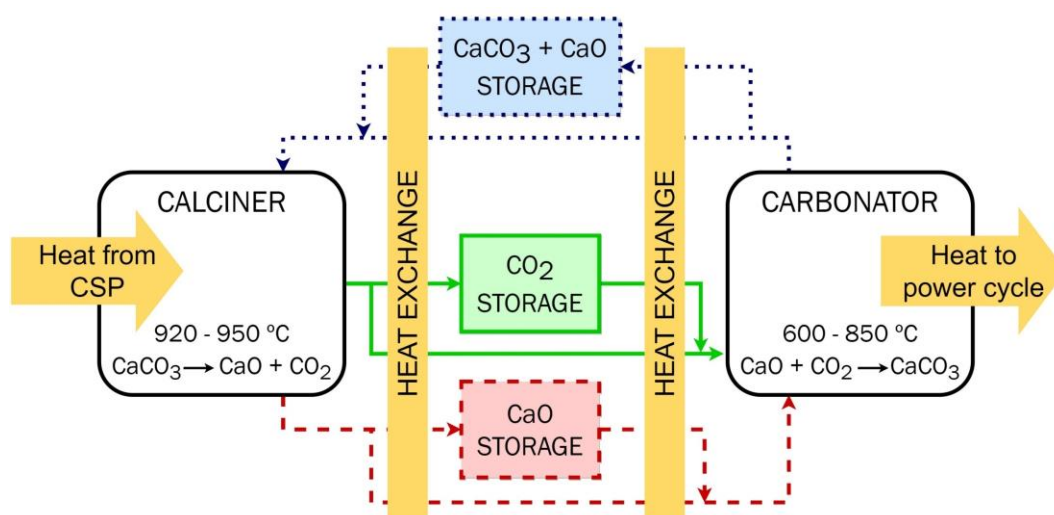

Figure 1. CaL TCES conceptual diagram.

The major drawback of the CaL reaction is the decay of sorbent capacity of CaO material with the number of cycles [57,58]. The loss of CaO reactivity is induced by thermal and chemical sintering caused by loss of porosity and pore plugging [59–62]. The CaO activity during carbonation step is subjected to the operating conditions of the CaL process for TCES applications, such as calcination/carbonation temperature (920-950 °C and 600-850 °C, respectively) and reactors atmosphere (100% CO_2) [54,56]. Nevertheless, the recovery of solar energy at high temperature in the carbonation step could allow the integration of high-efficient power cycles (i.e. Brayton) [63]. The loss of sorbent reactivity is one of the main issues to be solved. The sorbent conversion decay has been deeply investigated in literature, obtaining well-adjusted models under CO_2 capture conditions. However, the scarcity of experimentation under energy storage conditions narrows down the development of sorbent deactivation modelling for CaL operation as TCES. Different solutions have been investigated in literature to limit or prevent the drop in CaO activity: (i) limestone pretreatments [64] (i.e. mechanical [65,66], thermal [55,67], steam [68–70]), (ii) doped or modified sorbents [71,72], even adding inert stabilizers/promoters [73] (i.e. ZrO_2 [74–76], Al_2O_3 [76,77], eutectic alkali chloride salts [78]), (iii) improvements in natural limestone [61], or (iv) development of synthetic Ca-based sorbents [79], even introducing dark inert materials to

enhance the absorption of solar radiation [71,80,81]. Most of the sorbent activity enhancement techniques have been developed for CO_2 capture, such as (i) mechanical [65,66], thermal [55] and steam [70] pretreatments or (ii) doping of sorbents with ZrO_2 [74,76], Al_2O_3 [76,77]. Under TCES conditions, another technique to minimize the sintering issue at high operating temperatures, and therefore the deactivation of the sorbent, is to pressurize the calciner and carbonator reactors. Ortiz et al. proposed the calcination reaction in a low-pressure (0.01 bar) entrained flow reactor at 765 °C, reducing energy losses and CaO sintering [82].

Partially carbonated particles are found after the exothermic carbonation reaction, coexisting CaO and $CaCO_3$ in the same particle. The carbonated solids are stored or directed to the calciner during sunlight hours, closing the loop. The circulation and storage of unreacted solid material could negatively affect system efficiency [83]. The lower CaO reactivity, the larger amount of inactive solid material convey to the calciner [84]. As discussed above, the sorbent conversion is not complete and unreacted solids circulate throughout the CaL TCES system. The present PhD Thesis focuses on the issues raised by the efficiency improvement associated to the solids management.

Up to now, research efforts are aimed at scaling the CaL system as TCES, making it economically feasible. Primarily, the limitations in heat transfer during carbonation and calcination are some of the main problems to be solved. Moreover, several research lines have been carried out in recent years are presented below, proposing different operational schemes to couple the CSP plant with (i) the storage system based on CaL and (ii) a high-efficient power block to produce electricity.

Regarding reactors design for TCES, research has focused so far on small-scale experimental tests and large-scale simulations. Experimental research on CaL TCES is scarce, limiting the validation of larger-scale reactor models [85,86]. Paul Scherrer Institute tested the solar calcination at 54 kW in a window-less cyclone gas-particle separator, reaching 85% of sorbent conversion and an energy efficiency of 88%. The solar calcination results led the up-scaling up to 55 MW under computational fluid dynamics simulations using a falling particle receiver [87]. Moreover, Lisbona et al. simulated a 3-stage solar falling particle calciner to keep the temperature profile almost isothermal and avoid excessive sorbent degradation, achieving an energy storage efficiency of 98.9% [54]. Fluidized bed (FB) has also been widely investigated for CaL TCES, given its proper gas-solid heat transfer [86]. Padula et al. simulated an autothermal FB to enhance the overall TCES efficiency [88]. While Tregambi et al. tested in lab-scale a FB heated by a solar simulator at 940–950 °C under CO_2, validating the loss of sorbent reactivity given the harsh temperature conditions [62]. Sarrión et al. also verified the sintering issue caused by high calcination temperatures (950 °C under pure CO_2) through an experimental test in a thermogravimetric analyzer [79]. The indirectly irradiated fluidized beds can be the most suitable calciner design for up-scaling the CaL TCES, once issues related to particle attrition and high temperature resistance of reactor components are addressed [89]. The carbonation reaction has been tested at 10 kW within the SOlar Calcium-looping integRAtion for ThermoChemical Energy Storage (SOCRATCES) project [90] in an entrained flow reactor cooled by air through external coils, using the air in a Stirling engine to produce power [91]. Bailera et al. found from simulations that those carbonators cooled by external coils cannot properly recover the exothermal energy at industrial scale (100 MW), leading to unreasonable dimensions (7 m in diameter and 52 m in length) [92]. Therefore, other potential configurations for heat removal must be evaluated at industrial carbonators for CaL TCES. The implications of reactor design in the overall efficiency of the large-scale plants must be considered: (i) a suitable design to evacuate the thermal energy during carbonation [92] and (ii) the complexity of reaching a smooth temperature profile in the calciner [54]. Even so, the CaL TCES technology is currently in a demonstration scale, being slightly

above similar energy storage technologies based on endothermic-exothermic thermochemical reactions [93].

Several process schemes have been proposed in literature for the integration of the CaL TCES system in CSP plants. The aim of these studies is to enhance the dispatchability, minimize the capital cost of the CSP facilities and assess the overall efficiency improvement of CSP plant with highly efficient power cycles. The capacity factor improvement is estimated through (i) the complementation of solar-based RES, CSP and photovoltaic [94,95], (ii) the oversizing of the solar field within the CSP plant [96] and/or (iii) the integration between CSP and combined cycle plants [97,98]. The hybrid solar-based configuration proposed by Bravo et al. achieved a capacity factor up to 73% [94], which is comparable to conventional thermal energy systems. Besides, the operational strategy for maximizing the annual net power supplied led to an overall efficiency upper bound of 33.8% through a multi-objective optimization. The target variables are related to economics and energy, such as (i) the plant investment cost, (ii) the levelized cost of electricity (LCOE) and (ii) the mismatch between power supply and energy demand defined as loss of power supply capacity (LPSC). The main objective is to minimize the value of the target variables given as input data (i) the hourly variability of solar radiation, (ii) the minimum continuous energy demand of the plant and (iii) the financial data. The optimized results provided the hourly energy flows and the technical and economic performance of the hybrid solar power plant [95]. The electricity demand during the day was supplied by both solar-based RES, while the energy stored during sunlight hours in the CaL TCES system is recovered when solar energy is unavailable [94,95]. The solar field oversizing allows to store during the sunlight hours the amount of CaO required when solar energy is unavailable, as investigated Tregambi et al. [96]. A daylight duration of 12.1 h is considered at steady state operation to produce methane, providing the CO_2 stream to a power to gas station from a CaL process based carbon capture performed by concentrated solar power [96]. The most recent configuration of CSP with combined power plant was investigated by Ortiz et al., reaching an overall efficiency of 45% [98]. The CSP plant supplies thermal energy to the combined power block and the storage system. The CaO is discharged during the night when the CSP plant is shutdown [97]. The hourly energy flows to/from storage and performance behaviour of the CaL solar combined cycle was obtained for four selected days with different daily solar resource profiles within a year, discharging at a constant rate the energy stored during sunlight hours [98]. Moreover, a low-pressure calcination was also proposed by Ortiz et al. [82] to enhance the sorbent conversion into the CaL solar combined cycle. An overall efficiency above 30% was achieved after analyzing the pattern of storage, power and efficiency of typical days for spring and summer. Again, the energy stored during the hours of sunlight is used proportionally in the hours without solar resource, neglecting demand patterns to establish the best operating strategies [82]. Secondly, the power blocks implemented in the simulations performed by these works are a combination of steam Rankine cycle and CO_2 Brayton cycles. The most reliable power block to be coupled with CSP plants is the steam Rankine cycle, given its wide deployment in first and second generation plants [99]. Even so, CO_2 power cycles have recently been assessed to enhance the overall efficiency of CSP plants (net electric production to net solar thermal input) up to (i) 40.4% in the case of supercritical CO_2 cycles [100] and (ii) 31-44% for CO_2 Brayton cycle [95,101–103]. Moreover, the cheapest alternative when comparing helium and CO_2 for supercritical cycles is CO_2 [63].

The key motivation of this PhD Thesis is the improvement of the integration and operation of the CaL process as TCES into CSP plants. Under the development of the present PhD Thesis, novel solids management strategies have been addressed to enhance the energy performance of the CaL TCES system as well as the size reduction of the plant equipment affected by the circulation of inactive solids. Moreover, the dynamic operation of the CaL TCES system has been deeply assessed to improve its financial feasibility, being hourly and seasonally variable both the solar

resource and the electricity demand influenced by energy prices. Thus, the next section describes the work develop during the PhD Thesis to solve the gaps found in the literature related the CaL TCES in CSP.

1.3. Operational optimization in Calcium Looping as thermochemical energy storage

In general, the CaL TCES system has been assessed under stationary operation in literature. The hourly, daily, seasonally and yearly variability of the solar resource has been considered only in recent research to find the best design and the optimum required size for large-scale plants, minimizing investment cost. However, most of these works proposed oversized CSP systems or CSP supported by other energy sources, mainly renewables. The energy stored in the CaL TCES system during daytime with solar availability is proportionally recovered during periods without total or partial solar resource. Thus, operation at different loads during the day is not contemplated. The design and size of the plant equipment could be strongly influenced by the dynamic operation of the CaL TCES system that, in turn, is influenced by the instability of the solar resource. Besides, the process configurations investigated in these works explore the effect on the efficiency of the CaL TCES system of the circulation of non-reactive particles. The potential reduction of unreacted material conveyed to the calciner and storage tank of carbonate is a hot topic to be assessed.

The core target of this PhD Thesis is the proposal and assessment of a novel integration scheme of CaL technology as a TCES in a CSP plant, enhancing the system efficiency and maximizing the daily income from the electricity sale for any availability of solar resource. The new configuration could lead to the minimization of energy losses associated to the circulation and storage of unreacted/not-carbonated solids in a large-scale CaL TCES system. Therefore, the present PhD Thesis addresses two main gaps found in literature: (i) the assessment of the CaL TCES system efficiency subjected to solids management and (ii) the real operation of the CaL TCES system under dynamic operation according to solar resource availability and price variability in the electricity market. The innovative contributions of the present PhD Thesis lie in improving the energy efficiency of the CaL TCES system, as well as in determining the optimized CaL TCES operational map and transient pattern of operation along the day considering energy demand and solar availability.

Once the *State of the art of thermal energy storage in concentrating solar power plants* is presented in previous section, the technical advances of the PhD Thesis are structured in three main sections to achieve the main goal. The first stage is devoted to the energy assessment of the large-scale Calcium Looping process as thermochemical energy storage under conventional configuration. Within the second stage, a novel solids management strategy is proposed in a new CaL TCES configuration, enhancing the system performance and minimizing energy losses related to the circulation of unreacted solids. Finally, a methodology to set the most profitable dynamic operation is proposed to improve the energy and economic savings for the novel CaL TCES configuration integrated into CSP plants. The results of the research developed during this PhD Thesis have been disseminated in six papers indexed in the Journal of Citation Reports (JCR), being four already published and two under review, and five international conferences, as shown in Table 2.

The *State of the art of thermal energy storage in concentrating solar power plants* section presents an extent review of the prospective of TES in the next third generation of CSP plants, including information related to the complete and ongoing worldwide research and development (R&D) TES CSP projects. The review paper was published in Energies in 2022.

First section of technical advances (*Energy assessment of Calcium Looping based thermochemical storage system*) includes a novel carbonator modelling to enhance the heat removal and its implications related to efficiency and sizing in a conventional CaL TCES process scheme at industrial scale. The obtained results about the novel carbonator design were presented in the 32nd International Conference on Efficiency, Cost, Optimization, Simulation and Environmental Impact of Energy Systems, which was held in 2019. The first energy assessment of the conventional CaL TCES configuration was exposed in the 3rd Congress of Aportando Valor al CO$_2$, which took place in 2019. The carbonator modelling coupled with the CaL TCES system at large-scale to assess the required storage size for the minimum technical partial load and the nominal load was presented in the 33rd International Conference on Efficiency, Cost, Optimization, Simulation and Environmental Impact of Energy Systems, taking place in 2020. The implications of the carbonator in CaL TCES system at industrial scale on the system efficiency were published in Energy in 2021.

Second section of technical progresses (*Novel Calcium Looping thermochemical storage proposed configuration*) comprehends the main part of the present PhD Thesis. The novel configuration proposed for CaL TCES system was published in Energy in 2021. While, the comparison in size and efficiency between the conventional and the novel CaL TCES configuration under the same operational conditions and the operating maps resulting for maximizing the system efficiency were published in Journal of Energy Storage in 2022. An experimental campaign was performed given the positive effects on the efficiency improvement of the novel configuration. Lab-scale tests for CaL process provided results for carbonation degree evolution at simulation conditions for reactors and the density of carbonated and calcined particles, which were presented in the 10th European Combustion Meeting, which was held in 2021. As a result of the experimental tests, the preliminary design of a unit for the separation of carbonated solids by density difference was exposed in the 24th Fluidized Bed Conversion Conference, tanking place in 2022. As a final point of this experimental campaign, the minimum fluidization velocity of the carbonated and calcined particles was measured, confirming the potential partial separation for cycled particles in a paper published in Chemical Engineering Journal within 2023.

Finally, the dynamic operation of the novel CaL TCES configuration as the ideal situation was assessed and economically optimized within the last section of technical advances of the present PhD Thesis (*Operational methodology and economic implications*). The methodology applied was based on (i) the maximization of daily incomes under any solar radiation and electricity sales prices and (i) the operating maps which maximized the system efficiency. The economic assessment of the final CaL TCES design has been accepted for publication in Journal of Energy Storage in 2023.

For future work, a kinetic model for carbonation reaction and the separation degree of carbonated particles must be addressed as a result of the experimental campaign at a lab-scale. The kinetic model to be developed could be validated for a relatively large number of carbonation/calcination cycles under CaL TCES conditions. Additionally, an average separation degree of carbonated material could be obtained by applying a partial separation model. The partial separation model could also be developed after experimental validation of partial classification between more and less carbonated particles. The carbonation and partial separation models could be applied to the simulation of the CaL TCES system under the novel configuration proposed in this

PhD Thesis. Likewise, the methodology developed in the framework of the present PhD Thesis could be implemented again for energy and economic assessment of the CaL TCES system under partial separation of carbonated material. The CaL TCES simulation model for industrial scale could provide results closer to reality, applying future models to develop (carbonation kinetics for TCES and partial separation of carbonated material) and methodology defined under the present PhD Thesis related to operational optimization of the CaL TCES system.

Table 2. Structure of the present PhD Thesis.

| Section		Papers	Conferences
State of the art of thermal energy storage in concentrating solar power plants		*"Thermal energy storage in concentrating solar power plants: A review of European and North American R&D projects"* 2022, Energies, 15, 8570.	
Energy assessment of Calcium Looping based thermochemical energy storage		*"Modelling Calcium Looping at industrial scale for energy storage in concentrating solar power plants"* 2021, Energy, 225, 120306.	*"On the modelling of a lime carbonator operating in a concentrated solar power plant for energy storage"* 32nd ECOS 2019
			"Calcium Looping como uso directo del CO_2 para el almacenamiento de energía solar" 3rd Aportando valor CO_2 2019
			"Solar Calcium Looping energy storage: Preliminary comparison between pilot and large scale" 33rd ECOS 2020
Novel Calcium Looping thermochemical storage proposed configuration		*"Design and operational performance maps of Calcium Looping thermochemical energy storage for concentrating solar power plants"* 2021, Energy, 220, 119715	
	Integration and operating alternatives	*"Operation maps in Calcium Looping thermochemical energy storage for concentrating solar power plants"* 2022, Journal of Energy Storage, 55, 105771	
	Technical feasibility of carbonated solids separation	*"Solar-driven Calcium Looping in fluidized beds for thermochemical energy storage"* 2023, Chemical Engineering Journal, 466, 142708	*"Improvement of performance of fluidized bed Calcium Looping for thermochemical solar energy storage: Modelling and experiments"* 10th ECM 2021
			"New strategies for solids management in a Ca-looping based TCES System" 24th FBC 2022
Operational methodology and economic implications		*"Optimized Ca-looping thermochemical energy storage under dynamic operation for concentrated solar power"* 2023, Journal of Energy Storage, Accepted for publication	

1.3.1. Energy assessment of Calcium Looping based thermochemical storage system

The most widespread TES within R&D projects in the last decade are the TCES. The third generation of CSP plants will require high temperature resistance TES materials to enable the implementation of high-efficient power blocks. Different research proposed several integrations between the CSP plant, the CaL TCES system and the power block to produce electricity. Among CaL TCES system, most of the configurations proposed in literature involve two main reactors (carbonator and calciner) with an independent intermediate storage of CO_2, CaO and partially carbonated particles (mixture of CaO and $CaCO_3$). Moreover, the implications of the reactors design on the efficiency of the CaL TCES system are not implemented in the simulations at large-scale performed in these works. Thus, the **first contribution** is to establish the initial design of the scheme proposed in the literature as a reference case. The conventional scheme of the CaL TCES process is energetically and operationally assessed, contemplating carbonator design implications when up-scaling to industrial scale. New variables are defined to better characterize the streams conveyed from and to the storage tanks and therefore the stored volume. The circulation of gas and solids in the CaL TCES system could define the stored and recovered thermal energy, as well as the efficiency of storage and retrieval processes.

Figure 2 illustrates the conventional CaL TCES configuration, considering a 100 MW_{th} of solar power at calciner receiver (Q_{CL}) for nominal load. The calciner reactor operates at 950 °C and carbonator at 850 °C, both under CO_2 atmosphere. A CaO average activity of 13.54% into the carbonator was assumed [92], considering an input of 1% of fresh limestone into calciner. To maintain the mass balance in the calciner, a CaO flow is purged. The intermediate storage tanks conditions are (i) 200 °C for carbonated particles from carbonator (ST1: $CaCO_3$/CaO + CaO) and calcium oxide from calciner (ST2: CaO) and (ii) 100 °C and 73 bar for CO_2 from calciner, being previously compressed and cooled in one stage (CCT). A discharging expansion (DE) is required to feed the CO_2 at carbonator conditions from CO_2 storage tank (ST3). Heat losses of 2% are considered for the heat exchangers which release thermal energy (EE). The heat exchangers named energy required (ER) release or demand thermal energy, except for ER-CaCO3 which always requires heat input. The same heat exchanger cannot work releasing and requiring energy. A stream always demands or releases energy under all conditions, being a limitation in the design of a heat exchanger. Research presented in the literature only shows the operation of the heat exchangers under steady state in the CaL TCES system, ignoring the behaviour under transient mode of those heat exchangers located between the reactors and the storage tanks. The software Engineering Equation Solver (EES) was used to model the conventional CaL TCES configuration [104].

The solar resource variability influences the operating mode of the system: storage (Figure 2 (a)) or retrieval (Figure 2 (b)). The energy storage operation mode (ESOM) comprises the operation of the CaL TCES system under carbonator energy demand below nominal power. While energy retrieval operation mode (EROM) considers operation points of the CaL TCES system when solar availability is lower than nominal. Storage and discharge fractions are defined to determine (i) the thermal energy paths, (ii) the solids and gas streams to and from the storage tanks, (iii) the volume required for the storage tanks and (iv) how the CaL TCES system works. The input variables in the energy are the available solar energy (Q_{CL}) and the energy demand from the carbonator (Q_{CR}). The mass and energy flows for each CaL TCES equipment are obtained as a result. The

storage and discharge fractions have been defined to set the operation maps of the CaL TCES system, given the wide possibilities of operation.
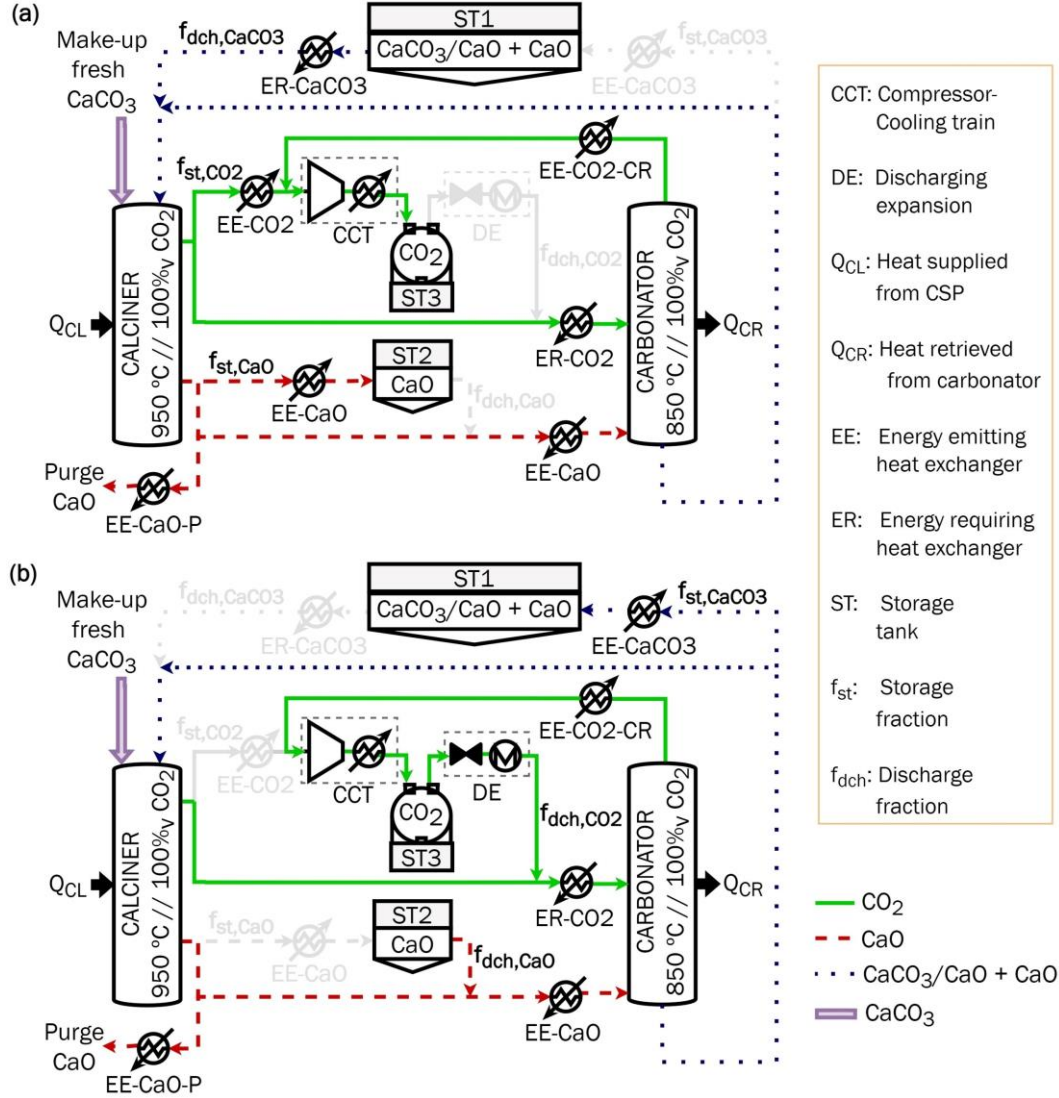
Figure 2. Conventional CaL TCES operation scheme under storage (a) and retrieval (b) operation modes.

When energy demand from carbonator decays below nominal, part of the captured solar energy is directed to energy storage (Figure 2 (a)). A storage fraction of lime and CO_2 flows, $f_{st,CaO}$ and $f_{st,CO2}$ in (Equation (2)) respectively, are sent to storage tanks ST2 and ST3. These fractions are defined as the ratio between the flow of CaO and CO_2 diverted to their corresponding storage tanks related and the maximum possible flow of CaO and CO_2 formed after calcination reaction (nominal operation of 100 MW_{th}), respectively. Carbonated material must be discharge from ST1 to form CaO and CO_2, storing the energy not required by the carbonator in the ST2 and ST3 tanks. The discharge fraction of carbonated solids, $f_{dch,CaCO3}$ in (Equation (3)), are the ratio between the carbonated material discharged from ST1 and the maximum amount of solids could fed the storage tank ST1 from carbonator when operates at full load.

$$f_{st,CaO} = f_{st,CO2} = \frac{\dot{m}_{st,CaO}}{\dot{m}_{st,max,CaO}} = \frac{\dot{m}_{st,CO2}}{\dot{m}_{st,max,CO2}} \qquad (2)$$

$$f_{dch,CaCO3} = \frac{\dot{m}_{dch,CaCO3}}{\dot{m}_{st,max,CaCO3}} \qquad (3)$$

Whenever solar energy is not enough to supply the energy demand in the carbonator (Figure 2 (b)), CaO and CO_2 are proportionally discharged from ST2 and ST3 to keep a constant inlet CaO/CO_2 molar ratio (R) of 6.8. The assumed value for R ensures a carbon capture efficiency of 90% during the carbonation stage. The discharge fraction of CaO and CO_2, $f_{dch,CaO}$ and $f_{dch,CO2}$ in (Equation (4)), defines the ratio between CaO and CO_2 discharged from ST2 and ST3 and the maximum flowrate of CaO and CO_2 diverted from calciner at nominal load (100 MW$_{th}$), respectively. The insufficient availability of solar energy diverts part of the carbonated material to storage (ST1). The storage fraction of carbonated material, $f_{st,CaCO3}$ in (Equation (5)), represents the mass flowrate ratio between carbonated solids diverted to ST1 from carbonator and the maximum stream could leave the carbonator at full operating capacity.

$$f_{dch,CaO} = f_{dch,CO2} = \frac{\dot{m}_{dch,CaO}}{\dot{m}_{st,max,CaO}} = \frac{\dot{m}_{dch,CO2}}{\dot{m}_{st,max,CO2}} \qquad (4)$$

$$f_{st,CaCO3} = \frac{\dot{m}_{st,CaCO3}}{\dot{m}_{st,max,CaCO3}} \qquad (5)$$

A novel carbonator modelling was proposed to quantify the implications of the partial load operation on the efficiency and storage tanks size of the CaL TCES conventional configuration at industrial scale under energy storage and retrieval operation modes. The operation load of both reactors (calciner/carbonator) are defined as the ratio between the input mass flow and the nominal input mass flow of carbonated material for calciner and CaO/CO_2 streams for carbonator. The minimum technical partial load of carbonator could influence storage tank size and the minimum thermal energy retrieved from carbonator to the power cycle. The carbonator was modelled as an entrained flow reactor, considering reaction kinetics from Ortiz et al. [56], gas and solid phase and heat transfer mechanism. The gas phase model provides information to the solid phase step to determine the velocity of the particles, according to Wen et al. [105]. The mole flows from both gas and solid phase were counted in the heat transfer module to compute reactor temperature. Moreover, the kinetic model receives information related to residence time to obtain sorbent conversion. The results of conversion and reactor temperature were reintroduced into the modules until they converged. A multi-tube configuration for heat transfer (i) conserving temperature profile was designed to scale up to large scale (100 MW$_{th}$) and (ii) keeping constant reactor length and velocity of gas-solid mixture relationship and ratio between reactor length and diameter of enclosure [106]. As a result, the carbonator dimensions for industrial scale would be 15 m in height and 3.3 m in diameter, resembling the behaviour of the small scale reactor with residence times between 6.5 and 7.5 s and carbonation conversion of 13.5%. Under nominal conditions, 80 MW$_{th}$ are available from carbonator to be diverted to a power cycle. The minimum technical partial load of carbonator to couple a power block is set at 0.239, retrieving 40 MW$_{th}$ to operate the power cycle with the minimum cooling flow requirements in the carbonator (half of its nominal value) [107].

The energy implications of the carbonator modelling on the CaL TCES system efficiency were assessed at a single operating point for each pair of carbonator/calciner loads (L_{CR} and L_{CL}).

The definition of two efficiencies provides information of the energy feasibility of the CaL TCES system: storage and available thermal energy efficiencies. The energy analysis carried out through the definition of efficiencies was published within the research paper *"Modelling Calcium Looping at industrial scale for energy storage in concentrating solar power plants"* 2021, Energy, 225, 120306 [108]. Under ESOM, the lime and CO_2 storage fraction ($f_{st,CaO}$) counterbalances the discharge of carbonated solids from ST1 ($f_{dch,CaCO3}$), being the lime and CO_2 discharge fraction ($f_{dch,CaO}$) and the carbonated storage fraction ($f_{st,CaCO3}$) equal to zero. The discharge fraction value of carbonated material ($f_{dch,CaCO3}$) corresponds to the difference between calciner and carbonator loads. Under EROM, the lime and CO_2 storage fraction ($f_{st,CaO}$) and the discharge of carbonated solids from ST1 ($f_{dch,CaCO3}$) are set to zero, being the lime and CO_2 discharge fraction ($f_{dch,CaO}$) equal to the carbonated storage fraction ($f_{st,CaCO3}$) equal to zero. The discharge fraction value of carbonated material ($f_{dch,CaCO3}$) corresponds to the difference between calciner and carbonator loads. Table 3 shows the operational points initially evaluated to define the operation map for conventional CaL TCES systems.

Table 3. Operation points assessed under each operation mode for conventional CaL TCES configuration.

Operating parameters	Operation mode	
	Energy storage (ESOM)	Energy retrieval (EROM)
Reactor loads		
Calciner load (L_{CL})	0 to 1	
Carbonator load (L_{CR})	0 to 1	
Storage/Discharge fractions		
CaO storage fraction ($f_{st,CaO}$)	(L_{CL}-L_{CR})	0
CaO discharge fraction ($f_{dch,CaO}$)	0	(L_{CL}-L_{CR})
Carbonated solids storage fraction ($f_{st,CaCO3}$)	0	(L_{CL}-L_{CR})
Carbonated solids discharge fraction ($f_{dch,CaCO3}$)	(L_{CL}-L_{CR})	0

Figure 3 shows the resulting operation maps under storage and retrieval operation modes through storage and discharge fractions. The green zone represents the fractions which define the optimized operation under ESOM. The blue area depicts the flows management between reactors and storage tanks under an optimized EROM.
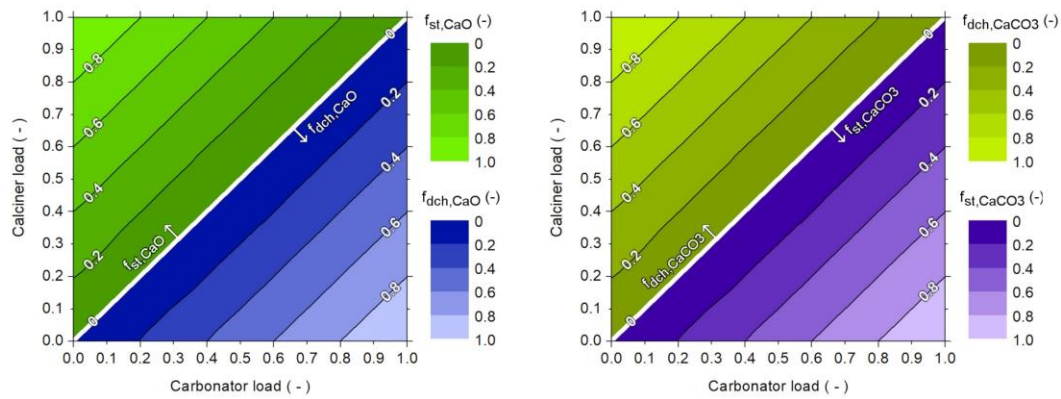
Figure 3. Operation maps for conventional CaL TCES scheme.

The lower the carbonator demand and the greater the solar energy availability, the greater discharge from storage tank ST1 and greater storage of CaO (ST2) and CO_2 (ST3) after calcination. The higher carbonator demand and the lower solar energy availability, the higher discharge from storage tanks ST2 (CaO) and ST3 (CO_2) and higher storage of partially carbonated solids into storage tank ST1 after carbonation step, given the low operating load on the calciner. These operation maps provide information about how operate the CaL TCES system and manage the gas and solids streams to/from the storage tanks to obtain an energetically optimized storage or retrieval process.

The efficiency during the storage step (η_{st}) compares the stored energy and the net energy consumed in the storage process. Figure 4 illustrates the maximum storage efficiency distribution for each operation point gathered in the optimized operation maps under ESOM.
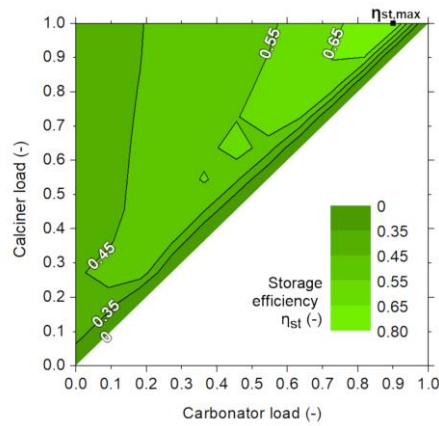

Figure 4. Storage efficiency under ESOM.

The maximum storage efficiency (76%) is reached for (1, 0.9) calciner and carbonator loads ($\eta_{st,max}$ in Figure 4), corresponding to the minimum specific storage consumption (SSC). The SSC determines the thermal and electrical energy invested during ESOM to store the mass unit of CaO. This term is useful to provide the energy consumption associated to the lime discharged from ST2 during EROM. The SSC ranges between 770-1324 MJ/t_{CaO} for high/zero carbonator loads, respectively. Figure 5 represents the thermal energy availability efficiency (η_{av}) related to the operation maps obtained for ESOM and EROM.
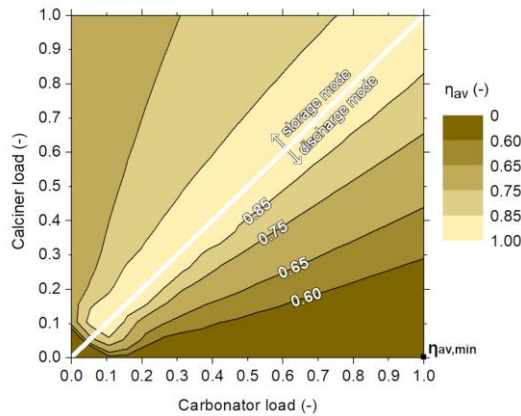

Figure 5. Thermal energy availability efficiency under ESOM and EROM.

The available thermal energy efficiency (η_{av}) for ESOM compares the available heat to the thermal energy invested in the CaL TCES system for calcination reaction and solids preheating before calcination from storage tank ST1. The thermal availability efficiency (η_{av}) under EROM considers the relation between heat available from the carbonator and EE heat exchangers and the thermal energy consumed. The thermal available energy efficiency profiles are similar for both energy operation modes: storage and retrieval. The minimum energy available efficiency (55%) is reached when solar energy is unavailable and the energy demand is maximum ($\eta_{av,min}$ in Figure 5). The highest thermal availability efficiencies are achieved for similar calciner/carbonator loads since the lower management of solids from/to storage tanks.

Regarding storage tanks size of CO_2 (ST3), CaO (ST2) and carbonated material (ST1) (Equation (6)), the storage and discharge fractions define the inlet/outlet flowrates, while the number of hours provides the time interval to integrate.

$$V_{st}\left(t\right) = \int_{t_0}^{t} \left(\frac{\dot{m}_{in} - \dot{m}_{out}}{\rho}\right) dt + V_{st,0} \tag{6}$$

The maximum storage flowrate of CO_2 and CaO takes place when calciner operates at nominal load and carbonator operates at minimum load (0.239) under ESOM. A density of 2710 kg/m³ and 1800 kg/m³ are considered for $CaCO_3$ and CaO, respectively. The maximum storage stream of carbonated solids is given under EROM when carbonator operates at nominal load and no solar resource is available. The size of the storage tanks ST1 and ST2 for 15 hours of operation up to 11400 m³ and 5700 m³ with a void fraction inside the tank of 30% [109]. While the CO_2 density is defined at storage conditions (100 ºC and 73 bar), reaching a storage tank ST3 volume of 8256 m³. Table 4 shows a summary of the results obtained for the energy implications on the conventional CaL TCES system.

Table 4. Results summary for energy assessment of conventional CaL TCES configuration.

Main conventional CaL TCES configuration results	
Efficiencies*	Range (min/max) (%)
Energy storage (η_{st})	46/76
Thermal energy availability (η_{av})	55/90
Volume tanks§	Required volume (m³)
Carbonated material storage tank (ST1)	11400
CaO storage tank (ST2)	5700
CO_2 storage tank (ST3)	8256

* Comprising minimum carbonator partial load of 23.9%.
§ Assuming a void fraction of 30% and a storage time of 15 h.

The influence of the reactor design at large scale on (i) the available heat and (ii) the partial load operation of the CaL TCES system were quantified in this study. One single operating point was assessed for each pair of calciner/carbonator loads, being able to operate some heat exchangers releasing or demanding energy, subsequently hindering the design of thermal energy integration. Secondly, the large size required for storage shows the high circulation of solids between the storage tanks and the reactors which energetically penalize the CaL TCES system. Therefore, a novel CaL TCES configuration was proposed and studied to enhance energy efficiency associated to solids management.

## 1.3.2. Novel Calcium Looping thermochemical storage proposed configuration

The high circulation and storage of unreacted inert solids in the conventional CaL TCES configuration open a window for finding operational strategies which improve the efficiency of the CaL TCES system. The **second contribution** of the present PhD Thesis is to enhance energy efficiency subjected to the convey of unreacted inert solids in the CaL TCES system. A novel CaL TCES configuration scheme was proposed to evaluate the effect of an ideal total separation of carbonated/reacted and not-carbonated/unreacted solids at the outlet of the carbonator on the plant dimensions. Moreover, the operational behaviour of the novel CaL TCES configuration was preliminary assessed under a wide range of operating points for each operation mode, (i) allowing simultaneous energy storage/release and (ii) assuming nominal loads for calciner under ESOM and for carbonator under EROM.

Figure 6 illustrates the proposed novel CaL TCES configuration. The solar power at calciner receiver (Q_{CL}) for nominal load at 100 MW$_{th}$. The analysed operating conditions of reactors (i.e. temperature, atmosphere), number of storage tanks, heat exchangers and the compression-cooling train (CCT) are analogous to those of the conventional CaL TCES system.

Since there are no literature regarding kinetic models of the CaL process based on TCES, a carbonation model derived from carbon capture conditions has been implemented. The CaO average activity (22.6%) during carbonation step was determined applying extremely conservative constrains: (i) the kinetic model described by Grasa et al. for carbon capture conditions (650 °C and 10-15%$_v$ CO_2 concentration) [110] and (ii) age distribution of solids inventory computed when no solid material is stored into storage tanks [111]. The carbonator kinetic model includes a deactivation constant of 0.52 and a residual conversion of 7.5% [110]. A CaO purge flow of 4% of the total CaO formed after calcination and a constant CaO/CO_2 molar ratio (R) of 4.26 entering the carbonator were assumed to ensure a carbon capture at carbonator of 90%. A carbonator nominal power of 88.33 MW$_{th}$ (Q_{CR}) is reached by applying the carbonator model when the maximum flow rate of the calcination products (CaO and CO_2) is introduced in the carbonator. The definition of the parameters of the carbonator model is gathered in the research paper *"Design and operational performance maps of Calcium Looping thermochemical energy storage for concentrating solar power plants"* 2021, Energy, 220, 119715 [112].

For the very first time in literature, a new equipment named solid-solid separation unit (SSU in Figure 6) was integrated after the carbonation stage to fully separate the carbonated material into (i) unreacted solids (CaO) and (ii) completely carbonated solids ($CaCO_3$/CaO). The unreacted CaO is recirculated into the carbonator while the carbonated material is directed to storage tank ST1 or to the calciner. The total separation of carbonated material could redefine the energy consumptions and plant dimensions under the most advantageous situation. The software Engineering Equation Solver (EES) were used to model the novel CaL TCES configuration [104].

The present novel CaL TCES configuration (Figure 6) continues with the same operating points methodology, considering the definitions of storage/discharge fractions to/from the storage tanks, respectively. The value of storage and discharge fractions were discretized in ten steps from 0 to 1 to assess the whole range of operating points which lead to a given combination of calciner/carbonator loads. Moreover, the discharge fractions must be below the value of the storage fraction, preventing the discharge of more material than stored.
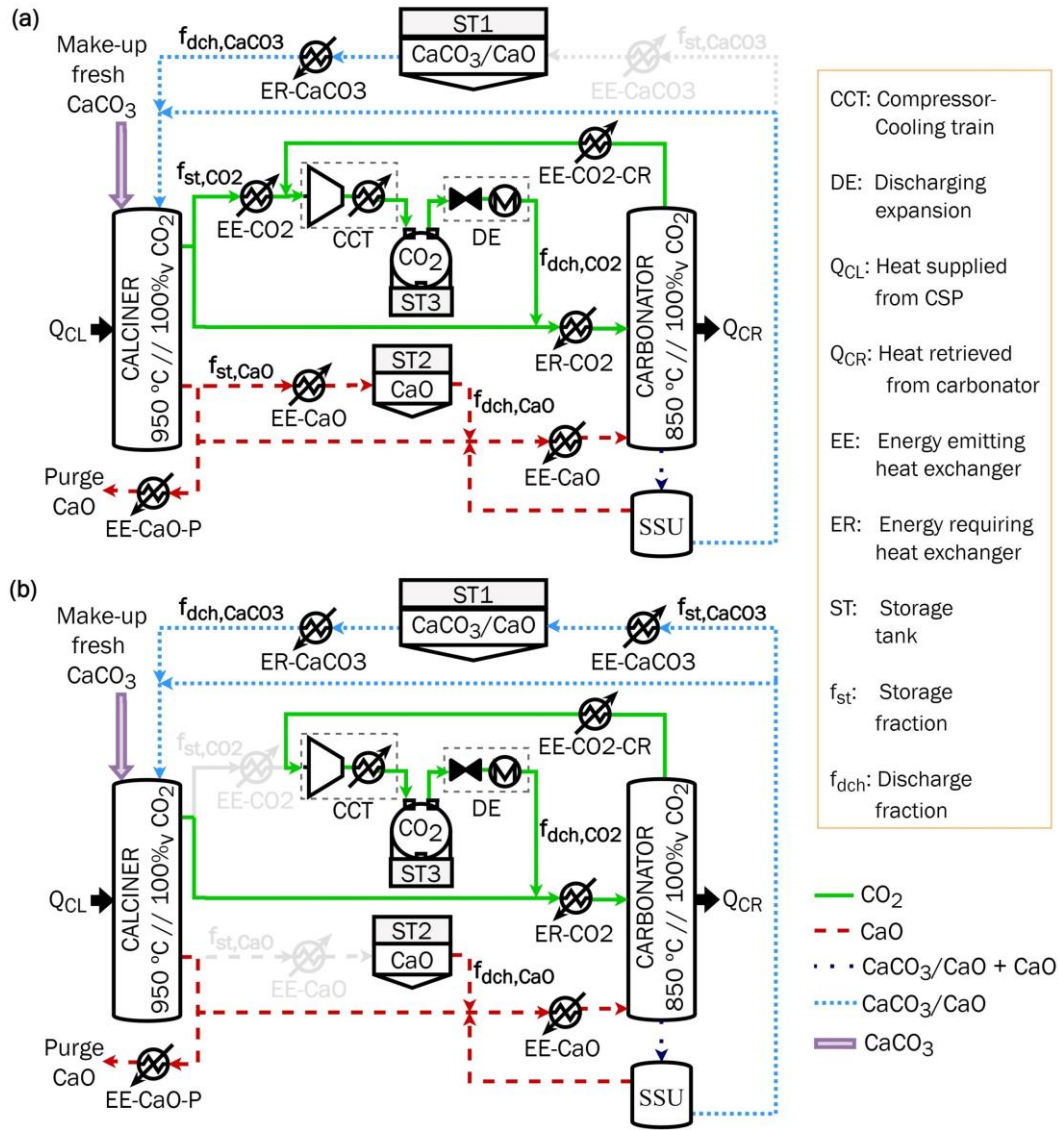
Figure 6. Novel CaL TCES configuration scheme under storage (a) and retrieval (b) operation modes.

Under ESOM, the whole range between 0 and 1 of the CaO and CO_2 discharge fractions ($f_{dch,CaO}$) is assessed for each value of the CaO and CO_2 storage fraction ($f_{st,CaO}$), assuming a complete circulation of carbonated material from SSU to calciner ($f_{st,CaCO3}$ = 0) which operates at nominal power (100 MW$_{th}$). The resulting operation maps provide information about the range of the size of the plant equipment when calciner operates at nominal conditions.

Under EROM, the whole range of the $CaCO_3$ discharge fraction ($f_{dch,CaCO3}$) between 0 and 1 is assessed by each value of the $CaCO_3$ storage fraction ($f_{st,CaO}$), assuming a directly circulation of calcination products (CaO and CO_2) to carbonator ($f_{st,CaO}$ = 0), which operates at nominal load (88.33 MW$_{th}$). The resulting operation maps provide information about the range of the size of the plant equipment when carbonator operates at nominal conditions. Table 5 shows the operational points initially evaluated to assess the influence of storage/discharge fractions combinations on the equipment size.

Table 5. Operation points assessed under each operation mode for novel CaL TCES configuration.

Operating parameters	Operation mode	
	Energy storage (ESOM)	Energy retrieval (EROM)
Reactor loads		
Calciner load (L_{CL})	1	0 to 1
Carbonator load (L_{CR})	0 to 1	1
Storage/Discharge fractions		
CaO storage fraction ($f_{st,Cao}$)	$f_{dch,CaCO3}$ to 1	0
CaO discharge fraction ($f_{dch,Cao}$)	0 to L_{CR} (being $<f_{st,cao}$)	$(1-L_{CL})$
Carbonated material storage fraction ($f_{st,CaCO3}$)	0	$f_{dch,Cao}$ to 1
Carbonated material discharge fraction ($f_{dch,CaCO3}$)	$(1-L_{CR})$	0 to L_{CL} (being $<f_{st,caco3}$)

The volume required for the storage tanks were lower than 2795 m^3 for the solids (1515 m^3 ST1 and 1280 m^3 ST2) and over 10000 m^3 for CO_2, considering the same storage conditions and storage time (15 hours) as the conventional CaL TCES scheme. The maximum flows leaving the calciner directed to ST2 and ST3 are obtained when calciner operates at nominal load and carbonator is shut down. The carbonated stream stored in ST1 is maximum when carbonator operates at nominal load and solar energy is totally unavailable. The size reduction of the solids storage tanks (ST1 and ST2) is significant. This size is minimized when the carbonator is off in both CaL TCES configurations.

Regarding heat exchangers, the size range has been analyzed under more operating points than the conventional CaL TCES system. The maximum required sizes are identified for the heat exchangers located before and after the storage tanks, which can be found under EROM or ESOM (i.e. the maximum power demanded from ER-CaCO$_3$ heat exchanger is 41.38 MW$_{th}$, achieving (i) under ESOM when the calciner operates at nominal load and the carbonator is shut-down or (ii) under EROM when both reactors operate at nominal load and the carbonated material are directed to ST1 prior to being fed into the calciner). Table 6 shows a summary of the results obtained for the sizing of the novel CaL TCES system.

Table 6. Results summary of the dimensioning of novel CaL TCES configuration.

Main novel CaL TCES configuration results	
Heat exchanger size*	Range (min/max) (MW$_{th}$)
CO_2 heat recovery directed to ST3 (EE-CO2)	0/-24.22
CO_2 preheating before carbonation step (ER-CO2)	-3.10/20.52
CaO heat recovery directed to ST2 (EE-CaO)	0/-20.50
CaO preheating before carbonation step (ER-CaO)	-2.91/18.02
Carbonated solids heat recovery directed to ST2 (EE-CaCO3)	0/-40.55
Carbonated solids preheating before calcination step (ER-CaCO3)	0/41.38
Volume tanks§	Required volume (m^3)
Carbonated material storage tank (ST1)	1515
CaO storage tank (ST2)	1280
CO_2 storage tank (ST3)	10436

* Heat exchangers affected by storage/discharge fractions. Energy demand (-) and energy retrieval (+).
§ Assuming a void fraction of 30% and a storage time of 15 h.

The effect of the solid-solid separation unit (SSU) on the equipment size was quantified in this study. This assessment of the operating maps evidences the reduction of energy consumption and equipment size in the novel CaL TCES scheme. Thus, the inclusion of the SSU could promote energy savings for the CaL TCES system, given the reduction of the storage tanks size due to the non-circulation of unreacted solids between reactors. However, the energy profit provided by the implementation of the SSU and its technical feasibility must be exhaustively assessed. Therefore, a comparison between the conventional and novel CaL TCES configuration was proposed under the same operating conditions in the next study to assess the effect of the carbonated solids separation on the energy requirements and plant sizing. The study must be extended to each pair of possible carbonator/calciner loads between 0 and 1, selecting for the definition of the operation maps those operation points which maximize the storage efficiency for ESOM and the thermal energy available efficiency for EROM. Moreover, the operational behaviour of the heat exchangers named ER must be technically suitable. Regarding the storage conditions of CO_2 and its prior compression-cooling stage, the storage tank size and energy requirement must be minimized, respectively. Finally, the separation of the partially carbonated solids must be experimentally tested to assess the technical feasibility of a fluidized bed classifier to separate the carbonated solids by density difference.

1.3.2.1.   Integration and operating alternatives

The energy and size savings of the total separation of carbonated solids were quantified compared to the conventional CaL TCES system under the same operating conditions. The operation maps of both CaL TCES configurations could illustrate the maximum efficiencies of the CaL TCES system. The **third and fourth contributions** of this PhD Thesis are (i) to quantify the effect of the carbonated solids separation on the energy efficiency and equipment size and (ii) to define the operation maps under both CaL TCES configurations which maximize the energy storage efficiency under ESOM and thermal energy availability efficiency under EROM. Moreover, the operating points selected under each pair of carbonator/calciner loads must meet specific technical, energy, design criteria and equipment load limitations which have been structured into a clear methodology to define the optimized operation maps.

Both CaL TCES configurations (see Figure 2 and Figure 6) share the operating conditions of (i) calciner and carbonator reactors, (ii) storage tanks and CCT and (iii) heat exchangers.

The calciner size is set at 100 MW$_{th}$ under nominal conditions (Q_{CL}), operating at 950 ºC in a pure CO_2 atmospheric pressure [113]. The carbonation reaction occurs at 850 ºC and a CO_2 concentration of 100%$_v$ at 1.2 bar to enhance solids circulation between reactors [102].

The average sorbent activity was computed by the carbonator model defined by Grasa et al. under carbon capture terms (650 ºC and CO_2 concentration of 10-15%$_v$) [110]. The reactive particles age distribution within carbonator was also defined under a conservative situation when solid material conveys directly between reactors [111]. The carbonator kinetic model parameters were set to 0.52 for the deactivation constant and 7.5% for residual conversion [110]. The constant CaO/CO_2 molar ratio (R) entering the carbonator was established at 4.26 for both CaL TCES configurations: conventional (Figure 2) and novel (Figure 6). As a result, the average sorbent activity was 20.4% and 22.6%, assuming a CaO purge of 3.09% and 4% for conventional and novel

configuration, respectively. The carbonator nominal power (Q_{CR}) reached 69 and 88.33 MW$_{th}$ for conventional and novel CaL TCES scheme, respectively.

The solids storage conditions (ST1 and ST2 in Figure 2 and Figure 6) were set at 200 ºC under atmospheric pressure, a temperature within the range proposed in the literature from ambient to 200-700 ºC [114]. The ST3 stored CO_2 at 35 ºC and 75 ºC, after being compressed and cooled (CCT) in four interleaved stages with a pressure ratio of 3 under each compression stage to limit energy demand. When CO_2 must be discharged from ST3, the discharging expansion (DE) composed by an expansion valve and a heat exchanger which reduces the temperature and pressure of the gas to ambient and carbonator pressure conditions (1.2 bar), respectively.

Regarding heat exchangers, those named EE were able to release thermal energy comprising a 2% of heat losses. Among the heat exchangers named ER, ER-CaCO3 always demanded thermal energy and the rest required or provided thermal energy. Both configurations were simulated with Engineering Equation Solver (EES) software [104], extracting CO_2 properties from EES internal data and solid substances (lime [115] and limestone [116]) properties from external data sources.
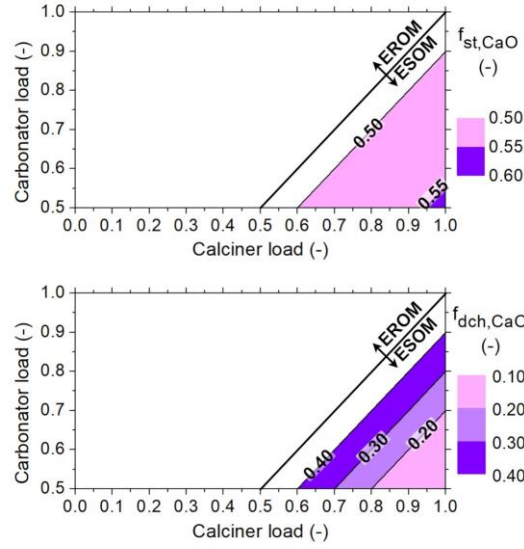
The operation maps under both CaL TCES configurations are defined by the storage and discharge fractions for each pair of calciner/carbonator load which provide the highest efficiency and fulfil the technical criteria. The criteria for operating point selection were described within the research paper *"Operation maps in Calcium Looping thermochemical energy storage for concentrating solar power plants"* 2022, Journal of Energy Storage, 55, 105771 [117]. Table 7 shows the operating points assessed under both CaL TCES configurations.

Table 7. Operation points assessed under each operation mode for conventional and novel CaL TCES configurations.

| Operating parameters	Operation mode	
	Energy storage (ESOM)	Energy retrieval (EROM)
Reactor loads		
Calciner load (L_{CL})	0 to 1	0 to <L_{CR}
Carbonator load (L_{CR})	0 to <L_{CL}	0 to 1
Storage/Discharge fractions		
CaO storage fraction ($f_{st,CaO}$)	$f_{dch,CaCO3}$ to L_{CL}	0
CaO discharge fraction ($f_{dch,CaO}$)	0 to L_{CR} (being <$f_{st,CaO}$)	(L_{CR}-L_{CL})
Carbonated material storage fraction ($f_{st,CaCO3}$)	0	$f_{dch,CaO}$ to L_{CR}
Carbonated material discharge fraction ($f_{dch,CaCO3}$)	(L_{CL}-L_{CR})	0 to L_{CL} (being <$f_{st,CaCO3}$)

Under ESOM, the storage fraction of carbonated material was assumed zero ($f_{st,CaCO3} = 0$) and the discharge fraction from ST1 counterbalance the load difference between calciner and carbonator reactors ($f_{dch,CaCO3} = L_{CL} - L_{CR}$).

The ESOM operating map (see Figure 7) defined by CaO storage and discharge fractions ($f_{st,CaO}, f_{dch,CaO}$) must comprise the operating points which (i) maximize the energy storage efficiency, (ii) keep the ER heat exchangers always demanding thermal energy, (iii) ensure a continuous flow of recoverable energy, limiting the minimum load of 50% to EE-CO2, EE-CaO and carbonator and (iv) minimize the thermal energy consumption, limiting the maximum load of 50% to ER-CaCO3.

Figure 7. Operation maps under ESOM for both CaL TCES configurations: conventional and novel.

The maximum storage efficiency map ($\eta_{st,max}$) and the stored power under each CaL TCES configuration are illustrated in Figure 8. Under both CaL TCES configurations, conventional (SC1) and novel (SC2), the lowest values within the maximum storage efficiency map are reached when the difference between the loads of both reactors is minimal. Under both CaL TCES configurations, the pair of carbonator/calciner loads of 0.5/0.6 is the least efficient within the maximum storage efficiency map, reaching an efficiency of 48% for SC1 and a 64% for SC2 within the storage stage.
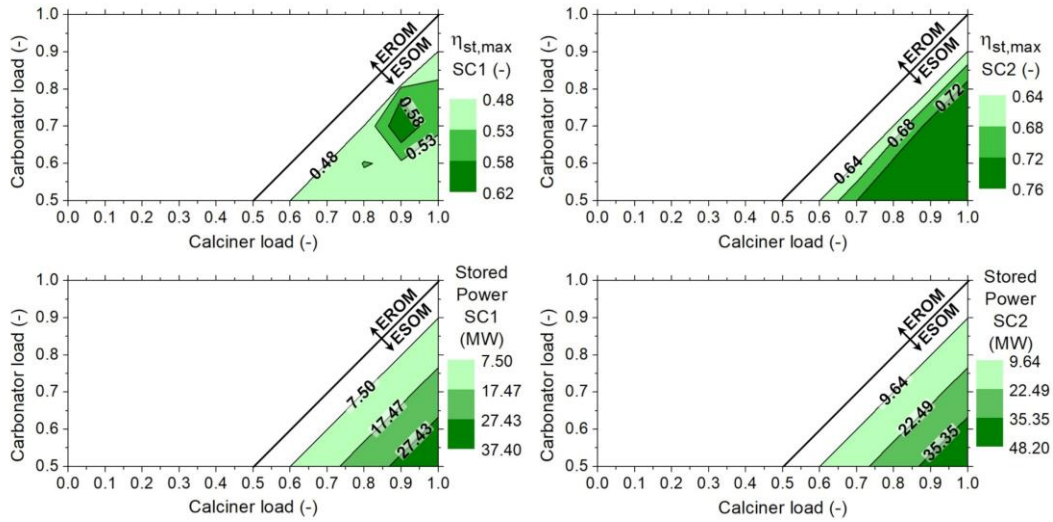
Figure 8. Maximum energy storage efficiency under ESOM for conventional (SC1) and novel (SC2) CaL TCES configurations.

The energy storage efficiency under novel configuration (SC2 in Figure 8) is greater than in conventional configuration (SC1 in Figure 8). The maximum energy storage efficiency under SC2 (76%) is reached when calciner operates at nominal load and carbonator load is 0.7. A maximum energy storage efficiency of 62% is achieved for SC1, being the pair of carbonator/calciner loads

0.8/1. The energy consumption is lower when total carbonated solid separation is considered, given the removal of preheating requirements of unreacted/inert material before calcination. Moreover, the energy that can be potentially stored increases under novel configuration (SC2). The recirculation of unreacted material into the carbonator reduces energy requirements of inert solids preheating prior calcination step, being able to calcinate 20% more limestone under SC2.

Under EROM, the CaO storage fraction was assumed zero ($f_{st,CaO} = 0$) and the discharge fraction from ST2 counterbalances the load difference between carbonator and calciner reactors ($f_{dch,CaO} = L_{CR} - L_{CL}$).

The EROM operating map (see Figure 9) defined by storage and discharge fractions of carbonated material ($f_{st,CaCO3}, f_{dch,CaCO3}$) includes those operating points which (i) maximize the thermal energy availability efficiency, (ii) keep the ER heat exchangers always demanding thermal energy, (iii) ensure a continuous flow of recoverable energy, limiting the minimum load of 50% to EE-CaCO3, and carbonator and (iv) minimize the thermal energy consumption, limiting the maximum load of 50% to ER-CaCO3.
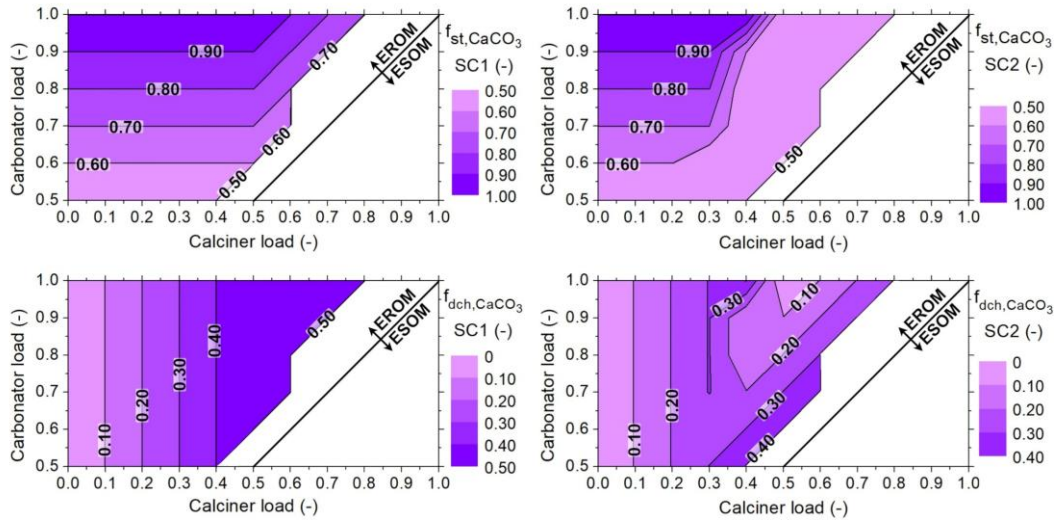
Figure 9. Operation maps under EROM for conventional (SC1) and novel (SC2) CaL TCES configurations.

The map of maximum energy retrieval efficiencies ($\eta_{av,max}$) and the retrieved power from storage under each CaL TCES configuration are illustrated in Figure 10. Higher thermal energy availability efficiency is reached when the amount of retrieved energy is diminished under the novel CaL TCES configuration (SC2). The lower circulation of solids through the ER-CaO heat exchanger implies lower energy requirements to preheat this stream. The highest values within the maximum energy retrieval efficiency map are reached when the difference between the calciner/carbonator is minimal. A maximum thermal energy availability efficiency of 86% and 91% are reached for a pair of carbonator/calciner loads of 0.7/0.6, under SC1 and SC2 respectively.

Under both CaL TCES configurations, the maximum thermal energy availability is reduced for lower calciner and higher carbonator loads (see Figure 10). The lowest maximum energy retrieval efficiencies are found when calciner is shut down under both CaL TCES configurations, being 56% for SC1 and 68% for SC2. Since solar resource is unavailable, the carbonator thermal energy demand is supplied by stored energy from storage tanks ST2 and ST3 (see Figure 2 and Figure 6).
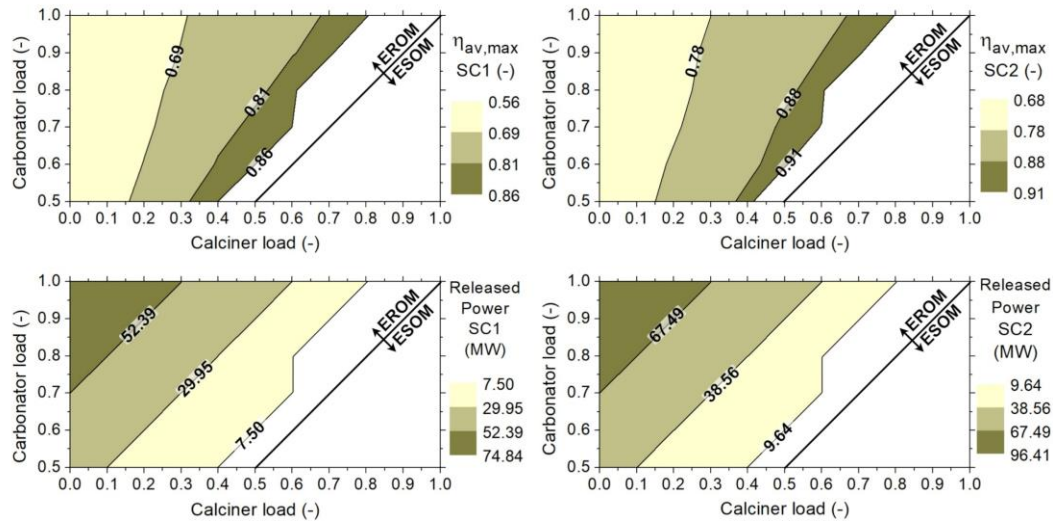
Figure 10. Maximum energy storage efficiency under EROM for conventional (SC1) and novel (SC2) CaL TCES configurations.

Regarding heat exchangers size, the CO_2 storage line showed an increase of 15% from conventional to novel CaL TCES configuration. The CO_2 stream after calcination step is higher under novel CaL TCES configuration, given the increase amount of calcined material. The total separation of carbonated solids could reduce down to 53% the heat exchangers from carbonated solids storage line and to 74% the equipment related to CaO storage line. The effect of the SSU was clearly reflected in the size of the equipment affected by solid streams. Table 8 collects the range size of the main equipment situated between the storage tanks and the reactors and the efficiencies under both CaL TCES configurations.

Table 8. Results summary of the effect of carbonated solids separation after carbonation step.

Main results of conventional and novel CaL TCES configuration	CaL TCES configuration	
	Conventional	Novel
Heat exchanger size*	Range (min/max) (MW$_{th}$)	
CO_2 heat recovery directed to ST3 (EE-CO2)	0/-21.14	0/-24.33
CO_2 preheating before carbonation step (ER-CO2)	0.33/19.52	0.38/22.46
CaO heat recovery directed to ST2 (EE-CaO)	0/-78.88	0/-20.50
CaO preheating before carbonation step (ER-CaO)	0.22/69.32	0.06/18.01
Carbonated solids heat recovery directed to ST2 (EE-CaCO3)	0/-85.86	0/-40.51
Carbonated solids preheating before calcination step (ER-CaCO3)	0/43.81	0/20.67
Efficiencies§	Range (min/max) (%)	
Energy storage (η_{st})	48/62	64/76
Thermal energy availability (η_{av})	56/86	67/91

* Heat exchangers affected by storage/discharge fractions. Energy demand (-) and energy retrieval (+).
§ Minimum carbonator partial load of 50%.

The present PhD Thesis has shed light on the threshold values of the equipment size and the energy savings that could be achieved. Under both CaL TCES configurations, operating maps were defined, maximizing the system efficiency. The energy saving is possible with the reduction of the circulation of unreacted solids between reactors. After analyzing the favourable energy

results, an experimental campaign was performed (i) to assess the technical feasibility of carbonated solids separation based on density differences and (ii) to validate the carbonator model simulation.

1.3.2.2. Technical feasibility of carbonated solids separation

The promising results obtained from the CaL TCES simulations under both configurations (conventional and novel) promoted an experimental analysis to validate the model results. Thus, the **fifth contribution** of this PhD Thesis under the experimental campaign is (i) to determine the experimental carbonation degree under CaL TCES conditions and (ii) to assess the technical feasibility of carbonated solids separation by density difference. The sorbent deactivation with carbonation/calcination cycles has been thoroughly tested under carbon capture conditions. However, the experimental CaO deactivation under CaL as TCES has been scarcely studied in literature. Moreover, the effect of the sorbent conversion on the particle density distribution and the minimum fluidization velocity of carbonated and calcined material were investigated. A novel and suitably adjusted carbonation degree characterization was developed in relation with the particle bulk density for large-scale CaL TCES systems. The promising positive effect of the total separation of carbonated solids on the energy efficiency and size of the CaL TCES system promoted the experimental assessment of the technical feasibility of the SSU. A correlation analysis between the particle density and the minimum fluidization velocity of carbonated and calcined material was performed to validate the separation by density difference on the solid-solid classifier.

Sorbent degradation assessment under solar calcination conditions

The carbonation degree was determined under carbonation and calcination conditions assumed in the CaL TCES simulation scheme (see Figure 2 and Figure 6). Three experimental tests were performed using two lab-scale facilities: electrically heated fluidized bed (EHFB) [118] and directly irradiated fluidized bed (DIFB) [62]. The description of both facilities was presented in the international conference paper *"Improvement of performance of fluidized bed Calcium Looping for thermochemical solar energy storage: Modelling and experiments"* 2021, proceedings of 10th European Combustion Meeting [119]. The solid inventory of two of the experimental tests was a mixture of limestone and sand, taking place in each FB reactor. The third experimental test was performed in the EHFB using only limestone as inventory. The main difference between the lab-scale reactors is the energy supply mode during calcination step. The EHFB receives thermal energy during calcination reaction without solar flux effect. The DIFB simulates a solar radiation to cover the energy demand at calcination step. The effect of the solar radiation on the sorbent conversion was assessed during the first 20 carbonation/calcination cycles. The materials, experimental conditions and procedure and data characterization appear in the research paper *"Solar-driven Calcium Looping in fluidized beds for thermochemical energy storage"* 2023, Chemical Engineering Journal, 466, 142708 [120]. The experimental carbonation degree was computed by the Equation (7), including the weight change between carbonated (m^{carb}) and calcined (m^{calc}) material after each reaction step for each cycle (*N*). The CaO content (x_{CaO}) in the calcined natural Italian limestone selected for the experimental test is 97.4%. MW in the Equation (7) stands for molecular weight.

$$X_N = \frac{(m_N^{carb} - m_{N-1}^{calc})}{m_{N-1}^{calc} x_{CaO}} \frac{MW_{CaO}}{MW_{CO_2}} \tag{7}$$

The experimental data for carbonation degree computed by Equation (7) under the three tests were adjusted according to a deactivation model based on initial activity decay (IAD), applying Equation (8).

$$X_N = X_1 N^{-k} \tag{8}$$

The parameters used for the sorbent deactivation model (IAD) were the initial activity constant (X_1) and the decay constant (k). The best fitting values for the three carbonation degree experimental tests are presented in Table 9.

Table 9. Best fitting parameters for the IAD model.

IAD sorbent deactivation model parameters	X_1 (-)	k (-)
Limestone and sand inventory		
Directly irradiated fluidized bed (DIFB)	0.61	1.02
Electrically heated fluidized bed (EHFB)	0.60	0.658
Limestone inventory		
Electrically heated fluidized bed (EHFB)	0.62	0.435

The fitting curves of the obtained experimental carbonation degree data under each of the 20 analyzed cycles is illustrated in Figure 11.
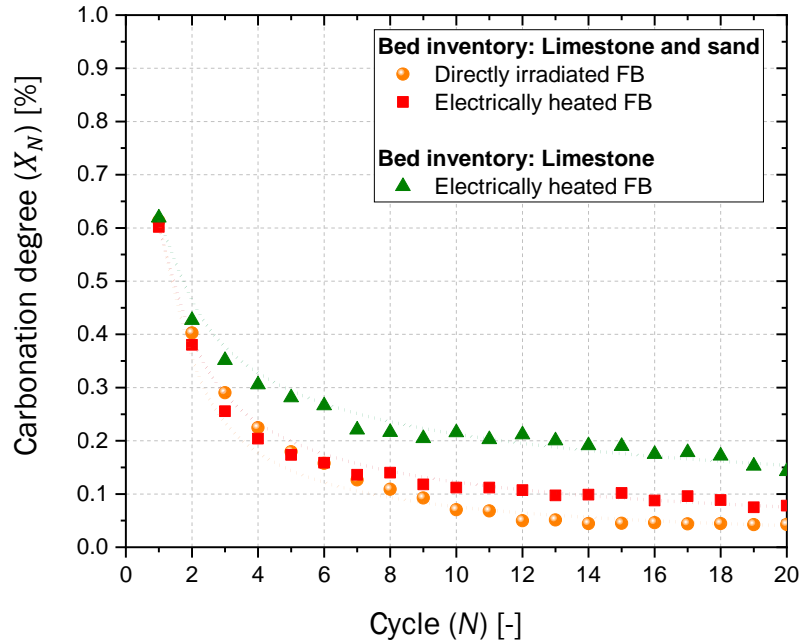
**Figure 11.** Fitting of experimental carbonation degree data.

The CaO average conversion achieves the 14% and 16% for DIFB and EHFB using sand and limestone as bed inventory, respectively. The EHFB experimental test with only limestone reaches the 25% of sorbent average conversion during the 20 calcination/carbonation cycles.

The CaO activity decays more sharply when limestone and sand are mixed in the bed inventory. A mechanochemical interaction between sand and lime could be the cause during the fluidization, forming calcium silicates, also observed by Valverde et al. [121]. The limestone inventory suffers a sintering resistance of 34% and 57% higher than the inventory composed by sand and limestone (EHFB and DIFB, respectively). Thus, the carbonator modelling must be governed by the sorbent deactivation model with parameters related to the limestone inventory.

Relationship between carbonation degree and bulk density

Besides the carbonation degree measurement by weight change between calcined/carbonated material from experimental data characterization, the relationship between bulk density and conversion decay was investigated. These results were used to define a new equation which allows the estimation of the conversion decay from bulk density. The bulk density of carbonated and calcined material was measured after each reaction step performed in the EHFB facility, comprising both bed inventories: (i) limestone and (ii) limestone and sand.

The bulk density of carbonated material under limestone bed inventory decays with the number of cycles upon loss of sorbent activity, keeping the density of carbonated particles practically constant after a first increase due to loss of porosity (see Figure 12). However, the bulk density when the bed inventory includes sand, increases for calcined material and keeps constant for carbonated particles. Once again, the physical interaction of sand with carbonated and calcined particles is corroborated, reducing its porosity and increasing its density as shown in Figure 12.
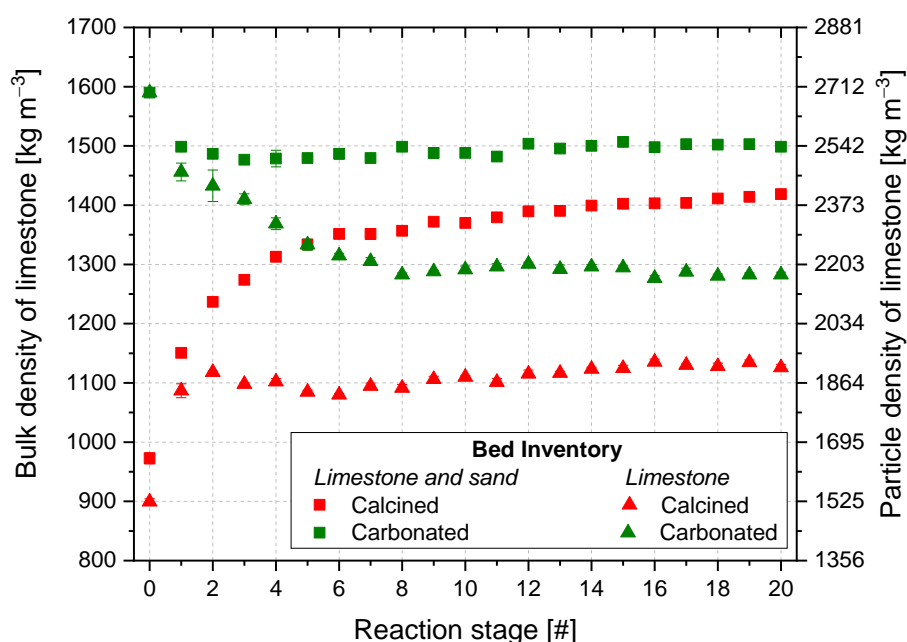

Figure 12. Bulk and particle density of carbonated and calcined material under both bed inventories.

A novel correlation between the sorbent conversion and the bulk density was developed and shown in Equation (9), given the influence shown of the carbonation degree on the particle density throughout the 20 cycles analyzed.

$$X_N = \left(\frac{\rho_N^{carb} V_N^{carb} - \rho_{N-1}^{calc} V_{N-1}^{calc}}{\rho_{N-1}^{calc} V_{N-1}^{calc}} \right) \frac{\mathrm{MW}_{CaO}}{x_{CaO} \mathrm{MW}_{CO_2}} \approx \left(\frac{\rho_N^{carb}}{\rho_{N-1}^{calc}} - 1 \right) \frac{\mathrm{MW}_{CaO}}{x_{CaO} \mathrm{MW}_{CO_2}} \qquad (9)$$

Thus, the experimental carbonation degree data can be quantified through the bulk density of carbonated (ρ^{carb}) and calcined (ρ^{calc}) material, assuming zero change in volume occupied by the bed of carbonated (V^{carb}) and calcined (V^{calc}) material.

Figure 13 illustrates the adequate/suitable approximation of the calculation of the CaO conversion, applying both data characterization methods: weight change method (dots) and bulk density (line).
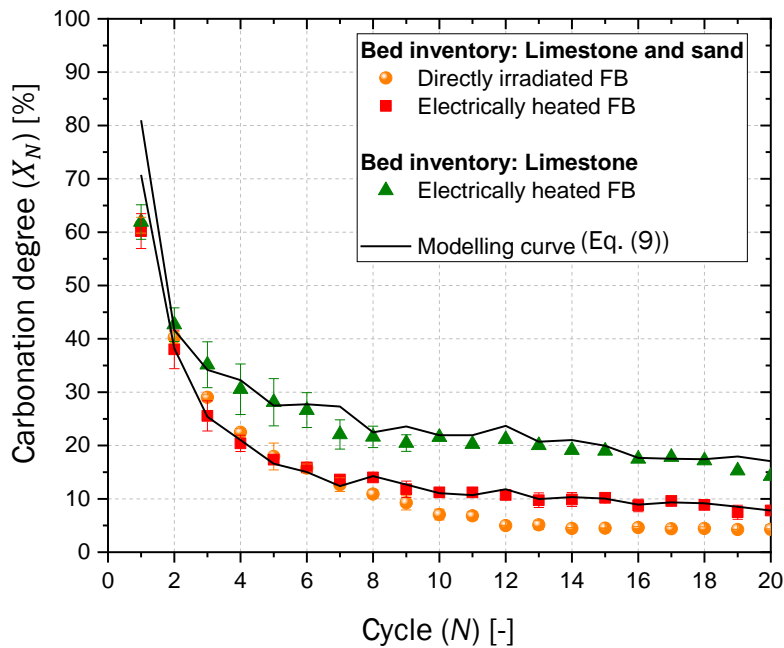
Figure 13. Experimental carbonation degree data determined by weight change and bulk density.

The measurement of the carbonation degree by means of the bulk density represents a new alternative to be applied even in large-scale CaL TCES plants, simply requiring sampling the bed before and after each carbonation stage and measuring its density.

Relationship between particle density and minimum fluidization velocity

In order to assess the technical feasibility of carbonated particles separation, the minimum fluidization velocity of carbonated and calcined particles was experimentally determined, measuring the pressure drop vs. the superficial gas velocity.

Figure 14 shows the experimental minimum fluidization velocity of carbonated and calcined particles computed by analysing the curves of pressure drop vs. superficial CO_2 velocity for a bed

inventory of limestone. The minimum fluidization velocity of calcined particles hardly shows any variation during the 20 cycles analyzed, increasing by less than 8%. The greatest difference in minimum fluidization velocity between the initial and final cycle is found within the carbonated particles, decreasing a 20%. Thus, the difference of minimum fluidization velocity between calcined and carbonated particles is wider for more reactive particles than less reactive ones. This difference ranges from 3.7 m/s for fresh material to 1.5 m/s for highly-cycled material.
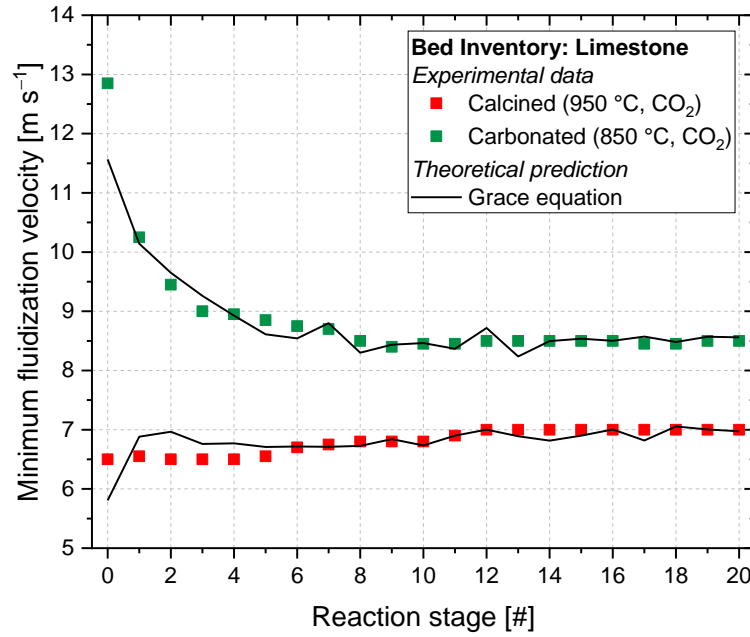
Figure 14. Experimental minimum fluidization velocity for carbonated and calcined particles.

Experimental measurements of particle size and density of carbonated and calcined particles were essential to determine the theoretical curve of the minimum fluidization velocity (Grace equation [122]). The particle size was defined by the Sauter diameter, post-processing particle size distribution data obtained after each carbonation and calcination cycle. The particle density (see Figure 12) for carbonated (ρ_p^{carb}) and calcined (ρ_p^{calc}) material was quantified through their respective bulk densities by Equation (10), assuming a typical constant bed voidage for packed bed of 0.41 for both calcined (ε_{bed}^{calc}) and carbonated (ε_{bed}^{carb}) material.

$$\rho_{pN}^{calc} = \frac{\rho_N^{calc}}{1 - \varepsilon_{bedN}^{calc}}\,; \qquad\qquad \rho_{pN}^{carb} = \frac{\rho_N^{carb}}{1 - \varepsilon_{bedN}^{carb}} \tag{10}$$

A satisfactory/suitable adjustment of the Grace curve based on semi-empirical correlations was illustrated in Figure 14. The influence of the particle density on the minimum fluidization velocity of both carbonated and calcined material was satisfactorily evidenced.

As expected, the experimental minimum fluidization velocity follows the same trend as the particle density defined by Equation (10), both for carbonated and calcined particles comprising only limestone as bed inventory. Thus, the carbonated material after carbonation step could be separated by density difference in a solid-solid fluidized bed classifier [123].

Table 10 shows the main results provided by the experimental tests related to carbonation degree, particle density and minimum fluidization velocity for carbonated and calcined material of the CaL process as TCES system.

Table 10. Summary results from experimental campaign of the CaL as TCES.

Main results from experimental test of the CaL as TCES system		
Carbonation sorption activity (%)	$1^{st}/20^{th}$ cycle	Average
DIFB (limestone+ sand)	61/4	14
EHFB (limestone + sand)	60/8	16
EHFB (limestone)	62/14	25
Particle density* (kg/m³)	$1^{st}/20^{th}$ cycle	Difference
Calcined particles	1847/1906	59 (+3%)
Carbonated particles	2474/2186	288 (-12%)
Minimum fluidization velocity* (m/s)	$1^{st}/20^{th}$ cycle	Difference
Calcined particles	6.5/7	0.5 (+7%)
Carbonated particles	10.2/8.5	1.7 (-17%)

*Bed inventory only limestone.

The experimental campaign carried out to determine the carbonation degree was achieved under the conditions of the CaL process as TCES at a laboratory scale. Moreover, the facilities implemented to perform the test (DIFB and EHFB) allow to evaluate operating conditions resembling real situation. Most of existing research has developed the sorbent deactivation models from experimental data obtained by thermogravimetric analysis [56,60,124], where operating conditions are more controlled than in FB. Thus, the experimental sorbent activity obtained for the limestone bed approximates the conversion expected under a large-scale operation.

The second test measured bulk density of carbonated and calcined particles. It served to generate a new characterization model for the carbonation degree, as well as to satisfactorily correlate the physical properties of granular solids with the minimum fluidization velocity. Additionally, the physical interaction between sand and limestone was verified, negatively penalizing the sorbent activity by reducing its porosity.

The last experimental procedure carried out related to carbonated solids separation confirms the potential partial separation of more and less carbonated particles. The partial separation could be achieved by particle density differences in a fluidized bed classifier [123]. The particle density and the minimum fluidization velocity could be the characteristic parameters used to monitor and control the operation of the solid-solid classifier based on density difference to partially separate the particles after carbonation step.
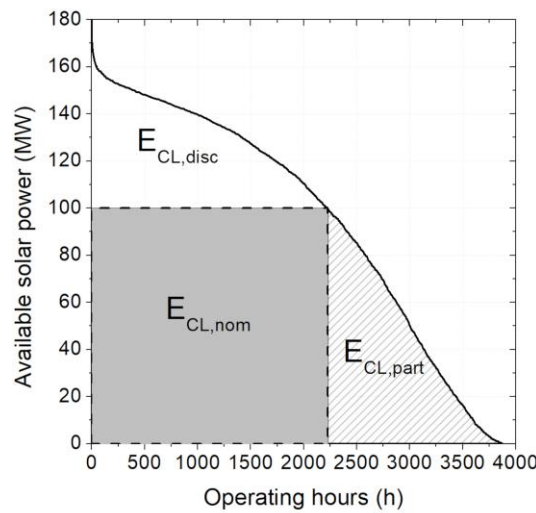
The experimental results of sorbent deactivation under TCES were applied to the next PhD Thesis step through the implementation of a new carbonation model based on experimental carbonation degree to the simulation of the novel CaL TCES configuration. An operational methodology to maximize the economic profit of the novel CaL TCES scheme must be defined. This methodology could be based on the optimized operation maps which maximize the energy savings and reduces the equipment plant size. The maximum economic profit of the CaL TCES could be assessed considering an ideal total separation of carbonated solids.

1.3.3. Operational methodology and economic implications

The operation of the novel configuration of the CaL TCES system with total carbonated solid separation is economically assessed in this section. The real operation of a CaL TCES with solid separation could only lead to a partial separation of carbonated solids as confirmed with experimental test results. Thus, the income for the CSP plant with complete separation of solids could represent the maximum possible revenue under an ideal scenario. The effect of the seasonal variability of solar resource and electricity prices could be accounted to assess the most profitable operation of a CSP plant with a CaL TCES. The **final contribution** of the present PhD Thesis is focused on the definition of a methodology to define the operation pattern which maximizes the daily incomes and CaL TCES system efficiency for any daily solar radiation and electrical prices.

The novel CaL TCES configuration (see Figure 6) was selected to apply the methodology developed during the last stage of this PhD Thesis. The operational conditions (temperature and pressure) of reactors, storage tanks and heat exchangers are described in section *Integration and operating alternatives*. The reactor sizes were defined by (i) maximizing the solar calciner power in a certain location and (ii) applying a carbonator model adjusted to the sorbent activity experimental data obtained during carbonation. The calciner size was computed by the direct normal irradiation (DNI) of the location which was selected, assuming (i) a heliostats area of 290482 m^2 and (ii) annual optical and thermal efficiencies of 64.7% and 92.8%, respectively [125]. Figure 15 shows the Load Duration Curve, representing the number of operating hours per year in which a specific solar power is available. The maximization of the solar thermal energy input (grey area in Figure 15) provides the optimal calciner size in a formal way, resulting 100 MW$_{th}$. Thus, the grey area ($E_{CL,nom}$) is the solar thermal energy supplied at nominal load, whereas the stripped area represents the solar thermal energy supplied to the calciner at partial load ($E_{CL,part}$). The surplus solar resource above the calciner nominal load is discarded ($E_{CL,disc}$).

Figure 15. Load Duration Curve for calciner optimal size assessment.

The experimental sorbent deactivation considered was based on the results obtained for limestone and sand inventory using the EHFB facility. These preliminary experimental results were

reported in a conference paper [119] prior to the final results shown in section *Technical feasibility of carbonated solids separation*. The experimental carbonation degree obtained under the EHFB conditions was tuned adjusting to the kinetic model developed by Valverde et al. [126,127] for CaL as TCES. The reactive particles age distribution for carbonation was also defined under the conservative situation of direct circulation between reactors [111]. The carbonator model parameters were set to 1.10 for the deactivation constant and 6% for residual conversion. The constant CaO/CO_2 molar ratio (R) entering the carbonator was established at 7.28. The assumed value for R ensures a carbon capture efficiency of 90% in carbonator reactor. As a result, the average sorbent activity was 13.21%, assuming a CaO purge of 4% and reaching a carbonator nominal power (Q_{CR}) of 88 MW$_{th}$. A detailed description of the reactor sizes definition appears in the research paper *"Optimized Ca-looping thermochemical energy storage under dynamic operation for concentrated solar power"* 2023, Journal of Energy Storage, accepted for publication.

The defined methodology has a wide application, being able to manage inputs from any location and electricity price market. A specific case study was analysed to apply the defined methodology in order to obtain quantitative results under a specific availability of solar resource and energy demand. The variable inputs included in the CaL TCES operational methodology were: (i) the solar resource variability in a selected location and (ii) the electricity price governed by the country in which the location is situated. A location within the Spanish province of Seville (37.443ºN, 6.25ºW) was selected to extract the daily solar resource input from the Photovoltaic Geographical Information System (PVGIS) tool of EC [128]. The electricity price (EP) was gathered from the Spanish electrical grid [129] during a standard year without accounting for the effect of international situations (i.e. war, pandemic). Eight representative days were selected within a year to validate the developed operating methodology, comprising maximum and minimum of DNI and EP within each season of a year.

The target variable is the daily income calculated as the sum of the 24th hourly incomes per day. The hourly income is defined as the product of the electric energy retrieval and the EP, assuming a thermal to electrical performance relative to the steam Rankine power block (35.55%) [99]. The energy retrieval comes from the carbonator (Q_{CR}) or the energy released by EE heat exchangers and carbonator (Q_{AV}). Thus, the income accounts for the electricity production from the energy recovered from the carbonator only (In_{CR}) or from the combined energy available in the system of the EE heat exchangers and the carbonator (In_{AV}). Moreover, two main operation constraints were imposed: (i) the daily stored energy must be preserved and (ii) the operation maps within each operation mode must be used to choose the operation point. The energy stored at the end of the day corresponds to the available energy in the storage tank at the beginning of the day. The full energy storage mode is contemplated, when the calciner is operated and carbonator is shut down. Even so, the operating points must keep the ER heat exchangers always demanding thermal energy and whenever possible ensure a continuous flow of recoverable energy with minimal consumption, limiting to 50% (i) the minimum load of EE-CO2, EE-CaO, EE-CaCO3 and carbonator and (ii) the maximum load of ER-CaCO3. Moreover, the operating point under each calciner/carbonator load must maximize the energy storage for ESOM and the thermal energy availability for EROM.

The objective of developing this methodology is to maximize the daily income per representative day as target variable. A genetic method included in the EES software [130] and developed by the National Center for Atmospheric Research (NCAR) [131] was applied to maximize the target variable. The genetic method algorithm requires (i) independent input variables and (ii) three internal parameters to identify the optimal value for the variable to be maximized (number of individuals, number of generations and the maximum mutation rate). The carbonator loads for

each hour per day are the independent variables, setting the lower and the upper threshold to 0 and 1, respectively. The maximum values were assigned for each internal parameters (individuals: 250, generations: 2048 and maximum mutation rate: 0.7), achieving greater robustness in the calculations. The optimal solution for the maximization of the daily income (target variable) was found when calculations finished. The results extracted from the operational methodology were daily profiles of (i) the energy retrieval based on EP, (ii) the CO_2, CaO and partially carbonated solids stored and (iii) the operating pattern. Table 11 shows the main results from the operational method based on the daily variability of the solar resource and EP.

Table 11. Summary results from applying operational methodology to novel CaL TCES configuration.

Main operational method results		
Energy retrieval vs EP*	Average DNI	EP profile
Minor carbonator outages	Medium-High	Pronounced peaks
Carbonator operates from sunrise to end day	High	Uniform
Production concentration start and end day	Medium- high	Pronounced peaks
Production concentration end day	Low	Pronounced peaks
Volume tanks§	Required volume (m³)	
Carbonated material storage tank (ST1)	651.34	
CaO storage tank (ST2)	596.36	
CO_2 storage tank (ST3)	2232.23	
Operating pattern	Average DNI	EP profile
Major operation under ESOM	High	Uniform
Major operation under full ESOM	Low	Pronounced peaks
Major operation under EROM	Low	Pronounced peaks (end day)

* Comprising minimum carbonator partial load 0 or greater than 50%.
§ Assuming a void fraction of 30% and densities for CO_2 ($\rho_{CO2\,(35°C,75bar)}$ = 273.71 kg CO_2/m³ [117], CaO and $CaCO_3$ ($\rho_{p,CaO}$ = 1793 kg CaO/m³ and $\rho_{p,CaCO3}$ = 2930 kg $CaCO_3$/m³ [119]).
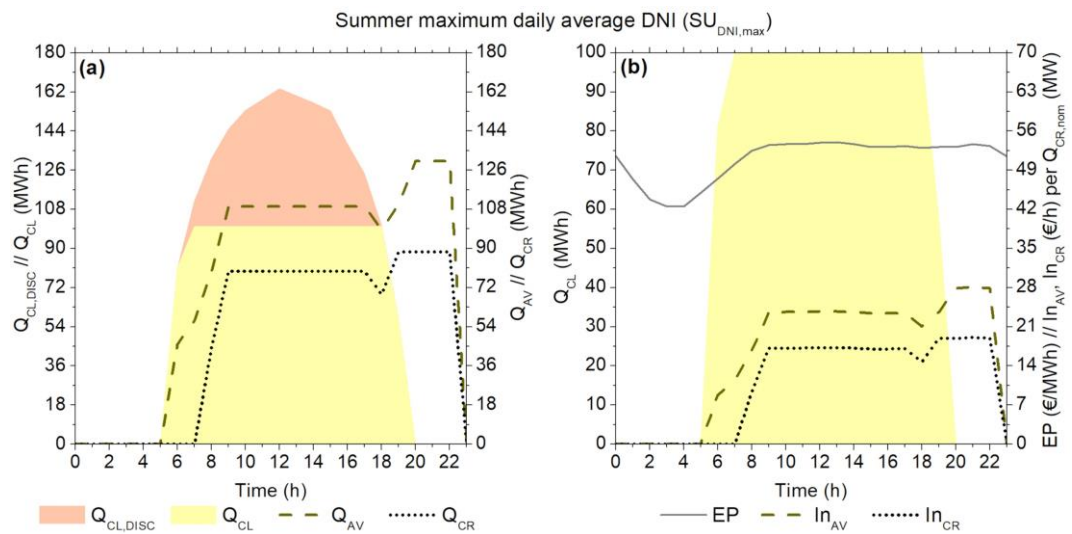

Figure 16. Energy retrieval (a) and incomes (b) obtained under high DNI and uniform EP profile.
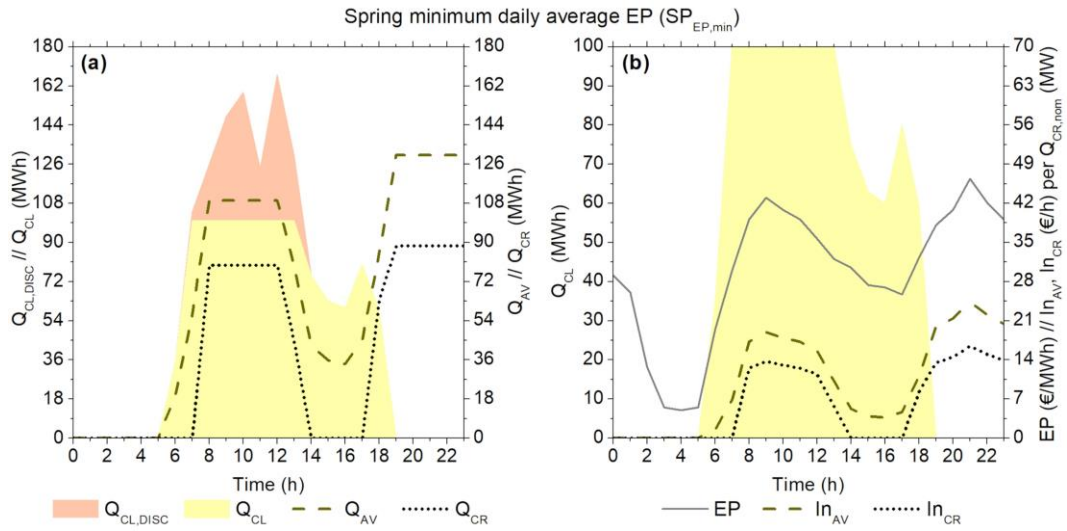
Figure 17. Energy retrieval (a) and incomes (b) obtained under medium DNI and sharp EP profile.

The energy retrieval matches with hours of maximum EP to obtain the maximum income. The higher the number of hours with available solar resource and uniform EP profile (Figure 16), fewer outages in energy recovery from the carbonator. When EP profile is sharp (Figure 17), the energy retrieval is concentrated in the hours with highest EP, usually during early morning and/or at the end of the day. The energy retrieval is only from EE-CaO, EE-CaO-P and EE-CO2 (see Figure 6) when the novel CaL TCES scheme operates within full ESOM. Thus, the energy retrieval can be continuous from sunrise to the end of the day when carbonator operates within the highest EP hours per day.
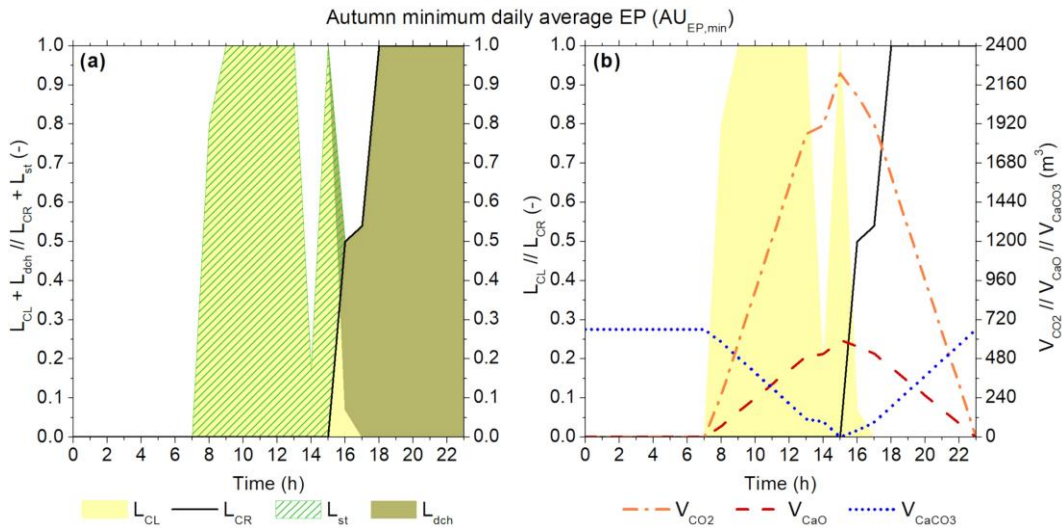

Figure 18. Energy storage/discharge (a) and stored volume profiles (b) under representative day reporting required storage tanks size.

The maximum energy stored per day indicates the required size for the storage tanks (Figure 18). The maximum volume stored for gas and solids within the assessed representative days takes place during a day with sharp EP profile and average solar resource. The inclusion of

the SSU leads a size reduction between 13% and 45.5% for solids storage tanks ST1 (carbonated material) and ST2 (CaO), respectively, comparing with data found in literature [98].

The higher solar resource availability, the greater number of operating hours of the CaL TCES system under ESOM (Figure 19). When the highest EP are concentrated from the second half of the day, the CaL TCES system operates under full ESOM from the beginning of the day until carbonator starts the operation (Figure 19). Under EROM, the maximum thermal energy availability occurs when the difference between carbonator and calciner load is minimum. The obtained daily operating pattern which maximize the daily income (see Figure 19) only included a limited number of operation points which correspond to threshold points within the defined operation map. Most of carbonator/calciner loads combinations are not included in the optimized daily pattern of operation points. Most of those situations considered in the optimized pattern correspond to (i) full storage operation mode and (ii) full retrieval operation mode without availability of solar energy.
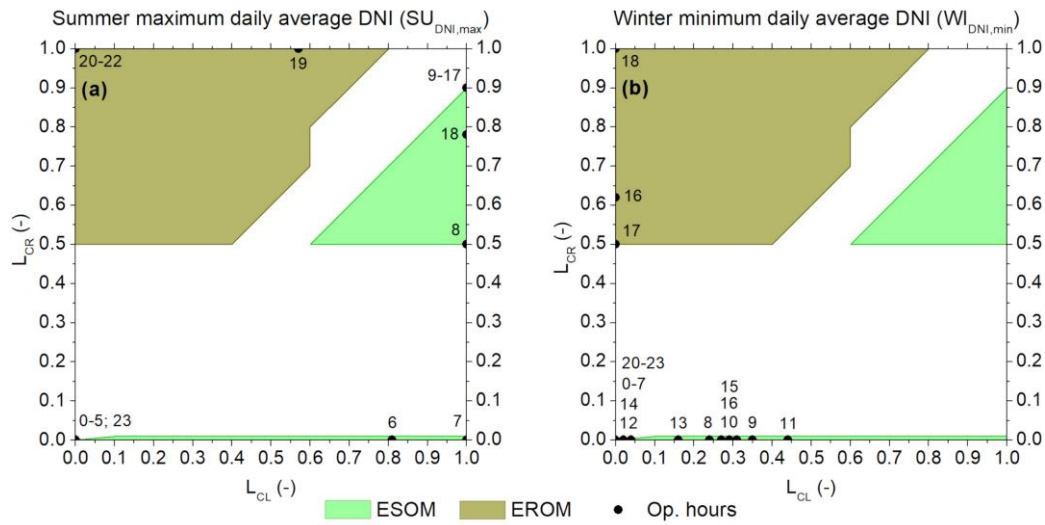
Figure 19. Operating pattern under high DNI (a) and EP pronounced peaks at the end of day (b).

The final stage of the present PhD Thesis points out the importance of assessing the dynamic operation of a CaL TCES system under transient state. A methodology based on the hourly, daily and seasonally variability of the solar resource and the electricity prices has been defined. The energy retrieval from the CaL TCES system takes places maximizing the daily income to be economically profitable. Moreover, the CaL TCES system operates maximizing the energy savings and minimizing the size of the plant equipment, providing the operating range of the heat exchanger network through the resulting operating pattern. The methodology applied to define the operation pattern of the novel CaL TCES configuration leads to the maximum economic profit reachable. The real CaL TCES configuration with a partial separation of carbonated solids could achieve lower incomes than the results presented for the complete separation of carbonated solids. However, higher energy efficiency and smaller plant size than the conventional configuration could be guaranteed.

Future work should address the real operation of CaL TCES system with partial separation. A partial separation degree between more and less carbonated material from carbonator should be computed and a carbonator kinetic model could be developed, comprising the experimental results obtained under the CaL conditions as TCES.

2. Published papers

The international conference and JCR journal papers published during the present PhD Thesis which are included in the compendium of publications of this PhD Thesis manuscript are presented in this section.

The first published JCR journal paper is included in the section *Energy assessment in Calcium Looping based thermochemical energy storage* within the present manuscript.

- Bailera M, Pascual S, Lisbona P, Romeo LM. *Modelling Calcium Looping at industrial scale for energy storage in concentrating solar power plants*. Energy (2021), 225, 120306.
https://doi.org/10.1016/j.energy.2021.120306

The following four publications are incorporated in the section *Novel Calcium Looping thermochemical storage proposed configuration*, being three of them JCR journal papers and one an international conference paper.

- Pascual S, Lisbona P, Bailera M, Romeo LM. *Design and operational performance maps of Calcium Looping thermochemical energy storage for concentrating solar power plants*. Energy (2021), 220, 119715.
https://doi.org/10.1016/j.energy.2020.119715

- Pascual S, Lisbona P, Romeo LM. *Operation maps in Calcium Looping thermochemical energy storage for concentrating solar power plants*. Journal of Energy Storage (2022), 55, 105771.
https://doi.org/10.1016/j.est.2022.105771

- Pascual S, Di Lauro F, Lisbona P, Romeo LM, Tregambi C, Montagnaro F, Solimene R, Salatino P. *Improvement of performance of fluidized bed Calcium Looping for thermochemical solar energy storage: Modelling and experiments*. Proceedings of 10th European Combustion Meeting (2021), pp. 1430-1435.

- Tregambi C, Di Lauro F, Pascual S, Lisbona P, Romeo LM, Solimene R, Salatino P, Montagnaro F. *Solar-driven Calcium Looping in fluidized beds for thermochemical energy storage*. Chemical Engineering Journal (2023), 466, 142708.
https://doi.org/10.1016/j.cej.2023.142708

One more published JCR journal paper is dedicated to the section *State of the art of thermal energy storage in concentrating solar power plants.*

- Pascual S, Lisbona P, Romeo LM. *Thermal energy storage in concentrating solar power plants: A review of European and North American R&D projects*. Energies (2022), 15, 8570.
  https://doi.org/10.3390/en15228570

The remaining paper *Optimized Ca-looping thermochemical energy storage under dynamic operation for concentrated solar power* which are included in the compendium of publications has been accepted for publication in Journal of Energy Storage in 2023. The JCR journal research paper is the core of the last PhD thesis section *Operational methodology and economic implications*. A copy of the acceptance letter for the last paper to be published can be found in *Appendix A* of the present PhD thesis.

Modelling calcium looping at industrial scale for energy storage in concentrating solar power plants

Manuel Bailera [a, *], Sara Pascual [a], Pilar Lisbona [b], Luis M. Romeo [a]

[a] *Escuela de Ingeniería y Arquitectura. Universidad de Zaragoza, Campus Río Ebro, María de Luna 3, 50018, Zaragoza, Spain*
[b] *Fundación Agencia Aragonesa para La Investigación y El Desarrollo (ARAID), Zaragoza, Spain*

A B S T R A C T

Ca-Looping represents one of the most promising technologies for thermochemical energy storage. This process based on the carbonation-calcination cycle of CaO offers a high potential to be coupled with solar power plants for its long-term storage capacity and high temperatures. Previous studies analyzed different configurations of CaL integrated into power cycles aiming to improve efficiency. However, most of these assessments based on lumped models did not account for scale effect in the most critical reactor. In this work, a detailed 1D-model of a large-scale carbonator is included in the comprehensive model of the integrated facility. The results obtained served to assess the available heat, the minimum technical part load of this equipment, the required size of the storage tanks and the overall efficiency of the plant. The main issue in the operation of large-size carbonator is the heat removal, thus a multi-tube internally cooled reactor is proposed. The designed carbonator provides 80 MWth at nominal operation and 40 MWth at minimum part load operation. The sizing of storage tanks depends on the operation management, ranging between 5700–11,400 m^3 for 15 h. Different efficiencies of the system were defined and presented through operating maps, as a function of the reactor loads.

1. Introduction

Deploying renewable energy sources (RES) contributes to the decarbonisation of energy systems [1]. However, curtailments are necessary when RES represent above 10% of the annual electricity generation [2], since operators only control 5—10% of wind and solar dispatch [3]. To face this situation, the European Commission proposed energy storage as solution [4] since 10—20% variable RES shares are estimated for about 50 regions in the world by 2023 [5].

In this study, we focus on concentrating solar power (CSP) plants. Dispatch of CSP has a peak around noon and significant variations over minutes or hours due to cloud coverage. To manage electricity production, half of the CSP plants worldwide use thermal energy storage (TES) [6]. TES systems retain thermal energy within specific materials and release it when needed. According to the physical phenomena occurring while absorbing/releasing the energy, thermal energy storage is classified in sensible TES, latent TES and thermochemical energy storage (TCES).

Sensible TES use materials with high specific heat (131—4187 J/ kg·K) to store/release the energy by heating/cooling their mass. These systems are simple, reliable and cheap, but the energy storage density is low (1001—4453 kJ/m^3·K) [7]. Most of sensible TES used in commercial CSP plants are based on molten salts [8], combining two tanks (packed beds) of high and low temperature for short- and long-term storage [9].

Latent TES use materials with high latent heat (112—260 kJ/kg), to store/release the energy during phase transitions at constant temperature, what reduces fluctuations in electricity production [7]. Phase change takes place between liquid and solid, in order to have small variations in volume (<10%) [10] and high energy storage densities (50—150 kWh/t). However, the low thermal conductivity of these materials (<0.5 W/m·K) prolongs the time of charging and discharging energy [7]. To obtain large heat exchange surfaces in latent TES, shell and tubes configurations are commonly used [11, 12].

Thermochemical energy storage systems are based upon reversible chemical reactions (endothermic in one direction and exothermic in the other) to store/release energy through a cyclic process. As TCES works at very high temperatures (450—1300 °C), it is the most promising candidate for thermal energy storage in new generation CSP plants working above 800 °C [7, 13]. Moreover, TCES

* Corresponding author.
E-mail address: mbailera@unizar.es (M. Bailera).

Nomenclature

Symbols

a_2	pre-exponential factor, 1/s
α	fitting parameter for the equilibrium pressure, K
$\bar{a}$	heat transfer area, m^2
A	specific projection area of the dispersed particles, m^2/kg
A_v	geometry-dependent absorptance of the gas body,
$\mathscr{A}$	pre-exponential factor, atm
$\boldsymbol{A}$	calculation parameter,
b	calculation parameter, 1/s
Cp	specific heat, kJ/(kmol·K)
CS	sensible heat, MW
d, D	diameter, m
E_2	carbonation activation energy, kJ/mol
f	fraction,
f_p	pressure correction factor,
fRe_D	friction factor,
g	gravity, m/s^2
Gz	Graetz number,
h	convective heat transfer coefficient, kW/(m 2 K)
h	specific enthalpy, kJ/kmol
k	thermal conductivity, kW/(m·K)
K	emission or absorption coefficient of the gas phase, 1/m
ℓ	heat transfer length, m
l_{mb}	mean beam length, m
load	carbonator load (ratio between the input mass flow and the nominal input mass flow),
L	length, m
L_p	particle load at operation conditions, kg/m^3
$\dot{m}$	mass flow rate, kg/s
n	exponent factor,
$\dot{n}$	mole flow rate, kmol/s
N	number of cooling tubes,
Nu	Nusselt number (local),
$\overline{Nu}$	Nusselt number (average),
O_{Lev}	offset in the extended Lévêque solution,
per	perimeter, m
P	pressure, bar
Pr	Prandtl number,
$\dot{q}'$	heat flow per unit of length, kW/m
$\dot{Q}$	rate of heat flow, MW or kW
$\overline{Q}$	mean relative absorption or backscattering efficiency of a particle,
r	reaction rate, 1/s
r	radius, m
r_*	ratio between inner and outer radius,
R	molar ratio CaO/CO$_2$,
R	thermal resistance, K/kW
Re_D	Reynolds number based on hydraulic diameter,
$\mathscr{R}$	ideal gas constant, kJ/(kmol·K)
s_{eq}	equivalent layer thickness, m
S_{eff}	effective cross-sectional area of reactor, m^2
SSC	specific storage consumption
t	reacting time or residence time, s
t_0	time to reach half of residual conversion, s
T	temperature, K
v	velocity, m/s
V	volume, m^3

$\dot{V}$	volumetric flow rate, m^3/s
X	conversion,
X_k	residual conversion,
ΔL	length of the discretized slice, m
ΔS_2^0	carbonation entropy change, J/(mol·K)
ΔH_2^0	standard enthalpy change of carbonation, kJ/mol
ΔH_r	enthalpy of carbonation, kJ/kmol

Greek symbols

α	absorptivity,
β	calculation parameter,
γ	calculation parameter,
ε	emissivity,
η	efficiency,
η_{av}	available energy efficiency (ratio between the available heat and the energy invested),
η_{CR}	carbonator efficiency (ratio between the heat recovered and the energy invested),
η_{st}	storage efficiency (ratio between the stored energy and the energy invested),
λ_1, λ_2	calculation parameter,
μ	viscosity, kg/(m·s)
ρ	density, kg/m^3
σ	Stefan-Boltzmann constant, kW/(m^2·K^4)
Φ	optical thickness for the gas solid dispersion,

Subscripts and superscripts

abs	absorption
av	available thermal energy
bsc	backscattering
c	carbonator
cf	cooling fluid/cooling tube
CL	in the calciner or for calcination
conv	convection
CR	in the carbonator or for carbonation
dch	discharge
emi	emission
eq	equilibrium
EROM	energy release operation mode
ESOM	energy storage operation mode
f	fresh
g	gas
h	hydraulic diameter
i	initial value or discretization index for axial position
in	inner or inlet
iw	wall in contact with the cloud of gas and particles
j	component j
L	covered length
Li	axial position at length L_i from top
max	maximum or nominal capacity
out	outer radius/diameter or outlet
ow	wall in contact with the cooling fluid
p	purge or particle
rad	radiation
s	solid
st	storage
t	terminal velocity
tb	cooling tubes
tube	carbonator's tube
w	wall
0	initial
∞	fully developed heat transfer

provides seasonal storage with no heat losses (the energy is stored in the chemical bound of the compounds) with higher energy densities than sensible and latent TES (about 240–1090 kWh/t) [14]. Among many materials for TCES (hydrides, metal oxides and carbonate salts), the calcium looping reaction (CaL), $CaO_3 \leftrightarrow CaO + CO_2$, stands out because the material is cheap and earth-abundant, products are non-toxic, and energy storage density reaches 390 kWh/t [14, 15].

The utilization of CaL for TCES was proposed by Barker in 1974 [16], and the scientific community intensified its research during the last decade. Recently, several papers dealt with the integration of CaL TCES with different power cycles [17, 18], efficiency optimization [19, 20, 21], and management of the storage system [22]. Ortiz et al. [17] and Tesio et al. [18] assessed different power plant options to find the technology that leads to better performance when integrated with calcium looping TCES. Both of them concluded that best results are achieved with CO_2 power cycles (CO_2 closed Brayton cycle according to Ortiz, and supercritical CO_2 power block according to Tesio). After identifying the most suitable technology, they optimized the efficiency of the concept by studying different plant layouts. They found overall efficiencies (net electric production to net solar thermal input) in the range 32–44% for the CO_2 closed Brayton cycle [19, 20], and 40.4% for the supercritical CO_2 cycle [21]. Regarding management, Bravo et al. used a multi-objective optimization framework to determine the best operational strategy. However, authors state that further research on this issue is necessary to reach authoritative conclusions, as economic aspects were not included in the optimization [22].

So far, the reactors design has not been taken into account in the existing studies which are mainly based on lumped models of the process. However, the extension of the chemical reactions in the carbonator and calciner clearly affects the mass flows, the management of storages and the overall efficiency of the plant [14]. The main reason is that experiments on calcium looping applied to TCES are scarce making difficult the validation of detailed models of the reactors [23]. Solar calcination ($CaO_3 \rightarrow CaO + CO_2$, endothermic) has been tested by the Paul Scherrer Institute in a cyclone gas-particle separator with a window-less aperture. Solar thermal input of the prototype was 54 kW, reaching 85% limestone conversion with 88% energy efficiency [24]. Carbonation ($CaO + CO_2 \rightarrow CaO_3$, exothermic), within the framework of solar CaL, is tested in the SOCRATCES project. They use an entrained flow reactor of 10 kW thermal output, cooled by external cooling coils. The cooling fluid is air, which is later used in a Stirling engine to produce power [25].

At industrial scale, the computational fluid dynamics simulations of the Paul Scherrer Institute show that solar calcination may operate effectively at 55 MW thermal inputs by using a falling particle receiver. In this type of reactors, a curtain of falling $CaCO_3$ particles absorb the solar radiation that enters through the aperture of the receiver [24]. Regarding carbonation, Bailera et al. showed that energy could not be properly recovered in entrained flow reactors when scaled-up to industrial scale, if they are cooled by external coils. Since the reactor heats up, the reaction reaches the equilibrium temperature and it progresses limited by the rate at which heat is evacuated. This leads to unfeasible dimensions of reactors (7 m diameter and 52 m length for carbonators of 100 MW solar input) [26]. Therefore, other potential configurations must be evaluated to improve the heat removal in industrial carbonators for CaL TCES.

In this work, we focus on the two main gaps found in literature when assessing the utilization of calcium looping as thermo-chemical energy storage in concentrating solar power plants: (i) the design of a suitable reactor for carbonation at industrial scale and (ii) the analysis of the concept taken into account the reactor design

and its behavior at part load operation. Thus, the novelty of this work consist in quantifying a realistic efficiency for CaL TCES at industrial scale. First, the paper introduces the concept of calcium looping TCES in CSP, establishing the case under study. Then, the methodology presents the carbonator modelling and the design criteria from few kW to 100 MW scale. Results show how part load operations in carbonator modify mass flows and the storage management (CaO, $CaCO_3$ and CO_2). Finally, we quantify the overall performance of the plant.

2. Calcium looping for energy storage in CSP plants

The energy storage system based on calcium looping process consists of two reactors, namely calciner and carbonator. In the calciner, solids fall from the top, and solar radiation provides thermal energy for calcination (Eq. (1)). In our study, we consider 100 MW of solar power input as nominal operation. If the availability of solar energy is less than the nominal power, the calciner will operate at partial load. The calciner load is defined as the ratio between the available solar power input and the nominal solar power input (100 MW). The solids mass flow is a mixture of limestone and lime (197.7 kg/s), and its inlet temperature is set at 850 °C through the heat exchanger HE-ER$_{CaCO3+CaO}$ (Fig. 1). The operating temperature inside the calciner is kept below 950 °C, to limit degradation of the solid particles [19].

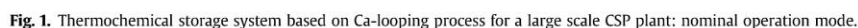$$CaCO_3 \leftrightarrow CaO + CO_2 \quad \Delta H_R^0 = 180 \; kJ\Big/mol \tag{1}$$

Lime and CO_2 are obtained after calcination of limestone. These products are conveyed to the second reactor, where carbonation takes place and the stored chemical energy is recovered (reverse of Eq. (1)). The heat released is transferred to the power block through a cooling fluid. The inlet temperature of the carbonator is set at 850 °C [20], for which reason the heat exchangers HE-ER$_{CaO}$ and HE-ER$_{CO2}$ are used. Finally, the solids leaving the carbonator are conveyed again to the calciner, thus closing the loop.
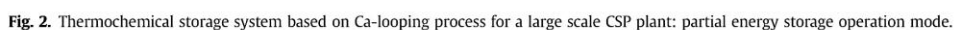
Full calcination can be assumed at the outlet of the calciner. However, the mass composition after carbonation depends on the average sorption activity of the solid population, as only part of the CaO particle will react with the CO_2 [27]. An average maximum conversion of 13.54% is assumed for the selected limestone [26, 28, 29] and the molar ratio CaO:CO_2 at the carbonator inlet is set at 6.8:1 [28, 29, 30].

Additionally, a small fraction of lime is purged from the system ($f_p = 1\%$) and the corresponding amount of fresh limestone is added to compensate the removal of calcium. The addition of fresh limestone to the system increases the average sorption activity of lime population given the decay of sorption capacity of individual lime particles with the number of cycles. In this layout, lime is purged after calcination, while limestone is added at the inlet of calciner. It must be noted that there is a net input of carbon and oxygen into the system, because the carbon dioxide released from fresh limestone calcination is accumulated. Therefore, a small amount of CO_2 has to be removed from the loop to close the carbon mass balance. Actually, the only CO_2 exiting the carbonator is this net mass input coming from the difference between the fresh $CaCO_3$ and the purged CaO, as the molar ratio in the carbonator was set to consume the rest of CO_2 during reaction.

This mode of operation corresponds to the nominal point used for carbon capture applications in which neither storage nor discharge of energy take place. The energy entering the calciner is recovered in the carbonator without delaying power production. This mode of operation is not useful for energy storage applications but its proper description is significant to understand the performance of the calcium looping. In the following subsections, the

3

Fig. 1. Thermochemical storage system based on Ca-looping process for a large scale CSP plant: nominal operation mode.

layout of the system under storage and discharge operation modes is described.

2.1. Energy storage operation mode

When the electricity demand from the system decays or the selling price of electricity does not cover the operating cost, part of the solar energy handled in the CSP is stored. Under energy storage operation, a fraction of the lime ($f_{st,CaO}$) and CO_2 ($f_{st,CO2}$) obtained through calcination are stored instead of conveyed to the carbonator (Fig. 2). Thus, the thermal power released in the carbonator is reduced, and the stored products allow producing thermal energy in a later period. Additionally, to keep constant the mass flow entering the calciner, solids must be added to the loop through the discharge from a limestone and lime reservoir. The discharge flow of this tank is defined as a fraction of the nominal solid flow leaving the carbonator outlet ($f_{dch,\,CaCO3}$).

If the fraction of CaO and CO_2 sent to storage tanks increases, the load of the carbonator may be reduced below its minimum partial load, requiring to shut-down the reactor (the part load in the carbonator is defined as the ratio between the input mas flow and the nominal input mass flow). Under this situation, the plant starts operating only in storage mode, not producing thermal power in the carbonator (Fig. 3). The discharge fraction from the limestone reservoir $f_{dch,\,CaCO3}$ will depend on the amount of solar energy entering the receiver.

In this study, the properties of stored CO_2 are 100 °C and 73 bar [20], through a compression stage including two cooling steps to 50 °C (HE-EE$_{CO2}$) and 100 °C (HE-EE$_{CO2,C}$). Solids storage temperature and pressure are 200 °C (HE-EE$_{CaO}$) and 1 bar [19].

2.2. Energy release operation mode

Whenever solar energy is not enough to keep carbonator

Fig. 2. Thermochemical storage system based on Ca-looping process for a large scale CSP plant: partial energy storage operation mode.

Fig. 3. Thermochemical storage system based on Ca-looping process for a large scale CSP plant: energy storage operation mode.

working at a specific load, the plant can run under energy release mode. In this case, part of the previously stored lime and CO_2 are now discharged from their reservoirs to enter in the carbonator and produce the desired thermal power (Fig. 4). The CO_2 and CaO leaving the storage tanks are defined as a fraction of the nominal flow of CO_2 ($f_{dch,CO2}$) and CaO ($f_{dch,CaO}$) at calciner outlet. Additionally, as there is not enough available solar energy to completely calcine the mass flow exiting the carbonator, part of this is diverted to storage ($f_{st,CaCO3}$) before closing the loop.

When solar power is not available, the operation is limited to release stored energy (Fig. 5). The mass flows discharged from the reservoirs depend on the demanded thermal power to be produced. In our study, whether we store or release energy, the fractions of CaO and CO_2 entering and exiting the tanks will be the same in order to keep constant the CaO:CO_2 molar ratio in the carbonator (i.e., $f_{st,CaO} = f_{st,CO2}$ and $f_{dch,CO2} = f_{dch,CaO}$). Heat losses of

heat exchangers are assumed as 2% of the total released energy.

3. Methodology

Methodology covers carbonator modelling, design criteria and assessment of the storage tanks required for the correct management of the plant.

3.1. Carbonator modelling

The energy removed from the carbonator represents the main source of heat sent to the power cycle. However, the operating load in the carbonator remarkably varies throughout the day due to cloud coverage, the solar radiation pattern and the demand of electricity. Therefore, its design must be assessed to quantify the effects of partial load operation in the overall efficiency of the system. In this sense, a detailed model of a large scale carbonator reactor has been developed. Besides, the minimum technical load in the carbonator have an effect on the size of storage tanks, and will determine the minimum amount of heat available for the power cycle.

The carbonator is an entrained flow reactor in which reactants entrance is located at the top. This is a complex system where heterogeneous exothermic chemical reactions take place together with heat transport phenomena. The model considers carbonation kinetics, heat transfer mechanisms and the specific geometry of the reactor, in order to compute axial profiles of conversion, temperature and residence time under different operating loads. The reactor was discretized in 100 slices of constant length, for which the equations presented in the following subsections were computed. In the case of those equations that comprise an integration, some of the variables are assumed constant along the slice to perform the integration (whenever the case, it is mentioned in the text).

Fig. 6 illustrates the flowchart of the carbonator model for one slice of the discretized reactor. There are four main blocks that simulate the solid phase, the gas phase, the kinetics and the heat transfer. The 'gas phase' module provides information to the 'solid phase' module in order to compute the downward velocity of the
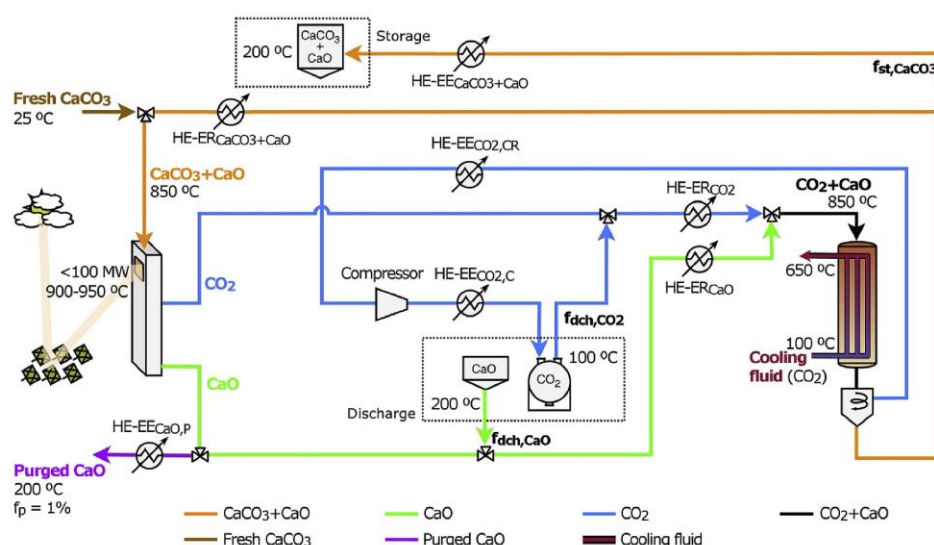

Fig. 4. Thermochemical storage system based on Ca-looping process for a large scale CSP plant: partial energy discharge operation mode.
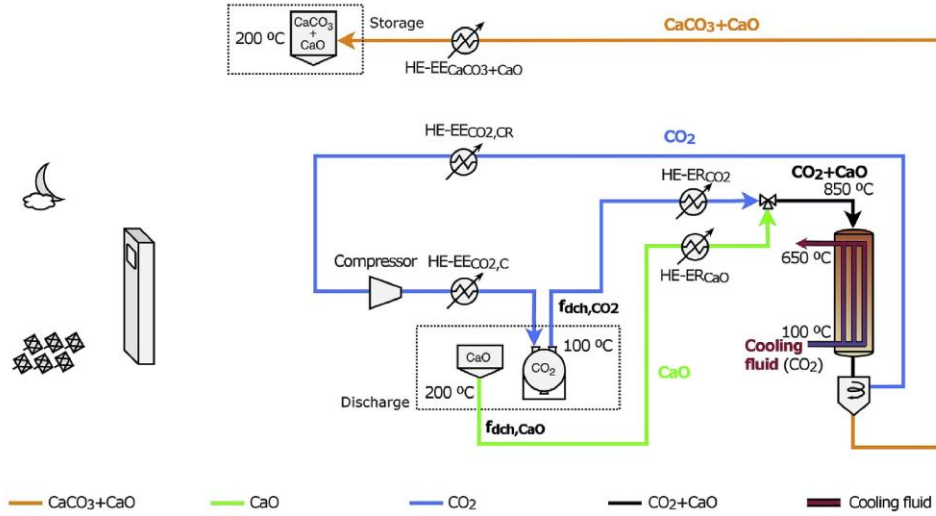
Fig. 5. Thermochemical storage system based on Ca-looping process for a large scale CSP plant: energy discharge operation mode.

solids falling through the reactor. Then, the 'solid phase' module provides the residence time of the solids to the 'kinetics' module to calculate the conversion. Also, both the 'gas phase' and the 'solid phase' modules transfer the mole flows data to the 'heat transfer' module in order to calculate the final temperature inside the reactor. At this point, the computed values of conversion and temperature must be re-introduced in the different modules (iterative process) until they converge. Once convergence is achieved, the data on residence times, conversion and temperature are provided to the next discretized slice. The former allows computing the total residence time, while conversion and temperature are used as initial values in the iterative loops of the next slice.

It must be noted that each slice does not only depends on the previous one, but also in the following one because of the heat transfer model. Since the reactor uses a counter-current cooling configuration, the initial temperature of the cooling fluid is provided by the following slice, which is not yet solved. The boundary condition that fixed the inlet temperature of the cooling fluid, in the last slice, allow to solve this indetermination. The final temperature of the cooling fluid is computed in the first slice. The list of boundary conditions that allow solving the system is presented in Table 1. These variables are commented in the following subsections.

3.1.1. Kinetic model

The kinetic equation used in the model was published by Ortiz et al. [31]. The carbonation reaction is described by Eq. (2), giving the conversion of CaO as a function of time and reaction rate,

$$X(t) = \frac{X_k}{1 + e^{-r(t - t_0)}} \quad (2)$$

where X_k is the conversion at the end of the reaction controlled phase (assumed as 0.1354 in this work) and t_0 the time taken to reach $X_k/2$ conversion (equal to 1.515 s). The reaction rate, r, is given by Eq. (3) as a function of temperature and CO_2 partial pressure,

$$r = a_2 \cdot e^{\left(-\frac{E_2}{\mathscr{R}T}\right)} \cdot \left(\frac{P}{P_{eq}} - 1\right) \cdot \left(\frac{P}{P_{eq}} + e^{\left(\Delta S_2^0/\mathscr{R}\right)} e^{\left(-\Delta H_2^0/\mathscr{R}T_s\right)}\right)^{-1} \quad (3)$$

where E_2 is 20 kJ/mol, αS_2^0 is −68 J/mol·K and αH_2^0 is −160 kJ/mol. Besides, $P_{eq} = \mathscr{A} \cdot exp(-\alpha/T)$, where $\mathscr{A}$ is 4.083·107 atm, and α is 20,474 K.

3.1.2. Solid phase

The time spent by the solids traversing the reactor corresponds to the reaction time (i.e., the time used in Eq. (2)). This is given by the entraining downflow velocity of the solids, which depends on its terminal velocity and the gas velocity. According to Wen et al. [32], the downward velocity, v_s, of small particles under low Reynold numbers is computed by Eq. (4):

$$v_s = v_{s,i} \cdot e^{-bt_s} + (v_g + v_t) \cdot \left(1 - e^{-bt_s}\right) \quad (4)$$

where $v_{s,i}$ is the initial velocity of the solid, v_g is the velocity of the gas phase (volumetric flow divided by the cross section), and v_t is the terminal settling velocity of the particle in a static fluid. The parameter b, and the velocity v_t are given by Eq. (5) and Eq. (6):

$$b = \frac{18\mu}{\rho_s d_p^2} \quad (5)$$

$$v_t = \frac{(\rho_s - \rho_g)d_p^2 g}{18\mu} \quad (6)$$

where μ is the viscosity of the gas, ρ_s is the density of the solid, ρ_g is the density of the gas, d_p is the diameter of the solid particles (assumed 60 μm), and g the gravity.

Integrating Eq. (4) gives the reactor length as a function of the residence time of solids, Eq. (7),
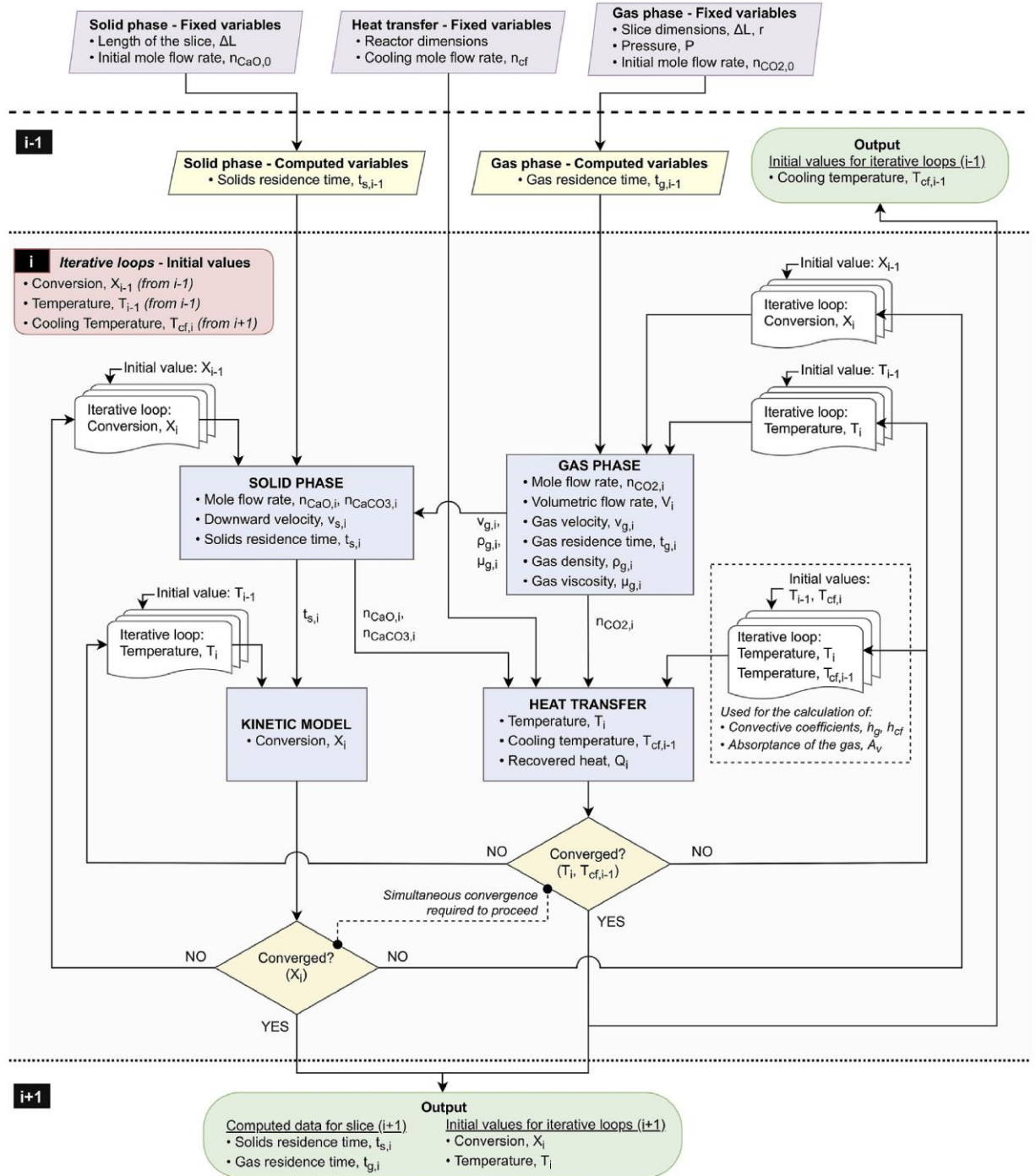
Fig. 6. Carbonator modelling flowchart for the discretized slice of index i, and its interactions with the previous (i-1) and next (i+1) slice.

$$L = \int_0^{t_{s,L}} v_s \, dt_s = \frac{v_{s,i}}{b}\left(1 - e^{-bt_s}\right) + \left(v_g + v_t\right) \cdot \left(t_s - \frac{1 - e^{-bt_s}}{b}\right) \quad (7)$$

Eq. (7) is integrated for each slice of the discretized reactor, so it can be assumed that v_g, v_t and b are constants in the range of integration (they are calculated at the specific temperature and pressure of the gas in each slice). Thus, total residence time

7

45

Table 1
Boundary conditions of the simulation.

	$L_i = 0$	$L_i = L$	$r = r_{out,c}$
Solid phase			
mole flow rate, $\dot{n}_{CaO}$	$\dot{n}_{CaO,c,0}$ (Eq. (58))	–	–
mole flow rate, $\dot{n}_{CaCO3}$	$\dot{n}_{CaCO3,c,0} = 0$	–	–
velocity, v_s	$v_{s,0} = 0.01\ m/s$	–	–
residence time, t_s	$t_{s,0} = 0$	–	–
Gas phase			
mole flow rate, $\dot{n}_{CO2}$	$\dot{n}_{CO2,c,0}$ (Eq. (59))	–	–
velocity, v_g	$v_{g,0} = \dot{n}_{CO2,c,0} \cdot (1 - X_0) \cdot \mathscr{R} \cdot T_0/(P \cdot S_{eff})$	–	–
residence time, t_g	$t_{g,0} = 0$	–	–
Kinetic model			
conversion, X	$X_0 = 0.00078$	–	–
Heat transfer			
Temperature of reactants, T	$T = 850\ °C$	–	–
Temperature of cooling, T_c	–	$T_c = 100\ °C$	–
Heat transferred, $\dot{q}'$	–	–	$\dot{q}' = 0$

considers the variation in temperature and gas volume along the reactor.

3.1.3. Gas phase

For the sake of simplicity, we assume that the fluid of a slice is not mixed with the fluid of any other slice ahead or behind (flat velocity profile). This implies that the residence time in the reactor is the same for all elements of the fluid. The residence time of the gas is given by Eq. (8),

$$t_g = \int_0^L \frac{S_{eff}}{\dot{V}}\ dL \tag{8}$$

where $\dot{V}$ is the volumetric flow rate and S_{eff} is the effective cross-sectional area of reactor (i.e., cross-sectional area minus the area occupied by solids). Eq. (8) is integrated for each slice, so $\dot{V}$ and S_{eff} are constant in the interval of integration, and the residence time in that interval becomes $t_{g,i} = L_i \cdot S_{eff}/\dot{V}_i$.

Besides, it is assumed that the pressure inside the reactor remains constant at 2.0 bar. The volumetric flow rate as a function of the conversion is given by Eq. (9),

$$\dot{V}_{Li} = \frac{\dot{n}_{CO2,0} \cdot (1 - X_{Li}) \cdot \mathscr{R} \cdot T_{Li}}{P} \tag{9}$$

3.1.4. Heat transfer

In this section, it is presented (i) the energy balance on the gas-solid mixture in which carbonation takes place, (ii) the heat transference (convective and radiative) from gas-solid mixture to the walls, (iii) the conduction through walls to the cooling fluid, and (iv) the energy balance of the cooling fluid. It should be noted that heat transfer equations depend on the carbonator configuration and geometry, which have been selected differently depending on the scale (see Section 3.2). To this regard, clarifications are made when required.

3.1.4.1. Reactants side.
The energy balance in the cloud of gas and particles is described by Eq. (10), considering the exothermal heat from carbonation and the heat exchange per length of reactor (from L_{i-1} to L_i):

$$\sum_j Cp_j \cdot \dot{n}_{j,L_i} \cdot (T_{L_i} - T_{L_{i-1}}) = -\Delta H_r \cdot \left(\dot{n}_{CaCO3,L_i} - \dot{n}_{CaCO3,L_{i-1}} \right) \\ - \dot{q}'_{L_i} \cdot (L_i - L_{i-1}) \tag{10}$$

where Cp_j and $\dot{n}_j$ are the specific heat and mole flow of component j, respectively, T is the temperature of the cloud of gas and particles (assumed to be homogeneous in the slice), αH_r is the enthalpy of reaction (-178 kJ/mol), and $\dot{q}'_{L_i}$ is the heat flow throughout the wall per unit of axial length. This heat flow through the wall accounts for radiation, $\dot{q}'_{rad,L_i}$, and convection, $\dot{q}'_{conv,L_i}$, in the form of Eq. (11):

$$\dot{q}'_{L_i} = \dot{q}'_{rad,L_i} + \dot{q}'_{conv,L_i} \tag{11}$$

Radiation is given by Eq. (12):

$$\dot{q}'_{rad,L_i} = \frac{\varepsilon_w}{\alpha_{g+p} + \varepsilon_w - \alpha_{g+p} \cdot \varepsilon_w} \cdot \sigma \cdot \left(\varepsilon_{g+p} \cdot T_{L_i}^4 - \alpha_{g+p} \cdot T_{iw,L_i}^4 \right) \cdot \ell \tag{12}$$

where α_{g+p} and ε_{g+p} are the absorptivity and emissivity of the gas-particle mixture [33], ε_w the emissivity of the wall, σ is the Stefan-Boltzmann constant, T is the temperature of the cloud of gas and particles (assumed to be homogeneous in the slice), and T_{iw} is the temperature of the inner wall (wall in contact with the cloud of gas and particles). The variable ℓ is defined in such a way that $\ell = \bar{a}/(L_i - L_{i-1})$, and $\bar{a}$ is the surface area where the heat transfer takes place within the slice, which depends on the geometry of the reactor.

The model for the calculation of the emissivity (ε_{g+p}) and absorptivity (α_{g+p}) of the gas-particle mixture is borne out of 'VDI Heat Atlas', Part K4 [33]. They can be described as

$$\varepsilon_{g+p} = (1 - \beta) \cdot \left(\frac{1 - \exp(-\Phi_{emi,g+p})}{1 + \beta \cdot \exp(-\Phi_{emi,g+p})} \right) \tag{13}$$

$$\alpha_{g+p} = (1 - \beta) \cdot \left(\frac{1 - \exp(-\Phi_{abs,g+p})}{1 + \beta \cdot \exp(-\Phi_{abs,g+p})} \right) \tag{14}$$

with

8

46

$$\beta = \frac{\gamma - 1}{\gamma + 1} \tag{15}$$

$$\gamma = \sqrt{1 + \frac{2 \cdot \overline{Q}_{bsc}}{\overline{Q}_{abs}}} \tag{16}$$

$$\Phi_{emi.g+p} = \left(\overline{Q}_{abs} \cdot A \cdot L_p + K_{emi.g} \right) \cdot l_{mb} \cdot \gamma \tag{17}$$

$$\Phi_{abs.g+p} = \left(\overline{Q}_{abs} \cdot A \cdot L_p + K_{abs.g} \right) \cdot l_{mb} \cdot \gamma \tag{18}$$

Where $\overline{Q}_{bsc}$ and $\overline{Q}_{abs}$ are the particle scattering and absorption coefficients, $K_{emi.g}$ and $K_{abs.g}$ are the gas scattering and absorption coefficients, L_p is the particle loading, l_{mb} is the mean beam length of radiation within the relevant geometry, and A is the specific projection area of the dispersed particles.

The particle scattering and absorption coefficients ($\overline{Q}_{bsc}$ and $\overline{Q}_{abs}$) are taken from the limestone's data graph included in the Heat Atlas (reference [33], section K4, page 993) as a function of the particle diameter. The specific projection area of the dispersed particles, A, is calculated from their diameter, d_p, and density, ρ_p, by Eq. (19).

$$d_p = \frac{3}{2 \cdot \rho_p \cdot A} \tag{19}$$

The gas scattering and absorption coefficients, $K_{emi.g}$ and $K_{abs.g}$, are computed from

$$K_{emi.g} = -\frac{\ln(1 - \varepsilon_g)}{l_{mb}} \tag{20}$$

$$K_{abs.g} = -\frac{\ln(1 - A_v)}{l_{mb}} \tag{21}$$

where ε_g is the emissivity of the gas and A_v is the absorptance. The values of ε_g are taken from the data graph included in the Heat Atlas (reference [33], section K3, page 982) as a function of pressure, temperature and the equivalent layer thickness. The latter is tabulated in Ref. [33], section K3, page 981, for different geometries. Regarding the absorptance A_v, it is a function of the wall temperature, the gas temperature and the emissivity of the gas, following:

$$A_v = f_{p,CO_2} \cdot \left(\frac{T_g}{T_w} \right)^{0.65} \cdot \varepsilon_g \tag{22}$$

The parameter f_{p,CO_2} is a pressure correction factor, which at 2.0 bar is equal to 1.019. This is given by equation (23), where s_{eq} is the equivalent layer thickness (tabulated in Ref. [33], section K3, page 981, for different geometries).

$$f_{p,CO_2} = 1 + (\lambda_1 - 1) \cdot \exp\left[-0.5 \cdot \left(\log \frac{\lambda_2}{100 \cdot p_{CO2} \cdot s_{eq}} \right)^2 \right] \tag{23}$$

with

$$\lambda_1 = \frac{\left[0.1 \cdot \left(\frac{T_g}{1000} \right)^{-1.45} + 1 \right] \cdot p \cdot \left(1 + 0.28 \cdot \frac{P_{CO2}}{P} \right) + 0.23}{0.1 \left(\frac{T_g}{1000} \right)^{-1.45} + p \cdot \left(1 + 0.28 \cdot \frac{P_{CO2}}{P} \right) + 0.23} \tag{24}$$

$$\lambda_2 = \begin{cases} 0.225 \cdot \left(\frac{T_g}{1000} \right)^2 & for\ T_g > 700\ K \\[2mm] 0.054 \cdot \left(\frac{T_g}{1000} \right)^2 & for\ T_g \le 700\ K \end{cases} \tag{25}$$

Regarding convection, which is the other term of heat flow in Eq. (11), it is given by Eq. (26)

$$\dot{q}'_{conv,L_i} = h_{g,L_i} \cdot (T_{L_i} - T_{iw,L_i}) \cdot \ell \tag{26}$$

where T is the temperature of the cloud of gas and particles (assumed to be homogeneous in the slice), T_{iw} is the temperature of the inner wall (wall in contact with the cloud of gas and particles) and h_g the convective coefficient [34]. The variable ℓ is defined in such a way that $\ell = \bar{a}/(L_i - L_{i-1})$, and $\bar{a}$ is the surface area where the heat transfer takes place within the slice, which depends on the geometry of the reactor.

The convective coefficient at each axial position is calculated by Eq. (27) [34]:

$$h_{g,L_i} = \frac{Nu_{Li} \cdot k_{Li}}{D_h} \tag{27}$$

Where Nu is the Nusselt number, k the thermal conductivity of the gas (at T_{L_i} and P_{L_i}), and D_h the hydraulic diameter. The latter is defined according to Eq. (28), which relates the cross-sectional area of the flow, S_{eff}, and the perimeter of the section, *per*.

$$D_h = \frac{4 \cdot S_{eff}}{per} \tag{28}$$

It should be noted that the hydraulic diameter depends on the geometry of the reactor. In our study, we use two types of configuration (see Fig. 7): an annular single-tube (reactants in the outer side) and a tube bundle in triangle configuration (reactants in the shell side). The hydraulic diameter for these two cases are:

$$D_{h(annular)} = 2 \cdot \left(r_c - r_{cf} \right) \tag{29}$$

$$D_{h(bundle)} = \frac{2 \cdot \left(r_c^2 - N \cdot r_{cf}^2 \right)}{\left(r_c + N \cdot r_{cf} \right)} \tag{30}$$

where r_c is the radius of the carbonator tube (the enclosing), r_{cf} is the radius of the cooling tube, and N the number of cooling tubes.

The Nusselt number, which is necessary in Eq. (27), also depends on the geometry of the reactor. In the case of an annular configuration, the correlations developed by Bennett are used [35]. Specifically, the correlation corresponding to boundary conditions of adiabatic outer wall and constant inner wall temperature (in our simulation, we use the average temperature of the cooling wall for the calculation of the Nusselt number). The Nusselt number in the inner surface, at an axial position L_i (of the total length L) is given by Eq. (31):

$$Nu_{Li(annular)} = \overline{Nu}_{L(annular)} \cdot \left(1 - \frac{\left(\frac{Gz_{Li}^{n/3}}{3}\right) \bigg/ \left(Gz_{Li}^{n/3} + \left(\frac{Nu_\infty - O_{Lev}}{A \cdot (fRe_D)^{1/3}}\right)^n\right)}{1 + \left(\frac{O_{Lev}}{A \cdot (fRe_D)^{1/3}}\right) \bigg/ \left(Gz_{Li}^{n/3} + \left(\frac{Nu_\infty - O_{Lev}}{A \cdot (fRe_D)^{1/3}}\right)^n\right)^{1/n}} \right) \tag{31}$$

Where $\overline{Nu}_{L(annular)}$ is the average Nusselt number over the total axial length of the reactor, fRe_D is the friction factor, Nu_∞ is the Nusselt number for fully developed heat transfer, O_{Lev} is the offset in the extended Lévêque solution, n is an exponent factor, A is a constant factor equal to 0.40377, and Gz_{Li} is the Graetz number for a duct of length L_i. These variables are computed by Eq. (32)–(37).

$$\overline{Nu}_{L(annular)} = \left[\left(A \cdot (fRe_D \cdot Gz_{Li=L})^{1/3}\right)^n + (Nu_\infty - O_{Lev})^n \right]^{1/n} + O_{Lev} \tag{32}$$

$$fRe_D = 32 \cdot \left(\frac{1 - r_*}{r_*}\right) \cdot \left(\frac{-2 \cdot r_*^2 - (1 - r_*^2)/\ln(r_*)}{1 + r_*^2 + (1 - r_*^2)/\ln(r_*)}\right) \tag{33}$$

$$Nu_\infty = 4.224 - 1.492 \cdot r_*^{-1/3} + 1.972 \cdot r_*^{-2/3} + 0.1370 \cdot r_*^{-1} \tag{34}$$

$$O_{Lev} = Nu_\infty^2 \big/ 310 + 0.911 \cdot Nu_\infty - 4.81 \quad (4 < Nu_\infty < 24) \tag{35}$$

$$n = A^3 \cdot exp(fRe_D / 350 + 3.6) \quad (70 < fRe_D < 400) \tag{36}$$

$$Gz_{Li} = D_h \cdot Re_{D,Li} \cdot Pr_{Li} / L_i \tag{37}$$

Where A is the same constant factor than before (equal to 0.40377), r_* is the ratio between the inner and outer radius (i.e., between de radius of the cooling tube and the carbonator tube, Eq.

(38)), $Re_{D,Li}$ is the Reynolds number based on the hydraulic diameter at the axial position L_i (Eq. (39)), and Pr is the Prandtl number at the axial position L_i (Eq. (40)):

$$r_* = r_{cf} \big/ r_c \quad (1/50 \leq r_* < 1) \tag{38}$$

$$Re_{D,Li} = \frac{\dot{m}_{Li} \cdot D_h}{S_{eff} \cdot \mu_{Li}} \tag{39}$$

$$Pr_{Li} = Cp_{Li} \cdot \mu_{Li} / k_{Li} \tag{40}$$

Alternatively, in the case of a tube bundle configuration with longitudinal flow, the Nusselt number is calculated through the correlations of Taborek [36]. Taborek only provided the correlations for the average Nusselt number over the total length of the reactor, instead of the local Nusselt number at position L_i. The correlation for the laminar region follows Eq. (41), which will be the case of our reactor (correlations for the transition and turbulent flow can be seen in Ref. [36]):

$$\overline{Nu}_{L(bundle)} = \left[Nu_\infty^3 + 9.261 \cdot Re_{D,L} \cdot Pr_L \cdot D_h / L \right]^{1/3} \quad (Re_D < 500) \tag{41}$$

Where Nu_∞ is equal to 4.12 (in this case, it represents the solution as Re tends to 0), $Re_{D,L}$ is the Reynolds number calculated as Eq. (39) with the corresponding $D_{h(bundle)}$ of Eq. (30), Pr_L is the
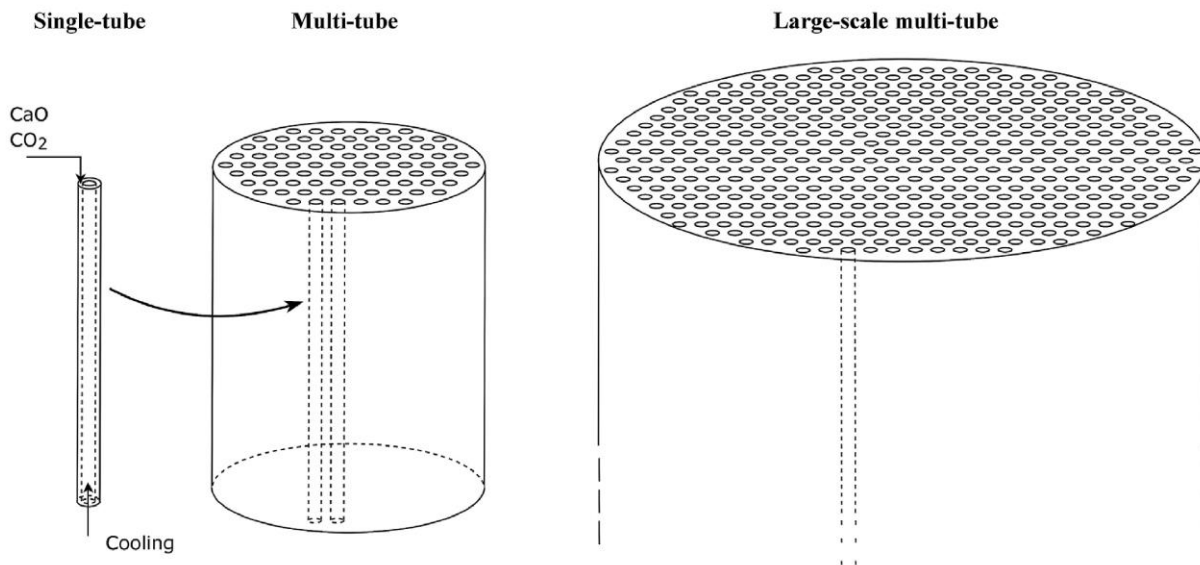

Fig. 7. Carbonator configurations for small and large scale.

Prandtl number as Eq. (40), D_h is the hydraulic diameter for tube bundle (Eq. (30)) and L is the total length of the reactor.

In order to compute the local Nusselt number for the tube bundle configuration, the correlation of Taborek can be differentiated according to Eq. (42) [37] (note that this expression is only valid for ducts of constant wall temperature):

$$Nu_{Li} = \frac{d}{dL}\left(\overline{Nu}_L \cdot L\right)\Big|_{L=L_i} \tag{42}$$

Thus, the local Nusselt number in a tube bundle (shell side) can be computed through Eq. (43) as:

$$Nu_{Li(bundle)} = \frac{Nu_\infty^3 + 6.174 \cdot Gz_{Li}}{\left(Nu_\infty^3 + 9.261 \cdot Gz_{Li}\right)^{2/3}} \quad (Re_D < 500) \tag{43}$$

where Nu_∞ is equal to 4.12 and the Graetz number is calculated with Eq. (37) using the corresponding $D_{h(bundle)}$ of Eq. (30).

3.1.4.2. Cooling side. The heat conducted through the wall separating the cooling and reactants is given by Eq. (44), which allows computing the temperature of the wall side that is in contact with the cooling fluid, T_{ow}:

$$\frac{\dot{q}'_{L_i}}{N} = \frac{T_{iw,L_i} - T_{ow,L_i}}{R_{tube} \cdot L_i} \tag{44}$$

$$R_{tube} = \frac{ln\left(\frac{r_{out}}{r}\right)}{2\pi \cdot k_{tube} \cdot L_i} \tag{45}$$

where R_{tube} is the thermal resistance of the cooling tube, r_{out} and r the outer and inner radius of the cooling pipe, N the number of cooling tubes, and k_{tube} the thermal conductivity of the tube (0.025 kW/m·K).

Once the temperature of the inner wall of the cooling tube is known, the energy balance on the cooling fluid is performed, by Eq. (46):

$$Cp_{cf} \cdot \dot{n}_{cf} \cdot \left(T_{cf,L_i-1} - T_{cf,L_i}\right) = \dot{q}'_{L_i} \cdot (L_i - L_{i-1}) \tag{46}$$

where Cp_{cf} and $\dot{n}_{cf}$ are the specific heat and mole flow of the cooling fluid. It should be noted that Eq. (46) is valid for a countercurrent heat exchange, and therefore it is heated from position L_i to L_{i-1} (carbonation goes from position L_{i-1} to L_i).

The heat transferred to the cooling fluid per unit of axial length, Eq. (47), is composed by the convective and radiative terms:

$$\dot{q}'_{L_i} = \dot{q}'_{rad,\,cf,L_i-1} + \dot{q}'_{conv,cf,L_i-1} \tag{47}$$

Radiation is given by Eq. (48):

$$\dot{q}'_{rad,\,cf,L_i-1} = \frac{\varepsilon_w}{1 - (1 - \varepsilon_w)\left(1 - A_{vcf,L_i}\right)} \\ \cdot \sigma \cdot \left(A_{vcf,L_i} \cdot T^4_{ow,L_i} - \varepsilon_{cf} \cdot T^4_{cf,L_i}\right) \cdot \ell_{cf} \tag{48}$$

where $A_{v,cf}$ is the geometry-dependent absorptance of the cooling fluid (calculated through Eq. (22), since we assume CO_2 as cooling fluid), ε_w the emissivity of the wall, σ is the Stefan-Boltzmann constant, T_{ow} is the temperature of the wall in contact with the cooling fluid, and T_{cf} is the temperature of the cooling fluid. The variable ℓ is defined in such a way that $\ell = \bar{a}/(L_i - L_{i-1})$, and $\bar{a}$ is the surface area where the heat transfer takes place within the slice. In the section of Eq.

Regarding convection, which is the other term of heat flow in Eq.

$$\dot{q}'_{conv,cf,L_i-1} = h_{cf,L_i-1} \cdot \left(T_{ow,L_i} - T_{cf,L_i-1}\right) \cdot \ell_{cf} \tag{49}$$

where h_{cf} is the convective coefficient of the cooling fluid, T_{ow} is the temperature of the wall in contact with the cooling fluid, and T_{cf} is the temperature of the cooling fluid. The variable ℓ is defined in such a way that $\ell = \bar{a}/(L_i - L_{i-1})$, and $\bar{a}$ is the surface area where the heat transfer takes place within the slice, which depends on the geometry of the reactor.

The convective coefficient at each axial position is calculated by Eq. (27), with the corresponding D_h computed with Eq. (28). In the cooling side, we have a circular tube configuration, so the hydraulic diameter is the one presented in Eq. (50):

$$D_{h(tube)} = 2 \cdot r_{cf} \tag{50}$$

The Nusselt number for this configuration is calculated through the correlation of Nellis G and Klein S (Eq. (51)) [34]. This expression provides the average Nusselt number over the length of the cooling tube, assuming constant temperature wall:

$$\overline{Nu}_{L(tube)} = 3.66 + \frac{(0.049 + 0.020/Pr_L) \cdot Gz_L^{1.12}}{1 + 0.065 \cdot Gz_L^{0.7}} \tag{51}$$

To compute the local Nusselt number at an axial position L_i, Eq. (42) is used, obtaining the following expression (Eq. (52)):

$$Nu_{Li(tube)} = 3.66 \\ + \frac{Gz_{Li}^{1.12} \cdot \left(1.8473 \cdot Gz_{Li}^{0.7} \cdot Pr_{Li} + 0.754 \cdot Gz_{Li}^{0.7} - 5.88 \cdot Pr_{Li} - 2.4\right)}{10^3 \cdot Pr_{Li} \cdot \left(1 + 0.065 \cdot Gz_{Li}^{0.7}\right)^2} \tag{52}$$

where the Graetz and Prandtl numbers are calculated with Eq. (37) and Eq. (40).

With this methodology, the temperature along the carbonator can be calculated by knowing the initial temperature of reactants and cooling fluid.

3.2. Design criteria at different scales

The scale of the system is characterized by the solar power available in the calciner, $\dot{Q}_{CL}$ (from 10 kW to 100 MW). The corresponding input flows of CaO and CO_2 entering the carbonator (at nominal load) are computed through the energy balance in the calciner (Eq. (53)).

$$\dot{Q}_{CL} = h_{CaO}^{(950°C)} \cdot \dot{n}_{CaO,c,0} + h_{CO2}^{(950°C)} \cdot \dot{n}_{CO2,c,0} + h_{CaO}^{(950°C)} \cdot \dot{n}_{CaO,p} \\ - h_{CaCO3}^{(850°C)} \cdot \dot{n}_{CaCO3,c,out} - h_{CaO}^{(850°C)} \cdot \dot{n}_{CaO,c,out} \\ - h_{CaCO3}^{(25°C)} \cdot \dot{n}_{CaCO3,f} \tag{53}$$

where h_j^T is the specific enthalpy of the component j at temperature T, $\dot{n}_{j,c,0}$ is the mole flow of component j entering the carbonator (which are outlet flows in the calciner), $\dot{n}_{j,c,out}$ is the mole flow of component j exiting the carbonator (which are inlet flows in the calciner), $\dot{n}_{CaO,p}$ is the lime purged after exiting the calciner, and $\dot{n}_{CaCO3,f}$ is the fresh limestone introduced in the calciner to replace the purge. All these mole flows can be written as a function of $\dot{n}_{CaO,c,0}$ (Eq. (54) to Eq. (57)) by fixing the conversion achieved in the carbonator (assumed as $X_K = 0.1354$) and the CaO:CO_2 molar ratio

11

$(R = 6.8776)$.

$$\dot{n}_{CO2,c,0} = \frac{\dot{n}_{CaO,c,0}}{R} \qquad (54)$$

$$\dot{n}_{CaCO3,c,out} = \dot{n}_{CaO,c,0} \cdot X_K \qquad (55)$$

$$\dot{n}_{CaO,c,out} = \dot{n}_{CaO,c,0} \cdot (1 - X_K) \qquad (56)$$

$$\dot{n}_{CaO,p} = \dot{n}_{CaCO3,f} = \dot{n}_{CaO,c,0} \cdot \left(\frac{1}{R} - X_K \right) \qquad (57)$$

Operating in Eq. (53) and using enthalpy data from Aspen Plus database, it is found Eq. (58) and Eq. (59) for the calculation of the nominal input flows of CaO and CO_2 in the carbonator as a function of the solar power entering the calciner.

$$\dot{n}_{CaO,c,0} = \frac{\dot{Q}_{CL}}{32,162.19 \left[\frac{kJ}{kmol} \right]} \quad or \quad \dot{m}_{CaO,c,0} = \frac{\dot{Q}_{CL}}{573.53 \left[\frac{kJ}{kg} \right]} \qquad (58)$$

$$\dot{n}_{CO2,c,0} = \frac{\dot{Q}_{CL}}{221,198.68 \left[\frac{kJ}{kmol} \right]} \quad or \quad \dot{m}_{CO2,c,0} = \frac{\dot{Q}_{CL}}{5,027.24 \left[\frac{kJ}{kg} \right]} \qquad (59)$$

In addition to the input flow calculation, some design criteria have been followed to keep similar conversion and temperature profiles along the reactor at different scales. First, a single tube reactor with inner cooling has been modelled, looking for proper heat removal at small scale (10 kW). This reactor is made of two concentric tubes of small diameter. The reactants flow from top to bottom through the outer tube, while cooling fluid flows in counter-current throughout the inner tube (Fig. 7). The aim is to recover few kW at this stage. The required input flows for 10 kW are 0.0174 kg/s of CaO and 0.0020 kg/s of CO_2.

Once proper dimensions are fixed for single-tube, a multi-tube configuration is stablished. This multi-tube reactor encloses 150–200 cooling tubes, between which the reactants flow from top to bottom. In principle, the cooling pipes are of the same diameter and length that the one used in single-tube configuration (the enclosure is also of the same length than the cooling pipes). The cooling tubes are set in triangular configuration and the distance among them is fixed in order to keep the cross-sectional area in proportion to the increment of reactants volume. In other words, the cross-sectional area through which the reactants flow is N times the area of the single tube configuration, being N the number of cooling tubes inside the enclosure of the multi-tube. This configuration is aimed to reach the MW scale (about $\dot{Q}_{CL} = 2$ MW), by keeping similar temperature profiles along the reactor.

Lastly, the large-scale multi-tube configuration is designed by keeping constant the ratio between the length of the reactor and the velocity of the gas-solid mixture flowing downward (L/v), and the ratio between the length of the reactor and the diameter of the enclosure (L/d) [38]. Besides, the number of cooling tubes is increased, instead of increasing their diameter. The aims of this configuration is to achieve the 100 MWth scale and to quantify the behavior at partial load. Again, we look for conserving temperature profiles, and outlet temperatures of both products and cooling fluids, since power production is the main objective of this reactor.

3.3. Operation modes and efficiency definitions

The two operations considered in this study are energy storage

operation mode (ESOM) and energy release operation mode (EROM). Under these modes, a large number of operation points leads to different pairs of calciner-carbonator powers and different values of storage power. The operation points are related to the mass flowrates stored or released from the tanks.

3.3.1. Energy storage operation mode

Two parameters are used to describe the operation points of ESOM: the fraction of the lime produced in the calciner that is sent to storage, and the fraction of limestone in the tank that is discharged.

The storage fraction of lime, $f_{st,CaO}$ in Eq. (60), is the ratio between the mass flowrate diverted to the CaO storage tank and the maximum mass flowrate that could leave the calciner operating at full capacity (100 MW).

$$f_{st,CaO} = \frac{\dot{m}_{CaO,st}}{\dot{m}_{CaO,max}} \qquad (60)$$

The discharge fraction of limestone, $f_{dch,CaCO3}$ in Eq. (61), is the ratio between the mass flowrate discharged from the limestone tank and the maximum mass flowrate that could leave the carbonator operating at full capacity.

$$f_{dch,CaCO3} = \frac{\dot{m}_{CaCO3+CaO,dch}}{\dot{m}_{CaCO3+CaO,max}} \qquad (61)$$

All the potential pairs of these two parameters cover the operation points encompassed during ESOM.

The specific storage consumption (SSC) expressed in Eq. (62) provides the amount of total energy (thermal and electrical) required to store a mass unit of lime. This value is useful to understand whether the storage process is profitable or not in terms of energy under specific operation points. It must be kept in mind the qualitative interest of the parameter but its limitation as quantitative measure given the mix of energy types in its definition. The energy consumed in the process includes the fraction of heat used to produce the lime sent to the storage tank ($\dot{Q}_{CL,st}$), the preheating of the limestone discharged from the storage tank which is later stored in the form of lime ($\dot{Q}_{HE\ ER\ CaCO3,st}$) and the electric power demanded in the compression of the stored carbon dioxide ($\dot{W}_{compressor}$).

$$SSC = \frac{\dot{Q}_{CL,st} + \dot{Q}_{HE\ ER\ CaCO3,st} + \dot{W}_{compressor}}{\dot{m}_{CaO,st}} \qquad (62)$$

A storage efficiency, η_{st}, is defined by Eq. (63) to compare the amount of stored energy and the net energy consumed during the storage process. The stored energy comprises the sensible heat of the stored substances (lime and carbon dioxide, $CS_{CO2+CaO,st}$) and the chemical energy potentially stored in the lime which will be latter carbonated, $\alpha H_R^0 \alpha \dot{n}_{CaCO3,CR}$. This parameter provides an idea of the portion of energy that is stored and the portion that is lost during the storage process.

$$\eta_{st} = \frac{\dot{Q}_{st,CaO}}{\dot{Q}_{CL,st} + \dot{Q}_{HE\ ER\ CaCO3,st} + \dot{W}_{compressor}}$$

$$= \frac{CS_{CO2+CaO,st} + \Delta H_R^0 \cdot \dot{n}_{CaCO3,CR}}{\dot{Q}_{CL,st} + \dot{Q}_{HE\ ER\ CaCO3,st} + \dot{W}_{compressor}} \qquad (63)$$

Another significant value for the operation is the efficiency of the carbonator in reference to the energy provided by this equipment, η_{CR}, Eq. (64). It compares the amount of power released in the carbonator and the energy invested. The latter includes the heat of

calcination required to produce the lime fed into the carbonator, $\dot{Q}_{CL,CR}$, and the preheat of this limestone prior the calciner, $\dot{Q}_{HE\ ER\ CaCO3,CR}$.

$$\eta_{CR} = \frac{\dot{Q}_{CR}}{\dot{Q}_{CL,CR} + \dot{Q}_{HE\ ER\ CaCO3,CR}} \qquad (64)$$

Finally, an efficiency related to the available thermal energy is defined by Eq. (65). This efficiency compares the available heat to the energy invested. The available heat accounts for the thermal power released in the carbonator, and the thermal power provided by the different heat exchangers (EE heat exchangers always provide thermal power, while ER heat exchangers only provide thermal power under ESOM).

$$\eta_{av(ESOM)} = \frac{\dot{Q}_{CR} + \sum \dot{Q}_{HE\ EE} + \dot{Q}_{HE\ ER\ CO2} + \dot{Q}_{HE\ ER\ CaO}}{\dot{Q}_{CL} + \dot{Q}_{HE\ ER\ CaCO3}} \qquad (65)$$

3.3.2. Energy release operation mode

Analogously, the storage fraction of the limestone produced in the carbonator, Eq. (66), and the discharge fraction of lime from the storage tanks, Eq. (67), describe the set of operation points that conform the energy release operation mode.

$$f_{st,CaCO3} = \frac{\dot{m}_{CaCO3+CaO,st}}{\dot{m}_{CaCO3+CaO,max}} \qquad (66)$$

$$f_{dch,CaO} = \frac{\dot{m}_{CaO,dch}}{\dot{m}_{CaO,max}} \qquad (67)$$

The storage fraction of limestone, $f_{st,CaCO3}$, represents the ratio between the mass flowrate diverted to the storage tank from the outlet stream of the carbonator and the maximum mass flowrate which could leave the carbonator operating at full capacity. The discharge fraction of lime, $f_{dch,CaO}$, is the relation between the mass flowrate discharged from the CaO tank and the maximum mass flowrate of CaO leaving the calciner at full load.

The energy efficiency in the carbonator, η_{CR}, under EROM is calculated through Eq. (68). The energy invested in this process includes (i) all the heat of calcination demanded in the calciner, $\dot{Q}_{CL}$, (since no calcined material is diverted to storage tanks under EROM) (ii) the storage consumption of the mass flowrate of lime discharged from the tanks, (iii) the preheating of this limestone before introduced into the calciner, $\dot{Q}_{HE\ ER\ CaCO3}$ and (iv) the preheating of the mass flowrates of lime and carbon dioxide, $\dot{Q}_{HE\ ER\ CO2}$ and $\dot{Q}_{HE\ ER\ CaO}$ (if needed).

$$\eta_{CR} = \frac{\dot{Q}_{CR}}{\dot{Q}_{CL} + SSC \cdot \dot{m}_{CaO,dch} + \dot{Q}_{HEERCaCO3} + \dot{Q}_{HEERCO2} + \dot{Q}_{HEERCaO}} \qquad (68)$$

Under EROM, the thermal efficiency of the system is defined by Eq. (69). In this case, the available heat only includes the thermal power from the carbonator and EE heat exchangers.

$$\eta_{av(EROM)} = $$
$$\frac{\dot{Q}_{CR} + \sum \dot{Q}_{HE\ EE}}{\dot{Q}_{CL} + \dot{Q}_{HE\ ER\ CaCO3} + SSC \cdot \dot{m}_{CaO,dch} + \dot{Q}_{HE\ ER\ CO2} + \dot{Q}_{HE\ ER\ CaO}} \qquad (69)$$

3.4. Sizing of storage tanks

The sizing of storage tanks accounts for the operating mode and the introduced/extracted mass flowrates of CO_2, CaO and $CaCO_3$. The operating mode dictates the number of hours and the storage/discharge fractions. Storage and discharge fractions directly define the inlet and outlet flowrates, while the number of hours provides the time interval to integrate. The storage volume of the tanks is calculated through Eq. (70).

$$V_{st}(t) = \int_{t_0}^{t} \left(\frac{\dot{m}_{in} - \dot{m}_{out}}{\rho} \right) dt + V_{st,0} \qquad (70)$$

The maximum storage flowrate of CO_2 and CaO takes place when solar calciner operates at nominal load and carbonator operates at minimum load.

4. Results

In this section, the model validation and the results for the small- and large-scale carbonators are presented. Besides, it is assessed the partial load operation for the large-scale carbonator. Lastly, a model of the coupled CaL TCES and CSP systems is run at threshold operation conditions to provide the sizing of storage tanks.

4.1. Model validation

The first important issue to be validated is the independency of results with respect to the number of discretized elements (i.e., with the length of each discretized slice). As case of study, it has been chosen the single-tube configuration operating at 50% partial load (the part load in the carbonator is defined as the ratio between the input mass flow and the nominal input mass flow). Fig. 8 presents the relative error that exists in the most important computed variables versus the number of discretization elements, with respect to 300 discretization elements (in a 4-m reactor, the latter means slices of 1.3 cm). It can be seen that the relative error
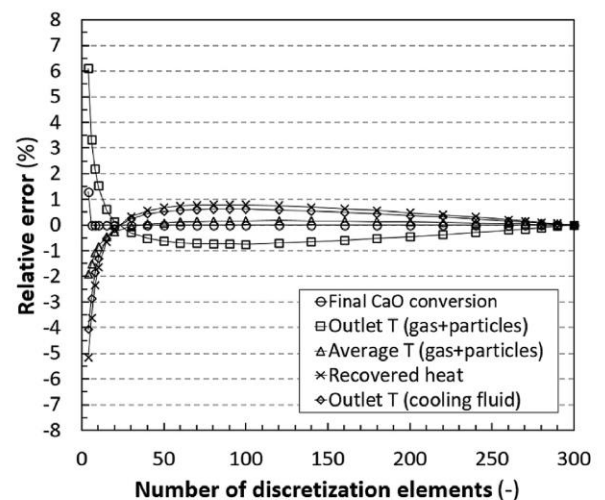

Fig. 8. Relative error in the most relevant computed variables vs. the number of discretization elements (with respect to 300 discretization elements).
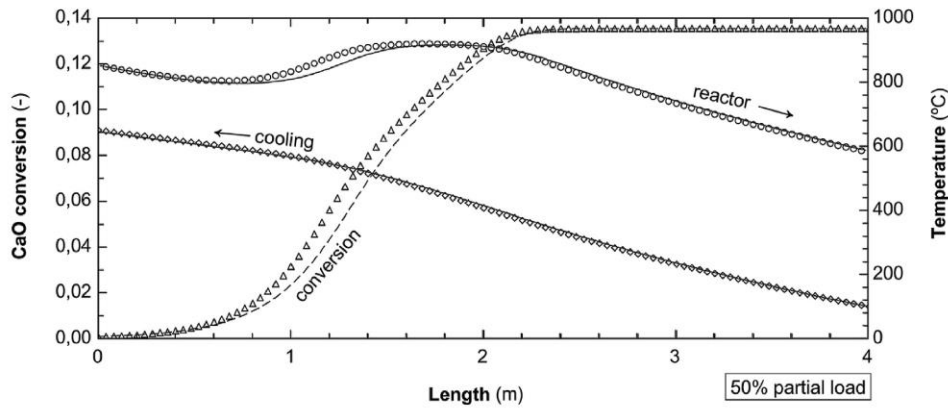
Fig. 9. Comparison between 100 (symbols) and 300 (lines) discretization elements, for the results on CaO conversion and temperature profiles (reactor and cooling sides) vs. length (from top to bottom), in a single-tube carbonator operating at 50% partial load.
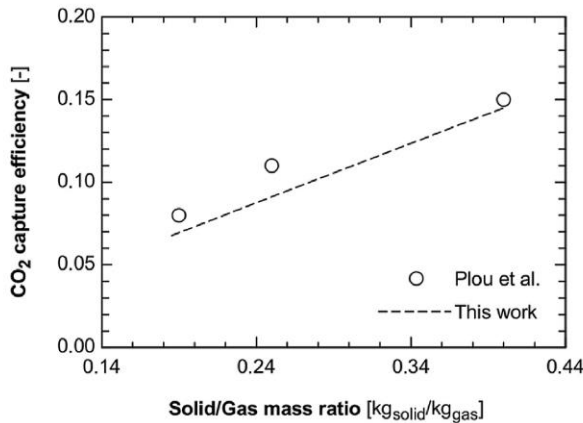

Fig. 10. CO_2 capture efficiency achieved in the entrained flow reactor of Plou et al. [39] *and in the simulations of this study under the same setup, as a function of the solid/gas mass ratio.*

remains below 1% in all cases whenever the number of discretization elements is above 15. Therefore, we select 100 discretization elements for the simulations presented in Section 4.2.

These small variations in the computed variables come from assuming constant volume flow in Eq. (8) when integrating over the length of each discretized element. This can be clearly seen in Fig. 9 when comparing the temperature and conversion profiles of a simulation with 100 discretization elements (depicted with symbols) with a simulation with 300 discretization elements (depicted with lines). In those regions in which the variation of volume flow occurs faster (i.e., with higher reaction rates), the error becomes noticeable. It must be noted that, since the case chosen as example is operating at 50% partial load, the reaction occurs in a shorter length, what accentuates the relative error. If the reactor operates at full load, the variation in volume is less steep, and the error less significant.

Furthermore, the selected operating conditions in our simulations make CO_2 to react almost completely, so any variation in volume flow is remarkable compared to the total volume flow in the reactor. This makes the relative error to be more significant. Still, our simulation keeps relative errors below 1% in the variables

of interest. In the case of analysing a reactor setup with higher ratio of CO_2:CaO, the error would be even lower.

The second important issue to be validated is the reproducibility of experimental results. In this aspect, the model is validated using experimental results of an entrained flow carbonator from Plou et al. [39]. The reactor of Plou et al. is a 24-m spiral-shaped stainless steel tube, with an external diameter of 3/8" (inner diameter of 7.54 mm). The gas velocity used during the experiments avoids saltation conditions within the entrained flow regime (i.e., avoids falling of particles towards the wall). The reactor is kept isothermal at 650 °C along the whole path. Three different materials were analyzed: two types of high-purity calcined lime and one cement raw meal. The results of the material tagged as "Lime #1" are used in this study for comparison as it has a similar value of X_k (i.e., conversion at the end of the reaction controlled phase) and t_0 (i.e., the time taken to reach a $X_k/2$ conversion) than the material assumed in the simulations of this study. Lime #1 has $X_k = 0.10$ and t_0 about 2 s, while the material used in our simulations has $X_k = 0.1354$ and $t_0 = 1.515$ seconds. These are typical conversions of highly deactivated materials.

Fig. 10 shows the CO_2 capture efficiency, which is defined as the CO_2 captured versus the maximum possible according to the equilibrium. The experiments were carried out with a gas velocity of 13.5 m/s at 650 °C and 1 bar (about $2.4 \cdot 10^{-4}$ kg/s). The gas is composed of 10% CO_2 and 90% air. The mass ratio between the solid and the gas was varied between 0.125 and 0.400 by modifying the mass of CaO entered in the reactor.

The results show a good agreement with the experiments of Plou et al. for Lime #1. The measured residence time is 1.8 s, while the simulated residence time 1.78 s for the gas and 1.77 s for the solids.

4.2. Carbonator assessment

The technical data regarding the three carbonators under study are presented in Table 2 (single-tube at lab scale, 7.6 kW, multi-tube at pilot scale, 1.4 MW, and the large-scale multi-tube, 79.9 MW). The reactants enter at 850 °C and 2 bar, and the cooling fluid is CO_2 entering at 100 °C and 50 bar. The mass of the cooling fluid is calculated to set its exit temperature at 650 °C.

The CaO conversion and temperature profiles along the reactor are preserved at the different scales (Fig. 11). At pilot scale (multi-tube reactor), the convective coefficient diminishes one order of magnitude in the reactants side; i.e. shell side. Therefore, the

14

Table 2
Technical data of the studied carbonators.

	Single-tube	Multi-tube	Large-scale multi-tube	
Carbonator				
Length (m)	4.0	5.0	15.0	Design criteria (Section 3.2)
Enclosure inner diameter (m)	0.074	0.970	3.3	Design criteria (Section 3.2)
CaO mass inlet (kg/s)	0.01740	3.2533	178.6	Eq. (58)
CO_2 mass inlet (kg/s)	0.00198	0.3712	20.8	Eq. (59)
Final CaO conversion (%)	13.53	13.54	13.54	Output of the model
Gas residence time (s)	7.1	10.0	7.55	Output of the model
Solid residence time (s)	4.8	6.6	6.51	Output of the model
Inlet T (°C)	850.0	850.0	850.0	Boundary condition
Outlet T (°C)	850.7	844.8	841.1	Output of the model
Average T (°C)	850.8	871.5	850.6	Output of the model
Pressure (bar)	2.0	2.0	2.0	Fixed
Reynolds (−)	34−493	0.4−5.5	1.5−21.3	Output of the model
Cooling tubes				
Length (m)	4.0	5.0	15.0	Design criteria (Section 3.2)
Inner diameter (m)	0.02	0.02	0.02	Design criteria (Section 3.2)
Number of tubes (−)	1	187	2705	Design criteria (Section 3.2)
CO_2 mass inlet (total) (kg/s)	0.0121	2.32	127.4	Output of the model (fixed $T_{cf,0}$)
Recovered heat (MW)	0.0076	1.45	79.9	Output of the model
Inlet T (°C)	100.0	100.0	100.0	Boundary condition
Outlet T (°C)	650.0	650.0	650.0	Fixed
Pressure (bar)	50.0	50.0	42.8−50.0	Output of the model
Reynolds (−)	9862−19,995	10,098−20,476	38,411−77,804	Output of the model

reactor has to be extended 1 m in length (from 4 m in single tube to 5 m in multi-tube) in order to bring the products again to 850 °C and thus recover their sensible heat. Otherwise, part of the exothermal heat from carbonation would not be recovered in the reactor.

Besides, when following the criteria of constant L/v and L/d ratios to pass from mid to large scale, the mass of cooling fluid per tube has to be increased to maintain its exit temperature at 650 °C. Doing so, the length of the reactor can be shortened to 15 m (instead of the 19 m that would result from the L/d restriction). The final configuration is suitable for a large-scale carbonation, in terms of operating temperature (average 850.6 °C, computed as $\sum_{i=1}^{100} T_{Li}/100$), residence time (6.5−7.5 s) and dimensions (15 m length and 3.3 m diameter).

Once the reactor at large-scale is defined, partial load operation is assessed (the part load in the carbonator is defined as the ratio between the input mass flow and the nominal input mass flow). Reducing the load in the carbonator means that the inlet mass flowrates of reactants are proportionally reduced, so the available exothermal heat from carbonation will diminish. Therefore, the amount of cooling fluid that can be heated diminishes (always keeping its exit temperature at 650 °C). The definition of minimum partial load of the reactor corresponds with the point in which the cooling mass flowrate is reduced to the half of its nominal value; i.e. the minimum flowrate of cooling fluid will be 63.7 kg/s of CO_2 at 650 °C (below this mass flow we assumed that the coupling with the power block cannot longer take place) [40]. This point corresponds to a partial load of 23.9% in the carbonator (Fig. 12) (only the 23.9% of the nominal input flow of CO_2 and CaO is entering the carbonator).

When load is reduced, the volume of reactants is lowered and so does their velocity throughout the reactor. The reaction ends earlier, and the cooling fluid starts recovering sensible heat from the products. Fig. 13 illustrates this fact for a 50% partial load. Thus, the total recovered heat does not diminish linearly with part load (see Fig. 12), and follows Eq. (71) when fitted to a polynomial expression by the least squares method.

$$\dot{Q}_c = 3.27 + 184.5 \cdot \text{load} - 137.8 \cdot \text{load}^2 + 30.0 \cdot \text{load}^3 \qquad (71)$$

4.3. Plant management and size of storages

The distribution of storage and discharge fractions versus carbonator and calciner loads are shown in Fig. 14. Under energy storage mode, the storage fraction of the lime ($f_{st,CaO}$) and CO_2 ($f_{st,CO2}$) is maximum for those operating regions in which the load of the calciner is high while the load of the carbonator is low. In the same way, the $CaCO_3$ discharge fraction ($f_{dch, CaCO3}$) from its storage tank increases from 0 to 1 if the calciner load rises and the carbonator load is reduced. However, since the minimum partial load of the carbonator is 23.9% according to our design, the maximum storage fraction of lime and CO_2 and the maximum discharge fraction of $CaCO_3$ will be 0.761. Regarding the release operation mode, the discharge fraction of the lime ($f_{dch,CaO}$) and CO_2 ($f_{dch,CO2}$) from storage tanks is maximum for operating points with low calciner and high carbonator loads. Likewise, the storage fraction of the $CaCO_3$ ($f_{st,CaCO3}$) obtained through carbonation increases from 0 to 1 if the calciner load is reduced and the carbonator load rises. These storage and discharge fractions operation maps are useful to establish how to operate the plant and manage the storage.

The maximum storage flowrates of CO_2, CaO and limestone are illustrated in Fig. 15 (assuming 0 void fraction inside the tanks of the solids). The maximum storage volumes are obtained applying Eq. (70) when solar calciner operates at nominal load and carbonator operates at its minimum operation load. The CaO density considered to calculate the volumetric flowrate is 1800 kg/m³, the density of $CaCO_3$ is 2710 kg/m³, and the void fraction inside the tank is 30% [41]. Tank sizes ranges from 330 to 514 m³ for 1 h of storage operation, and up to 5700−11,400 m³ for 15 h. In the latter case, the storing volume required is 8256 m³ for CO_2 in gas phase, 5824 m³ for CaO and 7926 m³ for the mixture of CaO−$CaCO_3$.

It should be noted that, when stored, the apparent density of a solid material is reduced due to the void space between particles. In a randomly packed bed of spheres, the apparent density can be reduced up to 60% [41]. This effect has not been taken into account in the data presented in Fig. 15, but it has been considered in the
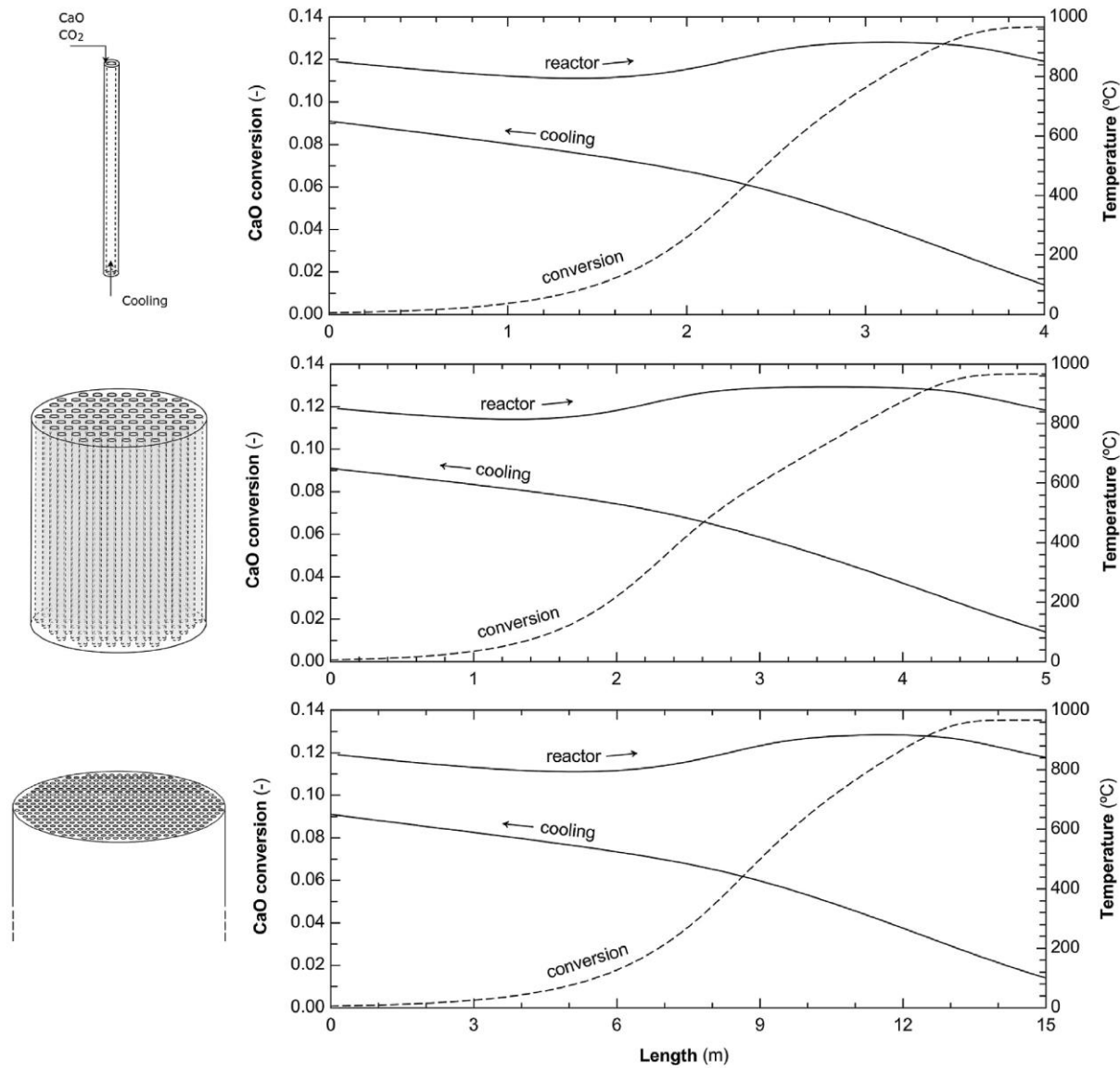
Fig. 11. CaO conversion and temperature profiles (reactor and cooling sides) vs. length (from top to bottom) for the single-tube, multi-tube and large-scale multi-tube configurations. Profiles are kept similar at the different scales (arrows depict the direction of the flow).

data presented in the text.

4.4. Overall efficiency of the plant at part load

The efficiencies defined to characterize the plant operation present differences between the energy storage mode and discharge mode. Under energy storage mode, the specific storage consumption (Eq. (62)) has been calculated for each possible pair of carbonator/calciner loads, ranging from 770 MJ/t_{CaO} to 1324 MJ/t_{CaO}. The minimum specific storage consumption corresponds to high carbonator load, while the maximum value refers to operating points in which carbonator reactor is shut-down.

The specific storage consumption is related to the energy storage efficiency. The distribution of the energy storage efficiency

versus carbonator and calciner loads is shown in Fig. 16. The maximum storage efficiency (76%) is obtained when the solar calciner operates at nominal load and the carbonator load is 90%, which corresponds to the minimum specific storage consumption. The lower is the storage of CaO and CO_2, the lower is the energy consumed in the energy storage process.

The carbonator efficiency as a function of the carbonator and calciner loads is illustrated in Fig. 17. The carbonator efficiency is clearly differentiated according to the operating mode in which the system is located (storage or release). For each possible pair of carbonator/calciner loads, the carbonator efficiency is obtained applying Eq. (68) if there is energy discharge and Eq. (64) if there is energy storage. Under energy release mode, the carbonator efficiency is reduced for high carbonator and low calciner loads. This
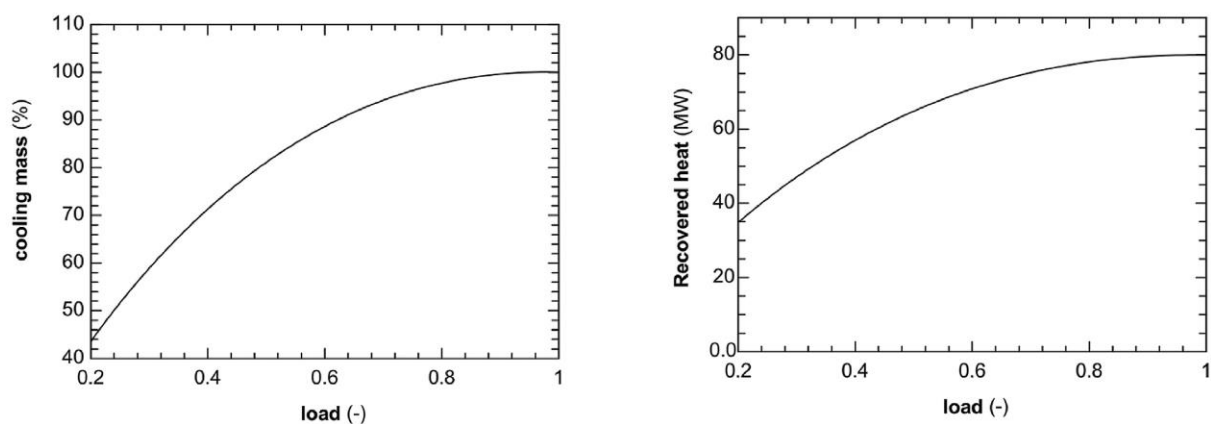
Fig. 12. Cooling mass flow and recovered heat vs. operating load (ratio between the input mass flow in the carbonator and its nominal input mass flow) for the large-scale multi-tube. Outlet temperature of cooling fluid is kept at 650 °C.
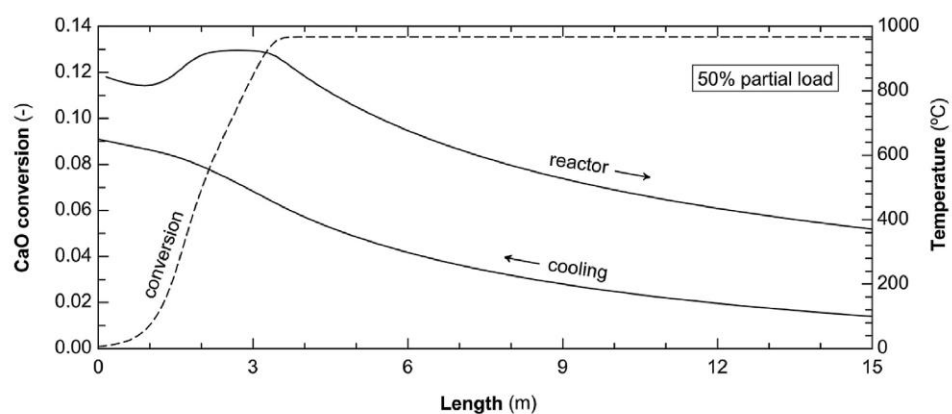
Fig. 13. CaO conversion and temperature profiles vs. length (from top to bottom) for the large-scale multi-tube at 50% partial load (arrows depict the direction of the flow).
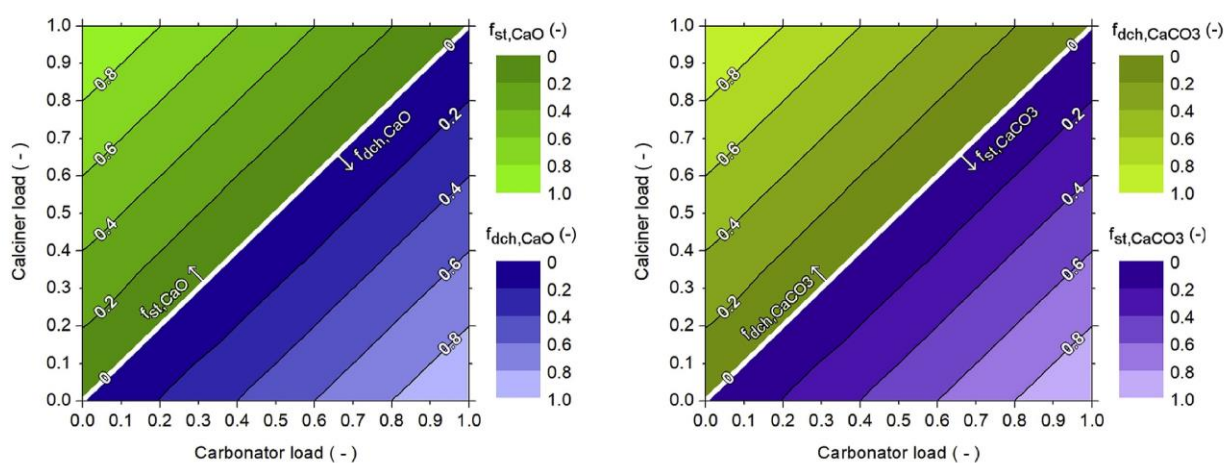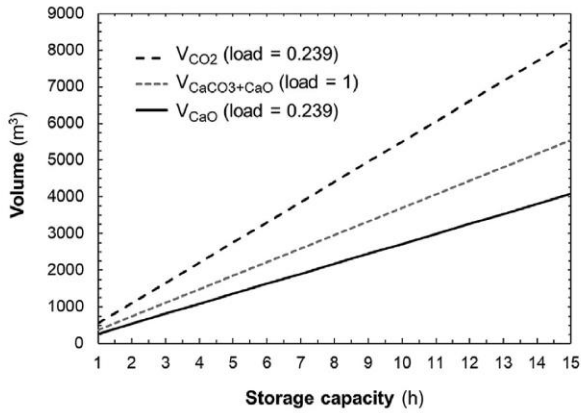

Fig. 14. Storage and discharge fractions operation map.

17

Fig. 15. Maximum storage tanks volumes for different storing timeframes (ideal case with 0 void fraction inside the tank).

Fig. 17. Carbonator efficiency operation map.

Fig. 16. Storage efficiency operation map.
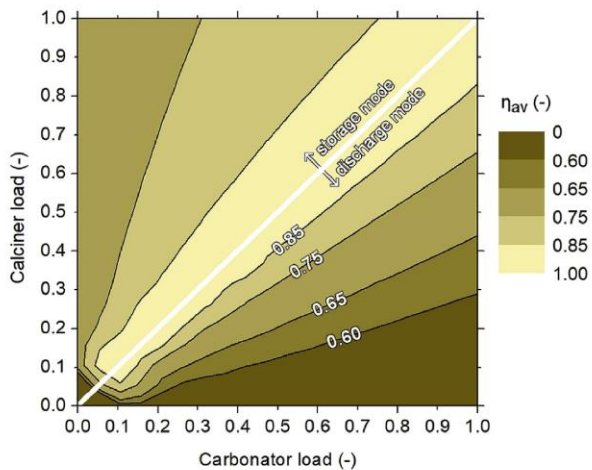
Fig. 18. Available energy efficiency operation map.

occurs because the energy released in the carbonator in that case comes mainly from the tanks (i.e., it is energy that was previously stored). The minimum carbonator efficiency is 20%, which corresponds to the operating point of the maximum energy demand without solar energy available. Regarding energy storage mode, the carbonator efficiency is greater for low calciner and carbonator loads. This occurs because the energy required from the system to release energy in the carbonator is reduced. Theoretically, the maximum carbonator efficiency is 84%, which corresponds to the operating point with a carbonator load of 10% and a calciner load of 20%. However, since the minimum partial load of the carbonator is 23.9% according to our technical design, the maximum carbonator efficiency will be 81%. This corresponds to the operating point with carbonator load of 23.9% and calciner load of 30%. On the other hand, if there is no storage or discharge of energy (i.e., all the energy received in the calciner is directed to the carbonator), the maximum carbonator efficiency (85%) is obtained with carbonator

and calciner loads of 23.9%.

The available energy efficiency of the system as a function of the carbonator and calciner loads is illustrated in Fig. 18. For each pair of carbonator/calciner loads, the available energy efficiency is computed by Eq. (69) when energy discharge takes place and by Eq. (65) when energy is stored. Under energy release mode, the available energy efficiency diminishes at high carbonator and low calciner loads because the energy required by the overall system to produce available energy increases. The minimum available energy efficiency is 55%, which corresponds to the operating point of the maximum energy demand without solar energy available. Regarding energy storage mode, the available energy efficiency increases with energy demand. Theoretically, the maximum available efficiency is 91%, which corresponds to the operating point in which the carbonator load is 20% and the calciner load is 23.9%. However, since the minimum partial load of the carbonator is 23.9% due to technical reasons, the maximum available energy efficiency will be limited to 90%, with a carbonator load of 23.9% and a calciner load of 30%. Besides, in those cases in which all the energy

received in the calciner is directed to the carbonator (there is no release or storage), the maximum available energy efficiency (97%) is obtained with carbonator and calciner loads of 23.9%. Actually, the highest available energy efficiencies are achieved around the operation points in which the circulation of mass flow between calciner and carbonator is almost direct (i.e., either the storage is minimal or the energy discharge is negligible).

5. Conclusions

Two main research gaps were identified in the existing studies of CaL as TCES for CSP: (i) a specific design of large-scale carbonator and (ii) an overall concept analysis accounting the influence of the reactor design on the available heat and the part load operation. Thus, a detailed entrained flow carbonator model was developed to support the scaling-up and design process of a large-scale carbonator. The final industrial design (15 m in length and 3.3 m in diameter) is able to process 187.6 kg/s of CaO and 20.8 kg/s of CO_2 at nominal load, typically operating at 850 °C and 2 bar. It is observed that the carbonation behavior at large scale can be similar to the behavior at small scale; with residence times of 6.5–7.5 s and outlet CaO conversion of 13.5%.

The heat removed from the carbonator through internal cooling tubes (127.4 kg CO_2 with 650 °C outlet temperature) amounts to 80 MWth and is diverted to the power cycle. The minimum part load of the carbonator is achieved for 23.9% of nominal inlet reactants flows. The available heat at this minimum load is 40 MWth since, besides the heat from the carbonation reaction, part of the sensible thermal energy of the reactor is recovered.

In terms of plant management, useful operation maps were obtained to size and manage the storage tanks of the CaL products. To store energy during 15 h of operation in a 100 MWth solar power plant, the required CO_2 tank volume is 8256 m^3, the CaO tank 5824 m^3 and the CaO–CaCO$_3$ tank 7926 m^3. The specific energy demand of storage process ranges between 770 and 1324 MJ/t$_{CaO}$, depending on the calciner and carbonator load. The maximum storage efficiency is 76%.

The carbonator efficiency was mapped versus the calciner and carbonator loads. The highest carbonator efficiencies (80–81%) were obtained at low partial loads. Under release operating mode, the lowest carbonator efficiencies (20–30%) are found for (high-low) values of the pair (carbonator load-calciner load). This situation corresponds to high discharge fractions of CaO and CO_2 from the storage tanks and presents a significant energy demand for their preheating. Under energy storage operation mode, the influence of partial loads on the carbonator efficiency is softer since energy demand for solid preheating plays a minor role in the whole energy balance.

Lastly, the available energy efficiency was calculated (55–97%) and a quite similar behavior for both operation modes was observed. This efficiency is higher when the part loads of both reactors (calciner and carbonator) are similar since lower mass flows have to be discharged and preheated from the storage tanks.

Future research should focus on the energy optimization of the system, the design and sizing of the equipment involved (heat exchangers, calciner, compression-refrigeration train for CO_2 storage, etc.) and the selection of technically feasible operating points under transient operation modes.

Author contribution

Manuel Bailera: Conceptualization, Methodology, Software, Validation, Formal analysis, Writing – original draft, Writing – review & editing, Visualization. Sara Pascual: Conceptualization, Methodology, Software, Formal analysis, Writing – original draft, Writing – review & editing, Visualization. Pilar Lisbona: Conceptualization Methodology, Writing – original draft, Writing – review & editing. Luis M Romeo: Conceptualization, Writing – original draft, Writing – review & editing, Funding acquisition.

Declaration of competing interest

The authors declare that they have no known competing financial interests or personal relationships that could have appeared to influence the work reported in this paper.

Acknowledgments

References

[1] Eurostat. Greenhouse gas emissions by sector (source: EEA) (code: tsdcc210). n.d, http://ec.europa.eu/eurostat/web/environment/air-emissions-inventories/main-tables. [Accessed 17 February 2017]. accessed.

[2] IEA. World. Energy outlook 2018. International Energy Agency; 2018. https://doi.org/10.1787/weo-2018-2-en.

[3] Pierre I, Bauer F, Blasko R, Dahlback N, Dumpelmann M, Kainurinne K, et al. Flexible generation: backing up renewables. 2011.

[4] European Commission. Commission staff working document: energy storage – the role of electricity. 2017.

[5] IEA. Status of power system transformation 2019. Power system flexibility. International Energy Agency; 2019.

[6] Concentrating Solar Power Projects. National Renewable Energy Laboratory; 2018.

[7] Achkari O, El Fadar A. Latest developments on TES and CSP technologies – energy and environmental issues, applications and research trends. Appl Therm Eng 2020;167:114806. https://doi.org/10.1016/j.applthermaleng.2019.114806.

[8] Kearney D, Kelly B, Herrmann U, Cable R, Pacheco J, Mahoney R, et al. Engineering aspects of a molten salt heat transfer fluid in a trough solar field. Energy 2004;29:861–70. https://doi.org/10.1016/S0360-5442(03)00191-9.

[9] Mohan G, Venkataraman MB, Coventry J. Sensible energy storage options for concentrating solar power plants operating above 600 °C. Renew Sustain Energy Rev 2019;107:319–37. https://doi.org/10.1016/j.rser.2019.01.062.

[10] Letcher TM. Storing energy: with special reference to renewable energy sources. Elsevier Inc.; 2016. https://doi.org/10.1515/ci-2016-0627.

[11] Almendros-Ibáñez JA, Fernández-Torrijos M, Díaz-Heras M, Belmonte JF, Sobrino C. A review of solar thermal energy storage in beds of particles: packed and fluidized beds. Sol Energy 2019;192:193–237. https://doi.org/10.1016/j.solener.2018.05.047.

[12] Prieto C, Cabeza LF. Thermal energy storage (TES) with phase change materials (PCM) in solar power plants (CSP). Concept and plant performance. Appl Energy 2019;254:113646. https://doi.org/10.1016/j.apenergy.2019.113646.

[13] Prieto C, Cooper P, Fernández AI, Cabeza LF. Review of technology: thermochemical energy storage for concentrated solar power plants. Renew Sustain Energy Rev 2016;60:909–29. https://doi.org/10.1016/j.rser.2015.12.364.

[14] Chen X, Zhang Z, Qi C, Ling X, Peng H. State of the art on the high-temperature thermochemical energy storage systems. Energy Convers Manag 2018;177:792–815. https://doi.org/10.1016/j.enconman.2018.10.011.

[15] Khosa AA, Xu T, Xia BQ, Yan J, Zhao CY. Technological challenges and industrial applications of CaCO3/CaO based thermal energy storage system – a review. Sol Energy 2019;193:618–36. https://doi.org/10.1016/j.solener.2019.10.003.

[16] Barker R. The reactivity of calcium oxide towards carbon dioxide and its use for energy storage. J Chem Technol Biotechnol 1974;24:221–7. https://doi.org/10.1002/jctb.2720240405.

[17] Ortiz C, Chacartegui R, Valverde JM, Alovisio A, Becerra JA. Power cycles integration in concentrated solar power plants with energy storage based on calcium looping. Energy Convers Manag 2017;149:815–29. https://doi.org/10.1016/j.enconman.2017.03.029.

[18] Tesio U, Guelpa E, Verda V. Integration of ThermoChemical energy storage in concentrated solar power. Part 1: energy and economic analysis/optimization. Energy Convers Manag X 2020:100039. https://doi.org/10.1016/

j.ecmx.2020.100039.

[19] Ortiz C, Romano MC, Valverde JM, Binotti M, Chacartegui R. Process integration of Calcium-Looping thermochemical energy storage system in concentrating solar power plants. Energy 2018;155:535–51. https://doi.org/10.1016/j.energy.2018.04.180.

[20] Chacartegui R, Alovisio A, Ortiz C, Valverde JM, Verda V, Becerra JA. Thermochemical energy storage of concentrated solar power by integration of the calcium looping process and a CO2 power cycle. Appl Energy 2016;173: 589–605. https://doi.org/10.1016/j.apenergy.2016.04.053.

[21] Tesio U, Guelpa E, Verda V. Integration of ThermoChemical energy storage in concentrated solar power. Part 2: comprehensive optimization of supercritical CO2 power block. Energy Convers Manag X 2020;6:100038. https://doi.org/10.1016/j.ecmx.2020.100038.

[22] Bravo R, Ortiz C, Chacartegui R, Friedrich D. Hybrid solar power plant with thermochemical energy storage: a multi-objective operational optimisation. Energy Convers Manag 2020;205:112421. https://doi.org/10.1016/j.enconman.2019.112421.

[23] Zsembinszki G, Sole A, Barreneche C, Prieto C, Fernández AI, Cabeza LF. Review of reactors with potential use in thermochemical energy storage in concentrated solar power plants. Energies 2018;11. https://doi.org/10.3390/en11092358.

[24] Koepf E, Alxneit I, Wieckert C, Meier A. A review of high temperature solar driven reactor technology: 25 years of experience in research and development at the Paul Scherrer Institute. Appl Energy 2017;188:620–51. https://doi.org/10.1016/j.apenergy.2016.11.088.

[25] Karasavvas E, Panopoulos KD, Papadopoulou S, Voutetakis S. Study of a drop-tube carbonator reactor for CSP-calcium looping based on a heterogeneous reaction model. Chem Eng Trans 2019;76:877–82. https://doi.org/10.3303/CET1976147.

[26] Bailera M, Lisbona P, Romeo LM, Díez LI. Calcium looping as chemical energy storage in concentrated solar power plants: carbonator modelling and configuration assessment. Appl Therm Eng 2020:115186. https://doi.org/10.1016/j.applthermaleng.2020.115186.

[27] Rodriguez N, Alonso M, Grasa G, Abanades JC. Heat requirements in a calciner of CaCO3 integrated in a CO2 capture system using CaO. Chem Eng J 2008;138: 148–54. https://doi.org/10.1016/j.cej.2007.06.005.

[28] Lisbona P, Martínez A, Lara Y, Romeo LM. Integration of carbonate CO2 capture cycle and coal-fired power plants. A comparative study for different sorbents. Energy Fuels 2010;24:728–36. https://doi.org/10.1021/ef900740p.

[29] Martínez A, Lara Y, Lisbona P, Romeo LM. Operation of a mixing seal valve in calcium looping for CO2 capture. Energy Fuels 2014;28:2059–68. https://doi.org/10.1021/ef402487e.

[30] Martínez A, Lara Y, Lisbona P, Romeo LM. Energy penalty reduction in the calcium looping cycle. Int J Greenh Gas Control 2012;7:74–81. https://doi.org/10.1016/j.ijggc.2011.12.005.

[31] Ortiz C, Valverde JM, Chacartegui R, Perez-Maqueda LA. Carbonation of limestone derived CaO for thermochemical energy storage: from kinetics to process integration in concentrating solar plants. ACS Sustainable Chem Eng 2018;6:6404–17. https://doi.org/10.1021/acssuschemeng.8b00199.

[32] Wen CY, Chaung TZ. Entrainment coal gasification modeling. Ind Eng Chem Process Des Dev 1979;18:684–95. https://doi.org/10.1021/i260072a020.

[33] Kabelac S, Vortmeyer D, VDI. VDI heat Atlas Part K - radiation. In: VDI heat Atlas. Second. Springer-Verlag Berlin Heidelberg; 2010.

[34] Nellis G, Klein S. Heat transfer. Cambridge University Press; 2008.

[35] Bennett TD. Exact solutions to the thermal entry problem for laminar flow through annular ducts. J Heat Tran 2020;142:1–12. https://doi.org/10.1115/1.4046345.

[36] Taborek J. Double-pipe and multitube heat exchangers with plain and longitudinal finned tubes. Heat Tran Eng 1997;18:34–45. https://doi.org/10.1080/01457639708939894.

[37] Bennett TD. Correlations for the Graetz problem in convection − Part 1: for round pipes and parallel plates. Int J Heat Mass Tran 2019;136:832–41. https://doi.org/10.1016/j.ijheatmasstransfer.2019.03.006.

[38] Zlokarnik M. Scale-up in chemical engineering. Wiley-VCH Verlag GmbH & Co. KGaA; 2002.

[39] Plou J, Martínez I, Grasa GS, Murillo R. Experimental carbonation of CaO in an entrained flow reactor. React Chem Eng 2019:899–908. https://doi.org/10.1039/c9re00015a.

[40] Taler J, Zima W, Ocłoń P, Grądziel S, Taler D, Cebula A, et al. Mathematical model of a supercritical power boiler for simulating rapid changes in boiler thermal loading. Energy 2019;175:580–92. https://doi.org/10.1016/j.energy.2019.03.085.

[41] Song C, Wang P, Makse HA. A phase diagram for jammed matter. Nature 2008;453:629–32. https://doi.org/10.1038/nature06981.

20

58

Design and operational performance maps of calcium looping thermochemical energy storage for concentrating solar power plants

S. Pascual [a, *], P. Lisbona [b], M. Bailera [a], L.M. Romeo [a]

[a] *Escuela de Ingeniería y Arquitectura, Universidad de Zaragoza, Zaragoza, Spain*
[b] *Fundación Agencia Aragonesa para La Investigación y El Desarrollo (ARAID), Zaragoza, Spain*

A R T I C L E   I N F O

A B S T R A C T

Calcium-looping thermochemical energy storage associated to concentrating solar plants appears as promising technology given its potential to increase the storage period and energy density of the stored material. Up to now, research efforts focused on the global efficiency of the TCES associated to different power cycles under fixed modes of operation: day or night. However, TCES will never operate under a stationary situation but will experience different operation points to adapt to solar availability and energy demand from the power cycle. The aim is to analyse the influence of those variables which define the operation points, under energy storage and release modes, in the design of the heat exchangers network, storage tanks and reactors involved in the TCES system. The equipment in the conceptual plant have been modelled accounting variable storage/discharge fractions in the mass balances. The results show a suitable capture efficiency, quantifies the stored power and define the size and performance of the heat exchangers required to operate the system. The behaviour of each heat exchanger and their relevance in heat integration with a power plant is derived. The novelty relies in the analysis of potential situations arising from different combinations of charge/discharge fractions of storage tanks.

© 2020 Elsevier Ltd. All rights reserved.

1. Introduction

The dispatch of concentrated solar power (CSP) plants presents a peak around noon, in addition to continuous variations due to cloud coverage, that make energy storage systems necessary to properly manage electricity production. Currently, the 54% of the CSP plants worldwide include thermal energy storage (TES) to increment their daily operating hours and maximize the electricity production [1]. These TES systems retain thermal energy within a specific material and release it when needed. According to the physical phenomena occurring while storing/releasing energy, thermal energy storage is classified in (i) sensible TES, (ii) latent TES and (iii) thermochemical energy storage (TCES).

Sensible TES uses materials with high specific heat (131–4187 J/kg·K) to store/release energy by heating/cooling their mass. Although the energy storage density of these systems is low (1001–4453 kJ/m³·K), they are simple, reliable and cheap, making them the most widely used TES system in commercial CSP plants [2]. Within sensible TES, molten salts are the most commonly

applied materials [3]. Their major drawback is the required range of working temperatures, since molten salts must be maintained above 200 °C to prevent solidification, and not exceed 550 °C to avoid its degradation [4].

Latent TES uses materials with high latent heat (112–260 kJ/kg) to store/release energy during a liquid-solid phase transition, in order to have constant temperature [2], small variations in volume (<10%) [5] and high energy storage densities (50–150 kWh/t). The main disadvantage of latent TES is the prolonged times of charging and discharging energy, because of the low thermal conductivity of these materials (<0.5 W/m·K) [2].

Thermochemical energy storage uses the reversibility of certain chemical equilibrium reactions (endothermic in one direction and exothermic in the other one) to store/release energy through a cyclic process. TCES system improves storage capacity compared to sensible and latent TES, through the introduction of materials with higher energy density (about 240–1090 kWh/t) [6] and minimal energy loss under seasonal storage since the energy is stored in the chemical bound of the compounds. Furthermore, since TCES operates in the temperature range of 450–1300 °C, it can also be integrated in new generation CSP plants, which operate above 800 °C [2,7].

* Corresponding author.
  E-mail address: saraps@unizar.es (S. Pascual).

One of the most promising TCES systems is based on the reversible calcination − carbonation reaction of $CaCO_3/CaO$, also known as calcium-looping (CaL) process [8]. Calcination reaction (Eq. (1)) is endothermic, producing carbon dioxide (CO_2) and calcium oxide (CaO) at 920−950 °C [9]. The thermal energy used in the calcination process should be energy intended to be stored or energy that would otherwise be wasted. Both products from calcination reaction can be independently stored until the stored energy is required to be recovered. The exothermic reaction (reverse Eq. (1)) is produced when the stored CO_2 and CaO are mixed at temperatures in the range 600−850 °C [10]. This carbonation reaction releases high temperature heat and produces $CaCO_3$ that can be stored, thus closing the loop.

$$CaCO_{3(s)} \leftrightarrows CaO_{(s)} + CO_{2(g)} \quad \Delta H_R^{\circ} = +178 \, kJ/mol \quad (1)$$
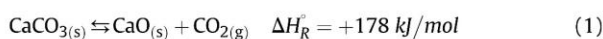
CaL process uses limestone ($CaCO_3$), which is a non-toxic, earth-abundant and cheap material (<10 €/t $CaCO_3$) [11]. Besides, $CaCO_3$ material presents high energy density, in the range 307−409 kWh/t [7,12]. The most important drawback of the CaL process is the decay of sorbent capacity of CaO material due to sintering [13], which becomes more relevant the higher is the number of carbonation-calcination cycles suffered by the solid particles [14,15]. This particular problem has been extensively studied in literature looking for different solutions: sorbent improvements by analyzing the multicycle activity of the natural $CaCO_3$ minerals [16], pre-processing limestone to enlarge the long-term performance of the sorbent upon iterated cycles [17], doping and modifying $CaCO_3$ [18,19], and developing synthetic Ca-based materials for energy storage [20].

Although the utilization of CaL for energy storage was already proposed in 1974 by Barker [8], was not until the last decade that several research works analysed its application in CSP plants. In this case, the calcination reaction would occur during sunlight hours whenever solar energy is available in the CSP. The calcination products (CaO and CO_2) can be total or partially stored, diverting the rest to the carbonator to produce energy. During night period, the stored CO_2 and CaO are always sent to carbonator to produce energy, aiming to keep at least a minimum operating load to avoid expensive shutdowns of the power plant.

The operation of this system is associated with power cycles for electricity production, therefore recent research mainly focus on the selection of the most suitable power block to be integrated with CaL TCES [21−23] and the subsequent optimization of the overall efficiency [24−27]. Also, some authors have studied the design of reactors [9,28] and the management of the storage system [29].

Ortiz et al. [21], Tesio et al. [22] and Karasavvas et al. [23] compared different power cycles aiming for the best performance when integrated with calcium looping TCES. All of them concluded that CO_2 power cycles provide the greatest results (supercritical CO_2 power block according to Tesio, and CO_2 closed Brayton cycle according to Ortiz and Karasavvas). After identifying the most suitable technology, they optimized the overall efficiency (net electric production to net solar thermal input) by assessing different plant layouts and operating conditions. In the case of supercritical CO_2 cycles, the efficiency was 40.4% [26], while for CO_2 closed Brayton cycle the higher efficiencies of the different authors were within the range 31−44% [24,25,27].

In terms of plant management, Bravo et al. [29] used a multi-objective optimization framework to define the operational strategy that would maximize the net energy supplied during one year of operation. They analysed 9 potential scenarios, obtaining capacity factors in the range 48−69% (referred to the operation of the CO_2 Brayton cycle) and efficiencies between 33.1% and 33.8% (net

electric production to net solar thermal input in the calciner).

Although the mentioned studies assume industrial plants, they do not consider the implications that reactor design may have on the overall efficiency at this scale. Only Bailera et al. [28] for carbonation and Lisbona et al. [9] for calcination, have started shedding light on this issue. Bailera et al. showed that carbonators cooled by external coils, when scaled-up to industrial scale, cannot properly evacuate the exothermal energy. Since the reaction gets inhibited, the carbonator dimensions for a 100 MW CSP plant become unreasonable (7 m in diameter and 52 m in length) [28]. Regarding calcination, Lisbona et al. assessed the temperature profile in a falling particle calcinator [9]. In this type of reactors, a curtain of falling $CaCO_3$ particles absorb the solar radiation that enters through the aperture of the receiver [30]. To keep the profile close to isothermal and avoid excessive degradation due to peaks of temperature, they proposed supplying the solar thermal energy through different stages along the calcinator. They concluded that a 3-stage calcinator provides an adequate balance between complexity, energy storage efficiency (98.9%), and temperature variation (895−993 °C) [9]. The main reason of the lack of studies regarding reactor design [31] is that experiments on CaL TCES are scarce. So far, solar calcination has been tested by the Paul Scherrer Institute in a window-less cyclone gas-particle separator with a solar thermal input of 54 kW (85% limestone conversion and 88% energy efficiency) [30], while carbonation is being tested within the SOCRATCES project in a 10 kW entrained flow reactor cooled by air through external coils [32]. Thus, the CaL TCES technology is currently in TRLs 5−6, which is in the upper range of similar energy storage technologies based on endothermic-exothermic thermo-chemical cycles [33].

The research gap found in most of these studies is that they are performed under stationary operation modes of the CaL TCES system. It means that both the fraction of calcination products diverted to storage during sunlight hours and the operating load of the carbonator during night period are fixed values. In this work, not only one single operation point is analysed at each mode of operation (energy storage and energy release), but a whole scanning of possible operation points is carried out. Therefore, the novelty of the paper is the analysis of the wide variety of potential situations that may take place, arising from the different combinations of charge/discharge fractions of the CaO, CO_2 and $CaCO_3$ storage tanks. Thus, it will cover scenarios such as low/high electricity demands, limited solar energy availability, variations in electricity prices, etc.

The main objective of this study is to determine the required size of the heat exchangers that are present in a CSP plant with CaL TCES under a wide range of potential scenarios, and stablish their operation maps versus the different charge/discharge fractions of the CaO, CO_2 and $CaCO_3$ tanks. The paper is structured in the following way: in section 2, the CSP plant integrated with calcium looping TCES and the energy storage/release operation modes are described; in section 3, the methodology used to model the plant and size the equipment is presented; in section 4, the results on heat exchangers requirements and operation maps are discussed; in section 5, the main conclusions of the study are remarked.

2. Plant description and operation modes

The thermal energy storage capacity of the CaL TCES system proposed in this study is 100 MWth at nominal conditions. As shown in Fig. 1, the system consists of two main reactors, a solar calciner and a carbonator, with intermediate storage tanks of CO_2, CaO and $CaCO_3$. The size and technical characteristics of these elements are described in the following paragraphs.
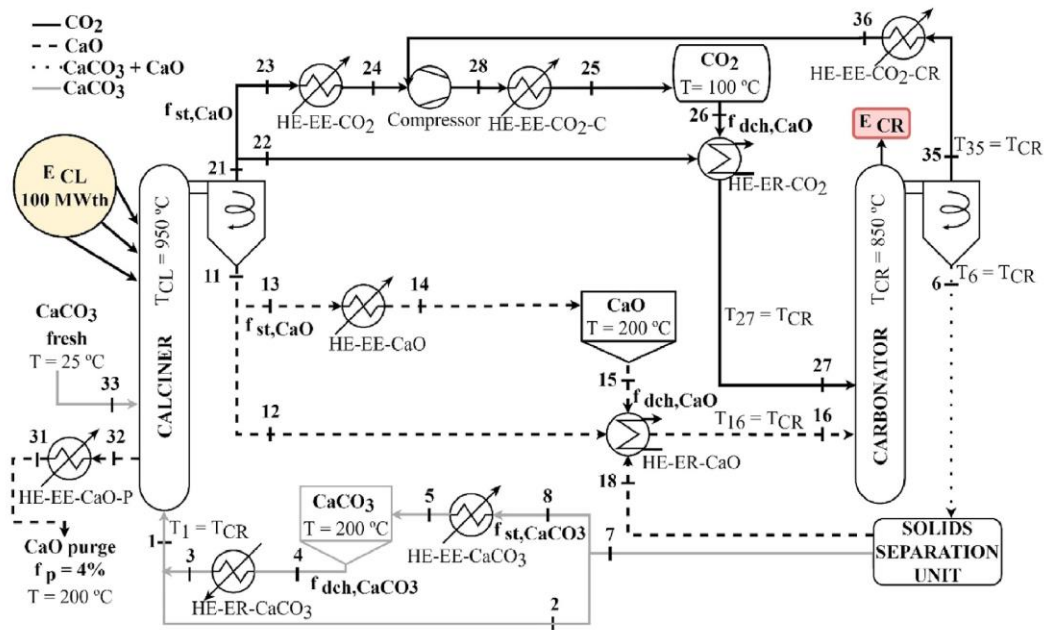
Fig. 1. Thermochemical storage system based on Calcium-looping process for a 100 MWth CSP plant.

2.1. Plant description

2.1.1. Concentrated solar power and solar field

The power required in the calciner is supplied by the solar energy captured in a concentration solar field. For this case study, a solar power tower plant located in the same site as the PS10 commercial plant in Seville (Spain) is considered [1]. This location has been selected given the high annual availability of the solar resource and the high solar irradiation. The annual Direct Normal Irradiance considered is 2012 kWh/m²/year [1]. The calciner is found inside the receiver of the solar power tower. The required solar field area is 250,000 m², considering an optical efficiency of 64.7% and a thermal efficiency of 92.8% [34]. Taking into account irradiance data from the PVGIS tool [35], the maximum power that could reach the interior of solar receiver would be 155 MW, while the average power during sunlight hours throughout the year is 83 MW. Therefore, it is reasonable to assume a thermal input of 100 MWth to the calciner under nominal operation conditions.

2.1.2. Calciner

The input flowrate of $CaCO_3$ to the calciner (stream 1) results from the addition of the limestone stream from the solids separation unit at 850 °C (stream 2) and the flowrate of $CaCO_3$ discharged from the limestone storage tank at 200 °C (stream 4). The inlet solid stream must be heated up to 850 °C. The calcination or sorbent regeneration process produces a continuous flowrate of CaO and CO_2, which can be stored (stream 13 and 23) or directed to the carbonator reactor to close the chemical Ca-looping (stream 12 and 22).

Since CaO quickly deactivates with the number of cycles, a stream of fresh limestone must be fed into the calciner to keep a reasonable age population and sorption activity. Besides, the operating temperature in the calciner does not exceed 950 °C in CO_2 pure atmosphere in order to avoid further degradation of CaO [24]. Therefore, the $CaCO_3$ supplied to the calciner reactor comes

from: (i) the contribution of fresh limestone and (ii) the $CaCO_3$ produced after carbonation reaction. Regarding the mass balance in the calciner, fresh limestone (stream 33 or F_0) counterbalances the purged solid material (f_p) which is set at 4% of the CaO molar flow generated in calcination reaction (stream 11 or $F_{CaO,outCL}$), as shown in Eq. (2).

$$f_p = \frac{F_0}{F_{CaO,outCL}} \tag{2}$$

2.1.3. Carbonator

Exothermal carbonation reaction takes place in the carbonator at 850 °C in pure CO_2 atmosphere [36]. Ideally, the carbonator operates in isothermal mode although it is difficult to achieve under normal operation [28]. The CaO stream discharged from the storage tank at 200 °C (stream 15) is mixed with a CaO stream diverted from the calciner outlet at 950 °C (stream 12) and a recycled CaO flow rate at 850 °C from the solids separation unit outlet (stream 18) before being introduced into carbonator at 850 °C.

The nominal power in the carbonator has been set considering the operation of the CaL facility without storage of materials, i.e. as a single capture cycle, and a heat input to the calciner of 100 MWth. In this case, the nominal power input (100 MWth) is used to calcinate an amount of sorbent which is fully directed to the carbonator to be completely carbonated releasing the maximum potential of thermal energy in this reactor, 88.33 MWth.

It is known that only a percentage of the CaO introduced in the carbonator (stream 16) will react with CO_2 (stream 27). This amount will depend on the average sorption activity of the population of particles circulating in the system [37]. A mixture of $CaCO_3$ and unreacted CaO is found at carbonator outlet (stream 6). To avoid the storage of a mixture of compounds, solid stream leaving the carbonator is completely separated into its two components,

CaO and CaCO₃, at high temperature (850 °C). This separation process allows to avoid the subsequent heating and cooling of CaO which otherwise would be directed the calciner and also allows to reduce the CaCO₃ storage tank size. The output stream of CaO is recirculated to the carbonator (stream 18), while the flowrate of CaCO₃ can be stored (stream 8) or directed to the calciner (stream 2), according to the operation mode. The unreacted CO₂ leaving the carbonator is stored together with the CO₂ from the calciner under established conditions and it will be fed into the carbonator again when required. The value of R and the average sorption activity (X_{ave}) define the carbon capture efficiency (η_{capt}) in the carbonator reactor (Eq. (3)).

$$\eta_{capt} = R \cdot X_{ave} = \frac{F_{CaO,inCR}}{F_{CO2,inCR}} \cdot X_{ave} = \frac{F_{stream\ 16}}{F_{stream\ 27}} \cdot X_{ave} \qquad (3)$$

2.1.4. Storage tanks

Temperature and pressure of the CO₂ storage depend on the storage tank size and phase of stored CO₂ [36]. In this study, CO₂ is stored in gas phase at 100 °C and 73 bar. CO₂ compression process to achieve these storage conditions includes a cooling stage down to 50 °C before compression to 73 bar and a final cooling to the storage temperature, 100 °C. CO₂ from storage tank is mixed with CO₂ from calciner before being introduced into carbonator at 850 °C. Solids storage temperature may ranges from ambient to 200–700 °C [24]. Solids storage temperature and pressure are set at 200 °C and 1 bar.

2.1.5. Heat exchangers

Heat exchangers (HE) illustrated in Fig. 1 will supply or remove thermal energy according to the operation mode of the overall TCES system. Heat exchangers designated as *EE* are able to provide energy under both modes of operation, storage or release mode. Heat losses of these *EE* heat exchangers are assumed to be a 2% of the power exchanged.

However, the heat exchanger designated as *ER-CaCO₃* always requires thermal energy input under any operating situation while the rest of *ER* heat exchangers provide or demand energy depending on the operation mode.

2.2. Operation modes

The management of the flow streams to and from the storage tanks will depend on the availability of renewable energy resource and/or the requirement of releasing thermal energy from the TCES, which will determine the operation mode: energy storage (ESOM) or energy release (EROM). First, storage and discharge fractions must be defined to describe the flows of gas and solids circulating in the system under each operation mode.

2.2.1. Storage and discharge fractions

Stationary operation is analysed in this study for both operation modes considering different combinations of discharge and storage fractions from and to storage tanks. Mapping a wide range of operation points will allow the estimation of the required size ranges of the equipment involved in the system.

The maximum CO₂ flow rate which can be diverted to the storage tank ($\dot{m}_{st,max,CO2}$) would correspond to the CO₂ flow rate leaving the calciner (stream 21) when the thermal energy received is 100 MWth (nominal operation of the solar calciner). The amount of CO₂ received in the storage tank ($\dot{m}_{st,CO2}$) will correspond to a fraction of this maximum CO₂ stream that actually leaves the calciner under nominal conditions ($f_{st,CaO}$), Eq. (4). The CO₂ leaving

the storage tank ($\dot{m}_{dch,CO2}$) is defined as a fraction of the maximum possible flowrate of CO₂ at calciner outlet ($f_{dch,CaO}$), Eq. (5).

The maximum CaO flow rate ($\dot{m}_{st,max,CaO}$) which could be sent to the storage tank corresponds to the CaO flowrate leaving the calciner (stream 11) when it is operated at nominal conditions; i.e. solar power received of 100 MWth. The CaO storage tank receives ($\dot{m}_{st,CaO}$) a fraction of this maximum CaO stream produced in the calciner under nominal conditions ($f_{st,CaO}$). The amount of CaO actually discharged from the storage tank ($\dot{m}_{dch,CaO}$) is also defined as a fraction of the maximum possible flow of CaO that leaves calciner ($f_{dch,CaO}$), as shown in Eq. (4) and Eq. (5), respectively. These storage and discharge fractions are analogous to those fractions of CO₂ in order to keep CaO/CO₂ molar ratio (R) constant.

$$f_{st,CaO} = \frac{\dot{m}_{st,CaO}}{\dot{m}_{st,max,CaO}} = \frac{\dot{m}_{st,CO2}}{\dot{m}_{st,max,CO2}} \qquad (4)$$

$$f_{dch,CaO} = \frac{\dot{m}_{dch,CaO}}{\dot{m}_{st,max,CaO}} = \frac{\dot{m}_{dch,CO2}}{\dot{m}_{st,max,CO2}} \qquad (5)$$

The maximum storage flowrate of CaCO₃ ($\dot{m}_{st,max,CaCO3}$) corresponds to the CaCO₃ flowrate leaving the carbonator (stream 7) when it operates under its nominal conditions, i.e. 88.33 MWth released in this equipment. The maximum CaCO₃ stream leaving the solids separation unit located downstream the carbonator can be totally or partially ($\dot{m}_{st,CaCO3}$) diverted to the CaCO₃ storage tank ($f_{st,CaCO3}$). On the other hand, the discharge CaCO₃ flowrate of this tank ($\dot{m}_{dch,CaCO3}$) is defined as a fraction of the maximum possible flow of CaCO₃ leaving the carbonator ($f_{dch,CaCO3}$), as shown in Eq. (6) and Eq. (7), respectively.

$$f_{st,CaCO3} = \frac{\dot{m}_{st,CaCO3}}{\dot{m}_{st,max,CaCO3}} \qquad (6)$$

$$f_{dch,CaCO3} = \frac{\dot{m}_{dch,CaCO3}}{\dot{m}_{st,max,CaCO3}} \qquad (7)$$

2.2.2. Energy storage operation mode (ESOM)

This operation mode will be activated whenever solar energy is available and becomes an input to the calciner instead to run the CSP plant. This could correspond to CSP daylight operation under very low electricity demand situation. As already defined, the nominal operation of the solar calciner receives 100 MWth. Under the energy storage mode, the CO₂ and CaO flowrates from the calciner are totally or partially directed to the storage tanks. The balance between stored energy and available heat from the system will vary depending on the amount of material directed to storage tank or to carbonator. Since a fraction of the mass streams leaving the calciner is stored and only the remaining part is circulated to the carbonator, the energy available in the carbonator will be correspondingly reduced with respect to nominal operation. The storage tank of limestone will be required to discharge material to feed the calciner and close the mass balance of the system.

2.2.3. Energy release operation mode (EROM)

This operation model will be activated whenever solar input to the calciner is not available but thermal energy is still required in the CSP plant. It could correspond to the operation of the CSP during high electricity demand periods or night hours. Under energy release mode, the received solar energy will always be lower than 100 MWth in the calciner. Thus, limestone flow rate from carbonator must be completely stored when no solar input is

available or partially diverted to the calciner when solar power is available. The flow rate of limestone diverted to the calciner will correspond to the amount of limestone which can be potentially calcined using the available solar energy. The storage tanks of CO_2 and CaO will be required to discharge material in order to maintain the energy availability in the carbonator.

3. Materials and methods

This section details the methodology followed for (i) the modelling of the carbonator to obtain the performance parameters of the Ca-looping and (ii) the evaluation of equipment sizing involved in the system according to the operation modes: energy storage or energy release. The model of the carbonator and calciner reactors and the model of the heat exchanger network have been implemented in Engineering Equation Solver (EES) software and they are used to quantify the influence of the variation of storage and release energy fractions in equipment sizing.

3.1. Carbonator model

According to a large number of investigations of the sorption behaviour of solid calcium oxide particles, it has been proven that carbonation conversion of sorbent particles undergoes a drastic fall after a relatively short number of carbonation-calcination cycles [38−40]. Abanades et al. [38] observed similar decay trends in the CO_2 capture capacity during the carbonation of calcines from natural limestones under a wide range of conditions. Furthermore, Wang et al. [39] suggested that the sintering of sorbents is the possible cause of the decreased activity in CO_2 absorption. In the same way Arias et al. [40] stated that the free surface of the sorbent is reduced during the carbonation/calcination cycles due to sintering and thus the carbonation conversion decays.

Different strategies are proposed to maintain an adequate average sorption capacity of the solid population and a sufficiently high efficiency of the carbonation process. One of these strategies is related to the optimal selection of fresh limestone flowrate or the equivalent stream of purged exhausted material [41]. The low cost of limestone allows the compensation of the CaO sorption degradation by increasing the feed of fresh limestone to the cycle [42].

A *Piaseck* limestone has been taken as a reference for degradation on the sorption capacity with the number of cycles [43]. The conversion of a particle of *Piaseck* limestone after N calcination cycles is calculated through Eq. (8).

$$X_N = \frac{1}{\frac{1}{1-X_r} + k \cdot N} + X_r \tag{8}$$

where k is the deactivation constant with a value of 0.52, X_r the residual conversion that takes a value of 0.075, and N the number of cycles to which the particle has been subjected [43].

However, not all the population of solid sorbent particles have suffered the same number of cycles and an age distribution is found in the solid inventory. There are particles that have just been fed to the system as fresh limestone ($N = 0$), others that have been carbonated and calcined only once ($N = 1$) and so on. Therefore, in order to calculate the average sorption capacity of the solid population, the age distribution of the population of sorbent particles must be known. This distribution is represented with the variable r_N and, for an extremely conservative situation in which no solid material is stored in the tanks, it can be calculated through Eq. (9).

$$r_N = \frac{f_p}{\left(1 + f_p\right)^N} \tag{9}$$

The variable r_N determines the fraction of CaO particles that circulate between the carbonator and the calciner with a certain number of cycles. The expression can be deduced through successive mass balances for the first cycles, where the CaO purge fraction (f_p), as shown in Eq. (2), is located in calciner [42,44].

The average conversion of the particle population (X_{ave}) can be calculated using Eq. (10) which uses (i) the fraction of CaO particles (r_N) that have undergone a number of carbonation-calcination N cycles and (ii) the conversion of a sorbent particle (X_N) in the N cycle [37].

$$X_{ave} = \sum_{N=1}^{N=\infty} r_N \cdot X_N \tag{10}$$

Once the average sorption capacity of the particle population is known, the CO_2 capture efficiency can be determined through the CaO/CO_2 molar ratio (R) introduced into the carbonator, as shown in Eq. (3).

3.2. Plant equipment sizing

The sizing of the elements involved in the CaL TCES system strongly depends on the pair of storage and discharge fractions which defines each operation point. Different operating points for each operation mode are determined at steady state, considering CaO purge set at 4% and a constant CaO/CO_2 molar ratio (R) for all operation schemes.

Under energy storage operation mode (ESOM), the energy input (E_{CL}) to the solar calciner is considered to be 100 MWth, while the $CaCO_3$ from the solids separation unit is completely directed to the calciner ($f_{st,CaCO3} = 0$) by-passing the storage tank of limestone. The operation points analysed for energy storage mode are defined by varying the CO_2 and CaO discharge fraction ($f_{dch,CaO}$) from 0 to 1 for each storage fraction ($f_{st,CaO}$) in a range of 0−1, considering increments of 0.1 for each fraction. Each operation scheme under energy storage mode will be defined by a pair of values ($f_{st,CaO}$, $f_{dch,CaO}$). For example, a storage fraction ($f_{st,CaO}$) set to 1 and a discharge fraction ($f_{dch,CaO}$) equal to zero defines an operation scheme in which all the thermal energy available in the solar calciner is stored in the form of CaO and CO_2 and the carbonator is not operated. However, if the storage fraction ($f_{st,CaO}$) drops to 0.7 and the discharge fraction ($f_{dch,CaO}$) is set to 0.1, it means that 70% of the maximum CaO and CO_2 flowrates from the calciner goes directly to its corresponding storage tank; while the remaining 30% is sent to the carbonator together with a 10% of the maximum flow of CaO ($\dot{m}_{st,max,CaO}$) and CO_2 ($\dot{m}_{st,max,CO2}$) which are discharged from the storage tanks. Therefore, the 40% of the maximum CaO and CO_2 flowrates from the calciner is directly circulated to the carbonator to release energy, while the remaining 60% is stored in their respective tanks. The energy stored under each scenario will depend on the storage and discharge fractions ($f_{st,CaO}$, $f_{dch,CaO}$). Therefore, it is only possible to store or discharge the maximum stored flow of CO_2 and CaO for each energy storage operation point. Furthermore, for a storage fraction ($f_{st,CaO}$) of 0.7, the maximum discharge fraction ($f_{dch,CaO}$) will be 0.7; i.e. the tank never discharges a flowrate higher than the received mass input. A large variety of operating schemes can be obtained under the energy storage operation mode. These schemes allow the generation of operation maps to calculate the required size of heat exchangers and compressor, and the range of energy released in the carbonator (E_{CR}).

Under energy release operation mode (EROM), the maximum power available in the carbonator (E_{CR}) is assumed to be 88.33 MWth as previously justified. The streams of CaO and CO_2 from

5

calciner are fully directed to the carbonator ($f_{st,CaO} = 0$). The operation schemes are defined by increasing the $CaCO_3$ discharge fraction ($f_{dch,CaCO3}$) from 0 to 1 for each storage fraction ($f_{st,CaCO3}$) in a range of 0−1, considering increments of 0.1 for each fraction. Each operation scheme under energy release mode will be defined by a pair of values ($f_{st,CaCO3}$, $f_{dch,CaCO3}$). For example, a storage fraction ($f_{st,CaCO3}$) set to 1 and a discharge fraction ($f_{dch,CaCO3}$) equal to zero defines an operation scheme in which solar energy is not available and the calciner must be shut-down; thus the $CaCO_3$ stream from carbonator must be kept in the corresponding storage tank. However, if the storage fraction ($f_{st,CaCO3}$) drops to 0.9 and the discharge fraction ($f_{dch,CaCO3}$) is set to 0.2, it means that 90% of the $CaCO_3$ flowrate from the solids separation unit goes directly to its corresponding storage tank: while the remaining 10% is sent to the calciner together with a 20% of the maximum flow of $CaCO_3$ ($\dot{m}_{st,max,CaCO3}$) which is discharged from the storage tank. Therefore, the 30% of the maximum $CaCO_3$ flowrate from the carbonator is directly circulated to the calciner, while the remaining 70% is stored in its respective tank.

The energy released under each scenario will depend on the storage and discharge fractions ($f_{st,CaCO3}$, $f_{dch,CaCO3}$). Therefore, it is only possible to store or discharge the maximum stored flow of $CaCO_3$ for each energy release operation scheme. In that case, for a storage fraction ($f_{st,CaCO3}$) of 0.9, the maximum discharge fraction ($f_{dch,CaCO3}$) will be 0.9. A large variety of operating schemes can be obtained for the energy release mode. These schemes allow the generation of operation maps to calculate the required size of heat exchangers and compressor, and the range of solar energy required in the calciner (E_{CL}).

The larger number of operation points analysed under both operation modes, the better mapping of the energy requirement or demand operation points.

4. Results and discussion

In this section, the results related to the efficiency of the sorption process taking place in the carbonator and the obtained operation maps are presented. Besides, the analysis of a wide variety of different operation schemes provides an estimation of the size range of the required equipment in the system.

4.1. Average sorbent conversion

The CO_2 capture efficiencies achieved in the carbonator are greater 90% for purged flows, f_p, of 4%. The two parameters that determine the capture efficiency are X_{ave}, a direct function of the purged stream of exhausted material, and the CaO/CO_2 molar ratio, R. The average conversion of the solid material, X_{ave}, is defined by the type of limestone chosen (*Piaseck*) which determines the evolution of sorbent conversion, X_N, with the number of cycles and the age distribution of solid population, r_N. Under a conservative scenario which does not account for the partial storage of the solid streams leaving the reactors, the average sorption capacity of the particle population using *Piaseck* limestone is X_{ave} of 22.58%. The value set for R is 4.26 which leads to a carbonation conversion efficiency for any operation point of 96.15%. Under that condition, the value given to the purged flow rate of exhausted material determines the maximum CaO and $CaCO_3$ flow at the carbonator outlet (stream 6).

A parametric analysis was carried out to assess the variation of average conversion of the solid population in the solid when the purge of exhausted material and the calcium to carbon dioxide ratio were varied. This variation has a direct effect on the carbon capture efficiency which has been illustrated in Fig. 2. Carbon capture
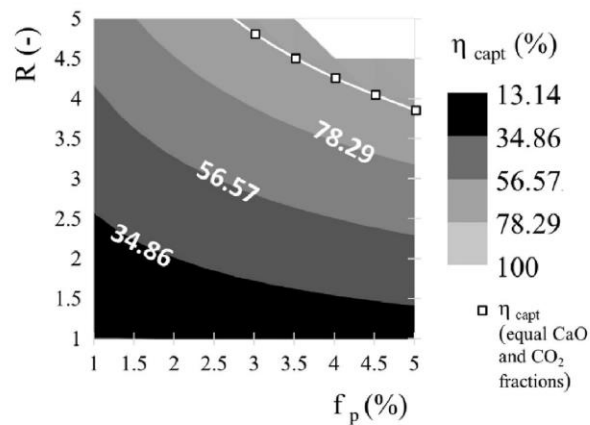

Fig. 2. Carbon capture efficiency in the system for different purged flowrates and CaO/CO_2 ratio.

efficiency (η_{capt}) ranges between 13.54% and 100%, Eq. (3), for a solids purge percentage between 1 and 5% and R values range from 1 to 5.

However, not all the pairs (R, f_p) represented in Fig. 2 are suitable for the operation of the CaL-CSP TCES. Only those points located on the white line represented in the figure are adequate for the operation requirements of the system. These points represents those situations in which CO_2 and CaO storage ($f_{st,CO2}$ and $f_{st,CaO}$) are equal as well as discharge ($f_{dch,CO2}$ and $f_{dch,CaO}$) fractions (limitations of the system). In this way, the R value and the average sorbent conversion (X_{ave}) will be kept constant for each operating point within both operating modes (ESOM and EROM).

The lowest carbon capture efficiency is 95.15%, corresponding to a R value of 3.86 and a purge of 5%, while the highest carbon capture efficiency (98.98%) is possible with a purge percentage of 3% and a R ratio of 4.81. Purge percentages (f_p) greater than 5% have not been considered because the increase of the sorbent average activity (X_{ave}) from that value is less sharp. Besides, a R value higher than 5 involves an extremely large solids circulation in the system and therefore the storage volume required is increased. Therefore, an intermediate value of carbon capture efficiency (96.15%) corresponding to a CaO/CO_2 molar ratio (R) of 4.26 and a CaO purge in the calciner (f_p) of 4% has been chosen.

4.2. Operation maps and equipment sizing

The results obtained from the analysed operation points, 100 for each mode of operation, provide relevant information on the size range of the equipment involved in the system.

4.2.1. Storage tank volumes

The maximum flow rates of carbon dioxide and calcium oxide which can be stored have been calculated and these values together with the densities of these substances are used to assess the proper range of the storage tanks. The maximum input flowrate to the CO_2 tank could achieve 24.37 kg/s, while CaO maximum flow could achieve a value of 29.86 kg/s. The storage conditions of the carbon dioxide are 100 °C and 73 bar which lead to a density of 126.1 kg/m³. The density of the calcium oxide is 1800 kg/m³ but considering a void fraction of 30% in the storage tank, the apparent density is around 1260 kg/m³.

In order to have a preliminary estimation of the maximum CO_2 and CaO storage tank volumes required for the operation of the

6

64

plant, the most extreme point of operation, load of calciner and the number of hours of operation must be set. The highest load corresponds to the nominal loads, already established as 100 MWth in the calciner. The point of operation for ESOM with larger material storage flow rates corresponds to the calciner operating at nominal load and carbonator off. A parametric analysis of the number of operating hours under limit operation point (ESOM) is carried out to observe the influence on the volumes of the storage tanks, Fig. 3.

CaO and CO_2 tank sizes ranges from 85 to 696 m^3 for 1 h of storing operation at maximum material storage flow rates, and up to 1280−10,436 m^3 for 15 h, respectively. This threshold represents a highly improbable situation since the solar calciner will rarely operate at full nominal load during the whole day. The maximum CO_2 storage volume obtained for 15 h exceeds 10,000 m^3. Although this storage volume represents only a threshold, the information is useful to revise the CO_2 storage conditions to reduce the storage tank size.

4.2.2. Stored power

The maximum potentially stored power under ESOM accounts for the sensible heat of CO_2 and CaO stored and the chemical potential linked to the recarbonation of CaO. The sensible heat amounts to 5.92 MW and the chemical potential that can be later released through the carbonation reaction implies a power of 21.39 MW. However, the maximum energy storage also implies a consumption of the CO_2 compressor of 11.55 MW. On the other hand, the power available in the carbonator (E_{CR}) can range between cero and 88.33 MW, according to the management of the CO_2 and CaO flow streams.

Fig. 4 illustrates the variation of the stored power under a wide range of ESOM operation points. As stated in section 3.2, we assume as a threshold value of the storage or discharge fractions the maximum stored flow rate of CO_2 and CaO for each energy storage operating point. In this way, stored power can be up to 27.31 MW, corresponding to the operating point in which the CaO and CO_2 storage fraction ($f_{st,CaO}$) is maximum and the carbonator does not operate ($f_{dch,CaO} = 0$). While the minimum energy storage occurs when the carbonator operates at nominal power (88.33 MWth) in ESOM ($f_{st,CaO} = f_{dch,CaO}$) and only the sensible heat of the CO_2 flow that leaves the carbonator towards the storage tank is stored.

The maximum input flow to the CaCO$_3$ tank may achieve a value of 53.29 kg/s and, accounting for the storage temperature of the
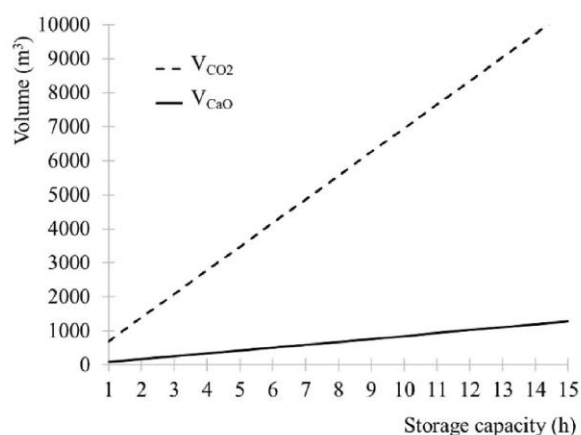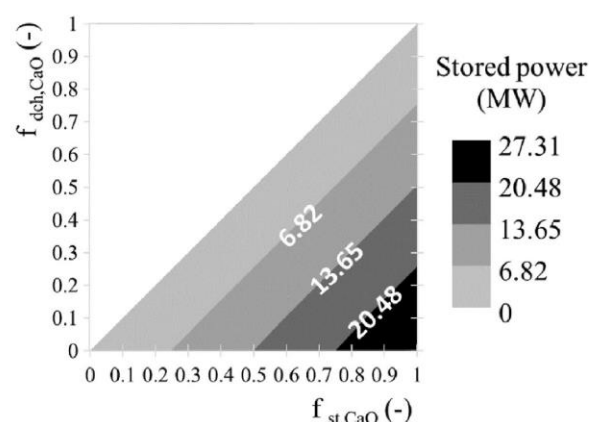

Fig. 4. Stored power under different ESOM points of operation.

solid, the maximum power accumulated in the form of sensible heat amounts to 11.68 MW. The solar power range available in the calciner (E_{CL}) can be between cero and 100 MW, the CaCO$_3$ flow stream input will be varied accordingly.

4.2.3. Heat exchangers network

The ranges of exchanged thermal power in each of the Heat Exchangers (HE) are presented in Table 1. The largest heat exchangers are found in the CaCO$_3$ line since these correspond to the highest solid flowrates. The negative sign (−) of the thermal power for a heat exchanger indicates an energy release, while a positive value (+) means that a specific heat exchanger requires an energy input. Under any operating conditions, the total heat losses of each heat exchangers are practically dependent on the storage fractions. The energy losses of the heat exchangers are lower under any EROM operation point since several heat exchangers are by-passed; i.e. all the heat exchangers at the beginning of the CaO (EE-CaO) and CO_2 (EE-CO$_2$) storage lines will be disconnected. On the contrary, under ESOM, only the EE-CaCO$_3$ heat exchanger, located before the CaCO$_3$ storage tank, will be by-passed.

The largest amount of available heat found in the HEN is provided by heat exchanger EE-CaCO$_3$ which can release up to 40.55 MW of thermal energy as the storage fraction of CaCO$_3$ (stream 7) increases under EROM. The maximum value of thermal energy released by EE-CaCO$_3$ heat exchanger is achieved when the storage fraction $f_{st,CaCO3}$ is 1 and the flow of CaCO$_3$ leaving the carbonator is stored at 200 °C. On the contrary, the EE-CaCO$_3$ heat exchanger is not under operation when the CaCO$_3$ flow rate is fully directed to the calciner, so the CaCO$_3$ storage fraction ($f_{st,CaCO3}$) will be zero.

Another significant heat exchanger is found in the storage line of limestone. The ER-CaCO$_3$ heat exchanger comes into operation to preheat the flow of CaCO$_3$ discharged from the storage at 200 °C to 850 °C. In this case, the heat exchanger designated as ER-CaCO$_3$ always demands an energy input; up to a maximum of 41.38 MW. ER-CaCO$_3$ will only be off for specific operation schemes where it is not required to discharge CaCO$_3$ from the storage tank ($f_{dch,CaCO3} = 0$).

The EE-CO$_2$ and EE CaO heat exchangers belong to the storage line and do not operate when CO_2 and CaO flow rates from calciner are fully directed to carbonator, after passing through ER-CO$_2$ and ER-CaO heat exchangers, respectively. However, they release thermal energy up to 20.50 and 24.22 MW, respectively, when the storage fraction $f_{st, CaO}$ is increased to 1.

Fig. 3. Volume of the CO_2 and CaO tanks required for maximum storage flow rates vs time.

Table 1
Range size of heat exchangers.

Energy flow description		T_{in}	T_{out}	Q	
		(°C)	(°C)	(MW)	
	Heat Exchanger			ESOM	EROM
CO_2	$EE-CO_2-C$	950	50	0 to −24.22	0
	$EE-CO_2-C$	506.9	100	−0.39 to −10.62	−0.39
	$EE-CO_2-CR$	850	50	−0.82 to 0	−0.82
	$ER-CO_2$	950	850	−3.10 to 20.52	20.52 to −3.10
		100			
CaO	EE-CaO	950	200	0 to −20.50	0
	EE-CaO-P	950	200	−0.82	0 to −0.82
	ER-CaO	950	850	−2.91 to 18.02	18.02 to −2.91
		850			
		200			
$CaCO_3$	$EE-CaCO_3$	850	200	0	−40.55 to 0
	$ER-CaCO_3$	200	850	0 to 41.38	41.38 to 0

The *EE-CO₂-C* and *EE-CO₂-CR* heat exchangers have a minimum threshold of thermal energy released of 0.39 and 0.82 MW, respectively, for any operating point of the energy release operation mode. The *EE-CO₂-C* heat exchanger cools the CO_2 flow before being stored at 100 °C and 73 bar to take advantage of the temperature reached after compression. The *EE-CO₂-CR* heat exchanger reduces the temperature of the CO_2 flow leaving the carbonator down to 50 °C, for its subsequent compression and storage. The minimum thermal energy released by both heat exchangers is solely related to the storage process of the CO_2 flow from the carbonator (stream 35). However, under the ESOM, the sharper increase of $f_{st,CaO}$, the larger thermal power release in the *EE-CO₂-C*. This power released in the *EE-CO₂-CR* is reduced to zero if the carbonator does not operate.

The thermal power recovered in the heat exchanger corresponding to the CaO purge (*EE-CaO-P*) presents a constant amount of 0.82 MW when calciner operates at nominal conditions. Although this value can be reduced to zero as the solar energy availability decreases.

Fig. 5 and Fig. 6 illustrate the operation maps of those heat exchangers which can demand or release thermal energy depending on the situation (i.e. storage and discharge fractions and operating loads in calciner and carbonator), the *ER-CO₂* and the *ER-CaO* heat exchangers. These heat exchangers are located before the introduction of CaO and CO_2 streams to the carbonator and their target is to keep the carbonator operation isothermal (850 °C). The maximum thermal power recovery in these heat exchangers is given when no CO_2 and CaO are discharged from storage ($f_{dch, CaO}$). The maximum thermal energy demand occurs when the CO_2 and CaO discharge fraction becomes maximum since both flowrates are

required to be preheated from 200 to 850 °C.

In the operation maps shown in Figs. 5 and 6, a specific operating point for the *ER-CaO* and *ER-CO₂* heat exchangers is highlighted and the values of heat exchanges are presented in the following. Under both operating modes, the selected operating point has a storage fraction of 0.9 and a discharge fraction of 0.1. Under the ESOM, the analysed heat exchangers require a low energy supply, being 1.51 MW for the *ER-CaO* heat exchanger and 1.74 MW for the *ER-CO₂* heat exchanger. While under EROM, both heat exchangers increase their energy demand up to 13.84 MW for the *ER-CaO* heat exchanger and 15.80 MW for the *EE-CO₂* heat exchanger. The lower amount of available solar energy under EROM, the less $CaCO_3$ flowrate from the carbonator diverted to the calciner. The reduction of the $CaCO_3$ flow rate introduced into the calciner implies an increase in the discharge flows of CaO and CO_2 from the storage tanks to keep constant the energy released in the carbonator.

The results obtained for the different operation points studied are shown for a single CaO purge value and the corresponding CaO/CO_2 molar ratio (R) which lead to a constant average conversion of the sorbent (X_{ave}) for any operating point at steady state. Future work including the parametric analysis of these variables and the study of their influence on the amount of stored energy or the energy exchange in the HEN will be of interest.

The analysis of a wide range of operation schemes allows the detailed sizing of the equipment included in the system. From the obtained results, it is observed that some of the largest heat exchangers modify their type of operation (demand or release of heat depending on the operation point under ESOM or EDOM). This information is relevant for the final design of the HEN which will be
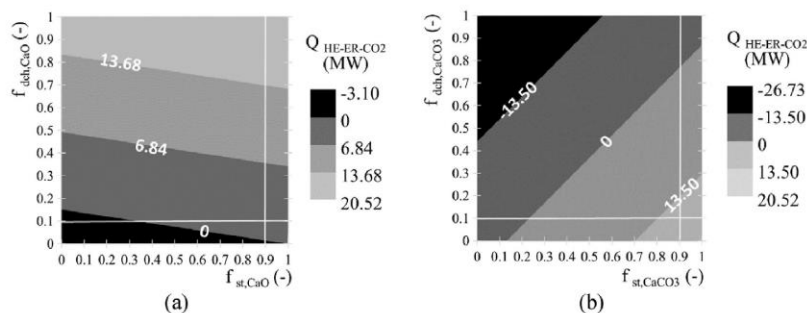
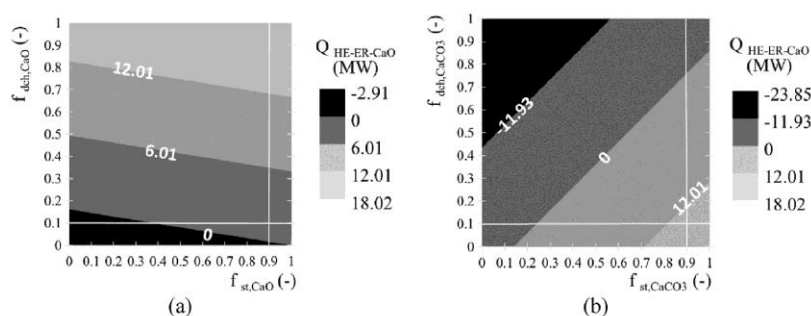**Fig. 5.** ER-CO₂ heat exchanger operation map under ESOM (a) and EROM (b).

8

66

Fig. 6. ER-CaO heat exchanger operation map under ESOM (a) and EROM (b).

eventually implemented in the integrated power plant. Further work should be done to develop a methodology which discriminate the operation points which are suitable for a logical operation of these heat exchangers.

5. Conclusion

The novelty of this study relies in the analysis of a wide number of potential points of operation that may take place arising from the different combinations of charge/discharge fractions of the CaO, CO_2 and $CaCO_3$ storage tanks.

In the present work, a large number of operating schemes for a CaL TCES system are evaluated to determine the impact of ESOM and EROM in the sizing of heat exchangers and reactors. The operating limitations of the system increment the dependence between R and f_p reducing the mechanisms to control the carbonation efficiency. Despite this fact, the conversion efficiency in the carbonator exceeds 90% by setting the CaO purge percentage in the calciner at 4%.

Results show that the storage tanks volumes needed for the energy storage could exceed 10,000 m^3 for CO_2 and 1200 m^3 for lime considering 15 h of operation at nominal load in the calciner. Besides, the maximum storage power reaches to 27.31 MW when the whole energy from the calciner at nominal load is stored. However, the storage tanks are oversized since the solar calciner will rarely operate at full nominal load during the whole day. Nevertheless, the CO_2 storage conditions should be reviewed to reduce the volume of the CO_2 storage tank and the solids separation at carbonator outlet should be studied in detail as strongly reduces the thermal demand of the system and the size of the storage tank of limestone. This separation process represents a technological challenge that is has not been solved yet. Further research on the techno-economic feasibility of the solid separation process would be required for the deployment of this storage option.

Operation maps created from the analysed schemes clearly establish the operation points in which power is stored, the amount of stored and released power and the size range of heat exchangers. The maximum power released (40.55 MW) is in the *EE-CaCO₃* heat exchanger under the energy release mode, when all the $CaCO_3$ flow from the carbonator is stored. The maximum power demand (41.38 MW) is from the *ER-CaCO₃* heat exchanger when it is required to discharge the maximum possible flow of $CaCO_3$ that can be stored. Heat exchangers designated as *EE* always release energy (ESOM and EROM) and heat exchangers called *ER* can release or demand energy depending on the defined storage and discharge fractions. Except for the *ER-CaCO₃* heat exchanger that always requires energy to preheat the flow of $CaCO_3$ from 200 °C to 850 °C. The discrimination of the operation points which conduct to one or other behaviour of the *ER* heat exchangers is key in the definition of the operation strategy under each mode of operation when the HEN is to be integrated with a power plant.

The main advantage of this study is the analysis of a greater number of operating points under both energy operation modes (storage/release). The number of operating points analysed is larger than in other studies due to the definition of storage and discharge fractions of CaO, CO_2 and $CaCO_3$. The analysis of these operating points allows to know the power range and the behaviour of the heat exchangers of the plant.

CRediT author statement

S. Pascual: Conceptualization, Methodology, Software. P. Lisbona: Conceptualization, Writing – review & editing, Visualization. M. Bailera: Writing – review & editing, Visualization. L.M. Romeo: Supervision.

Declaration of competing interest

The authors declare that they have no known competing financial interests or personal relationships that could have appeared to influence the work reported in this paper.

Acknowledgment

Nomenclature

Symbols

E	released or demand power, MW
f	fraction,
F	mole flow rate, kmol/s
k	CaO deactivation constant,
$\dot{m}$	mass flow rate, kg/s
Q	heat flow rate, MW
r	fraction of CaO particles,
R	molar ratio CaO/CO_2,
T	temperature, °C
V	volume, m^3

X	conversion,
ΔH_R^0	enthalpy of carbonation, kJ/mol
η	efficiency,

Subscripts and superscripts

0	$CaCO_3$ fresh
ave	average
capt	carbon capture
CR	carbonator
CL	calciner
dch	discharge
g	gas
in	input or inlet
max	maximum
N	number of carbonation-calcination cycles
out	output or outlet
p	purge or particle
r	residual
s	solid
st	storage

Acronyms and abbreviations

CaL	Calcium-looping
CSP	Concentrating Solar Power
EE	Energy Emitted
EES	Engineering Equation solver
ER	Energy Required
HE	Heat Exchanger
HEN	Heat Exchangers Network
SHS	Sensible Heat Storage
TCES	Thermochemical Energy Storage
TES	Thermal Energy Storage

References

[1] Concentrating Solar Power Projects. National renewable energy laboratory. 2018. https://solarpaces.nrel.gov/projects. [Accessed 29 January 2020].

[2] Achkari O, El Fadar A. Latest developments on TES and CSP technologies — energy and environmental issues, applications and research trends. Appl Therm Eng 2020;167:114806. https://doi.org/10.1016/j.applthermaleng.2019.114806.

[3] Kearney D, Kelly B, Herrmann U, Cable R, Pacheco J, Mahoney R, et al. Engineering aspects of a molten salt heat transfer fluid in a trough solar field. Energy 2004;29:861—70. https://doi.org/10.1016/S0360-5442(03)00191-9.

[4] González-Roubaud E, Pérez-Osorio D, Prieto C. Review of commercial thermal energy storage in concentrated solar power plants: steam vs. molten salts. Renew Sustain Energy Rev 2017;80:133—48. https://doi.org/10.1016/j.rser.2017.05.084.

[5] Letcher TM. Storing energy: with special reference to renewable energy sources. Elsevier Inc.; 2016. https://doi.org/10.1515/ci-2016-0627.

[6] Chen X, Zhang Z, Qi C, Ling X, Peng H. State of the art on the high-temperature thermochemical energy storage systems. Energy Convers Manag 2018;177: 792—815. https://doi.org/10.1016/j.enconman.2018.10.011.

[7] Prieto C, Cooper P, Fernández AI, Cabeza LF. Review of technology : thermochemical energy storage for concentrated solar power plants. Renew Sustain Energy Rev 2016;60:909—29. https://doi.org/10.1016/j.rser.2015.12.364.

[8] Barker R. The reactivity of calcium oxide towards carbon dioxide and its use for energy storage. Appl Chem Biotechnol 1974;24:221—7.

[9] Lisbona P, Bailera M, Hills T, Sceats M, Díez LI, Romeo LM. Energy consumption minimization for a solar lime calciner operating in a concentrated solar power plant for thermal energy storage. Renew Energy 2020;156:1019—27. https://doi.org/10.1016/j.renene.2020.04.129.

[10] Ortiz C, Valverde J, Chacartegui R, Perez-Maqueda L. Carbonation of limestone derived CaO for thermochemical energy storage: from kinetics to process integration in concentrating solar plants. ACS Sustain Chem 2018;6:6404—17.

[11] Abanades JC, Rubin ES, Anthony EJ. Sorbent cost and performance in CO2 capture systems. Ind Eng Chem Res 2004;43:3462—6. https://doi.org/10.1021/ie049962v.

[12] Khosa AA, Xu T, Xia BQ, Yan J, Zhao CY. Technological challenges and industrial applications of CaCO3/CaO based thermal energy storage system — a review. Sol Energy 2019;193:618—36. https://doi.org/10.1016/j.solener.2019.10.003.

[13] Alva G, Lin Y, Fang G. An overview of thermal energy storage systems. Energy 2018;144:341—78. https://doi.org/10.1016/j.energy.2017.12.037.

[14] Sarbu I. A comprehensive review of thermal energy storage. MDPI Sustain 2018;10:1—32. https://doi.org/10.3390/su10010191.

[15] Liu D. Progress in thermochemical energy storage for concentrated solar power : a review. Int J Energy Res 2018:1—16. https://doi.org/10.1002/er.4183.

[16] Benitez-guerrero M, Manuel J, Sanchez-jimenez PE, Perejon A, Perez-maqueda LA. Multicycle activity of natural CaCO 3 minerals for thermochemical energy storage in Concentrated Solar Power plants. Sol Energy 2017;153:188—99. https://doi.org/10.1016/j.solener.2017.05.068.

[17] Tregambi C, Salatino P, Solimene R, Montagnaro F. An experimental characterization of calcium looping integrated with concentrated solar power. Chem Eng J 2017;331:794—802. https://doi.org/10.1016/j.cej.2017.08.068.

[18] Da Y, Xuan Y, Teng L, Zhang K, Liu X, Ding Y. Calcium-based composites for direct solar-thermal conversion and thermochemical energy storage. Chem Eng J 2020;382:122815. https://doi.org/10.1016/j.cej.2019.122815.

[19] André L, Abanades S. Evaluation and performances comparison of calcium, strontium and barium carbonates during calcination/carbonation reactions for solar thermochemical energy storage. J Energy Storage 2017;13:193—205. https://doi.org/10.1016/j.est.2017.07.014.

[20] Sarrión B, Perejón A, Sánchez-Jiménez PE, Pérez-Maqueda LA, Valverde JM. Role of calcium looping conditions on the performance of natural and synthetic Ca-based materials for energy storage. J CO2 Util 2018;28:374—84. https://doi.org/10.1016/j.jcou.2018.10.018.

[21] Ortiz C, Chacartegui R, Valverde JM, Alovisio A, Becerra JA. Power cycles integration in concentrated solar power plants with energy storage based on calcium looping. Energy Convers Manag 2017;149:815—29. https://doi.org/10.1016/j.enconman.2017.03.029.

[22] Tesio U, Guelpa E, Verda V. Integration of ThermoChemical energy storage in concentrated solar power. Part 1: energy and economic analysis/optimization. Energy Convers Manag X 2020:100039. https://doi.org/10.1016/j.ecmx.2020.100039.

[23] Karasavvas E, Panopoulos KD, Papadopoulou S, Voutetakis S. Design of an integrated CSP-calcium looping for uninterrupted power production through energy storage. Chem Eng Trans 2018;70:2131—6. https://doi.org/10.3303/CET1870356.

[24] Ortiz C, Romano MC, Valverde JM, Binotti M, Chacartegui R. Process integration of Calcium-Looping thermochemical energy storage system in concentrating solar power plants. Energy 2018;155:535—51. https://doi.org/10.1016/j.energy.2018.04.180.

[25] Chacartegui R, Alovisio A, Ortiz C, Valverde JM, Verda V, Becerra JA. Thermochemical energy storage of concentrated solar power by integration of the calcium looping process and a CO 2 power cycle. Appl Energy 2016;173: 589—605. https://doi.org/10.1016/j.apenergy.2016.04.053.

[26] Tesio U, Guelpa E, Verda V. Integration of ThermoChemical energy storage in concentrated solar power. Part 2: comprehensive optimization of supercritical CO2 power block. Energy Convers Manag X 2020;6:100038. https://doi.org/10.1016/j.ecmx.2020.100038.

[27] Karasavvas E, Panopoulos KD, Papadopoulou S, Voutetakis S. Energy and exergy analysis of the integration of concentrated solar power with calcium looping for power production and thermochemical energy storage. Renew Energy 2020;154:743—53. https://doi.org/10.1016/j.renene.2020.03.018.

[28] Bailera M, Lisbona P, Romeo LM, Díez Ll. Calcium looping as chemical energy storage in concentrated solar power plants: carbonator modelling and configuration assessment. Appl Therm Eng 2020:115186. https://doi.org/10.1016/j.applthermaleng.2020.115186.

[29] Bravo R, Ortiz C, Chacartegui R, Friedrich D. Hybrid solar power plant with thermochemical energy storage: a multi-objective operational optimisation. Energy Convers Manag 2020;205:112421. https://doi.org/10.1016/j.enconman.2019.112421.

[30] Koepf E, Alxneit I, Wieckert C, Meier A. A review of high temperature solar driven reactor technology: 25 years of experience in research and development at the Paul Scherrer Institute. Appl Energy 2017;188:620—51. https://doi.org/10.1016/j.apenergy.2016.11.088.

[31] Zsembinszki G, Sole A, Barreneche C, Prieto C, Fernández AI, Cabeza LF. Review of reactors with potential use in thermochemical energy storage in concentrated solar power plants. Energies 2018;11. https://doi.org/10.3390/en11092358.

[32] Karasavvas E, Panopoulos KD, Papadopoulou S, Voutetakis S. Study of a droptube carbonator reactor for CSP-calcium looping based on a heterogeneous reaction model. Chem Eng Trans 2019;76:877—82. https://doi.org/10.3303/CET1976147.

[33] Yan Y, Wang K, Clough PT, Anthony EJ. Developments in calcium/chemical looping and metal oxide redox cycles for high-temperature thermochemical energy storage: a review. Fuel Process Technol 2020;199:106280. https://doi.org/10.1016/j.fuproc.2019.106280.

[34] Rinaldi F, Binotti M, Giostri A, Manzolini G. Comparison of linear and point focus collectors in solar power plants. Energy Procedia 2013;49:1491—500. https://doi.org/10.1016/j.egypro.2014.03.158.

[35] European Commission. PVGIS - photovoltaic geographical information system. 2019.

[36] Chacartegui R, Alovisio A, Ortiz C, Valverde JM, Verda V, Becerra JA. Thermochemical energy storage of concentrated solar power by integration of the calcium looping process and a CO2 power cycle. Appl Energy 2016;173: 589—605. https://doi.org/10.1016/j.apenergy.2016.04.053.

[37] Rodriguez N, Alonso M, Grasa G, Abanades JC. Heat requirements in a calciner of CaCO3 integrated in a CO2 capture system using CaO. Chem Eng J

10

68

2008;138:148−54. https://doi.org/10.1016/j.cej.2007.06.005.

[38] Abanades JC, Alvarez D. Conversion limits in the reaction of CO2 with lime. Energy Fuel 2003;17:308−15. https://doi.org/10.1021/ef020152a.

[39] Wang J, Anthony EJ. On the decay behavior of the CO2 absorption capacity of CaO-based sorbents. Ind Eng Chem Res 2005;44:627−9. https://doi.org/10.1021/ie0493154.

[40] Arias B, Abanades JC, Grasa GS. An analysis of the effect of carbonation conditions on CaO deactivation curves. Chem Eng J 2011;167:255−61. https://doi.org/10.1016/j.cej.2010.12.052.

[41] Romeo LM, Lara Y, Lisbona P, Escosa JM. Optimizing make-up flow in a CO2 capture system using CaO. Chem Eng J 2009;147:252−8. https://doi.org/

[42] Martínez A, Lara Y, Lisbona P, Romeo LM. Energy penalty reduction in the calcium looping cycle. Int J Greenh Gas Control 2012;7:74−81. https://doi.org/10.1016/j.ijggc.2011.12.005.

[43] Grasa GS, Abanades JC. CO$_2$ capture capacity of CaO in long series of carbonation/calcination cycles. Ind Eng Chem Res 2006;45:8846−51. https://doi.org/10.1021/ie0606946.

[44] Abanades JC. The maximum capture efficiency of CO2 using a carbonation/calcination cycle of CaO/CaCO3. Chem Eng J 2002;90:303−6. https://doi.org/10.1016/S1385-8947(02)00126-2.

10.1016/j.cej.2008.07.010.
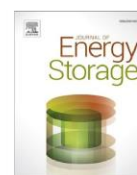
Research papers

Operation maps in calcium looping thermochemical energy storage for concentrating solar power plants

S. Pascual, P. Lisbona [*], L.M. Romeo

Mechanical Engineering Department, Escuela de Ingeniería y Arquitectura, Universidad de Zaragoza, 50018, Spain

ABSTRACT

Calcium Looping (CaL) process used as thermochemical energy storage system in concentrating solar plants has been extensively investigated in the last decade and the first large-scale pilot plants are now under construction. Existing research focuses on improving global efficiencies under steady-state and single modes of operation: energy storage or energy retrieval. However, TCES systems will operate under different operation points to adapt the load of its reactors to the solar availability and the energy demand from the power cycle. A thorough analysis of the operation modes provides an extremely large number of potential situations to operate the system. In this study, operation maps which maximize thermal energy availability and energy storage efficiency are defined. Furthermore, a novel approach for the management of partially carbonated solids is examined to reduce the circulation of inert material in the system based on preliminary experimental results which allows for a partial separation of carbonated solids. Two threshold scenarios are analysed: (i) no solids separation as considered in most CaL TCES studies and (ii) ideal total solids separation. The aims of this work are to set methodological criteria to define the optimal operation map and to assess the effect of partially carbonated solids separation on the energy penalties and equipment size. The inclusion of a solid separation stage leads to a maximum increase of energy storage efficiency of 26 % and a size reduction between 53 and 74 % of those heat exchangers affected by solids streams.

1. Introduction

Half of the existing concentrated solar power (CSP) plants include thermal energy storage (TES) to maximize operating hours and electricity production [1]. Since the CSP installation cost has decreased by 70 % in the last 10 years [2], CSP plants with TES will be able to compete with conventional fossil fuel-based baseload facilities for electricity production [3]. The integration of TES in CSP plants enhances their dispatchability with variable solar radiation or during the night [4]. Literature is plenty of works about the feasible options to do this integration, some of them include current status and research trends [4], innovations [5] and specifications and pros and cons of different concentrating solar technologies [6–8] that include high (i) operating temperatures (above 1000 °C), (ii) thermodynamic efficiencies for the CSP plant and (iii) nominal power capacities [5–7]. Cost analysis has been also presented [9] demonstrating that the variability of the TES material annual costs from one year to the next is lower than fossil fuels, whose price trend is less predictable. The amount of TES stored depends on (i) the specific heat of the medium, (ii) the temperature variation and

(iii) the amount of storage material option [8]. Most of the CSP plants currently under commercial operation or under construction use molten salts as a thermal storage medium [10]. Beyond molten salts, for sensible heat storage, water is also commercially used as thermal storage medium [11]. For latent heat storage, Phase Change Materials (PCMs) are used, although they show some limitations such as a low enthalpy of phase change, low thermal conductivity and instable at high temperatures [12,13]. The selection of the best TES system to each CSP technology is complex and must consider specific characteristics with regard to storage [14]. One of the preferred options is thermochemical energy storage (TCES) which makes use of the reversibility of chemical equilibrium reactions to store or to release energy through a cyclic process. TCES shows enhanced storage capacity and the minimum energy losses under seasonal storage in comparison with sensible and latent TES. Thus, TCES will be able to improve CSP conversion efficiency in the near future [15]. Moreover, TCES can also be easily integrated in CSP plants which operate above 800 °C [16,17] since it operates in the range of 450–1300 °C.

Among TCES system, the Calcium Looping process, firstly proposed

by Baker [18], is one of the most promising. Calcination reaction of limestone, Eq. (1), is endothermic and takes place during sunlight hours at 920–950 °C [19]. Calcination products, carbon dioxide (CO_2) and calcium oxide (CaO), can be total or partially stored, diverting the remaining flowrate to the carbonator to release energy.

$$CaCO_{3\ (s)} \leftrightarrows CaO_{(s)} + CO_{2\ (g)} \quad \Delta H_R^\circ = +178\ kJ/mol \quad (1)$$
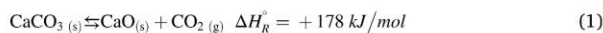
The energy density of $CaCO_3$ ranges between 390 and 490 kWh/t [20,21] and this value represents the main advantage of the CaL TCES technology. During night, or whenever extra thermal energy is required by the power cycle to fulfil electricity demand, the stored CO_2 and CaO may be fed into the carbonator to retrieve the stored thermal energy. The carbonation exothermic reaction, reverse Eq. (1), takes place between CO_2 and CaO at 600–850 °C [22] releasing high temperature heat. The generated $CaCO_3$ can be stored until sunlight hours when the calcination starts up again, closing the loop.

Energy storage density of CaL TCES is estimated by several authors using different definitions for comparison with other storage technologies applied to CSP plants. Sun et al. determine the energy density as the amount of stored energy per unit mass CaO (417 kWh/t after 10 cycles). In this case, the energy density is proportional to the carbonation conversion and represents the energy released in the carbonation reaction per mass CaO [23]. Di Lauro et al. define the density of energy storage for each carbonation/calcination step as the sum of (i) the chemical energy stored and (ii) the excess of sensible heat of the material respect to the discharged temperature (650 °C). The energy storage density reaches to 1419 MJ/m³ after 10 cycles, considering a tapped bulk density of 1590 kg/m³ for limestone. Moreno et al. established an energy storage density of 1220 MJ/m³ after 20 cycles for limestone, considering only the chemical energy stored [24]. These values are larger than the molten salts energy storage density (800 MJ/m³), taking into account only the sensible heat stored [25]. Other works estimate the energy storage density as the relation between (i) the energy stored as chemical, latent and sensible heat and (ii) the size of the storage tanks. The energy storage density obtained for a conventional CaL CSP system achieves 1300 MJ/m³, which is much higher than the energy storage density of a typical molten salt with a temperature change of 275 °C (near 400 MJ/m³) [26].

Regarding reactor design, several researchers have dealt with simulation activities for, both, carbonator [27,28] and calciner [19]. These works highlighted the importance of a proper design to evacuate the energy released during carbonation [28] and the difficulties for achieving a smooth temperature profile in the calciner [19]. New concepts based on autothermal fluidized bed reactor for calcination are investigated by Padula et al. to improve the overall TCES efficiency [29]. The advantages offered by fluidized bed technology related to gas-solid heat transfer have driven its adaptation to the new requirements of concentrated solar energy [30]. Besides, Ortiz et al. proposed an entrained flow reactor to perform the calcination under operating conditions of 765 °C and low-pressure (0.01 bar), minimizing energy losses and CaO sintering [31]. Within the potential reactors for the calcination of limestone in TCES systems (fluidized bed, entrained bed and rotary reactor), the indirectly irradiated fluidized beds seem to be the most suitable option [32]. Unfortunately, experimental results on CaL TCES pilot plants are still scarce limiting the potential validation of the reactor design modelling studies [30,33]. Important issues must be addressed for the scale-up of $CaCO_3$ calcination reactors, such as the particle attrition and the high temperature resistance of the reactor wall components [32].

The CaL TCES integrated with power cycles and the optimization of the overall efficiency has been extensively investigated [34–37]. Main literature findings conclude that CO_2 power cycles provide the greatest results. The efficiencies reported for different layouts and operating conditions achieved a 40.4 % in the case of supercritical CO_2 cycles [36], and ranged between 31 and 44 % for CO_2 closed Brayton cycle

[34,35,37,38]. Regarding Bryton cycles, Tesio et al. investigate the integration of two alternatives: helium and supercritical CO_2. The results show the greatest efficiency for helium cycle, whereas the supercritical CO_2 cycle is the cheapest alternative [39]. Secondly, the new improved CaL TCES designs found in literature enhance the dispatchability and minimize the cost of the CSP plants. Bravo et al. propose a hybrid solar configuration combining the CSP plant with CaL TCES with a photovoltaic (PV) plant, achieving a LCOE of 123 USD/MWh with a capacity factor of up to 73 % for the location assessed with the best solar resource [40]. Both plants produce electrical energy during the sunlight hours, partially storing energy in the CaL TCES system and covering electricity demand with part of the energy from the PV plant. The stored energy is released to cover energy demand under unavailability of solar energy [38,40]. Another way to improve the renewable share developed by Tregambi et al. is the integration of a CSP plant and CaL carbon capture technology with Power to Gas technology. The CaL process operates continuously 24 h/day, (i) storing CaO after calcination step during sunny hours and (i) feeding the CaO stored during the daytime to the carbonator when solar radiation is unavailable. The production of methane from captured CO_2 and hydrogen from water electrolysis is considered, covering the energy demand by PV plant or other renewable energy source. The overall efficiency from solar to methane production is between 20 and 22 % [41]. One of the most recently proposed configuration investigated by Ortiz et al. is based on the integration of the CaL TCES system in a combined cycle plant. The CSP plant provides solar energy to (i) the combined cycle and (i) the TCES system during the day. The energy stored in the CaL TCES system is released when solar radiation is unavailable to cover the energy demand of the power block [42]. The overall efficiency is almost 45 %, considering the solar resource of a specified location assessed [43].

In general, these studies present their results under stationary operation at nominal load with constant fractions of stored products during sunlight hours and constant operating loads of the carbonator during the night period. Nevertheless, this technology will operate under varying loads and, as a consequence, further analysis is required to describe the operational behaviour of the complete CSP plant. The amount of stored and discharged material will determine the size of heat exchangers, the transient load in the equipment and the integrations with power cycle or the use of the thermal energy as well as equipment cost and LCOE [44]. One of the novelties of this work relies in the analysis of a wide variety of the potential situations arising from the different combinations of charge/discharge fractions of the CaO, CO_2 and $CaCO_3$ storage tanks. The influence of the storage/discharge fractions on the behaviour of the plant equipment was assessed in a previous work published by the authors without considering the potential situations with simultaneous energy storage and retrieval [44]. A large number of potential operation points of the CaL-CSP system which can be operationally useful were disregarded from the previous analysis. However, the present work provides a much wider study including all the possible points and introducing a systematic methodology based on clear criteria to select and disregard the operation points under observation. Furthermore, the definition of the final operation maps in the present work maximizes the efficiency of the CaL TCES system. No research is found in literature about the optimum operational performance of CaL CSP and the different strategies to achieve high thermal energy availability or high energy storage efficiency.

Regarding energy penalties in the CaL TCES system, the circulation and storage of non-reactive solid material is one the most influential aspects on the energy efficiency of the system [45]. Low CaO activity in the carbonator leads to large amounts of inactive solid material circulating in the system [46]. A research gap also exists in the assessment of the potential reduction of inert solids circulation and storage. In this work, the effect on the energy penalty of the recirculation of partially converted CaO after carbonation reaction has been assessed.

Thus, the originality of the present work relies in (i) the establishment of optimal operation maps to guide the operation under transient

mode and (ii) the assessment of the implementation of a solids separation unit at carbonator outlet to reduce the energy demand and size of the CaL TCES system. The main objectives of the study are (i) to define adequate and methodological criteria to filter the operation points and select the feasible situations under real operation, (ii) to determine the required size and energy penalties for the optimal situations which meet technical, energy and design, equipment loads limitations and maximize significant operating parameters and (iii) to explore the effect of solids separation after carbonation reactor on the energy penalties and equipment size.

2. Systems description and operation modes

The system consists of two reactors, a calciner located inside the solar receiver and a carbonator, with intermediate storage tanks of $CaCO_3$ (ST1), CaO (ST2) and CO_2 (ST3) as illustrated in Figs. 1 and 2. A thermal input of 100 MWth to the solar calciner ($\dot{Q}_{CL}$) under nominal operation conditions is assumed considering a solar field as described in [44]. The calciner operates at atmospheric pressure and 950 °C under pure CO_2 atmosphere to ensure complete conversion [47]; thus, $CaCO_3$ is fully decomposed into CaO and CO_2. Depending on the operation mode, the CO_2 and CaO flowrates from the calciner are directed to the carbonator or diverted towards their corresponding storage tanks (ST3 and ST2).

Since CaO deactivates with the number of cycles, a stream of fresh limestone is fed in the calciner to keep a reasonable average sorption activity of the solid population. Thus, the $CaCO_3$ fed into the calciner reactor comes from both the contribution of fresh limestone and the $CaCO_3$ produced after carbonation reaction. Fresh limestone counterbalances the purged solid material (f_p) set as a percentage of the CaO molar flow formed in calcination reaction.

The carbonator operation conditions are set in 850 °C under pure CO_2 atmosphere and a pressure of 1.2 bar to improve the circulation of solids between calciner and carbonator [35]. The exothermic carbonation reaction is not complete and the average carbonation degree must be determined. The model used to determine the deactivation of the CaO particles is tuned adjusting the kinetic model described by Grasa et al. [48] obtained for 650 °C and an approximately CO_2 concentration between 10 and 15%vol. The amount of carbonated CaO and the energy released ($\dot{Q}_{CR}$) will depend on the average sorption activity of the population of particles circulating in the system [49]. Therefore, a mixture of $CaCO_3$ and CaO consisting of partially carbonated lime particles which present a range of densities between 2762 and 2930 kg/m^3 is found at carbonator outlet [50]. This experimentally measure density difference for the cycled particles points out the existing potential for

partial separation of these particles through fluidization processes. The CaO to CO_2 molar ratio introduced in the carbonator (R) and the average sorbent activity define the carbon capture efficiency in the carbonator reactor.

CO_2 is stored at 35 °C and 75 bar. The CO_2 compression-train includes four interleaved compression and cooling stages. The first three cooling stages reduce the temperature to 50 °C and the last stage down to the storage temperature, 35 °C. A pressure ratio of 3 is considered in each compression stage which limits the electricity consumption and makes use of the heat released in the cooling stages. The CO_2 discharged from the tank ST3 must reduce its pressure (75 bar) to the carbonator working pressure (1.2 bar) through an expansion valve (EV). Besides, the temperature of the discharged CO_2 is increased up to ambient temperature (HEAMB) before being introduced to the ER-CO2 heat exchanger. Depending on the operation mode, the CO_2 from the storage tank ST3 is mixed with CO_2 from calciner before being introduced into carbonator at 850 °C. Regarding solids storage conditions, lime and limestone storage temperature may range from ambient to 200–700 °C [34]. Storage temperature and pressure of solids are set at 200 °C and 1 bar. Both scenarios have been simulated with Engineering Equation Solver (EES) software [51], using internal data library for CO_2 properties and external data sources for solids substances: lime [52] and limestone [53].

Lastly, a network of heat exchangers (HE) will supply or remove thermal energy according to the operation mode of the CaL TCES system. Heat exchangers designated as EE, Figs. 1 and 2, are able to provide energy under any mode of operation with heat losses of a 2 %. However, the heat exchanger designated as ER-CaCO3 always requires thermal energy input while the rest of ER heat exchangers provide or demand energy depending on the operation mode. The heat exchange network will be designed to cover the thermal energy required by (i) heat exchangers named ER and (ii) an associated power block to produce electricity. Only the heating and cooling needs have been calculated. The thermal integration is beyond the scope of the present study and will be assessed in future works.

In this study, the CaL TCES system has been analysed under two threshold scenarios which consider (SC1) no separation of solids of the solid stream leaving the carbonator, Fig. 1, and (SC2) an ideal and total separation of the solid CaO-CaCO3 mixture generated in the carbonator, Fig. 2. Carbonation occurs on the surface of the particle producing a mixture of partially carbonated particles, thus, complete separation of CaO and $CaCO_3$ will never effectively happen and SC2 represents an unreal situation. However, it is used in the study as a threshold situation to easily estimate a minimum energy consumption and size of the equipment. The operating conditions of the main equipment in the CaL
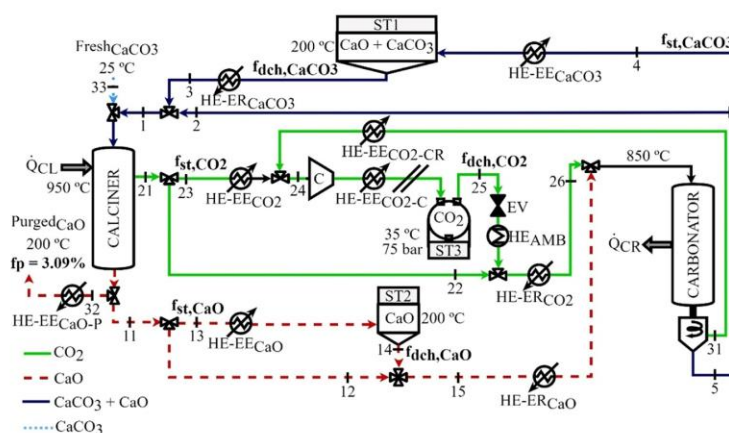

Fig. 1. CaL TCES system for a 100 MWth CSP plant w/o solid separation (SC1).
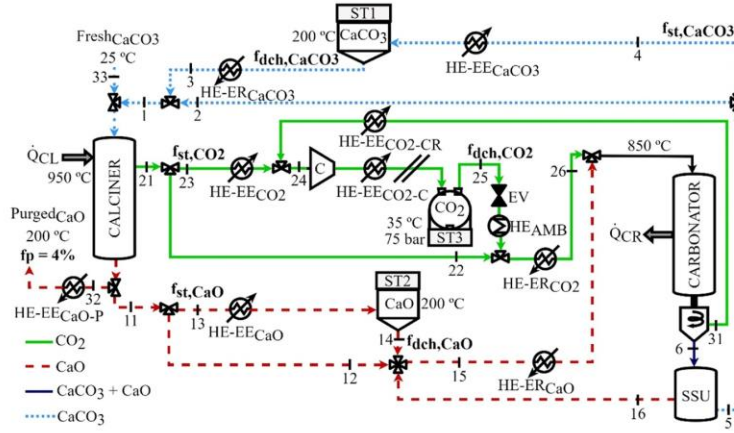
Fig. 2. CaL TCES system under total solids separation (SSU) scenario (SC2).

TCES system (calciner, carbonator, storage tanks, heat exchangers and compression-cooling train) are the same under both scenarios. The molar ratio between CaO and CO_2 (R) is set as 4.26 in both scenarios [27], leading to a f_p of 3.09 % and 4 % for SC1 and SC2, respectively. Besides, an average sorption activity of 20.4 % and 22.6 % is estimated for the sorbent under SC1 and SC2, respectively, considering a residual conversion of 7.5 % and a deactivation constant of 0.52 for the selected limestone, X_N, and a conservative age distribution of solid population as provided by Pascual et al. [44]. The different mass balances in the CaL TCES systems and the relevant performance parameters are described under both threshold scenarios.

2.1. CaL TCES w/o solid separation unit (Scenario 1 - SC1)

The first scenario does not consider solid separation at the outlet of the carbonator and is illustrated in Fig. 1. Under SC1, the input of solid particles to the calciner which must be heated up to 950 °C consists of a mixture of around 80 % lime and 20 % limestone and comes from the carbonator at 850 °C and the storage tank ST1 at 200 °C. The inlet stream of solids directed to the carbonator results from the mixture of the CaO stream discharged from storage tank ST2 (200 °C) and the direct CaO flowrate from calciner (950 °C).

Only a share of the solar input is used to calcine the limestone introduced in the calciner while a large amount of heat is invested in heating the CaO/CaCO3 solid mixture up to 950 °C. For this reason, the lower amount of CaO in the inlet solid mixture, the higher amount of calcined limestone and, therefore, the higher chemical energy stored in the solid stream leaving the calciner. Besides, the amount of solid particles circulating between reactors is significantly reduced, so the involved heat exchangers and storage tanks decrease their size.

The specific thermal energy required in the calciner is 2169.5 kJ/kg CaCO3 for a system without solids separation unit (SC1) and 1906.6 kJ/kg CaCO3 for a system with ideal and complete solids separation (SC2). This significant reduction of heat demand is related to the lower pre-heating needs for the solids stream introduced in the calciner.

2.2. CaL TCES with solid separation unit (Scenario 2 - SC2)

The second scenario under study considers the ideal situation of total solid separation at carbonator outlet (SC2) as shown in Fig. 2. This unreal solids separation assumes the total separation of the solid mixture into two pure streams of CaCO3 and CaO. In particular, the solid separation unit (SSU) receives the CaO/CaCO3 mixture from the carbonator and separates (i) the unreacted CaO which is recirculated into the carbonator and (ii) the limestone stream sent back to the calciner or to the

CaCO3 storage tank (ST1). This scenario will be useful to analyse the threshold values of equipment size and energy consumptions under the most advantageous case.

Under this second theoretical scenario, the calciner is only fed with CaCO3 in the solid inlet stream. Thus, the solar energy input is fully used to heat the limestone up to 950 °C and calcine the solid material. No solar energy is wasted in the heating of calcined material, CaO. For this reason, the amount of calcined limestone is increased for the same calciner power while the circulation of solids between reactors is reduced. The unreacted CaO after carbonation is separated and recirculated into the carbonator itself.

The greatest influence of the solid separation unit affects the equipment shown in Fig. 2: (i) the heat exchangers with solids streams involved (EE-CaO, ER-CaO, EE-CaCO3 and ER-CaCO3) and (ii) mainly CaO and CaCO3 storage tanks (ST2 and ST1).

2.3. Operation modes

Depending on the availability of solar energy and/or the demand of thermal energy required from the CaL TCES, the management of the gas and solids streams to and from the storage tanks will follow a different operation mode. Under both scenarios (SC1 and SC2), three operation modes are analysed: (i) energy storage operation mode (ESOM), (ii) direct operation mode (DOM) and (iii) energy retrieval operation mode (EROM).

2.3.1. Storage and discharge fractions

The operation under nominal power in the calciner, 100 MWth, provides the maximum available energy to be stored. Moreover, the maximum retrieved power will be achieved under nominal operation in the carbonator determined considering the direct operation of the carbonation-calcination cycle. The chemical energy content of the solid stream generated in the calciner under nominal conditions amounts to 69 MWth under SC1 and 88 MWth under SC2. This energy will be totally recovered in the carbonator under direct operation and represents the maximum released power and the nominal power in the carbonator. The maximum mass flows of gas and solids obtained when reactors operate at nominal power are presented in Table 1.

The maximum CO_2 and CaO flowrates ($\dot{m}_{st,max,CO2}$, $\dot{m}_{st,max,CaO}$) diverted to or discharged from the storage tanks ST3 and ST2 corresponds to the maximum CO_2 and CaO flowrates leaving the calciner when it operates at nominal power. The flowrates of CO_2 and CaO received in the storage tanks ST3 and ST2 ($\dot{m}_{st,CaO}$, $\dot{m}_{st,CO2}$) will correspond to a fraction of these maximum CO_2 and CaO streams, Eq. (2). The CO_2 and CaO leaving the storage tanks ST3 and ST2 ($\dot{m}_{dch,CaO}$, $\dot{m}_{dch,CO2}$)

Table 1
Mass flow of gas and solids under calciner and carbonator nominal powers.

Nominal power and mass flow description			No separation (SC1)	Total separation (SC2)
$P_{nom,CL}$	(MW)	Nominal power calciner	100	100
$P_{nom,CR}$	(MW)	Nominal power carbonator	69	88
$\dot{m}_{st,max,CO2}$	(kg/s)	Maximum mass flow CO_2 from CL	21.16	24.35
$\dot{m}_{st,max,CaO}$	(kg/s)	Maximum mass flow CaO from CL	114.77	29.83
$\dot{m}_{st,max,CaCO3}$	(kg/s)	Maximum mass flow $CaO/CaCO_3$ from CR	133.15	53.24[a]

[a] Only $CaCO_3$ from SSU.

are also defined as a fraction of the maximum CO_2 and CaO streams at calciner outlet, Eq. (3).

$$f_{st,CaO} = \frac{\dot{m}_{st,CaO}}{\dot{m}_{st,max,CaO}} = \frac{\dot{m}_{13}}{\dot{m}_{st,max,CaO}} \tag{2}$$

$$f_{dch,CaO} = \frac{\dot{m}_{dch,CaO}}{\dot{m}_{st,max,CaO}} = \frac{\dot{m}_{14}}{\dot{m}_{st,max,CaO}} \tag{3}$$

The maximum $CaO/CaCO_3$ flowrate ($\dot{m}_{st,max,CaCO3}$) diverted to or discharged from the storage tank ST1 corresponds to the maximum $CaO/CaCO_3$ flowrate leaving the carbonator when it operates at nominal power (69 MWth and 88 MWth for SC1 and SC2, respectively). The CaO/$CaCO_3$ stream received in the storage tank ST1 ($\dot{m}_{st,CaCO3}$) will correspond to a fraction of this maximum $CaO/CaCO_3$ flowrate, Eq. (4). The CaO and $CaCO_3$ leaving the storage tank ST1 ($\dot{m}_{dch,CaCO3}$) are defined as a fraction of the maximum mixture of CaO and $CaCO_3$ stream at carbonator outlet, Eq. (5).

$$f_{st,CaCO3} = \frac{\dot{m}_{st,CaCO3}}{\dot{m}_{st,max,CaCO3}} = \frac{\dot{m}_4}{\dot{m}_{st,max,CaCO3}} \tag{4}$$

$$f_{dch,CaCO3} = \frac{\dot{m}_{dch,CaCO3}}{\dot{m}_{st,max,CaCO3}} = \frac{\dot{m}_3}{\dot{m}_{st,max,CaCO3}} \tag{5}$$

2.3.2. Operation modes

The operating points for a given pair of calciner/carbonator loads are defined through the storage/discharge fractions. The maximum storage and discharge fraction as defined above are theoretical thresholds which, in this study, have been assumed as 1.

When the system is operated as Energy Storage Operation Mode (ESOM), the input of solar power is assumed to be equal or lower than the calciner nominal power, while the power released in the carbonator will be always below its nominal power for both SC1 and SC2. During this operation mode, the resulting CaO and CO_2 streams from calciner are partially or totally stored and the CaO and CO_2 storage fractions ($f_{st,CaO}$, $f_{st,CO2}$) are always higher than the discharge fractions ($f_{dch,CaO}$, $f_{dch,CO2}$). It is considered that no solids from the carbonator are diverted to storage ($f_{st,CaCO3} = 0$) under ESOM. Thus, the feasible operating points for each pair of carbonator/calciner loads are defined by a given discharge fraction of $CaCO_3$ ($f_{dch,CaCO3}$) and a range of storage fractions of CaO and CO_2. The minimum and maximum values of these fractions are presented in Table 2.

Under the Energy Retrieval Operation Mode (EROM), the solar power input in the calciner is considered to be below its nominal power. The thermal power released in the carbonator can be equal to or lower than its nominal power for each studied scenario (SC1 and SC2). The $CaCO_3$ storage fraction ($f_{st,CaCO3}$) is always higher than the $CaCO_3$ discharge fraction ($f_{dch,CaCO3}$) at all possible energy release operating points for each pair of calciner/carbonator loads. It is considered that no gas or solids from the calciner are diverted to storage ($f_{st,CaO} = 0$) under EROM. The technically operating points for each pair of reactor loads are defined by a given discharge fraction of CaO ($f_{dch,CaO}$) and a range of storage fractions of $CaCO_3$. The minimum and maximum values of these fractions are also shown in Table 2.

The third operation mode, Direct Operation Mode (DOM), presents a direct circulation between reactors without net storage or discharge of

Table 2
Definition of operation modes of the TCES system.

Operation parameters	Energy operation modes	
	ESOM	EROM
$\dot{Q}_{CL}$ (MW)	$\leq P_{nomCL}$	$< P_{nomCL}$
$\dot{Q}_{CR}$ (MW)	$< P_{nomCR}$	$\leq P_{nomCR}$
$Load_{CL}$ (−)	≤ 1	0 to $< L_{CR}$
$Load_{CR}$ (−)	0 to $< L_{CL}$	≤ 1
$f_{st,CaO}$ (−)	$f_{dch,CaCO3}$ to L_{CL}	0
$f_{dch,CaO}$ (−)	0 to L_{CR}	$(L_{CR}$-$L_{CL})$
$f_{st,CaCO3}$ (−)	0	$f_{dch,CaO}$ to L_{CR}
$f_{dch,CaCO3}$ (−)	$(L_{CL}$-$L_{CR})$	0 to L_{CL}

CaO $CaCO_3$ and CO_2. The calciner and carbonator are operated at the same load with respect to their respective nominal powers under DOM. This operation mode is not useful for TCES but for its implementation for carbon capture processes.

Table 2 summarizes the information for the different operating variables of the operating modes of the system described above (ESOM and EROM).

Thus, an operation point is completely defined by a pair of reactor loads (L_{CL}, L_{CR}) and the storage fraction of CaO/CO_2 ($f_{st,CaO}$) under ESOM and the storage fraction of $CaCO_3$ ($f_{st,CaCO3}$) under EROM. The rest of discharge and storage fractions are dependant of these parameters.

3. Criteria for operation point selection

The operation points included in the operation map of the CaL TCES system are narrowed down according to following aspects: the heat exchange equipment size, the carbonator load and thermal energy availability and the storage energy efficiency.

3.1. Design and technical criteria

Several situations are detected to be not technically feasible or energetically or economically disadvantageous. Thus, several criteria are established to narrow down the amount of studied operation points:

C.1. Under ESOM, it is assumed that no limestone is stored in ST1 ($f_{st,CaCO3} = 0$) while, under EROM, no lime is diverted to the storage tank ST2 ($f_{st,CaO} = 0$).

C.2. The operating points corresponding to the direct operation modes are discarded given the energy penalty imposed by the operation of the CaL system without producing a net thermal energy storage or retrieval.

C.3. Only those operating points in which ER-HE heat exchangers demand energy are considered technically suitable for the design of the facility.

C.4. A minimum partial load is required for the operation of the carbonator and the heat exchangers involved in the system to ensure the continuous operation of the CSP power block. The minimum operation load is set at 50 % for system equipment with nominal released power >15 MW (carbonator, EE-CO2, EE-CaO and EE-CaCO3).

5

C.5. A maximum energy demand is established for the ER-CaCO3 heat exchanger to limit its energy consumption and size. This threshold value is set as the 50 % of the maximum heat requirement in ER-CaCO3 obtained among the operation points analysed after C.3.

The performance of the system is only assessed for those operation points selected after the application of these five criteria. The selection of the most interesting points for each pair of loads (L_{CR}, L_{CL}) to define the operation map will be based on the evaluation of the thermal energy availability (η_{av}) and the storage energy efficiency (η_{st}).

3.2. Definition of energy availability, storage efficiency and specific storage consumption

Three parameters are defined to characterize the performance of the system depending on the mode of operation: the thermal energy availability, the storage efficiency and the specific storage consumption. The thermal energy availability ratio compares the available thermal energy of the system to the invested energy input. The storage efficiency compares the amount of stored energy and the net energy consumed during the storage process. The specific storage consumption presents the total amount of energy (thermal and electrical) required to store a mass unit of lime.

Under EROM, the thermal energy availability of the system is defined by Eq. (6). The available heat includes the thermal power from the carbonator and EE heat exchangers. The energy invested in this process includes (i) the heat of calcination demanded in the calciner, $\dot{Q}_{CL}$, (ii) the energy consumption related to the storage step of the lime discharged from the tank ST2, (iii) the thermal power demand in the heat exchangers named ER.

$$\eta_{av(EROM)} = \frac{\dot{Q}_{CR} + \sum \dot{Q}_{HE\,EE}}{\dot{Q}_{CL} + \sum \dot{Q}_{HE\,ER} + SSC \bullet \dot{m}_{CaO,dch}} \tag{6}$$

The total energy input to the system under ESOM only includes the required heat in the calciner, $\dot{Q}_{CL}$, and the heat demanded to preheat the gas and solid mass flowrates through the heat exchangers named ER. This thermal energy availability is defined by Eq. (7).

$$\eta_{av(ESOM)} = \frac{\dot{Q}_{CR} + \sum \dot{Q}_{HE\,EE}}{\dot{Q}_{CL} + \sum \dot{Q}_{HE\,ER}} \tag{7}$$

The storage efficiency may be calculated through Eq. (8). The stored energy accounts for the sensible heat of the stored material and the chemical energy stored in the lime which will be latter carbonated. The energy invested in the process includes the calcination heat required to produce the lime sent to ST2 ($\dot{Q}_{CL,st}$), the energy to preheat of the amount of limestone discharged from the storage tank ST1 which is later stored as lime in ST2 ($\dot{Q}_{HE\,ER\,CaCO3,st}$) and the electric power consumed in the compression of the stored carbon dioxide ($\dot{W}_{compressor}$). This parameter provides an estimation of the share of stored energy in comparison to the energy invested during the storage process.

$$\eta_{st} = \frac{\dot{Q}_{st,CaO}}{\dot{Q}_{CL,st} + \dot{Q}_{HE\,ER\,CaCO3,st} + \dot{W}_{compressor}}$$
$$= \frac{SH_{CO2+CaO,st} + \Delta H_R^0 \bullet \dot{n}_{CaCO3,CR}}{\dot{Q}_{CL,st} + \dot{Q}_{HE\,ER\,CaCO3,st} + \dot{W}_{compressor}} \tag{8}$$

The specific storage consumption (SSC), Eq. (9), indicates the energetic feasibility of the storage process under specific operation points. It must be kept in mind the qualitative interest of the parameter but its limitation as quantitative measure given the mix of energy types in its definition.

$$SSC = \frac{\dot{Q}_{CL,st} + \dot{Q}_{HE\,ER\,CaCO3,st} + \dot{W}_{compressor}}{\dot{m}_{CaO,st}} \tag{9}$$

4. Results and discussion

The operation points to be analysed are narrowed down based on initial assumptions and technical criteria. Once the number of cases are reduced, the energy availability ratio and storage efficiency are calculated to assess the most advantageous operation point for a given pair of calciner/carbonator loads.

4.1. Matrix of potential operational points

Each pair of reactors loads determines the net energy to be stored and/or discharged but a large number of operating points with different storage and discharge fractions may lead to the same net energy storage or release situation. However, the energy demand or availability in the different components of the system (heat exchangers, compressor) will vary depending on the values of the storage and discharge fractions. In this section, possible operating points are selected using those criteria previously defined.

Table 3 summarizes the range size of the heat exchangers and compressor-cooling train of the possible operation points applying criteria (C.1), (C.2) and (C.3). The sign (−) means heat power release or electric power demand whereas the sign (+) means the equipment requires heat.

The minimum load in the carbonator and the heat exchangers EE-CO2, EE-CaO and EE-CaCO3 is set at 50 % by Criterion 4 (C.4). The nominal power of each equipment corresponds to the values presented maximum in the column [Max] of Table 3 under both scenarios. The carbonator operates above 50 % of its nominal power under both operation modes (ESOM and EROM).

Regarding the heat exchangers, the minimum partial load for EE-CO2 and EE-CaO under the ESOM will be 50 % of their nominal power while EE-CaCO3 will be disconnected. Under EROM, EE-CaCO3 heat exchanger will operate above 50 % of its nominal power while EE-CO2 and EE-CaO are disconnected. On the other hand, the ER-CaO and ER-CO2 heat exchangers are dependent on the load of the carbonator and, therefore, of the CaO and CO_2 inlet flowrate in the carbonator, respectively. While the ER-CaCO3 heat exchanger will be designed to always work below a 50 % of the maximum energy requirement, (C.5). Fig. 3 illustrates the number of operation points discretizing the storage and discharge fractions from 0 to 1 in ten steps after also applying from (C.1) to (C.5).

The operating points, considering a minimum partial load of 50 % in the mentioned equipment and limiting the size of ER-CaCO3, amount to 69 points within ESOM and 114 points under EROM. The thermal energy availability and the energy storage efficiency will be calculated for all these operation points to provide information about the most favourable operation map when the following objectives are pursued within the system: (i) the maximization of the thermal energy availability (EROM) or (ii) the maximization of the energy storage efficiency (ESOM).

4.2. Thermal energy availability – Energy Retrieval Operation Mode

First, the operation map which maximizes thermal energy availability is determined. This parameter becomes especially relevant when the system is operated to recover the stored energy, EROM. The thermal energy availability was calculated for all the operating points shown in Fig. 3 and, then, those which led to the highest values were selected to create this operation map. For each pair of carbonator/calciner loads, the thermal energy availability is computed by Eq. (6) when energy retrieval takes place (EROM). The maximum thermal energy availability and the power discharged from storage tanks under both solid management scenarios (SC1 and SC2) are illustrated in Fig. 4.

Under both scenarios, the maximum thermal energy availability diminishes for lower calciner and higher carbonator loads. The maximum thermal energy availability range between 0.56 and 0.86 for SC1 and

Table 3
Ranges of plant equipment size after applying C.1, C.2 and C.3.

Energy flow description				SC1 - w/o SS		SC2 - 100%SS	
				Min	Max	Min	Max
Heat exchanger		T_{in}[a] (°C)	T_{out} (°C)	$\dot{Q}$ (MW)			
CO_2	EE-CO_2	950	50	−21.14	0.00	−24.33	0.00
	$\sum$EE-CO2-Ci	145–150[b]	50–35[b]	−10.75	−0.13	−11.44	−0.04
	EE-CO_2-CR	850	50	−2.46	−0.13	−0.82	−0.08
	ER-CO_2	950/15	850	19.52	0.00	22.46	0.00
CaO	EE-CaO	950	200	−78.88	0.00	−20.50	0.00
	EE-CaO-P	950	200	−2.44	0.00	−0.82	0.00
	ER-CaO	950/200/850[c]	850	69.32	0.00	18.01	0.00
$CaCO_3$	EE-$CaCO_3$	850	200	−85.86	0.00	−40.51	0.00
	ER-$CaCO_3$	200	850	87.61	0.00	41.34	0.00

Compressor train		T_{in}[a] (°C)	T_{out} (°C)	$\dot{W}$ (MW)			
CO_2 comp	$\sum C_i$ (up to 75 bar)	50	145–150[b]	−7.89	−0.09	−8.41	−0.03

[a] Several streams at different temperatures can be fed into a heat exchanger (T_1/T_2).

[b] The temperature of this stream may vary within a range (T_1-T_2).

[c] The stream at 850 °C is only fed to ER-CaO under SC2 since it corresponds to the recirculation from SSU to CR.
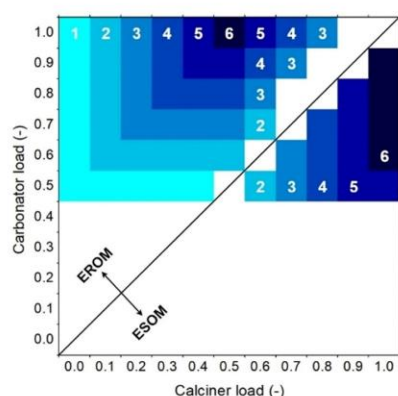
Fig. 3. Operation points distribution respect to calciner and carbonator loads under C.1., C.2, C.3, C.4 and C.5.

0.67 and 0.91 for SC2. The power retrieved from storage under EROM for both scenarios is also illustrated in Fig. 4. The lower power discharge, the higher the thermal energy availability for SC2 compared to SC1. The circulation of solids through the HE-ER-CaO is greater in SC1 than in SC2, so the energy required increases.

The operation map which maximizes the thermal energy availability is presented in the following, Fig. 5. Under EROM, the significant parameters which define an operation point are storage and discharge fractions of $CaCO_3$ ($f_{st,CaCO3}$, $f_{dch,CaCO3}$). As presented in Fig. 5, different operation maps are obtained for each scenario (SC1 and SC2) to maximize the thermal availability. The maximum thermal availability is achieved under more favourable conditions when solid separation is included (SC2). Under SC2, a lower amount of solids is sent to the storage tank of limestone (ST1) leading to smaller sizes of this equipment and a lower amount of solids is discharged from the tank implying a more limited energy penalty related to the preheating of this stream.

The range size of the equipment involved in the system for both scenarios is presented in Table 4. The negative sign (−) of the thermal power for a heat exchanger indicates an energy release, while a positive value (+) means that a specific heat exchanger requires an energy input.
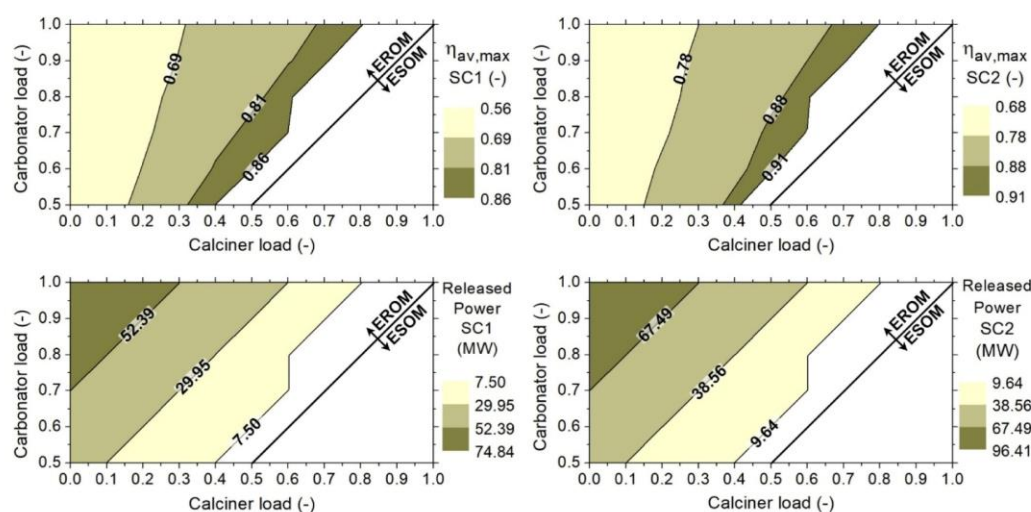
Fig. 4. Maximum thermal energy availability and released power under SC1 and SC2.
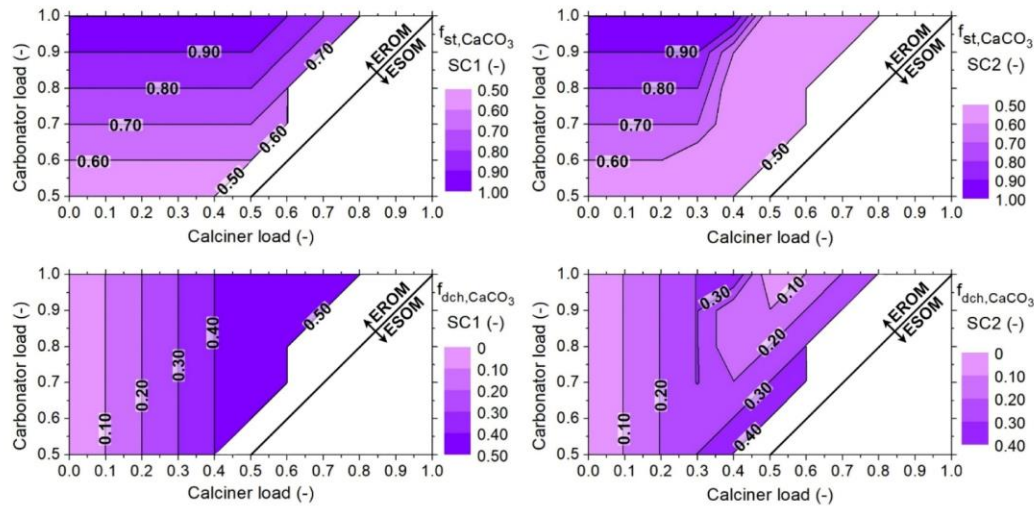
Fig. 5. Operation map under EROM (left: SC1 and right: SC2).

Table 4
Range size of plant equipment under maximization of available energy efficiency.

Energy flow description		T_{in}[a] (°C)	T_{out} (°C)	SC1 - w/o SS		SC2 - 100%SS	
				Min	Max	Min	Max
Heat exchanger				$\dot{Q}$ (MW)			
CO_2	EE-CO_2	950	50	−21.14	0.00	−24.33	0.00
	$\sum$EE-CO2-Ci	145–150[b]	50–35[b]	−10.75	−0.63	−11.44	−0.21
	EE-CO_2-CR	850	50	−2.46	−1.22	−0.82	−0.41
	ER-CO_2	950/15	850	19.52	0.33	22.46	0.38
CaO	EE-CaO	950	200	−78.88	0.00	−20.50	0.00
	EE-CaO-P	950	200	−2.44	0.00	−0.82	0.00
	ER-CaO	950/200/850[c]	850	69.32	0.22	18.01	0.06
$CaCO_3$	EE-$CaCO_3$	850	200	−85.86	0.00	−40.51	0.00
	ER-$CaCO_3$	200	850	43.81	0.00	20.67	0.00

Compressor train		T_{in}[a] (°C)	T_{out} (°C)	$\dot{W}$ (MW)			
CO_2 comp	$\sum$Ci (up to 75 bar)	50	145–150[b]	−7.89	−0.46	−8.41	−0.16

[a] Several streams at different temperatures can be fed into a heat exchanger (T_1/T_2).

[b] The temperature of this stream may vary within a range (T_1-T_2).

[c] The stream at 850 °C is only fed to ER-CaO under SC2 since it corresponds to the recirculation from SSU to CR.

The negative sign (−) of the electric power for the compressor train means an energy demand.

Only the energy consumed by the heat exchanger ER-CaCO3 is reduced by 50 % under both scenarios with respect to the maximum reference power that appears in Table 3, which is obtained after applying the criteria (C.1), (C.2) and (C.3). However, the energy is more efficiently recovered under SC2 than SC1.

4.3. Energy storage efficiency – Energy Storage Operation Mode

Under energy storage operation modes (ESOM), the most relevant parameter to assess the performance of the system is the stored energy efficiency. Thus, an operation map which maximizes the energy storage efficiency is also determined. The energy storage efficiency has been defined through Eq. (8) for the operating points under energy storage mode shown in Fig. 3 and the maximum values of storage efficiency for each pair of calciner/carbonator loads for both scenarios are illustrated in Fig. 6. The amount of stored energy is always the same for a given pair of calciner/carbonator loads, independently of the storage and discharge fractions.

The maximum energy storage efficiency range between 0.48 and 0.62 for SC1 and 0.64 and 0.76 for SC2. The greater amount of stored energy, the greater energy consumed. However, the energy storage efficiency for SC2 is clearly above the values obtained under SC1. The energy consumed in preheating the unconverted CaO before the calcination reaction disappear under SC2.

The specific storage consumption for each pair of calciner/carbonator loads is represented in Fig. 7. The values of SSC range between 5.93 and 6.60 MJ/kg for SC1 and 4.24 and 4.98 MJ/kg for SC2. The CO_2 flow through the compression-cooling train decreases due to the storage and discharge fractions of CaO and CO_2 ($f_{st,CaO}$, $f_{dch,CaO}$) are the minimum possible within the evaluated points. Thus, the electric energy consumption drops.

The greater energy storage efficiency (see Fig. 6), the less specific storage consumption. However, the SSC range for SC1 is above the values obtained in SC2. The maximum possible CaO flow rate to be stored under both scenarios corresponds to the CaO produced after $CaCO_3$ calcination. Under SC2 the $CaCO_3$ flow rate to be calcined is
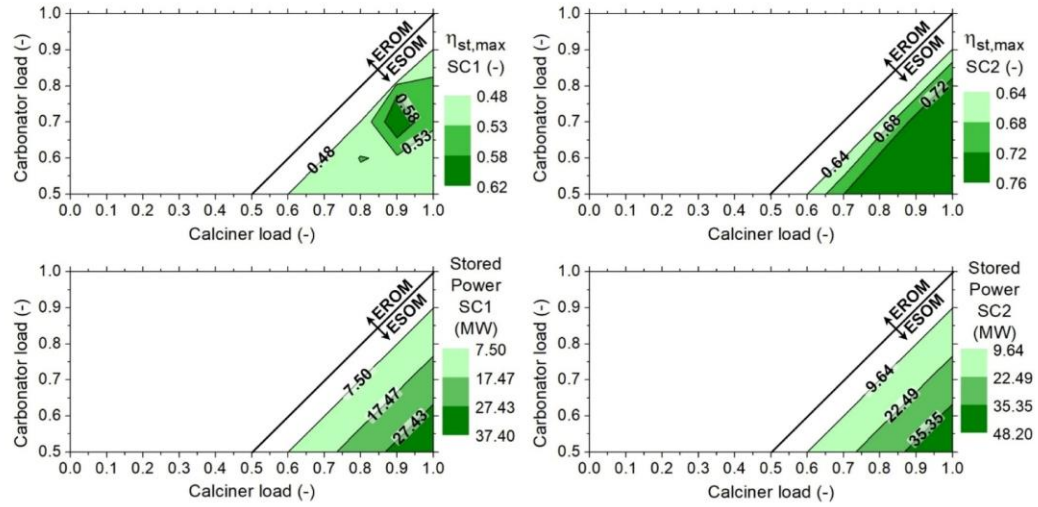
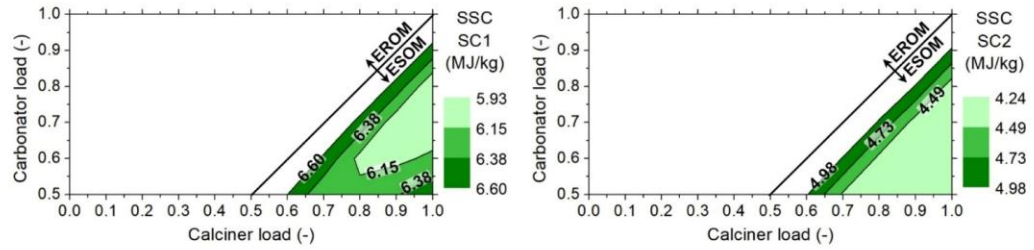**Fig. 6.** Maximum energy storage efficiency and stored power under SC1 and SC2.

Fig. 7. Minimum specific storage consumption under SC1 and SC2.

approximately 20 % greater than in SC1 because 'inert' solids do not circulate through the system (all the material introduced in calciner is limestone). Therefore, energy requirements are higher in SC1 than in

Fig. 8. Operation map under ESOM (SC1 and SC2).

SC2 due to unconverted CaO from carbonator is stored and discharged from storage tanks ST1 and ST2.

The operation map which maximizes the energy storage efficiency has only sense under ESOM and it is shown in Fig. 8. This operation map defined by the storage and discharge fractions of CaO and CO_2 ($f_{st,CaO}$, $f_{dch,CaO}$) is equivalent for both solid management scenarios (SC1 and SC2).

The values of thermal energy availability of the operation map defined for each pair of calciner/carbonator loads are represented in Fig. 9. The thermal energy availability ranges between 0.71 and 0.90 for SC1 and 0.64 and 0.93 for SC2.

The range size of the equipment involved in the system for both scenarios is presented in Table 5. The negative sign (−) of the thermal power for a heat exchanger indicates an energy release, while a positive value (+) means that a specific heat exchanger requires an energy input. The negative sign (−) of the electric power for the compressor train means an energy demand.

The ER-CaCO3 heat exchanger keeps the size reduction by 50 % under both scenarios with respect to the maximum reference power that appears in Table 3, which is obtained after applying the minimum partial load criterion. Besides, under both scenarios the maximum size of the EE-CaO and EE-CO2 heat exchangers and the compression-cooling train is reduced by 40 % respect to the maximum reference power represented in Table 3. The maximization of the energy storage efficiency implies a lower energy consumption. For a pair of calciner/carbonator loads, the maximum energy storage efficiency is reached when (i) the electricity consumed by compressor train is small and (ii) the CaO and CO_2 storage fraction is the minimum possible to achieve the energy
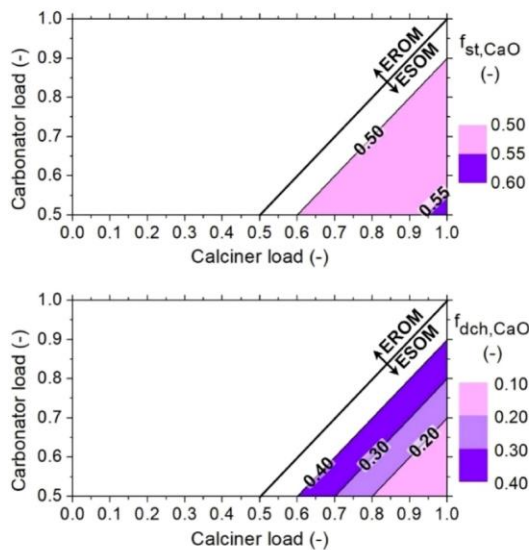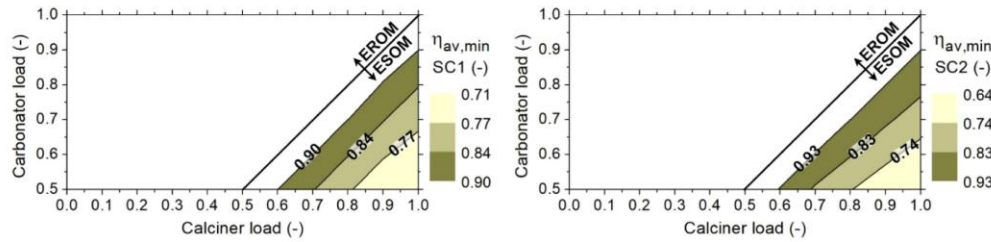
Fig. 9. Thermal energy availability and released power (SC1 and SC2).

Table 5
Range size of plant equipment under maximization of energy storage efficiency.

Energy flow description				SC1 - w/o SS		SC2 - 100%SS	
				Min	Max	Min	Max
Heat exchanger		T_{in}^{a} (°C)	T_{out} (°C)	$\dot{Q}$ (MW)			
CO_2	$EE\text{-}CO_2$	950	50	−12.69	0.00	−14.60	0.00
	$\sum EE\text{-}CO2\text{-}Ci$	145–150[b]	50–35[b]	−6.40	−0.63	−6.85	−0.21
	$EE\text{-}CO_2\text{-}CR$	850	50	−2.46	−1.22	−0.82	−0.41
	$ER\text{-}CO_2$	950/15	850	19.52	0.33	22.46	0.38
CaO	EE-CaO	950	200	−47.33	0.00	−12.30	0.00
	EE-CaO-P	950	200	−2.44	0.00	−0.82	0.00
	ER-CaO	950/200/850[c]	850	69.32	0.22	18.01	0.06
$CaCO_3$	$EE\text{-}CaCO_3$	850	200	−85.86	0.00	−40.51	0.00
	$ER\text{-}CaCO_3$	200	850	43.81	0.00	20.67	0.00

Compressor train		T_{in}^{a} (°C)	T_{out} (°C)	$\dot{W}$ (MW)			
CO_2 comp	$\sum C_i$ (up to 75 bar)	50	145–150[b]	−4.70	−0.46	−5.03	−0.16

[a] Several streams at different temperatures can be fed into a heat exchanger (T_1/T_2).
[b] The temperature of this stream may vary within a range (T_1-T_2).
[c] The stream at 850 °C is only fed to ER-CaO under SC2 since it corresponds to the recirculation from SSU to CR.

storage required under this pair of calciner/carbonator loads.

4.4. Heat availability and demand

The amount of available and demanded heat in the equipment under the whole range of situations included in the operation maps defined in Sections 4.2 and 4.3 are now assessed in detail. This information will be useful to understand the range of values in which each heat exchanger will be operated. However, the information presented in this section is aggregated and a more detailed and individual analysis of the behaviour of each independent heat exchanger is beyond the scope of this work.

When EROM is analysed, the threshold operation points which maximize the thermal availability presented in Fig. 5 are assessed. These operation points correspond to the pairs of reactor loads (L_{CL}, L_{CR}): (0.8, 1), (0.4, 0.5), (0, 1) and (0, 0.5). In SC1, the corresponding pairs of storage and discharge fractions ($f_{st,CaCO3}$, $f_{dch,CaCO3}$) are (0.7, 0.5), (0.5, 0.4), (1, 0.1) and (0.5, 0.1) while in SC2, they are (0.5, 0.3), (0.5, 0.4), (1, 0.1) and (0.5, 0.1). The operation map for ESOM is also analysed

through the assessment of the limit operation points which maximize the energy storage efficiency as presented in Fig. 8. These threshold operation points correspond to the pairs of reactor loads (L_{CL}, L_{CR}): (0.6, 0.5), (1, 0.9), and (1, 0.5). Under SC1 and SC2, the corresponding pairs of CaO storage and discharge fractions ($f_{st,CaO}$, $f_{dch,CaO}$) are (0.5, 0.4), (0.5, 0.4) and (0.6, 0.2).

4.4.1. Available heat

The available heat at different levels of temperature under EROM threshold operation points is represented in Fig. 10. The size of the heat exchange equipment is reduced to near a half when solids are separated and non-reacted CaO recirculated to the carbonator. It might be observed when the system is operated under EROM, the availability of very high-temperature heat (950–850 °C) is extremely low or it does not exist.

Under ESOM, the available heat for different levels of temperature in the threshold operation points is represented in Fig. 11. The range of operation of the heat exchangers under ESOM is much narrower than
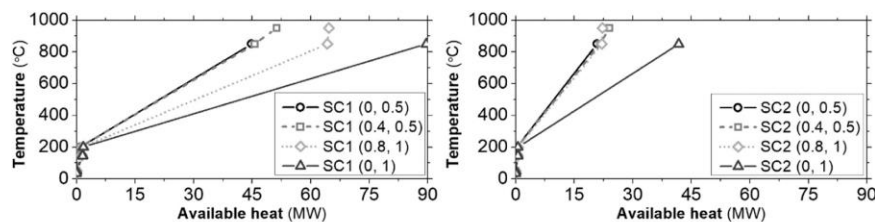

Fig. 10. Available heat at different temperatures for the threshold operation points in EROM (SC1 and SC2).
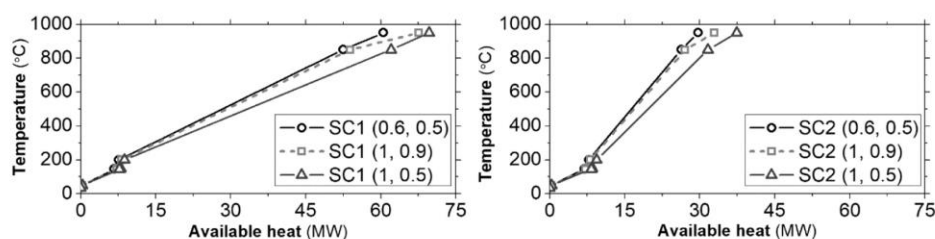
10

80

Fig. 11. Available heat at different temperatures for the threshold operation points in ESOM (SC1 and SC2).
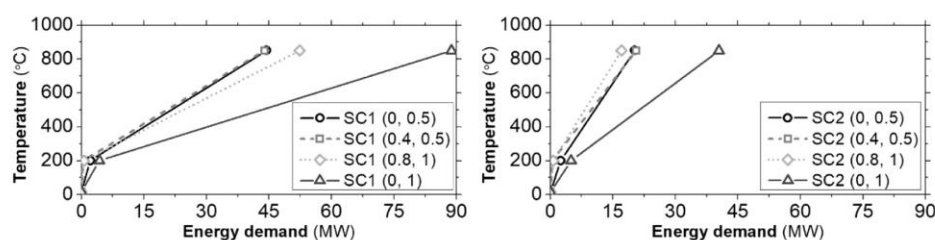

Fig. 12. Energy demand at different temperatures for the threshold operation points in EROM (SC1 and SC2).
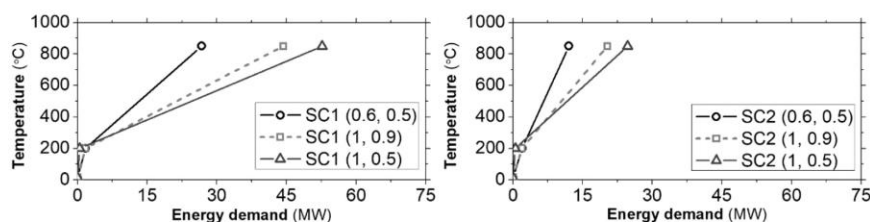

Fig. 13. Energy demand at different temperatures for the threshold operation points in ESOM (SC1 and SC2).

under EROM, facilitating the efficient operation of these equipment. Again, the presence of a solid separation unit (SC2) at the outlet of the carbonator reduces by approximately a half the size of the heat exchangers.

4.4.2. Demanded heat

The demanded heat for different levels of temperature under EROM threshold operation points is represented in Fig. 12. The size of the heat exchange equipment is extremely increased when no separation of solids is implemented. The strong reduction of the demanded heat is a very strong advantage of the inclusion of a solid separation unit. Further research must be done to determine the amount of demanded heat which can be covered with the available heat in the CaL TCES system and the amount which must be provided by external source.

Under ESOM, the demanded heat for different levels of temperature in the threshold operation points is represented in Fig. 13. The demand of thermal energy is reduced to near a half when the system is operated as an energy storage facility. Again, the separation of carbonated solids strongly limits the requirements of heat in the CaL TCES system.

Under each assessed operating point, the difference between the total amount of available and demanded heat has been computed. The sum of available heat is always greater than the total amount of demanded heat within all the limit operating points under EROM and ESOM. When solar energy is not available ($Load_{CL} = 0$), the SC2 presents a higher difference between available and demanded heat than SC1, up to 75 %. The lower the CaO discharged from the ST2 tank, the smaller the size of the heat exchanger named HE-ER-CaO. Thus, the CaO recirculation into the carbonator (SC2) raises the difference in size between release and demand heat exchangers. When the availability of solar energy increases,

the difference between availability and demand of thermal energy is greater in SC1 than in SC2. However, since the greater circulation of solids through the reactors within SC1, larger size is required for the heat exchangers.

5. Conclusions

The novelty of this study relies in three main aspects: (i) the identification of the most suitable operation maps under real operating conditions and (ii) the comparison between two scenarios regarding the management of solids at the outlet of the carbonation reactor and (iii) the quantification of heat power demand and availability.

It has been observed that the operation points which are feasible are limited by technical constraints and the operation map of the CaL TCES system banned a large amount of operation situations. The most suitable operating point under each pair of calciner/carbonator loads was selected according to: (i) maximization of thermal energy availability under EROM and (ii) maximization of stored energy efficiency under ESOM. The thermal energy availability for the operation map defined under EROM ranges between 56 and 91 % for both scenarios (SC1 and SC2). Energy storage efficiency is an average 16 % lower for EROM than for ESOM (max energy storage efficiency).

The separation of carbonated solids leads to an increase of the thermal energy availability and an improvement of energy storage efficiency. The specific storage consumption is strongly decreased when solids are completely separated. It can be concluded that the separation of solids improves the performance of the CaL TCES system under both modes of operation.

Regarding plant equipment size, the ER-CaCO3 heat exchanger

power demand can be reduced a 50 % if the criterion of maximum available energy is applied. While if the maximization of energy storage efficiency criterion is applied, the size of the equipment involved in the CaO and CO_2 storage lines (EE-CO2, EE-CaO and compression-cooling train) could be reduced a 40 %, in addition to the 50 % reduction in the ER-CaCO3 heat exchanger size. Comparing the ideal and complete separation of solids scenario (SC2) with the scenario without solid separation (SC1), a size reduction from 53 to 74 % could be reached in the heat exchangers influenced by solid streams (EE-CaO, EE-CaO-P, ER-CaO, EE-CaCO3 and ER-CaCO3) and by unreacted CO_2 leaving the carbonator (EE-CO2-CR). Regarding the rest of the plant equipment (EE-CO2, ER-CO2 and compression-cooling train), results from SC2 show a size increment between 7 and 15 % in comparison to SC1. In conclusion, the threshold values of stored and recovered energy and the size of the plant equipment are defined.

Future research should focus on the estimation of the real potential of partially carbonated solids separation based on density differences. Once the size of the system will be defined, the detailed integration of heat with the power plant should be carried out as well as the economic assessment of the heat exchange network.

Nomenclature

Symbols

f	fraction, −
L	load, −
$\dot{m}$	mass flow rate, kg/s
$\dot{n}$	mole flow rate, kmol/s
$\dot{Q}$	heat flow rate, MW
P	power, MW
R	molar ratio CaO/CO_2, −
T	temperature, °C
$\dot{W}$	electric flow rate, MW
ΔH_R^0	enthalpy of carbonation, kJ/mol
η	efficiency, −

Subscripts and superscripts

amb	ambient
av	availability
CR	carbonator
CL	calciner
dch	discharge
g	gas
in	input or inlet
max	maximum
nom	nominal
out	output or outlet
p	purge or particle
s	solid
st	storage

Acronyms and abbreviations

CaL	Calcium-looping
CSP	Concentrating Solar Power
DOM	Direct Operation Mode
EE	Energy Emitted
ESOM	Energy Storage Operation Mode
ER	energy required
EROM	Energy Release Operation Mode
EV	expansion valve
HE	heat exchanger
SC	scenario

SH	sensible heat
SSC	specific storage consumption
SSU	solids separation unit
ST	storage tank
TCES	thermochemical energy storage
TES	thermal energy storage

CRediT authorship contribution statement

S. Pascual: Conceptualization, Methodology, Software, Visualization, Writing – original draft. **P. Lisbona:** Conceptualization, Methodology, Writing – review & editing, Visualization. **L.M. Romeo:** Conceptualization, Writing – review & editing, Supervision.

Declaration of competing interest

The authors declare the following financial interests/personal relationships which may be considered as potential competing interests: Sara Pascual reports financial support was provided by Ministerio de Ciencia, Innovación y Universidades. Luis M. Romeo reports financial support was provided by Horizon 2020 Framework Programme. Luis M. Romeo reports financial support was provided by Gobierno de Aragón.

Data availability

Data will be made available on request.

Acknowledgment

References

[1] Concentrating solar power projects, National Renewable Energy Laboratory, 2022. https://solarpaces.nrel.gov/projects. (Accessed 1 July 2022).

[2] A. Zervos, R. Adib (Eds.), Renewables 2022. Global Status Report, REN21 Secretariat, 2022 https://www.ren21.net/wp-content/uploads/2019/05/GSR2022_Full_Report.pdf.

[3] S. Kraemer, in: CSP Doesn't Compete With PV – It Competes With Gas, 2017, pp. 1–3, solarpaces.org/csp-competes-with-natural-gas-not-pv/ (accessed July 1, 2022).

[4] T. Islam, N. Huda, A.B. Abdullah, R. Saidur, A comprehensive review of state-of-the-art concentrating solar power (CSP) technologies: current status and research trends, Renew. Sustain. Energy Rev. 91 (2018) 987–1018, https://doi.org/10.1016/j.rser.2018.04.097.

[5] D. Barlev, R. Vidu, P. Stroeve, Innovation in concentrated solar power, Sol. Energy Mater. Sol. Cells 95 (2011) 2703–2725, https://doi.org/10.1016/j.solmat.2011.05.020.

[6] U. Pelay, L. Luo, Y. Fan, D. Stitou, M. Rood, Thermal energy storage systems for concentrated solar power plants, Renew. Sustain. Energy Rev. 79 (2017) 82–100, https://doi.org/10.1016/j.rser.2017.03.139.

[7] S. Kuravi, J. Trahan, D.Y. Goswami, M.M. Rahman, E.K. Stefanakos, Thermal energy storage technologies and systems for concentrating solar power plants, Prog. Energy Combust. Sci. 39 (2013) 285–319, https://doi.org/10.1016/j.pecs.2013.02.001.

[8] A. Kumar, S.K. Shukla, A review on thermal energy storage unit for solar thermal power plant application, Energy Procedia 74 (2015) 462–469, https://doi.org/10.1016/j.egypro.2015.07.728.

[9] S.J. Wagner, E.S. Rubin, Economic implications of thermal energy storage for concentrated solar thermal power, Renew. Energy 61 (2014) 81–95, https://doi.org/10.1016/j.renene.2012.08.013.

[10] K. Vignarooban, X. Xu, A. Arvay, K. Hsu, A.M. Kannan, Heat transfer fluids for concentrating solar power systems – a review, Appl. Energy 146 (2015) 383–396, https://doi.org/10.1016/j.apenergy.2015.01.125.

[11] E. González-Roubaud, D. Pérez-Osorio, C. Prieto, Review of commercial thermal energy storage in concentrated solar power plants: steam vs. Molten salts, Renew. Sust. Energ. Rev. 80 (2017) 133–148, https://doi.org/10.1016/j.rser.2017.05.084.

[12] A. Mohammad, J. Khoshbaf, H. Groningen, C. Orozco, in: Thermal energy storage in CSP technologies: from commercialized to innovative solutions, 2018, pp. 0–26, https://doi.org/10.13140/RG.2.2.22026.57282.

[13] B. Xu, P. Li, C. Chan, Application of phase change materials for thermal energy storage in concentrated solar thermal power plants: a review to recent developments, Appl. Energy 160 (2015) 286–307, https://doi.org/10.1016/j.apenergy.2015.09.016.

[14] A. Palacios, C. Barreneche, M.E. Navarro, Y. Ding, Thermal energy storage technologies for concentrated solar power – a review from a materials perspective, Renew. Energy 156 (2020) 1244–1265, https://doi.org/10.1016/j.renene.2019.10.127.

[15] Innovation Outlook: Thermal Energy Storage, International Renewable Energy Agency (IRENA), Abu Dhabi, 2020 https://www.irena.org/publications/2020/Nov/Innovation-outlook-Thermal-energy-storage.

[16] O. Achkari, A. El Fadar, Latest developments on TES and CSP technologies – energy and environmental issues, applications and research trends, Appl. Therm. Eng. 167 (2020), 114806, https://doi.org/10.1016/j.applthermaleng.2019.114806.

[17] C. Prieto, P. Cooper, A.I. Fernández, L.F. Cabeza, Review of technology: thermochemical energy storage for concentrated solar power plants, Renew. Sustain. Energy Rev. 60 (2016) 909–929, https://doi.org/10.1016/j.rser.2015.12.364.

[18] R. Barker, The reactivity of calcium oxide towards carbon dioxide and its use for energy storage, Appl. Chem. Biotechnol. 24 (1974) 221–227.

[19] P. Lisbona, M. Bailera, T. Hills, M. Sceats, L.I. Díez, L.M. Romeo, Energy consumption minimization for a solar lime calciner operating in a concentrated solar power plant for thermal energy storage, Renew. Energy 156 (2020) 1019–1027, https://doi.org/10.1016/j.renene.2020.04.129.

[20] X. Chen, Z. Zhang, C. Qi, X. Ling, H. Peng, State of the art on the high-temperature thermochemical energy storage systems, Energy Convers. Manag. 177 (2018) 792–815, https://doi.org/10.1016/j.enconman.2018.10.011.

[21] X. Chen, X. Jin, X. Ling, Y. Wang, Exergy analysis of concentrated solar power plants with thermochemical energy storage based on calcium looping, ACS Sustain. Chem. Eng. 8 (2020) 7928–7941, https://doi.org/10.1021/acssuschemeng.0c01586.

[22] C. Ortiz, J. Valverde, R. Chacartegui, L. Perez-Maqueda, Carbonation of limestone derived CaO for thermochemical energy storage: from kinetics to process integration in concentrating solar plants, ACS Sustain. Chem. 6 (2018) 6404–6417.

[23] H. Sun, Y. Li, Z. Bian, X. Yan, Z. Wang, W. Liu, Thermochemical energy storage performances of ca-based natural and waste materials under high pressure during CaO/CaCO3 cycles, Energy Convers. Manag. 197 (2019) 3–12, https://doi.org/10.1016/j.enconman.2019.111885.

[24] V. Moreno, J. Arcenegui-Troya, P.Enrique Sánchez-Jiménez, A. Perejón, R. Chacartegui, J.Manuel Valverde, L.Allan Pérez-Maqueda, Albero: an alternative natural material for solar energy storage by the calcium-looping process, Chem. Eng. J. 440 (2022), https://doi.org/10.1016/j.cej.2022.135707.

[25] F. Di Lauro, C. Tregambi, F. Montagnaro, P. Salatino, R. Chirone, R. Solimene, Improving the performance of calcium looping for solar thermochemical energy storage and CO2 capture, Fuel 298 (2021), https://doi.org/10.1016/j.fuel.2021.120791.

[26] S. Wu, C. Zhou, P. Tremain, E. Doroodchi, B. Moghtaderi, A phase change calcium looping thermochemical energy storage system based on CaCO3/CaO-CaCl2, Energy Convers. Manag. 227 (2021), https://doi.org/10.1016/j.enconman.2020.113503.

[27] M. Bailera, S. Pascual, P. Lisbona, L.M. Romeo, Modelling calcium looping at industrial scale for energy storage in concentrating solar power plants, Energy 225 (2021), 120306, https://doi.org/10.1016/j.energy.2021.120306.

[28] M. Bailera, P. Lisbona, L.M. Romeo, L.I. Díez, Calcium looping as chemical energy storage in concentrated solar power plants: carbonator modelling and configuration assessment, Appl. Therm. Eng. 172 (2020), 115186, https://doi.org/10.1016/j.applthermaleng.2020.115186.

[29] S. Padula, C. Tregambi, R. Solimene, R. Chirone, M. Troiano, P. Salatino, A novel fluidized bed "thermochemical battery" for energy storage in concentrated solar thermal technologies, Energy Convers. Manag. 236 (2021), 113994, https://doi.org/10.1016/j.enconman.2021.113994.

[30] C. Tregambi, M. Troiano, F. Montagnaro, R. Solimene, P. Salatino, Fluidized beds for concentrated solar thermal technologies—a review, Front. Energy Res. 9 (2021) 1–26, https://doi.org/10.3389/fenrg.2021.618421.

[31] C. Ortiz, A. Carro, R. Chacartegui, J.M. Valverde, Low-pressure calcination to enhance the calcium looping process for thermochemical energy storage, J. Clean. Prod. 363 (2022), https://doi.org/10.1016/j.jclepro.2022.132295.

[32] M. Alvarez Rivero, D. Rodrigues, C.I.C. Pinheiro, J.P. Cardoso, L.F. Mendes, Solid–gas reactors driven by concentrated solar energy with potential application to calcium looping: a comparative review, Renew. Sustain. Energy Rev. 158 (2022), 112048, https://doi.org/10.1016/j.rser.2021.112048.

[33] G. Zsembinszki, A. Sole, C. Barreneche, C. Prieto, A.I. Fernández, L.F. Cabeza, Review of reactors with potential use in thermochemical energy storage in concentrated solar power plants, Energies 11 (2018), https://doi.org/10.3390/en11092358.

[34] C. Ortiz, M.C. Romano, J.M. Valverde, M. Binotti, R. Chacartegui, Process integration of calcium-looping thermochemical energy storage system in concentrating solar power plants, Energy 155 (2018) 535–551, https://doi.org/10.1016/j.energy.2018.04.180.

[35] R. Chacartegui, A. Alovisio, C. Ortiz, J.M. Valverde, V. Verda, J.A. Becerra, Thermochemical energy storage of concentrated solar power by integration of the calcium looping process and a CO2 power cycle, Appl. Energy 173 (2016) 589–605, https://doi.org/10.1016/j.apenergy.2016.04.053.

[36] U. Tesio, E. Guelpa, V. Verda, Integration of thermochemical energy storage in concentrated solar power. Part 2: comprehensive optimization of supercritical CO2 power block, Energy Convers. Manag. 6 (2020), 100038, https://doi.org/10.1016/j.ecmx.2020.100038.

[37] E. Karasavvas, K.D. Panopoulos, S. Papadopoulou, S. Voutetakis, Energy and exergy analysis of the integration of concentrated solar power with calcium looping for power production and thermochemical energy storage, Renew. Energy 154 (2020) 743–753, https://doi.org/10.1016/j.renene.2020.03.018.

[38] R. Bravo, C. Ortiz, R. Chacartegui, D. Friedrich, Hybrid solar power plant with thermochemical energy storage: a multi-objective operational optimisation, Energy Convers. Manag. 205 (2020), 112421, https://doi.org/10.1016/j.enconman.2019.112421.

[39] U. Tesio, E. Guelpa, V. Verda, Comparison of sCO2 and He Brayton cycles integration in a calcium-looping for concentrated solar power, Energy 247 (2022), 123467, https://doi.org/10.1016/j.energy.2022.123467.

[40] R. Bravo, C. Ortiz, R. Chacartegui, D. Friedrich, Multi-objective optimisation and guidelines for the design of dispatchable hybrid solar power plants with thermochemical energy storage, Appl. Energy 282 (2021), https://doi.org/10.1016/j.apenergy.2020.116257.

[41] C. Tregambi, P. Bareschino, E. Mancusi, F. Pepe, F. Montagnaro, R. Solimene, P. Salatino, Modelling of a concentrated solar power – photovoltaics hybrid plant for carbon dioxide capture and utilization via calcium looping and methanation, Energy Convers. Manag. 230 (2021), 113792, https://doi.org/10.1016/j.enconman.2020.113792.

[42] C. Ortiz, R. Chacartegui, J.M. Valverde, A. Carro, C. Tejada, J. Valverde, Increasing the solar share in combined cycles through thermochemical energy storage, Energy Convers. Manag. 229 (2021), 113730, https://doi.org/10.1016/j.enconman.2020.113730.

[43] C. Ortiz, C. Tejada, R. Chacartegui, R. Bravo, A. Carro, J.M. Valverde, J. Valverde, Solar combined cycle with high-temperature thermochemical energy storage, Energy Convers. Manag. 241 (2021), 114274, https://doi.org/10.1016/j.enconman.2021.114274.

[44] S. Pascual, P. Lisbona, M. Bailera, L.M. Romeo, Design and operational performance maps of calcium looping thermochemical energy storage for concentrating solar power plants, Energy 220 (2021), 119715, https://doi.org/10.1016/j.energy.2020.119715.

[45] F. Martinez Castilla, G. Guío-Pérez, D.C. Papadokonstantakis, S. Pallarès, D. Johnsson, Techno-economic assessment of calcium looping for thermochemical techno-economic assessment of calcium looping for thermochemical energy storage with CO 2 capture, Energies 14 (2021) 0–17.

[46] C. Ortiz, J.M. Valverde, R. Chacartegui, L.A. Perez-Maqueda, P. Giménez, The calcium-looping (CaCO3/CaO) process for thermochemical energy storage in concentrating solar power plants, Renew. Sustain. Energy Rev. 113 (2019), 109252, https://doi.org/10.1016/j.rser.2019.109252.

[47] V. Manovic, J.P. Charland, J. Blamey, P.S. Fennell, D.Y. Lu, E.J. Anthony, Influence of calcination conditions on carrying capacity of CaO-based sorbent in CO2 looping cycles, Fuel 88 (2009) 1893–1900, https://doi.org/10.1016/j.fuel.2009.04.012.

[48] G.S. Grasa, J.C. Abanades, CO2 capture capacity of CaO in long series of carbonation/calcination cycles, Ind. Eng. Chem. Res. 45 (2006) 8846–8851, https://doi.org/10.1021/ie0606946.

[49] N. Rodriguez, M. Alonso, G. Grasa, J.C. Abanades, Heat requirements in a calciner of CaCO3 integrated in a CO2 capture system using CaO, Chem. Eng. J. 138 (2008) 148–154, https://doi.org/10.1016/j.cej.2007.06.005.

[50] S. Pascual, F. Di Lauro, P. Lisbona, L.M. Romeo, C. Tregambi, F. Montagnaro, R. Solimene, P. Salatino, Improvement of performance of fluidized bed calcium looping for thermochemical solar energy storage: modelling and experiments, in: Proc. 10th Eur. Combust. Meet, 2021, pp. 1430–1435.

[51] F-Chart, Engineering Equation Solver (EES) software. https://www.fchartsoftware.com/ees/, 2022.

[52] M.W. Chase Jr., NIST-JANAF thermochemical tables, in: J. Phys. Chem. Ref. Data, Monogr. 9, Fourth Ed., 1998, pp. 1–1951, https://webbook.nist.gov/cgi/cbook.cgi?ID=C1305788&Type=JANAFS&Plot=on.

[53] G.K. Jacobs, D.M. Kerrick, K.M. Krupka, The high-temperature heat capacity of natural calcite (CaCO3), Phys. Chem. Miner. (1981) 55–59, https://doi.org/10.1007/978-3-642-37015-1_18.

Improvement of Performance of Fluidized Bed Calcium Looping for Thermochemical Solar Energy Storage: Modelling and Experiments

S. Pascual[1], F. Di Lauro[2], P. Lisbona[3], L.M. Romeo[1], C. Tregambi[4], F. Montagnaro[2], R. Solimene[*,5], P. Salatino[6]

[1]Departamento de Ingeniería Mecánica. Escuela de Ingeniería y Arquitectura (EINA). Universidad de Zaragoza. C/ María de Luna s/n, 50018, Zaragoza, Spain
[2]Dipartimento di Scienze Chimiche, Università degli Studi di Napoli Federico II, Complesso Universitario di Monte Sant'Angelo, 80126 Napoli, Italy
[3]Fundación Agencia Aragonesa para la Investigación y el Desarrollo (ARAID), Zaragoza, Spain
[4]Dipartimento di Ingegneria, Università degli Studi del Sannio, Piazza Roma 21, 82100 Benevento, Italy
[5]Istituto di Scienze e Tecnologie per l'Energia e la Mobilità Sostenibili, Consiglio Nazionale delle Ricerche, Piazzale Vincenzo Tecchio 80, 80125 Napoli, Italy
[6]Dipartimento di Ingegneria Chimica, dei Materiali e della Produzione Industriale, Università degli Studi di Napoli Federico II, Piazzale Vincenzo Tecchio 80, 80125 Napoli, Italy

Abstract

Calcium-looping (CaL) can be exploited as promising thermochemical energy storage (TCES) process in concentrated solar power (CSP) plants. The present research analyzes the influence of solids separation after carbonation in a CaL-CSP plant sizing. The results obtained from modelling and simulation of both threshold schemes (with/without solids separation) have shown a reduction of plant equipment size and energy consumption of the facility between 50 and 75% when solid separation unit is included. Based on these promising modelling results, experimental tests were performed to verify the technical feasibility of solids separation after partial carbonation, exploiting the difference of density (hence of minimum fluidization velocity) between calcined and carbonated particles. Experimental results show suitable conditions for partial separation of solids in fluidized bed for the first calcination/carbonation cycles.

Introduction

Calcium-looping process (CaL) based on the cyclic reactions of carbonation-calcination of limestone can be exploited as promising thermochemical energy storage (TCES) system in concentrated solar power (CSP) plants. Research has mainly been focused on the improvement of efficiency of different CaL integrations as TCES within power cycles [1,2], the management of the storage system [3] and the design or scaling up of the main reactors, carbonator [4–6] and calciner [7]. Fluidized beds have been identified as ideal reactors/receivers for CaL-CSP integration given the intimate gas–solid contact achieved by fluidization state and the high efficient collection of solar energy [8].

The integrated schemes presented in literature consider independent storage tanks for: i) CO_2 and lime (CaO) obtained after calcination and ii) a mixture of unconverted CaO (related to particles experiencing very short residence times) and partially carbonated lime (CL), the latter being in turn a mixture of CaO and $CaCO_3$ (because of uncomplete carbonation), obtained after carbonation step [5,6]. Under these conditions, the size of the CL storage tank will be extremely large as well as the size of the heat exchangers managing the solids flow circulating from carbonator to calciner. Up to now, the influence of the separation of the mixture of solids exiting the carbonator on the plant equipment size and the power plant consumption has not been assessed in detail. However, the analysis of a CaL-CSP operation maps under a solids separation scenario has allowed to know the behavior and power range of the heat exchangers involved in the plant [9].

The novelty of this research relies in the analysis of the CaL-TCES process including partial separation of solids at the outlet of the carbonator, in order to reduce the plant size and therefore the associated economic costs. The proposed system is a fluidized bed classifier able to separate the particles by density difference.

CaL-CSP simulation model

The CaL-CSP system consists of two main fluidized beds reactors, calciner and carbonator, with intermediate storage tanks of CO_2 and solids. The calciner is sized for 100 MW_{th} of solar input energy (E_{CL}) and working temperature is 950 °C under CO_2 pure atmosphere to ensure a high reaction rate [10]. The endothermic calcination reaction is assumed to be complete and the limestone in the calciner is fully transformed into lime and CO_2. The CO_2 and lime formed in calciner are directed to carbonator or diverted towards their corresponding storage tanks. Since CaO quickly deactivates with the number of cycles, a stream of fresh limestone is fed in the calciner to keep a reasonable sorption activity. The $CaCO_3$ to the calciner reactor comes from: (i) the contribution of fresh limestone and (ii) the $CaCO_3$ produced after carbonation reaction. Fresh limestone counterbalances the purged solid material (f_p) which is set as a percentage of the CaO molar flow generated in calcination reaction.

The carbonator operates at 850 °C under pure CO_2 atmosphere [1]. The exothermic carbonation reaction

---

(E_{CR}) is not complete with a carbonation degree decreasing upon iterated cycles. The carbonator model used to determine the deactivation of the CaO particles is tuned adjusting the kinetic model described by Grasa et al. [11] obtained for 650 ºC and an approximately CO_2 concentration between 10-15%vol. The amount of reacting CaO particles will depend on the average sorption activity of the population of particles circulating in the system [12]. Therefore, a mixture of $CaCO_3$ and CaO consisting of partially carbonated lime particles is found at carbonator outlet. Unreacted CO_2 leaving the carbonator is stored under established conditions. The CaO to CO_2 molar ratio introduced in the carbonator (R) and the average sorbent activity define the carbon capture efficiency in the carbonator reactor.

The CaL-CSP model has been evaluated under two limit scenarios after the carbonation step: (SC1) no separation and (SC2) an ideal and total separation of the mixture of $CaCO_3$ and CaO exiting the carbonator, to quantify its influence on performance, size and economics. A simplified outline of the CaL-CSP model under both scenarios is illustrated in Fig.1. The greatest influence of the solids separation unit occurs on the equipment shown in Fig.1: (i) heat exchangers with solids streams involved (*EE-CaO, ER-CaO, EE-CaCO3* and *ER-CaCO3*), (ii) fluidized bed reactors (carbonator and calciner) and (iii) mainly CaO and $CaCO_3$ storage tanks.
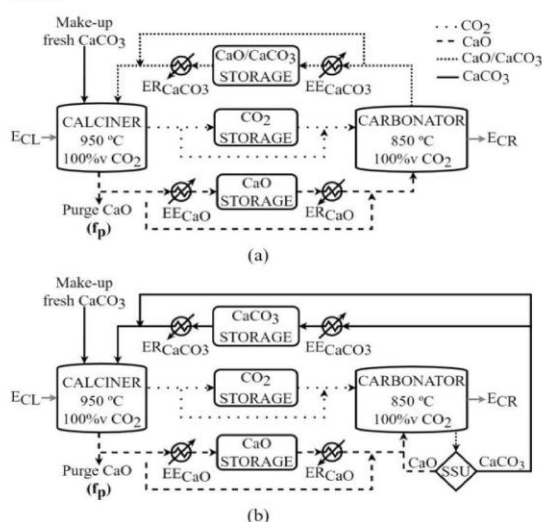

Figure 1. Simplified scheme CaL-CSP simulation model under SC1 (a) and SC2 (b).

Under scenario SC1 (Fig. 1 (a)), the solids input to the calciner (CL) is a mixture of approximately 80% lime and 20% limestone that must be heated up to 850 °C. The CL stream results from the addition of the direct flow from the carbonator at 850 °C and the discharge flow of solids stored at 200 °C. Regarding the inlet streams to the carbonator, the CaO stream discharged from the storage (200 °C) is mixed with the direct CaO flow from calciner

(950 ºC) before being introduced into carbonator at 850 ºC.

Under scenario SC2 (Fig.1 (b)), an idealized solids separation is considered assuming to be feasible the separation of the mixture of $CaCO_3$ and CaO. In particular, the separation unit (SSU) receives the mixture of $CaCO_3$ and CaO from the carbonator and separates (i) the unreacted CaO which is recirculated into the carbonator and (ii) the limestone stream sent to calciner or storage tank.

Both scenarios have been energetically compared under comparable operating conditions. A CaO purge percentage (f_p) is set in each case to keep the same constant value of R under both simulations. The molar ratio between CaO and CO_2 (R) is 4.26, whereas f_p is 3.09% and 4% for SC1 and SC2, respectively. The simulation results obtained under SC2 show a size reduction between 50 and 75% in the plant equipment influenced by solids streams compared to the CaL-CSP under SC1. Besides, the solids storage tanks size under SC2 is smaller than for scenario SC1 given the recirculation of unreacted CaO.

However, the model used under both scenarios present some limitations. First, the kinetic model used is based on the degradation of the sorption capacity of a *Piaseck* limestone in case of carbonation at 650 ºC and 10%vol of CO_2 atmosphere [11]. No experimental data of carbonation evolution under the actual operating conditions of the CaL for TCES were available in literature. Therefore, the carbonation degree should be determined experimentally under the operating conditions established in the CaL-CSP model. On the other hand, a model for solids separation has not been estimated. Only two threshold limit scenarios have been evaluated (with and without solids separation) from the energy point of view. The possible separation degree exploiting the difference in density between the unreacted CaO and the CL stream must be analyzed experimentally. Moreover, it is not possible a complete separation between CaO and $CaCO_3$ because the stream exiting the carbonator is made of partially carbonated lime particles containing both $CaCO_3$ and CaO. Thus, the separator could, in principle, separate only the more carbonated lime particles from the less converted particles.

Nevertheless, this preliminary research based on modelling allows the possibility of developing an experimental campaign to investigate the technical feasibility of, even if partial, solids separation.

Experimental tests methodology

Determination of carbonation degree. A lab-scale Directly Irradiated Fluidized Bed (DIFB) described by Tregambi et al. [13] was used to determine the carbonation degree under the CaL-CSP operating conditions described in the previous section. The experimental tests consisted of 20 consecutive calcination and carbonation cycles using an Italian natural limestone named "Sardo", ground and sieved in the 420−590 μm range, as reactive material [13]. A bed

inventory of 850 g was used, consisting in 700 g of inert sand (served as thermal flywheel but not required in industrial applications) and 150 g of reactive limestone. The fluidizing velocity was always set at 0.6 m/s during carbonation and calcination, a value approximately twice the minimum fluidization velocity of the inert sand. Both reactions took place in the same DIFB reactor by alternating the calcination-carbonation operating conditions. Consistently with realistic conditions of CaL-CSP system, only the calcination step was performed under radiative flux. Thermal supply in other stages of the experiment was ensured by radiant heaters and a gas preheater. During a typical carbonation degree test, the bed was charged with about 700 g of inert sand and heated up to 900 °C by using both the radiant heaters and the gas preheater with atmospheric air as fluidizing gas. Once the pre-set temperature was reached, the radiant heaters were powered off, the air stream was switched to CO_2 and, simultaneously, a sample of 150 g of limestone was fed to the reactor. Then, the solar simulator was powered on and its power tuned to reach a temperature of 950 °C. A time of 20 min was waited to perform the calcination reaction (calcination zero), after which the solar simulator was powered off and the reactor cooled down to 850 °C with atmospheric air stream. Once reached this temperature, the fluidizing gas was switched to CO_2 to perform the carbonation reaction (carbonation step), which was prolonged for 20 min. Finally, the solar simulator was powered on for 20 min and its power tuned to reach 950 °C so to perform the calcination reaction and complete the reaction cycle (calcination step). The reactor was then cooled down to 850 °C to eventually start a new carbonation/calcination loop.

Sorbent samples were recovered after each carbonation step to evaluate the carbonation degree of the material. These samples (1-2 g mass), carefully separated from the inert silica sand by sieving, were subjected to a calcination step in a muffle furnace at 950 °C in air for 1 h and the weight change was measured with an analytical balance (0.1 mg precision). The samples weight data were used to calculate the mean carbonation degree ($\bar{X}_{Ca}$) of the material after each carbonation step (N):

$$\bar{X}_{Ca}(N) = \frac{\frac{m_0 - m_F}{MW_{CO2}}}{\frac{m_F \cdot P_{CaCO3}}{MW_{CaO}}} \quad (1)$$

Where m_0 is the sample mass extracted after each carbonation step, m_F is the sample mass after the calcination step in the muffle furnace, P_{CaCO3} is the purity of the Sardo limestone, MW is the molecular weight. The average sorbent capacity up to the reaction cycle considered (N) is eventually computed in Eq. (2) as:

$$\bar{X}_{Ca,N} = \frac{\sum_{N=1}^{N} \bar{X}_{Ca}(N)}{N} \quad (2)$$

Bulk density test. The experimental tests to determine the bulk density of calcined and carbonated particles were performed in a different lab-scale Fluidized Bed (FB) without solar radiative flux simulation, described in detail in Tregambi et al. [14]. The operating conditions were the same of those used in the DIFB reactor. During a typical test, the bed was charged with about 150 g of inert sand and heated up to 900 °C by using radiant

heaters and atmospheric air as fluidizing gas. Once the pre-set temperature was reached, the sand was removed from the reactor and the air flow was switched to CO_2. A sample of 150 g of limestone was then fed to the reactor, which temperature was increased to 950 °C. When temperature reached 900 ºC, the calcination started. The calcination zero was prolonged for 20 min. The CO_2 flow was switched to air after the calcination zero (20 min). The calcined material with the inert sand was then removed from the reactor after 2 min of air atmosphere by exploiting a vacuum system. The material extraction after calcination was performed in air atmosphere to prevent material carbonation as a consequence of the temperature reduction during extraction. The inert sand was separated from the calcined material by sieving and put back into the reactor, which temperature was set at 850 ºC. Once the pre-set temperature was reached, the calcined material was introduced into the reactor to perform the carbonation reaction after changing the gas stream from air to CO_2. The carbonated material with the inert sand was removed from the reactor after 20 min with the same procedure as calcination step. Once the inert sand was separated from the carbonated material by sieving, it was put back into the reactor. The reactor was heated up to 900 ºC using air as fluidizing stream. Once the pre-set temperature was reached, the air flow was switched to CO_2 and carbonated material was introduced to start the next calcination step.

The reactive material recovered after each carbonation and calcination step was analyzed to evaluate the bulk density and the granulometric distribution. The bulk density was determined by measuring the weight and volume of the reactive material in a 50 mL graduated cylinder. The reactive material was slowly and manually poured within the cylinder up to a certain volume mark. The material bulk density was calculated as the weight divided by the volume reached in the glass cylinder. On the other hand, the reactive material was sieved considering the following particle diameter ranges: 420–590 μm, 300–420 μm, 200–300 μm, 100–200 μm, <100 μm. The weight of material collected in each of the sieve ranges described was measured to know the particle size distribution of the carbonated (CL) and calcined (unreacted CaO) material after each cycle.

Development and validation of a density model

A simple and theoretical model (TM) at particle scale during iterated cycles of calcination and calcination was developed based on the experimental test results obtained. The assumptions taken for the model were the following: (i) no attrition and fragmentation phenomena, (ii) sintering only takes place during calcination causing porosity and size reduction, (iii) particles do not change volume during carbonation step and (iv) bed porosity remains the same for calcination and carbonation and is assumed constantly equal to 0.45.

Based on this model, the bulk density experimental results for carbonated and calcined particles can be

1432

related to the carbonation degree according to the following equation:

$$X_{carb_i} = \frac{MW_{CaO}}{MW_{CO_2}}\left(\frac{\rho_{carb_i}}{\rho_{calc,i-1}} - 1\right) \qquad (4)$$

where $\rho_{carb,i}$ is the bulk density of carbonated particles (CL) at carbonation number i, $\rho_{calc,i-1}$ is the bulk density of calcined particles (unreacted CaO) at calcination step $i-1$ and $X_{carb,i}$ is the carbonation degree after i carbonation step.

In parallel, the model can be used to calculate (i) the effective particle density and (ii) the particle diameter after each calcination and carbonation step. The effective particle density is computed by Eq. (5) for carbonated particles and by Eq. (6) for calcined particles:

$$\rho_p^{carb_i} = \frac{\rho_{carb_i}}{(1-\varepsilon_{bed})} \qquad (5)$$

$$\rho_p^{calc_i} = \frac{\rho_{calc_i}}{(1-\varepsilon_{bed})} \qquad (6)$$

where $\rho_p^{carb_i}$ and $\rho_p^{calc_i}$ are the carbonated and calcined particle density at cycle i, while ρ_{carb_i} and ρ_{calc_i} are the bulk density obtained after carbonation and calcination step (i) from the experimental test. The void fraction assumed (ε_{bed}) was 0.45 for both carbonated and calcined material. The void fraction value is typically of the fluidized bed state and is similar to the value obtained considering the bulk density of the fresh limestone (1590 kg/m^3) and the calcium carbonate density (2930 kg/m^3).

The particle diameter is computed by Eq. (7) for carbonated particles at step $i+1$ and for calcined particles at step i:

$$\frac{d_p^{carb_{i+1}}}{d_p} = \frac{d_p^{calc_i}}{d_p} = \left(\frac{\rho_0 \cdot MW_{CaO}}{\rho_{calc_i} \cdot MW_{CaCO_3}}\right)^{1/3} \qquad (7)$$

where $d_p^{calc_i}$ is the diameter of the calcined particle at cycle i, which matches the diameter of the carbonated particle at cycle $i+1$ ($d_p^{carb_{i+1}}$). Whereas d_p is the initial particle diameter, taking as reference the mean particle diameter of Sardo limestone (505 μm) used as raw material. Finally, ρ_0 is the experimental bulk density of the fresh limestone. The relationship between $d_p^{carb_{i+1}}$ and $d_p^{calc_i}$ was justified by analyzing the particle diameter after each carbonation and calcination step obtained from the experimental test. The mean particle size after calcination i was practically similar to the mean particle size obtained after carbonation $i+1$.

Results from model computations were used to determine the theoretical minimum fluidization velocity by applying the Wen & Yu model [15]. The particle diameter and effective particle density values from the experimental model developed were used to obtain the theoretical minimum fluidization velocity for each calcination (unreacted CaO) and carbonation (CL) step.

Results and discussion

The mean carbonation degree for each of the 20 carbonation-calcination cycles is shown in Fig.2. The black dots curve corresponds to the average carbonation degree for the 20 cycles performed in the DIFB. The grey and white points curves are related to the mean carbonation degree value obtained within the FB reactor

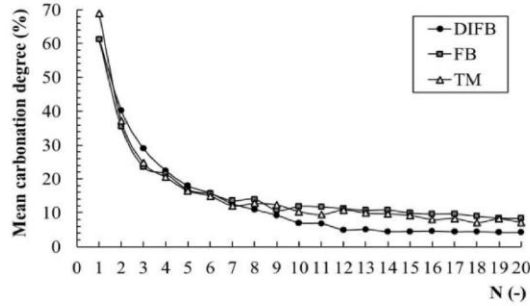and by the Theoretical Model (TM) developed applying Eq. (4), respectively.

Figure 2. Mean carbonation degree results under DIFB, FB and TM conditions.

Experimental data obtained using the DIFB and FB show similar results. Values of carbonation degree obtained within DIFB are slightly lower, probably because of a more severe sintering induced by the concentrated solar radiation [8,13]. The experimental carbonation degree results under the second test conditions (FB) are used to validate the theoretical carbonation degree model (TM). Both curves show practically the same trend.

The average sorbent capacity in the reaction cycle number 20, computed by Eq. (2), is 13.72% under DIFB conditions, and around 16% under FB or TM assumptions. Direct irradiation has a weak negative effect on the carbonation, mainly from cycle 10th to 20th, favoring the sintering of the material.

The effective bulk density of particles for carbonated and calcined particles after each cycle is illustrated in Fig.3. The black squares curve represents the carbonated particles density applying Eq. (5), while the white rhombs curve is obtained through Eq. (6) for the calcined particles density.
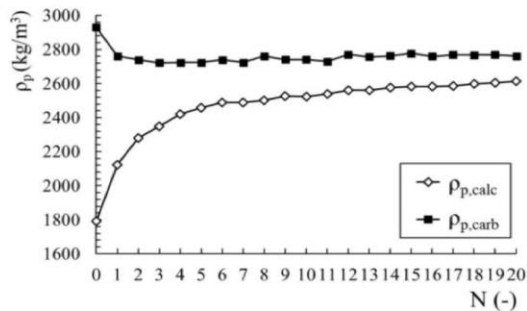

Figure 3. Effective particle density of carbonated and calcined particles.

The particle density after each carbonation (black dots curve) remains practically unchanged (about 2750 kg/m^3). The first value of the black dots curve (N = 0) corresponds to the effective particle density of the raw material (fresh limestone). The carbonated particle density value may be governed by the $CaCO_3$ compact structure. On the other hand, the calcined particles

1433

88

density increases rapidly until 6th and more slowly for the further steps. Thus, the effect of sintering on calcined particle density is clearer than carbonated particles density. Therefore, the particles density after each calcination increases proportionally to the reduction in the carbonation degree step by step.

The particle diameter results for carbonated and calcined material after each cycle is shown in Fig.4. The black squares curve represents the carbonated particles diameter, while the white rhombs curve is obtained for the calcined particles size, both applying Eq. (7).
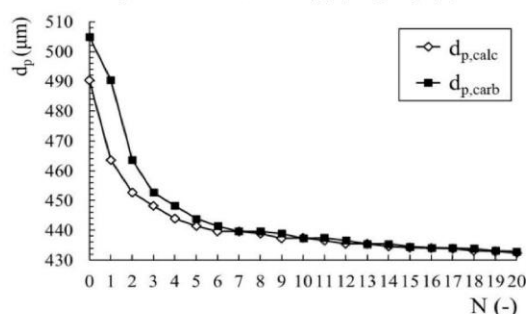

Figure 4. Theoretical particle diameter for carbonated and calcined material.

The particles size is reduced step by step in the calcination reaction for both carbonated and calcined particles. The size is kept in the range between 430 and 440 μm from cycle 6th to 20th. The smaller the particles size with number of carbonation-calcination cycles, the greater the sintering phenomenon influence and therefore an increase of the calcined particles density is produced. The mean particle size up to 20 cycles from the theoretical model amounts to 449 μm, whereas the average particle diameter obtained from the experimental data is 453 μm. Therefore, the theoretical model developed from the bulk density data collected approaches the experimentally determined particle size.

The theoretical minimum fluidization velocity (u_{mf}) for carbonated and calcined particles after each cycle is illustrated in Fig.5. The white rhombs curve represents the u_{mf} of the calcined particles or unconverted CaO, while the black squares curve shows the u_{mf} of carbonated particles or CL stream. Both were calculated considering air as fluidizing gas at ambient temperature (25 °C) to compare the theoretical results with the experimental data. The comparison between theoretical and experimental u_{mf} will be performed in future studies.

Nevertheless, as can be seen in Fig.5, the minimum velocity required for fluidization of carbonated particles during the first 5 cycles is between 27 and 11% higher than that of calcined particles. Since cycle 6th, the difference of u_{mf} between carbonated and calcined particles remains practically constant (u_{mf} of carbonated material is 7% more over u_{mf} of calcined material).
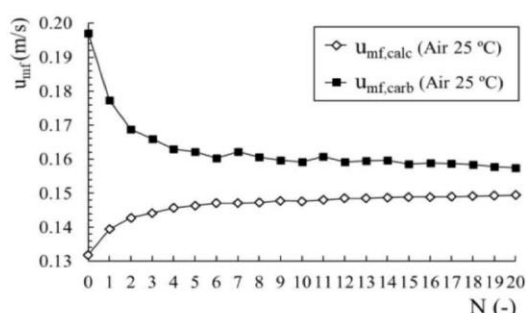

Figure 5. Theoretical minimum fluidization velocity of calcined and carbonated particles under experimental conditions (air 25 °C).

Fig.6 illustrated the theoretical minimum fluidization velocity using CO_2 as fluidizing gas at 850 °C. In the same way, the white rhombs curve represents the u_{mf} of the calcined particles or unconverted CaO, while the black squares curve shows the u_{mf} of carbonated particles or CL stream.
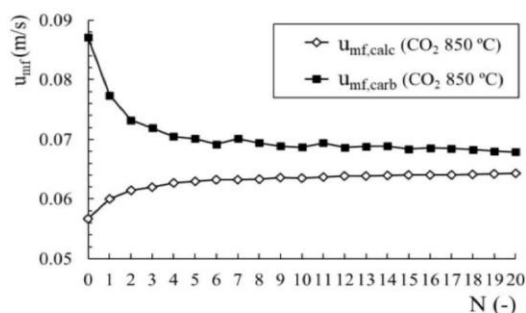

Figure 6. Theoretical minimum fluidization velocity of calcined and carbonated particles under real operating conditions (CO_2 850 °C).

The minimum velocity required for fluidization of the partially carbonated lime during the first 5 cycles is between 29 and 11% higher than that of unconverted CaO particles. Since cycle 6th, the difference of u_{mf} between carbonated and calcined particles remains practically constant (u_{mf} of CaO and $CaCO_3$ mixture is 8% more over u_{mf} of unconverted CaO).

Results show suitable conditions for partial separation of solids in a fluidized bed for particles subjected to few carbonation-calcination cycles. For future work, the experimental measurement of the minimum fluidization velocity must be performed to compare and validate the results obtained through the experimental model developed. In the same way, a sensitivity study of the sorbent purge percentage variation on the carbonation degree may be analyzed to improve the CaO average sorption capacity under the operating conditions selected in the CaL-CSP model.

Conclusions

In the present work, the partial separation of solids after carbonation reaction has been experimentally investigated under a CaL-CSP model operating

1434

89

conditions using fluidized bed reactors (850 °C and 950 °C for carbonation and calcination, respectively, reacting atmosphere always of 100% CO_2). A potential reduction in equipment size and energy flows between 50 and 75 % can be achieved when going from a system without solids separation to one with total separation of solids after carbonation step.

Results obtained show that the density of carbonated and calcined particles are related to the mean carbonation degree of the sorbent and the particle size. A model developed from experimental data is used to determine the particle density and diameter after each carbonation and calcination step. The theoretical minimum fluidization velocity calculated of calcined material (unreacted CaO) is lower than the carbonated material (partially carbonated lime) for the first cycles. A partial separation of solids may be technically feasible for particles with few cycles operated.

Acknowledgements

References

[1] R. Chacartegui, A. Alovisio, C. Ortiz, J.M. Valverde, V. Verda, J.A. Becerra, Thermochemical energy storage of concentrated solar power by integration of the calcium looping process and a CO_2 power cycle, Appl. Energy. 173 (2016) 589–605. https://doi.org/10.1016/j.apenergy.2016.04.053.

[2] U. Tesio, E. Guelpa, V. Verda, Integration of ThermoChemical Energy Storage in Concentrated Solar Power. Part 2: comprehensive optimization of supercritical CO_2 power block, Energy Convers. Manag. X. 6 (2020) 100038. https://doi.org/10.1016/j.ecmx.2020.100038.

[3] R. Bravo, C. Ortiz, R. Chacartegui, D. Friedrich, Hybrid solar power plant with thermochemical energy storage: A multi-objective operational optimisation, Energy Convers. Manag. 205 (2020) 112421. https://doi.org/10.1016/j.enconman.2019.112421.

[4] M. Bailera, P. Lisbona, L.M. Romeo, L.I. Díez, Calcium looping as chemical energy storage in concentrated solar power plants: Carbonator modelling and configuration assessment, Appl. Therm. Eng. (2020) 115186. https://doi.org/10.1016/j.applthermaleng.2020.115186.

[5] S. Pascual, M. Bailera, P. Lisbona, L.I. Díez, L.M. Romeo, Solar calcium looping energy storage: Preliminary comparison between pilot and large scale, ECOS 2020 - Proc. 33rd Int. Conf. Effic. Cost, Optim. Simul. Environ. Impact Energy Syst. (2020) 1511–1522.

[6] M. Bailera, S. Pascual, P. Lisbona, L.M. Romeo, Modelling calcium looping at industrial scale for energy storage in concentrating solar power plants, Energy. (2021) 120306. https://doi.org/10.1016/j.energy.2021.120306.

[7] P. Lisbona, M. Bailera, T. Hills, M. Sceats, L.I. Díez, L.M. Romeo, Energy consumption minimization for a solar lime calciner operating in a concentrated solar power plant for thermal energy storage, Renew. Energy. 156 (2020) 1019–1027. https://doi.org/10.1016/j.renene.2020.04.129.

[8] C. Tregambi, F. Di Lauro, F. Montagnaro, P. Salatino, R. Solimene, Limestone calcination-carbonation in a fluidized bed reactor/receiver for thermochemical energy storage applications, AIP Conf. Proc. 2126 (2019). https://doi.org/10.1063/1.5117757.

[9] S. Pascual, P. Lisbona, M. Bailera, L.M. Romeo, Design and operational performance maps of calcium looping thermochemical energy storage for concentrating solar power plants, Energy. 220 (2021). https://doi.org/10.1016/j.energy.2020.119715.

[10] V. Manovic, J.P. Charland, J. Blamey, P.S. Fennell, D.Y. Lu, E.J. Anthony, Influence of calcination conditions on carrying capacity of CaO-based sorbent in CO_2 looping cycles, Fuel. 88 (2009) 1893–1900. https://doi.org/10.1016/j.fuel.2009.04.012.

[11] G.S. Grasa, J.C. Abanades, CO_2 Capture Capacity of CaO in Long Series of Carbonation/Calcination Cycles, Ind. Eng. Chem. Res. 45 (2006) 8846–8851. https://doi.org/10.1021/ie0606946.

[12] N. Rodriguez, M. Alonso, G. Grasa, J.C. Abanades, Heat requirements in a calciner of $CaCO_3$ integrated in a CO_2 capture system using CaO, Chem. Eng. J. 138 (2008) 148–154. https://doi.org/10.1016/j.cej.2007.06.005.

[13] C. Tregambi, F. Di Lauro, F. Montagnaro, P. Salatino, R. Solimene, 110th anniversary: Calcium looping coupled with concentrated solar power for carbon capture and thermochemical energy storage, Ind. Eng. Chem. Res. 58 (2019) 21262–21272. https://doi.org/10.1021/acs.iecr.9b03083.

[14] C. Tregambi, F. Montagnaro, P. Salatino, R. Solimene, Solar-Driven Torrefaction of a Lignin-Rich Biomass Residue in a Directly Irradiated Fluidized Bed Reactor, Combust. Sci. Technol. 191 (2019) 1609–1627. https://doi.org/10.1080/00102202.2019.1607847.

[15] C.Y. Wen, Y.H. Yu, A Generalized Method for Predicting the Minimum Fluidization Velocity, A.I.Ch.E. J. (1966) 610–612.

1435

Solar-driven calcium looping in fluidized beds for thermochemical energy storage

Claudio Tregambi [a,b], Francesca Di Lauro [c], Sara Pascual [d], Pilar Lisbona [d], Luis M. Romeo [d], Roberto Solimene [b,*], Piero Salatino [b,e], Fabio Montagnaro [c]

[a] *Dipartimento di Ingegneria, Università degli Studi del Sannio, Piazza Roma 21, 82100 Benevento, Italy*
[b] *Istituto di Scienze e Tecnologie per l'Energia e la Mobilità Sostenibili, Consiglio Nazionale delle Ricerche, Piazzale Tecchio 80, 80125 Napoli, Italy*
[c] *Dipartimento di Scienze Chimiche, Università degli Studi di Napoli Federico II, Complesso Universitario di Monte Sant'Angelo, 80126 Napoli, Italy*
[d] *Departamento de Ingeniería Mecánica. Escuela de Ingeniería y Arquitectura (EINA). Universidad de Zaragoza, C/ María de Luna s/n, 50018 Zaragoza, Spain*
[e] *Dipartimento di Ingegneria Chimica, dei Materiali e della Produzione Industriale, Università degli Studi di Napoli Federico II, Piazzale Tecchio 80, 80125 Napoli, Italy*

ABSTRACT

Integration between Concentrated Solar Power (CSP) and Calcium Looping (CaL) is gaining consideration in the perspective of large shares of renewable energy sources, to smooth the variability of non-dispatchable energy input. The scope of this study is to investigate the CaL process for ThermoChemical Energy Storage (TCES), by performing a dedicated experimental campaign in fluidized bed under realistic process conditions suitable for CaL-CSP integration. Chemical deactivation of the limestone-based sorbent has been assessed by measuring the extent of Ca carbonation along iterated calcination/carbonation cycles, correlated with physico-chemical characterization of the sorbent at selected stages of the conversion. Properties that have been scrutinized were particle size distribution, bulk density, and particle size, density, and porosity of bed solids. The attainable values of energy storage density were evaluated as well.

A remarkable finding of the experimental campaign is the pronounced synergistic deactivation of limestone when it is co-processed with silica sand. Chemical interaction of CaO with the silica sand constituents at the process temperatures has been scrutinized as possible responsible for the loss of reactive CaO toward CO_2 uptake. Post-process of particle density data, together with N_2-intrusion porosimetric analysis, and quantitative and qualitative XRD analyses, suggests that the sand/lime interaction induces a strong reduction of the total and reactive sorbent porosity and, in turn, of reactivity.

Density-based classification to separate converted and unconverted limestone particles after the carbonation step has been evaluated with the goal of increasing process efficiency, by avoiding the circulation of streams with unreacted particles through the plant. For this purpose, the minimum fluidization velocity of calcined and carbonated particles has been measured after each reaction step at the relevant process temperature.

1. Introduction

The ambitious targets of the European Green Deal aim to cut the greenhouse gas emissions by at least 55% within 2030, and to achieve carbon neutrality by 2050 with net-zero greenhouse gas emissions. These objectives require a strong decarbonization of the power and energy sectors, with an ever-increasing exploitation of renewable energy sources. Among them, solar energy is bound to play a key role in the future economy because of its virtual unlimited potential and wide availability. However, a strategy to deal with its intermittent nature needs to be implemented to enable its massive deployment.

Concentrated Solar Power (CSP) technologies provide an effective path for exploitation of solar energy, allowing integration with thermal and thermochemical energy storage systems to overcome its intrinsic intermittency. In CSP systems, a field of heliostats (i.e., sun tracking mirrors) is used to focus and concentrate the solar energy onto a receiver. Here, a heat transfer medium is heated at moderate-to-high temperatures and eventually used to sustain energy intensive chemical/physical processes, or to drive thermodynamic cycles for energy generation. Most recent commercial CSP plants make use of molten salts (i.

---

e., a binary mixture of $NaNO_3$ and KNO_3) as heat transfer medium, which operate within the 290–565 °C temperature range. Storage of the hot medium in insulated vessels, rather than direct use (i.e., thermal energy storage), allows decoupling the two steps of solar energy collection and exploitation, enhancing the dispatchability of solar energy. Research efforts on the CSP technology are mostly prioritized on: i) increasing the maximum working temperature of the heat transfer medium, currently limited at 565 °C due to the molten salts degradation; ii) developing more efficient energy storage systems with respect to storage density, application temperature, and time scale of utilization. On one side, particle receivers are under the spotlight to overcome the temperature limitations of the molten salts: dense-solids suspensions can indeed safely work at temperatures of 1000 °C and over [1–3]. On the other side, use of reversible chemical reactions to store solar energy in the form of chemical bonds (i.e., ThermoChemical Energy Storage, TCES) is widely pursued [4–7]. Gas-solid chemical reactions are the most investigated. Indeed, their higher reaction enthalpy turns into potential higher values of energy storage densities and the easier separation of the reaction products favours the subsequent storage/transportation.

Particle receivers able to simultaneously work as solar receiver and chemical reactor can represent a breakthrough for the success of the CSP–TCES technology. For this reason, Fluidized Bed (FB) systems have been and are widely investigated [8–10]. Literature research studies spread from conventional FB with direct/indirect irradiation [11–13], to innovative design targeted at: i) increasing the axial thermal diffusivity by internal circulation [14–16], spout, pulsed or uneven fluidization [2,17–20]; ii) providing a more uniform residence time distribution by multistage operation [21–23]; iii) exploiting the sensible heat of the reaction products for the heating of the reactants by internal solid–solid heat exchangers [2,24,25].

The selection of the most appropriate chemical reaction for TCES is open to debate. Apart from solar fuels production, decomposition and recombination of metal hydroxides, carbonates, oxides and perovskites are among the most investigated processes, each with specific advantages and drawbacks [26–29]. In particular, reversible calcination-carbonation of Ca–based sorbents, Eq. (R1):

$$CaCO_3 \leftrightharpoons CaO + CO_2 \qquad (R1)$$

has been widely addressed recently, and its integration with CSP is being currently assessed, with different European research projects currently active [30,31].

The same reaction scheme has been widely investigated in literature for post combustion and atmospheric CO_2 capture, and is commonly referred to as Calcium Looping (CaL) [32–35]. CSP–CaL integrated processes targets both CO_2 capture [34,36,37] and TCES. The interest on this system for TCES applications mainly springs from: i) the fairly high reaction enthalpy of the chemical reaction ($|\Delta H_r^\circ|_{298K} = 178$ kJ mol^{-1}); ii) the high temperature at which solar energy can be retrieved (650–850 °C according to the process parameters), which allows integration with high-efficiency Rankine/Brayton cycles [38]; iii) the low cost of the raw material (i.e., limestone, a very cheap natural sorbent rich in $CaCO_3$). On the other side, the major weakness of the CaL cycle is the decay of material reactivity over iterated cycling, induced by loss of porosity (i.e., thermal/chemical sintering) and pore plugging [39–41]. Different techniques have been explored to prevent or limit the loss of reactivity, among which: production of composite materials with inert stabilizers/promoters [42] such as ZrO_2 [43–45], Al_2O_3 [46,47], CeO_2 or multiple Ce/Al/Zr additives [48], eutectic alkali chloride salts [49]; mechanical activation [50,51]; thermal pre-treatments [52,53]; use of steam [54–56]. More recently, introduction of inert materials in synthetic Ca–based sorbents has been scrutinized also with the aim of improving their optical performance in terms of solar energy absorptivity, through the synthesis of particles characterized by a darker colour [57–59]. On this topic, a peculiar natural sorbent with a higher

absorption of solar energy has also been tested with positive outcomes [60]. While improving material stability, it was recently found that the presence of inert compounds does not significantly affect the kinetics of carbonation, and a slight modification of the parameters of the random pore model may be sufficient to account for the presence of inert stabilizers [61]. Different process schemes have been proposed and investigated in literature for integration between CSP and CaL for TCES. Tregambi et al. [41] distinguished between open loop and closed loop conditions with respect to CO_2. In the open loop condition, CaO carbonation is performed at 650 °C using a stream coming from a CO_2 emitting industry, whereas calcination is performed at 850 °C using air, and the produced stream is released to the atmosphere. Differently, in closed loop conditions, calcination is performed at 940–950 °C under CO_2, that can then be recycled to the process. Experimental tests performed in a FB heated by a solar simulator demonstrated that the harsher conditions of closed loop during calcination induce a stronger loss of reactivity [41]. Castilla et al. [62] investigated a process scheme for simultaneous TCES and CO_2 capture, and performed a techno-economic analysis of the system. Sarrión et al. [63,64] proposed, instead, two different process configurations for a closed loop CO_2 cycle for TCES. In both schemes, carbonation is carried out at 850 °C under pure CO_2, to maximize the efficiency of the subsequent cycle for energy production. Calcination is instead performed either at 750 °C under a N_2/He atmosphere [63,64], or at 950 °C under pure CO_2 [64]. In the former case, use of membranes is proposed to separate the produced CO_2 from the carrier gas and close the looping cycle. Experimental tests have been performed only in a thermogravimetric analyzer, but proved again that harsher conditions during calcination promote material sintering. The closed loop CO_2 scheme, with carbonation/calcination at 850/950 °C under pure CO_2, has been investigated by model computations also by Pascual et al. [65], who proposed the addition of a solid–solid separation unit after the carbonator to separate converted and unconverted particles, thus avoiding the looping of unreacted streams, to increase process efficiency. Since CaO carbonation to yield $CaCO_3$ is generally proved to be a slow reaction step because of the time required for internal CO_2 diffusion [61], it is reasonable to consider that unconverted streams may leave the carbonator during continuous operation, thus supporting the usefulness/advantages of a Solid-Solid Separation Unit (SSU). The feasibility of this operation is, however, still to be demonstrated.

The aim of this study is to contribute to the existing knowledge on the CaL process for TCES, by performing a dedicated experimental campaign under realistic process conditions suitable for CaL-CSP integration, which are different from those typically investigated in literature for carbon capture and storage. The closed loop CO_2 scheme, considering carbonation/calcination at 850/950 °C under pure CO_2, has been selected because of its interesting features and because of the lack of experimental data in apparatus different from thermogravimetric analyzers. In this work, experimental tests were performed in FB reactors because of their peculiarity of acting, simultaneously, as particle receivers for solar radiation and multiphase chemical reactors. Decay of material reactivity and deactivation trend, as well as changes in granulometric distribution of the bed inventory over cycling, were deeply scrutinized. Attainable values of energy storage density were also computed. Moreover, the aim of increasing the overall process efficiency of the process has been pursued by avoiding the circulation of unreacted streams [65]. To this end, it was evaluated the possibility of separating converted (i.e., $CaCO_3$-based) and unconverted (i.e., CaO-based) particles after the carbonation step, exploiting the particle density difference. For the purpose, the minimum fluidization velocity of calcined and carbonated particles was experimentally measured after each reaction step at the relevant process temperature, to gather first data about the feasibility of this operation. Finally, the influence of silica sand on the CaL performance, when experiments were carried out using sand as ballast bed material, was highlighted.

2. Process scheme

The process plant devised for the closed loop CaL cycle for TCES is sketched in Fig. 1. The system entails two fluidized bed reactors (i.e., a solar calciner and a carbonator), three intermediate Storage Tanks (STs) required to decouple collection and exploitation of solar energy (i.e., one each for the calcined and carbonated material, one for the compressed CO_2), a SSU at the exit of the carbonator, and several Heat Exchangers (HEs) for heat recovery or preheating. A heat loss of 2% was assumed for each heat exchanger used for heat recovery. Operation of the process is described in the following. More extent information of the theoretical simulation of the CaL process as TCES is detailed by Pascual et al. [66]. A stream of carbonated material (consisting of partially carbonated particles because of uncomplete carbonation [41]) is fed from either the ST1 $CaCO_3$ storage tank (upon preheating from 200 to 850 °C through HE1) or from the carbonator itself to the calciner. Here, endothermic calcination occurs driven by concentrated solar energy (100 MW energy input as reference case). Gaseous atmosphere is 100% CO_2, therefore a process temperature of about 950 °C is required to guarantee fast reaction kinetics. The stream of pure CO_2 exiting the reactor is partially recycled as fluidizing gas to the reactor, and partially either sent to compression and ST3 (upon heat recovery from 950 °C to 50 °C in HE3) or directly fed to the carbonator. The CO_2 is stored in ST3 at 75 bar and 35 °C, after being previously compressed and cooled in 4 interleaved stages (CCT in Fig. 1). A pressure ratio of 3 was assumed for each of the four compression stages to finally reach the CO_2 storage pressure (75 bar). The energy penalty associated to the compression stages is the electrical energy consumption, rising to 8.41 MW maximum [66]. The first three cooled stages reduce the temperature to 50 °C and the fourth to the CO_2 storage temperature (35 °C). The heat from the cooled stages is recovered, being the heat losses of 2%. Similarly, particles leaving the calciner are sent to ST2 (upon heat recovery from 950 °C to 200 °C in HE6), or directly to the carbonator. Finally, the calciner also processes an additional stream of fresh limestone and purges a stream of spent material, which is required to compensate for the decay of material reactivity over cycling ("chemical loss") and for the elutriation of fine particles generated upon attrition/fragmentation phenomena ("physical loss") [67,68]. The fresh limestone is fed at ambient temperature (25 °C) and a heat recovery of the purged spent material is done through HE8 from 950 °C to 200 °C. The calcination step is in operation only upon availability of solar energy (ECL). When the collected solar energy needs to be retrieved (ECR), CaO and CO_2 are fed to the carbonator either from

the CaO/CO_2 storage tanks (ST2 and ST3) (upon preheating through HE7 and HE5, respectively) or directly from the calciner. The HE7 receives CaO streams from (i) calciner at 950 °C and (ii) ST2 at 200 °C to be preheated to carbonator conditions (850 °C). The HE5 preheats the CO_2 mixture from ST3 at 15 °C and calciner at 950 °C to 850 °C. The CO_2 from ST3 suffers a discharging expansion (DE in Fig. 1) before being fed into HE5 at 15 °C. Reactive atmosphere in the carbonator is 100% CO_2: carbonation is then performed at high temperature (850 °C) to maximize the efficiency of the subsequent thermodynamic cycle for power production. The carbonation reaction is generally a slow reaction step because of the time required for internal CO_2 diffusion. Fluidized beds may be viewed as continuously stirred tank reactors in terms of solid residence time distribution. Thus, it is reasonably to consider that the solid stream exiting the carbonator includes both carbonated particles (consisting of both CaO and $CaCO_3$, mostly concentrated in the core and shell of the particle, respectively) and unreacted (or less carbonated) particles. Unreacted CO_2 stream is found at carbonator outlet given the uncomplete exothermic carbonation reaction. The unreacted CO_2 from carbonator is sent to the CCT after a heat recovery from 850 °C to 50 °C in HE4. The carbonator model applied for the theoretical TCES simulation was based on the kinetic model described by Grasa et al. [69] under carbon capture conditions (650 °C and 10–15 $\%_v$ of CO_2). A SSU is then implemented for the separation of carbonated and unreacted particles: carbonated material is sent either to ST1 (upon heat recovery from 850 °C to 200 °C in HE2) or to the calciner, whereas unreacted or less reacted material is cycled back to the carbonator at 850 °C, closing the looping cycle. To allow the solid–solid separation, the SSU consists of a tapered fluidized bed reactor operated under transient fluidization regime, so as to induce segregation of lower density particles to the top of the column [70,71]. The inclusion of the total separation of carbonated and unreacted particles was firstly proposed by Pascual et al. [65] to enhance the energy efficiency of the CaL TCES system. Moreover, the effect of the SSU on the energy penalties and plant size reduction was assessed under theoretical simulation. The threshold scenarios (no separation and total separation of solids after carbonation step) were evaluated to provide information of the maximum and minimum energy and size requirements. A size reduction between 53 and 74 % was showed for heat exchangers affected by solid streams when the SSU is included [66].
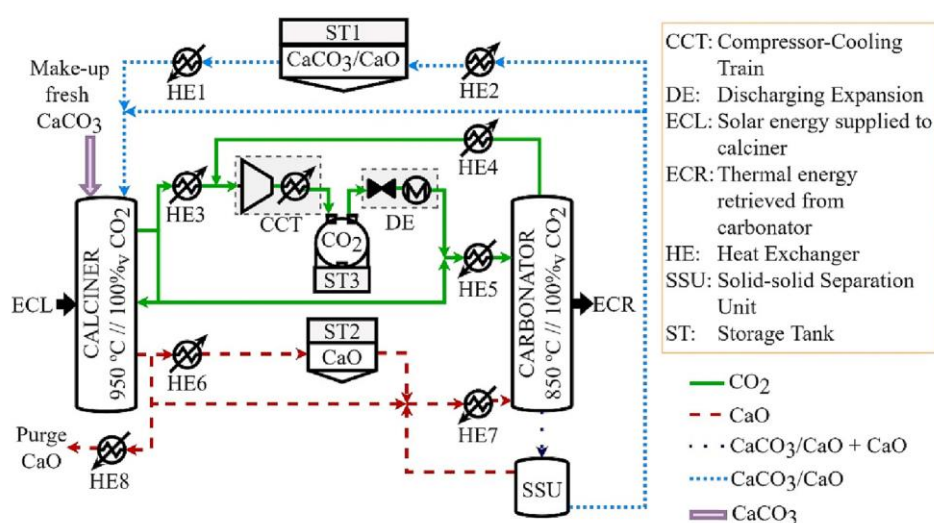

Fig. 1. Simplified conceptual scheme for closed loop CaL-CSP integration, taken as reference in this work.

3. Experimental

The experimental campaign consisted in CaL tests performed under operating parameters relevant for the process integration outlined in the previous paragraph. Tests were performed in semi–batch mode using a single FB reactor, by switching the process conditions between carbonation and calcination. Two different experimental rigs were used for the whole experimental campaign: i) a fluidized bed reactor equipped with a solar simulator, to mimic the effect of concentrated solar radiation and estimate the decay of reactivity over cycling; ii) an electrically heated fluidized bed reactor, to determine the changes in the particle properties (granulometric distribution, porosity and density) of the bed inventory over cycling, as well as the minimum fluidization velocity of the material after each reaction step.

3.1. Experimental apparatus

The FB reactor used for the CaL tests under solar simulated conditions is sketched in Fig. 2. The reactor has been used in previous experimental campaigns and a comprehensive description of the experimental rig can be found in [41,52]. The FB reactor has an internal diameter of 0.1 m and, starting from the bottom, is made of three components: i) a windbox with an upper perforated plate serving as gas distributor (0.5 mm holes on a triangular pitch); ii) a fluidized bed section, 0.1 m high; iii) a conical freeboard section (0.4 m high, internal cone angle of about 30°) with an upper optical window required to seal the reactor environment while allowing entrance of the concentrated solar radiation. At middle height of the conical section, four discharge ports (1 in. diameter) are provided for gas outlet. The reactor is heated by: i) a gas heater (manually controlled), able to heat the gaseous stream up to 700 °C; ii) two semicylindrical radiant heaters (driven by a PID controller) which surround the windbox and fluidized bed sections; iii) a solar simulator, made up by three 4 kW_e short–arc Xe–lamps coupled with elliptical reflectors, able to produce a peak flux of about 3 MW m^{-2} and a total irradiated power of about 3.2 kW_{th} on the bed surface. Electronic mass flow controllers are used for gas feeding to the reactor. Four K–type thermocouples are located within the system for temperature measurement: i) one at the exit of the gas preheater; ii) one within the windbox, 0.02 m below the distribution grid; iii) two inside the FB, 0.05 m over the distribution grid and 0.05 m from the reactor wall

(middle thermocouple), and 0.08 m above the distribution grid and 0.01 m from the reactor wall (up thermocouple).

The electrically heated FB reactor is depicted in Fig. 3. It features an internal diameter of 0.04 m and, starting from the bottom, is made of two components: i) a windbox section, 0.6 m high, with an upper stainless steel wire mesh serving as gas distributor; ii) a reaction plus freeboard section, 0.8 m high (the relative extension of the two zones depends on the bed inventory). Exhaust gas leaves the reactor at the top of the freeboard. Two semicylindrical radiant heaters (driven by a PID controller) surround the reaction/freeboard zone and the windbox zone for an overall length of about 0.6 m. A lateral port, located a few millimeters above the distribution grid, is used for the simultaneous temperature and pressure measurement inside the FB reactor by a K–type thermocouple and a piezoelectric pressure transducer, respectively. Electronic mass flow controllers are used for gas feeding. The reactor is also equipped with a vacuum system to discharge and collect the bed

Fig. 3. Electrically heated fluidized bed reactor.

FB:	Fluidized Bed
MF:	Mass-flow Controller
PT:	Pressure Transducer
RH:	Radiant Heaters
TC:	K-type Thermocouple
WB:	Windbox
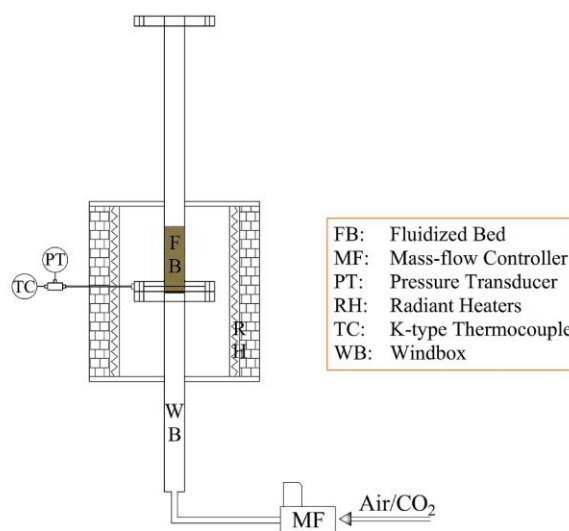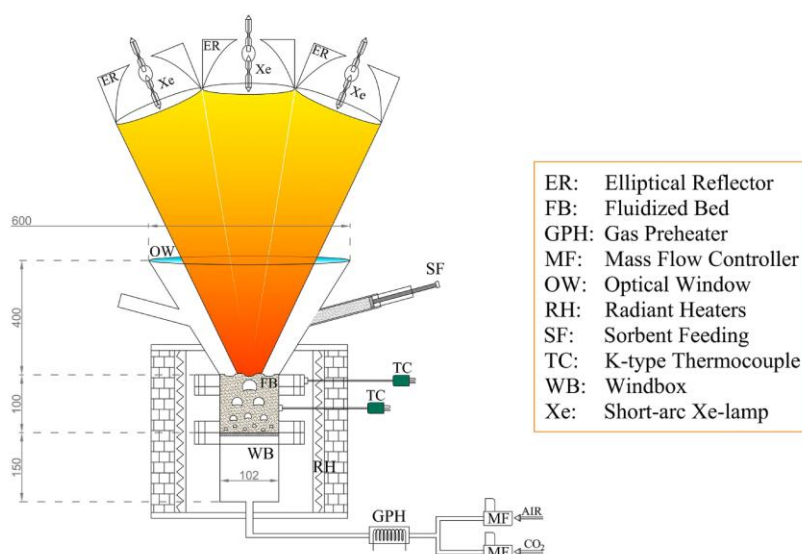
Fig. 2. Directly irradiated fluidized bed reactor. Dimensions in mm.

ER:	Elliptical Reflector
FB:	Fluidized Bed
GPH:	Gas Preheater
MF:	Mass Flow Controller
OW:	Optical Window
RH:	Radiant Heaters
SF:	Sorbent Feeding
TC:	K-type Thermocouple
WB:	Windbox
Xe:	Short-arc Xe-lamp

4

inventory under cold or hot conditions.

3.2. Materials

Two different materials were used in the experimental campaign: a silica sand from the Ticino river (Italy) and a natural Italian limestone, whose main properties summarized in Table 1. Besides SiO_2 (83.9 %$_{wt}$), the other constituents of the Ticino sand are Na_2O (1.8 %$_{wt}$), K_2O (2.4 %$_{wt}$), CaO (0.9 %$_{wt}$), MgO (1.0 %$_{wt}$), Al_2O_3 (8.4 %$_{wt}$), Fe_2O_3 (1.4 %$_{wt}$).

3.3. Experimental conditions and procedure

Regardless of the experimental rig, for all the CaL tests performed in this work the following process parameters, relevant to closed loop CaL–CSP integration, were used:

    i) reacting atmosphere of 100 %$_v$ CO_2 during both carbonation and calcination;

    ii) reaction time of 20 min for both reaction steps;

    iii) superficial gas velocity of 0.6 m s^{-1} throughout the process;

    iv) process temperature of 850 °C and 950 °C during carbonation and calcination, respectively.

Moreover, for the experimental runs performed in the directly irradiated FB, bed inventory consisted in a mixture of silica sand (82 %$_{wt}$) and limestone (18 %$_{wt}$). Silica sand acts as a thermal flywheel, smoothing and mitigating the temperature variations induced by the chemical reactions. This lime-to-sand ratio was used also in previous experimental campaigns [41,52], and is retained in this work also for a better data comparison. Differently, for the experimental runs performed in the electrically heated FB, bed inventory consisted in either a 1:1 mixture of silica sand and limestone, or limestone only. The smaller scale of the plant allows indeed a better temperature control, offering the possibility of working with higher percentage of lime. This also permitted to perform different characterizations on the reactive material.

3.3.1. Directly irradiated fluidized bed (Experimental procedure #1)

First, the system was charged with ~ 700 g of sand and heated up to 900 °C by the radiant and gas heaters, using air as fluidizing gas. Once achieved this temperature, the fluidizing gas was switched to CO_2 for 5 min to flush all the air from the reactor. The radiant heaters were powered off, and a sample of 150 g of limestone was fed to the reactor. Then, the solar simulator was turned on at the power required to keep the bed at 950 °C to perform the calcination step, assuming as reference the "up" thermocouple. After 20 min (calcination reaction time), the solar simulator was turned off, the fluidizing gas switched to air, and the radiant heaters turned on with a set point temperature of 850 °C. The fluidizing gas was then switched back to CO_2, to perform the carbonation step. After 20 min (carbonation reaction time), the radiant heaters were turned off and the bed was heated up to 950 °C by means of the solar simulator, to perform a new calcination step. The procedure was repeated until completion of 20 looping cycles. At the end of each carbonation step, a small sample of bed material (1–2 g) was collected for the subsequent determination of the carbonation degree of the sorbent. Sand and reactive material were separated by sieving.

Overall, the temperature control in the directly irradiated fluidized bed was quite satisfactory. During the calcination, after the initial transient heating to 950 °C, the average temperature recorded by the up and middle thermocouple was 955 ± 4 °C and 968 ± 5 °C, suggesting a slight bed overheating. During the carbonation, the temperatures recorded by the up and middle thermocouples were in good agreement, with an average value of 838 ± 11 °C.

3.3.2. Electrically heated fluidized bed

Three different experimental procedures were carried out in this facility: a) to assess the sorption degradation of limestone under CaL TCES conditions; b) to assess the interaction of sand presence in limestone degradation under CaL TCES conditions; c) to estimate the minimum fluidization velocity of the calcined and carbonated material upon iterated cycles.

3.3.2.1. Experimental procedure #2.
The following experimental procedure was applied to the tests performed with a bed inventory of limestone only. First, the system was charged with ~ 180 g of sand and heated up to 900 °C using air as fluidizing gas. Once achieved this temperature, the vacuum system was used to discharge the bed inventory, and the reactor was cleaned to remove any trace of sand. The fluidizing gas was switched to CO_2, and flowed for 2 min to completely flush the air from the reactor. Then, a sample of 180 g of limestone was fed to the reactor and the PID controller was set to 950 °C to perform the calcination step. After 20 min, heating of the FB was stopped, and the bed inventory was collected by the vacuum system. Before this operation, the fluidizing gas was switched back to air, to prevent a possible sorbent re-carbonation induced by the temperature reduction. The collected material was cooled down to ambient temperature, and weighted. It was then estimated the bulk density of the sample, by pouring the material in a 50 mL graduated cylinder and measuring the weight and occupied volume. Finally, the sample was sieved in the following size ranges: 0–100 μm, 100–200 μm, 300–420 μm and 420–590 μm, and each granulometric cut was individually weighted. All the material was eventually mixed back and fed into the still hot FB reactor under air atmosphere. The PID controller was set to 850 °C and, once reached this temperature, the fluidizing gas was switched to CO_2 to perform the carbonation step. After 20 min, heating of the FB was stopped, and the bed inventory was collected by the vacuum system under CO_2 atmosphere and cooled to ambient temperature. Overall weight (required to evaluate the carbonation degree), bulk density and granulometric distribution were determined as previously described. After that, the sample was fed back to the FB reactor under CO_2 atmosphere, and the PID controller was set to 950 °C, to perform a new calcination step. The procedure was repeated until completion of 20 looping cycles. Overall, the temperature control in the electrically heated fluidized bed was quite effective. During the calcination, apart from a brief overshoot of 10 °C during the initial transient heating to 950 °C, the average temperature was 950 ± 2 °C. Similar fluctuations were observed during the carbonation, with an average temperature of 850 ± 2 °C.

3.3.2.2. Experimental procedure #3.
A different experimental run was also performed by applying the same experimental procedure but using a bed inventory of sand and limestone (1:1 weight mixture). Material

Table 1
Main properties of the materials used in the experimental campaign.

Material	Bulk density, tapped [kg m^{-3}]	Size range [μm]	CaO content (calcined material) [%$_{wt}$]	u^t_{mf}(850–950 °C)* [m s^{-1}]
Limestone	1590	420–590	97.4	0.12–0.11
Ticino sand	1489	850–1000	0.9	0.35–0.33

* Minimum fluidization velocity, calculated according to Grace [72].

characterizations were carried out after separation of the sorbent from the sand, performed by sieving. The first calcination was however performed with limestone only, to produce a relevant amount of material for the subsequent cycles.

3.3.2.3. Experimental procedure #4. Finally, to estimate the minimum fluidization velocity, a different experimental run was performed, using again a bed inventory of reactive material only. The same experimental procedure described above was applied but, after each reaction step, the bed inventory was not discharged. Instead, an automated script developed in LABVIEW was run to measure the pressure drop vs. the superficial gas velocity in a "down–curve" from 30 to 0 cm s^{-1}, with 1 cm s^{-1} step. Curves were acquired at the process temperature of the relevant step, using CO_2 as fluidizing gas. Particular accuracy was dedicated to ensuring the temperature uniformity of the entire fluidized bed when decreasing the superficial gas velocity. To this aim, the bed was vigorously fluidized before the acquisition of each pressure drop measurement.

3.4. Data analysis and further characterization

The mean carbonation degree for the tests performed in the directly irradiated FB was evaluated using the samples of carbonated material collected after each carbonation step. The samples were individually calcined in a muffle furnace at 950 °C under air atmosphere, and the weight change was measured with an analytical balance (0.1 mg precision), so as to determine the mean carbonation degree as described in Di Lauro et al. [52].

For the tests performed in the electrically heated FB, the data of overall weight after each reaction step were used to compute the mean carbonation degree ($\overline{X}_{Ca}$) as:

$$\overline{X}_{Ca}(N) = \frac{\left(m_N^{carb} - m_{N-1}^{calc}\right)}{m_{N-1}^{calc} x_{CaO}} \frac{MW_{CaO}}{MW_{CO_2}} \tag{1}$$

where N is an index for the cycle number, m^{carb} and m^{calc} represent the overall weight of the carbonated and calcined sample, respectively, x_{CaO} is the mass fraction of CaO in the calcined sorbent (see Table 1), MW stands for molecular weight.

Mean carbonation degree data were further processed to compute the average energy storage density (E_{SD}) following the methodology described in Di Lauro et al. [52]. Computed values account for both the chemical heat and sensible heat contributions.

Data of Particle Size Distribution (PSD) were post–processed to evaluate the mean Sauter diameter.

The curves of pressure drop vs. superficial gas velocity were analyzed to compute the minimum fluidization velocity of the calcined and carbonated particles.

Finally, samples of lime retrieved after the last calcination step were subjected to X-Ray Diffraction (XRD) analysis, performed using a Rigaku MiniFlex 600 instrument, and to N_2–intrusion porosimetric analyses to investigate differences in specific surface area (through BET theory), total pore volume and pore size distribution (through BJH theory).

4. Results

4.1. Sorbent carbonation degree

Fig. 4 shows the mean carbonation degree of the sorbent obtained in the different experimental tests (*EP #1, #2* and *#3*). It is possible to observe that the mean carbonation degree decreases along with reaction cycles. Sintering phenomena and loss of reactivity are induced by the high temperature and high CO_2 concentration experienced by the sorbent during both reaction steps. With reference to experimental tests performed in the directly irradiated FB (*EP#1* where solid inventory includes limestone and sand), $\overline{X}_{Ca}$ decreases from about 61% ($N = 1$) to
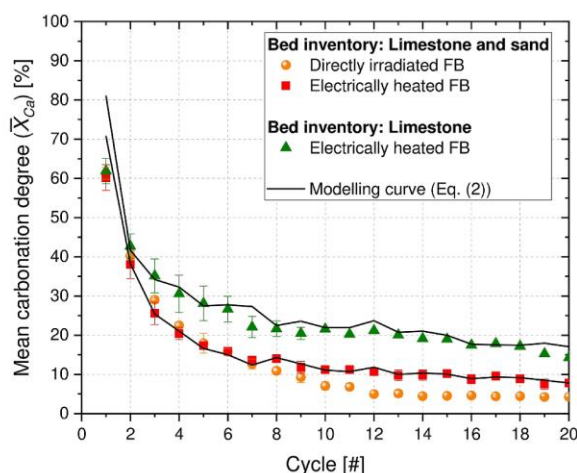

Fig. 4. Mean carbonation degree of the sorbent as a function of the cycle number and of the adopted operating conditions.

about 4% ($N = 20$), with an average value of 14% over the whole 20 reaction cycles. Performance of the tests carried out in the electrically heated FB with a bed inventory of limestone and sand (*EP #3*) do not differ sensibly: $\overline{X}_{Ca}$ decreases from about 60% ($N = 1$) to about 8% ($N = 20$), with an average value of 16% over the whole reaction cycles. The slightly worse performance achieved in the directly irradiated FB may be caused by the overheating of the bed surface induced by the highly concentrated solar radiation, as observed in previous research studies [11]. The temperature difference between the "middle" and "up" thermocouple ranged within 13.4 ± 3.2 °C across the different tests. The bed surface overheating was not measured in this work, but according to previous experimental studies it can be as high as 80 °C in the centre of the FB [11,41]. Differently, the tests performed in the electrically heated FB with a bed inventory of limestone only (*EP #2*) show better performance in terms of sorbent reactivity. The mean carbonation degree decreases indeed from about 62% (1st cycle) to about 14% (20th cycle), with an average value over the whole 20 cycles of about 25%. This was an unexpected result that needed further investigation. In particular, it was scrutinized in literature a possible chemical interaction between the silica sand constituents and lime particles, with the formation of unreactive compounds, which can subtract reactive CaO, and induce a loss of reactivity. Dicalcium silicate (Ca_2SiO_4, i.e. belite), one of the main constituents of the Portland cement clinker [73,74], is formed when raw meals for cement production are used as sorbents in CaL process for CO_2 capture [75]. It was claimed that its formation reduces the CO_2 sorption capacity of the cement raw meals subtracting CaO sites available for the carbonation reaction [76]. Valverde et al. [77] also observed the formation of calcium silicates from the interaction of a calcium-based sorbent and a SiO_2 nanostructured powder under CaL conditions. However, in this case the addition of nanostructured SiO_2 increases the carbonation degree improving the CO_2 accessibility to the CaO sites. Experimental data plotted in Fig. 4 shows a detrimental effect of Ticino silica sand on lime reactivity, in analogy with the findings obtained with cement raw meals used in CaL process for CO_2 capture [75]. A further consequence of this result is related to the use of additives, devoted to improving the fluidizability of small particles of limestone and/or its optical performance in terms of absorption of concentrated solar energy. Their addition to sorbent particles should be carefully evaluated because of possible interaction with lime and consequent decrease in reactivity.

Post-processing of $\overline{X}_{Ca}(N)$ data has been carried out by postulating here the following IAD "Initial Activity Decay" equation:
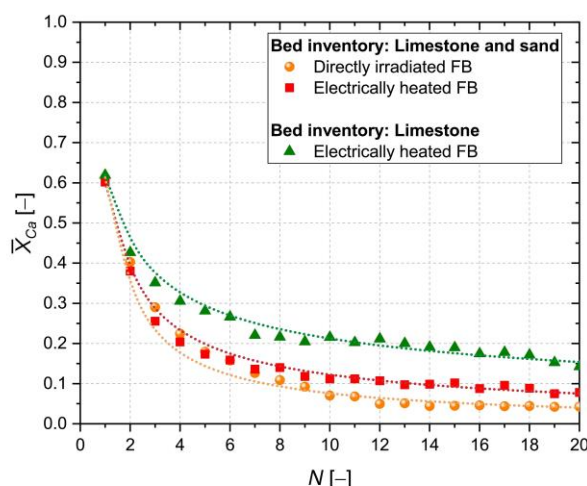
6

C. Tregambi et al.

Fig. 5. Fitting of experimental carbonation degree data by the IAD Eq. (2).

Table 2
Values for the decay constant (IAD model) for the cases under investigation.

	k_2 [–]	R^2 [–]
Limestone and sand inventory Directly irradiated FB	0.91	0.97
Limestone and sand inventory Electrically heated FB	0.69	0.98
Limestone inventory Electrically heated FB	0.46	0.97

$$\overline{X}_{Ca}(N) = k_1 N^{-k_2} \qquad (2)$$

where k_1 is the initial activity constant, that measures the efficacy of the sorbent when $N = 1$ ($\overline{X}_{Ca}(N = 1) = k_1$), and k_2 is the decay constant that considers the resistance of the sorbent to sintering phenomena (the higher k_2, the worst the sintering resistance). While Fig. 5 shows data fitting, Table 2 lists the best-fitting values for k_2 (along with the values for the coefficient of determination). Sintering resistance for the sorbent
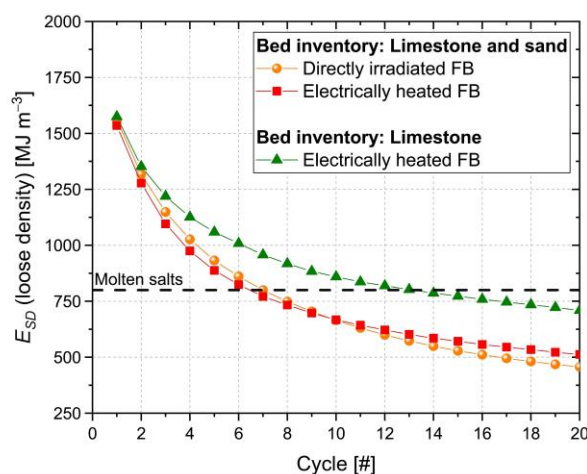

Fig. 6. Average energy storage density up to the reaction cycle considered vs. reaction stage, under the adopted operating conditions.

in the case of limestone inventory and electrically heated FB (*EP #2*) resulted ca. 33% and 49% higher vs. the cases with limestone and sand inventory (electrically heated (*EP #3*) and directly irradiated FB (*EP #1*), respectively), to confirm the ranking discussed above.

4.2. Density of energy storage

Fig. 6 shows the average values of energy storage density up to the reaction cycle considered vs. reaction cycle, for the different experimental runs. Data were computed under a conservative scenario by considering the loose density of limestone, which is about 13% lower than the tapped density value [52]. The energy storage density of the molten salts is also plotted as reference material, though a more comprehensive comparison should also account for the different technology and operating conditions of the two processes (i.e., thermal energy storage with molten salts and TCES with CaL). For the tests with a bed inventory of limestone and sand, the average values of E_{SD} are quite similar for the two experimental rigs and decrease from about 1550 MJ m^{-3} (1 looping cycle) to 485 MJ m^{-3} (20 looping cycles). Under these process conditions, the CaL system outperforms the molten salts only up to an average sorbent life of 6 cycles. From the 8th cycle onwards, the molten salts system appears to be superior. Data obtained in this study appear to be worse than those shown in Di Lauro et al. [52] for limestone in closed loop configuration, where carbonation was performed at 650 °C and 15 %$_v$ CO$_2$. This arises because of: i) a slightly lower reactivity of the sorbent in the present study, probably induced by the higher temperature and CO$_2$ concentration experienced during carbonation (mean carbonation degree at the 20th reaction cycle is of 13.7% in this work vs. 15.3% in Di Lauro et al. [52]); ii) a lower amount of sensible energy storage in this work (to perform carbonation, CaO is cooled from 950 °C to 850 °C in this work and from 950 °C to 650 °C in Di Lauro et al. [52]). Data of E_{SD} obtained with a bed inventory of limestone only are slightly better, especially at increasing looping cycles. Values decrease from about 1575 MJ m^{-3} (1 looping cycle) to 710 MJ m^{-3} (20 looping cycles). Even if the performance in terms of E_{SD} is comparable to that of molten salts when an average sorbent life of 10–20 cycles is considered, it should be recalled that, in this CaL process, thermal energy at the carbonator is released at a much higher temperature (i.e., 850 °C), with a consequent higher overall efficiency in the subsequent thermodynamic cycle for energy production. Moreover, the share of chemical heat storage over the total is very high. It values about 91% at the first cycle for all the tests, and decreases to 79% (10 looping cycles) and 70% (20 looping cycles) for the tests performed with a bed inventory of lime and sand, and to 84% (10 looping cycles) and 80% (20 looping cycles) for the tests performed with a bed inventory of limestone only.

4.3. Particle size distribution

Fig. 7 shows information on the attrition/fragmentation of the bed inventory for the experimental runs performed in the electrically heated FB. Data are plotted either as cumulative PSD for selected calcination stages (Fig. 7–A) or as mean Sauter diameter (d_{Sauter}) vs. reaction number (Fig. 7–B).

Figure 7–A highlights a progressive fragmentation/shrinkage of limestone particles along with reaction cycles. Particles mostly shift from the 420–590 μm to the 300–400 μm size range, whereas the mass fraction of smaller size ranges (less than 300 μm) only slightly increases. The effect is more pronounced for the tests performed with a bed inventory of limestone and sand, suggesting that the presence of sand enhances the fragmentation/shrinkage of limestone particles. Particle size reduction appears to be mostly concluded at the 10th calcination for tests with a bed inventory of limestone only, as the PSD for the 10th and 20th calcined samples mostly overlap. Differently, when the bed inventory of limestone and sand is used, the PSD for the 10th and 20th calcined samples still shows significant differences. Discussed data are
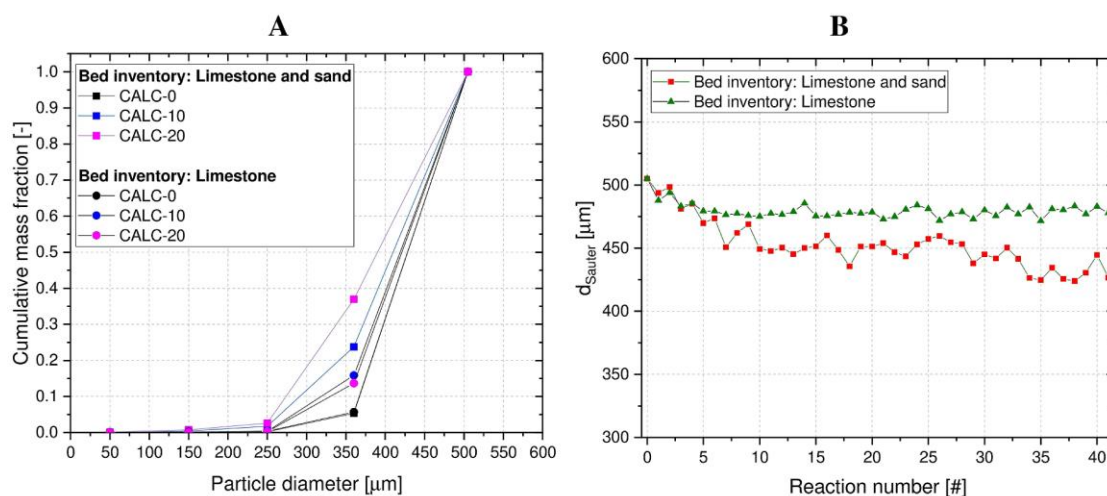
Fig. 7. A) Cumulative particle size distribution for selected calcination stages (CALC-0 refers to the samples after the initial calcination); B) Mean Sauter diameter of the bed inventory vs. reaction number (reaction number 0 refers to the starting limestone samples).

further confirmed by the trend of d_{Sauter} highlighted in Fig. 7–B. Starting from the 505 μm value of the limestone samples fed to the reactor, d_{Sauter} decreases to about 475 μm and 425 μm for the tests with a bed inventory of limestone only and limestone and sand, respectively. With regards to tests with limestone only, the value of 475 μm is approached already at the 10th reaction step (corresponding to the 5th carbonation). Differently, tests with a bed inventory of limestone and sand show a first stabilization of d_{Sauter} at about 450 μm from the 10th reaction step on, followed by a second decrease towards 425 μm from the 30th reaction step on, which suggests a further weakening/shrinkage of the material structure upon iterated reaction cycles. Fig. 7 also highlights that, in both tests, the fraction of material below 150 μm is mostly negligible, as it always accounts for less than 1%. It is reasonable that finer particles are also formed during the process, but are elutriated from the system. For this reason, the make-up stream of fresh limestone used in the process (see Fig. 1), should be intended to also compensate for this net mass loss [67].

4.4. Particle density

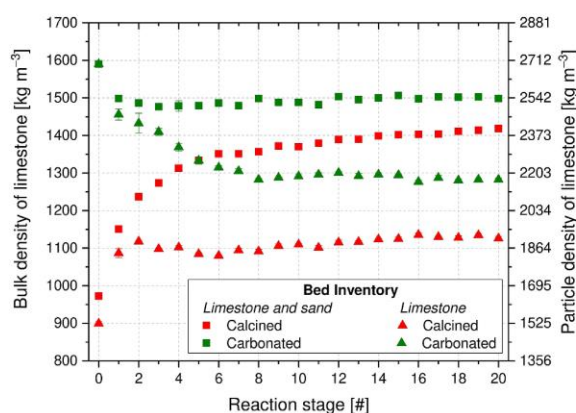Fig. 8 shows the bulk density of limestone particles after each

Fig. 8. Bulk and particle density of limestone particles for calcined and carbonated samples, in tests performed with a bed inventory of limestone and sand, and limestone only.

reaction step for the tests performed with the bed inventory of limestone and sand and limestone only. As expected, the density values of calcined particles are always lower than those of the corresponding carbonated ones. However, the trend of density with reaction stage quite differs for the two experimental tests. Indeed, in tests with sand, the density of the calcined particles increases along with reaction cycles, whereas that of the carbonated particles is mostly constant after a decrease during the very first cycles. Differently, in tests without sand, the density of the calcined particles is mostly constant after an increase during the first reaction cycles, whereas that of the carbonated particles decreases along with the reaction cycles, especially during the first 8 carbonation steps. Further, for both carbonated and calcined particles, the density values obtained in tests with sand are always higher than those obtained in tests without sand. Data obtained when working with the bed inventory of limestone only are probably the easiest to explain: the density of carbonated samples decreases with reaction cycles because of the lower carbonation degree as the number of cycles progresses, whereas the density of calcined samples is mostly constant after a first increase resulting upon loss of porosity. Differently, data obtained when working with sand show that the density of the calcined samples increases because of the interaction with sand, whereas that of the carbonated samples remains mostly constant because the decrease induced by the lower carbonation degree is offset by the increase induced by the interaction with sand. This explanation is further corroborated by the higher density values detected in tests with sand. Data were post-processed to evaluate the density increase that could have been induced from belite formation, quantitatively evaluated on the basis of the reduction of carbonation degree [75,76] with respect to the tests without sand. It was found that the formation of belite can only justify an increase of 5% of materials density. It is noteworthy that the sand may also physically act on the sorbent particles reducing their porosity and, in turn, increasing the particle density of both calcined and carbonated samples.

The bulk density of the calcined and carbonated samples upon iterated cycles has been further worked out to better correlate the physical properties of the granular solids along the course of the CaL process. In particular, the obtained data can be used to estimate the mean conversion degree during the carbonation step, and the particle density and porosity of the calcined and carbonated samples, upon calcination/carbonation iterated cycles.

The mean carbonation degree can be calculated exclusively by the bulk density of batches of calcined and carbonated particles once it is

assumed that the volume occupied by the granular solids does not significantly change during each single carbonation step. Equation (1) can then be rearranged as:

$$\overline{X}_{Ca}(N) = \left(\frac{\rho_N^{carb} V_N^{carb} - \rho_{N-1}^{calc} V_{N-1}^{calc}}{\rho_{N-1}^{calc} V_{N-1}^{calc}}\right) \frac{MW_{CaO}}{x_{CaO} MW_{CO_2}} \approx \left(\frac{\rho_N^{carb}}{\rho_{N-1}^{calc}} - 1\right) \frac{MW_{CaO}}{x_{CaO} MW_{CO_2}} \tag{3}$$

where ρ^{carb} and ρ^{calc} are the bulk density of the carbonated and calcined particles, respectively, and V^{carb} and V^{calc} represent the volume occupied by the bed of carbonated and calcined particles, respectively. The results obtained from Eq. (3) are reported in Fig. 4 and, thereby, compared with the conversion degree calculated by Eq. (1). The comparison highlights that the method based on the measurements of bulk densities accurately agrees with the data obtained from samples weight. This result can be used to set up alternative methods to estimate the conversion degree during the carbonation step in, even large-scale, CaL systems, simply sampling the granular solids both first and after each carbonation step.

The particle density of the calcined and carbonated materials at a generic N cycle, ρ_{pN}^{calc} and ρ_{pN}^{carb}, respectively, can be estimated from the corresponding bulk densities by the following equations:

$$\rho_{pN}^{calc} = \frac{\rho_N^{calc}}{1 - \varepsilon_{bedN}^{calc}}; \quad \rho_{pN}^{carb} = \frac{\rho_N^{carb}}{1 - \varepsilon_{bedN}^{carb}} \tag{4}$$

where $\varepsilon_{bedN}^{calc}$ and $\varepsilon_{bedN}^{carb}$ are the bed voidage during the bulk density measurement for the calcined and carbonated materials at a generic N cycle, respectively. Assuming a constant bed voidage equal to 0.41, a typical value for packed bed, the particle density can be easily evaluated, and the obtained data points can be read in Fig. 8 together with the bulk density values.

The particle porosity of the calcined and carbonated particles, in turn, can be calculated by the following equations, assuming as reference the density of pure CaO for the calcined particles, and a mean value (based on the carbonation degree) between the density of pure CaO and CaCO₃, for the carbonated particles:

$$\varepsilon_{pN}^{calc} = 1 - \frac{\rho_N^{calc}}{\rho_{CaO}};$$

$$\varepsilon_{pN}^{carb} = 1 - \frac{\rho_N^{carb}}{\dfrac{\overline{X}_{Ca}(N)MW_{CaCO_3} + (1 - \overline{X}_{Ca}(N))MW_{CaO}}{\dfrac{\overline{X}_{Ca}(N)MW_{CaCO_3}}{\rho_{CaCO_3}} + \dfrac{(1 - \overline{X}_{Ca}(N))MW_{CaO}}{\rho_{CaO}}}} \tag{5}$$

where ρ_{CaO} and ρ_{CaCO_3} are the density of pure CaO and CaCO₃, set equal to 3340 kg m⁻³ and 2710 kg m⁻³, respectively. It is worth to note that the contribution of solid compounds, formed by the chemical interaction between lime and silica sand, to the absolute particle density has been neglected.

Finally, it can be defined as "reactive" the porosity that vanishes during the carbonation step as:

$$\varepsilon_{pN}^{react} = \varepsilon_{pN-1}^{calc} - \varepsilon_{pN}^{carb} \tag{6}$$

The "reactive" porosity represents the internal porosity of the particles, which is occupied by the CO_2 molecules reacting with CaO to form CaCO₃ during the carbonation step. The particle porosity and the "reactive" porosity are shown as a function of the reaction stage in Fig. 9 for all the investigated conditions.

Data in Fig. 9-A counter-mirror those of Fig. 8. The analysis of the data of particle porosity for the samples obtained processing only limestone particles highlights, as also reported in literature [78], that the reduction of reactivity of limestone is due to the reduction of porosity of the calcined particles during the first cycles, and the concurrent sintering of the carbonated particles along the iterated cycles. The porosity of carbonated particles increases upon iterated cycles in agreement with a larger amount of porosity no more accessible by CO_2 molecules during carbonation. A different scenario appears when analyzing the experimental data of the tests carried out using limestone with silica sand particles. The interaction with silica sand particles strongly influences the phenomenology: the porosity of calcined particles steadily decreases along the iterated cycles, whereas the porosity of carbonated particles increases only during the first cycles. Moreover, in presence of sand, particle porosity values are remarkably lower than the corresponding ones in the case without sand. The "reactive" porosity trend along iterated cycles (Fig. 9-B) confirms what already observed, and highlights a difference in the "reactive" porosity of about 0.04 in favour of the only limestone case.
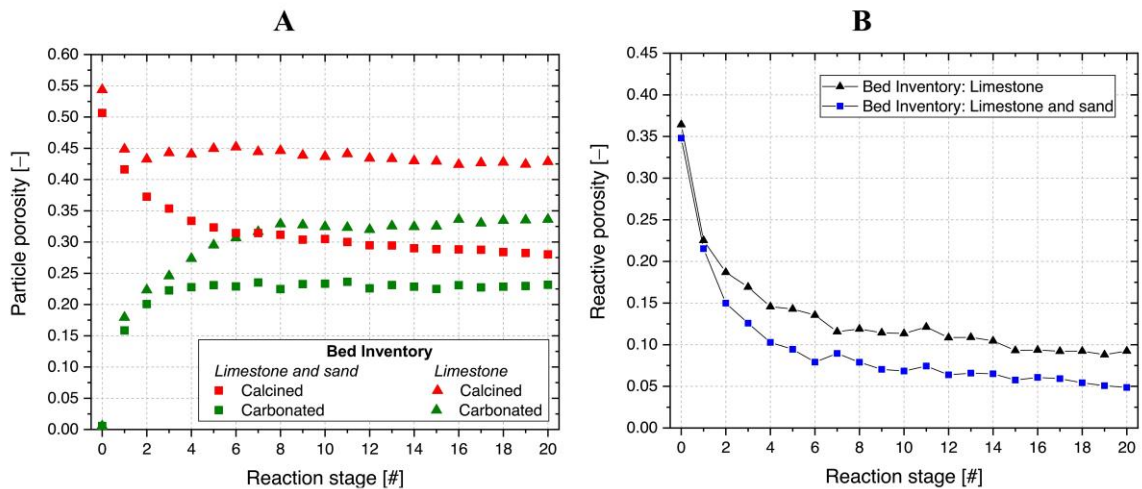

Fig. 9. Particle (A) and "reactive" (B) porosity of limestone particles for calcined and carbonated samples in tests performed with a bed inventory of limestone and sand, and limestone only.
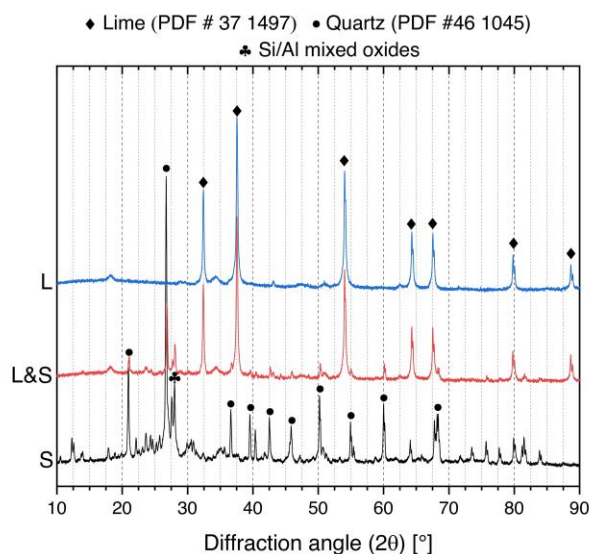
Fig. 10. XRD profiles of: lime samples retrieved after the last calcination step in the electrically heated FB, for tests performed with a bed inventory of limestone only (L) and limestone and sand (L&S); pure sand (S).

4.5. XRD and visual analyses

Fig. 10 shows the XRD profiles of the lime samples retrieved after the last calcination step for the tests performed in the electrically heated FB, together with that of pure sand. It is possible to observe that:

- the XRD spectrum of the sand exhibits several characteristics peaks of quartz (SiO_2), and a few minor peaks related to other compounds and impurities present in the sample;
- the XRD spectrum of the calcined sample retrieved from the tests performed with a bed inventory of limestone only exactly matches the crystalline signature of lime (CaO);
- the XRD spectrum of the calcined sample retrieved from the tests performed with a bed inventory of limestone and sand exhibits, apart from the peaks related to lime, several additional peaks that match either those of quartz, or those of the other compounds found in the sand.

XRD data seems to rule out a bulk chemical interaction between sand and lime since no peaks related to new crystalline phases were detected. It is likely that a potential chemical interaction takes place only at the particle surface, given the sizes of sorbent and sand particles used in this study. For the sake of completeness, it should be underlined that sand-derived peaks found in the calcined sample may arise, apart from very

fine sand particles trapped in the lime pores, also from sand particles that, upon iterated attrition/fragmentation, approached the size of lime ones and were thus not trapped by the sieves. A quantitative XRD analysis was also performed to assess the extent of sand contamination, and of belite formation. Belite formation was again not detected while the sand percentage turned out to be 5–6%. Such low values cannot justify the density differences observed in the two samples, and support the discussion on the reduction of particles porosity previously highlighted (see §4.4).

Fig. 11 shows a picture of these three samples. The comparison highlights that lime particles retrieved from the test performed with a bed inventory of sand and lime features a slightly darker colour, probably as a consequence of the physical and chemical interaction with the sand.

4.6. Porosimetric analyses

The results of the porosimetric analyses reveal that the specific surface is quite low in all the samples (1–2 m^2 g^{-1}) calcined at the 20th cycle, and similar to values reported in other studies under severe calcination conditions [41]. The cumulative pore volume distribution of the different samples is, instead, shown in Fig. 12. The lime sample processed in the electrically heated FB without sand, that is the best in terms of mean carbonation degree, is characterized by the highest value of total pore volume (0.165 cm^3 g^{-1}), mostly of which are mesopores (~88%). When lime is processed together with sand, the distribution is quite different depending on the reactor used. Lime processed in the electrically heated FB, that has intermediate performance in terms of mean carbonation degree, has the lowest value of total pore volume (0.047 cm^3 g^{-1}) but a significant share of both micropores and smaller mesopores (~80%), probably formed due to the sand/sorbent interaction. Differently, lime processed in the directly irradiated FB, that has the worst performance in terms of mean carbonation degree, has an intermediate value of total pore volume (0.106 cm^3 g^{-1}), but half of them are macropores and are thus less relevant for the reactivity of the material. The formation of larger pores may have been induced by the thermal sintering due the bed surface overheating produced by the simulated solar radiation. It seems that the sand/sorbent interaction might have played a less important role in these tests, probably due to the different hydrodynamics related to the larger scale of the used reactor.

4.7. Minimum fluidization velocity

Fig. 13 shows the minimum fluidization velocity of carbonated and calcined samples in tests performed using a bed inventory of limestone only (*EP #4*). It is recalled that data were acquired at the process temperature of the reaction step (i.e., 850 °C for carbonation, 950 °C for calcination), using CO_2 as fluidizing gas. The trend of the minimum fluidization velocity recalls that of the bulk density (see Fig. 8). For calcined samples, the minimum fluidization velocity slightly increases

Fig. 11. Picture of: lime samples retrieved after the last calcination step in the electrically heated FB, for tests performed with a bed inventory of limestone only (L) and limestone and sand (L&S); pure sand (S).
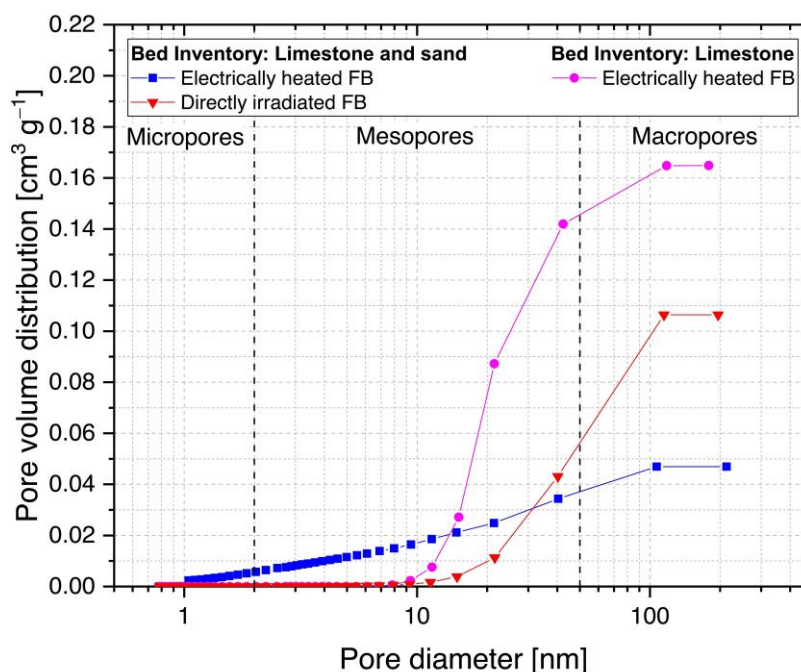
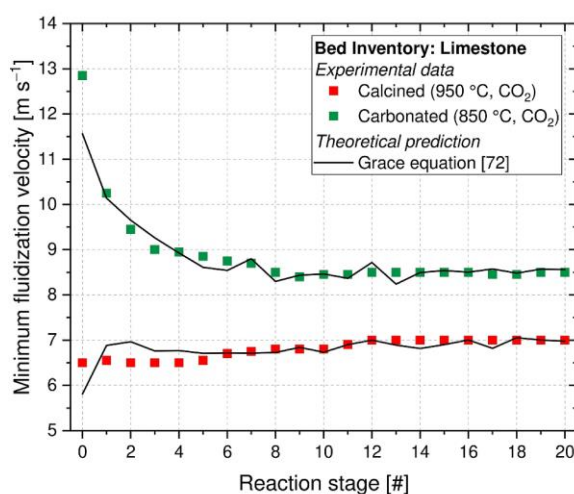**Fig. 12.** Cumulative pore volume distribution of the different samples, after the last calcination step.

Fig. 13. Minimum fluidization velocity for calcined and carbonated sorbent samples at the relevant process temperature, using CO_2 as fluidizing gas, obtained from experimental data and theoretical approach.

from an initial value of about 6.5 cm s^{-1} (initial calcination) to about 7 cm s^{-1} (20th reaction stage). Conversely, for carbonated samples, the minimum fluidization velocity decreases from about 10.2 cm s^{-1} (1st reaction stage) to about 8.5 cm s^{-1} (20th reaction stage). Overall, a difference between the minimum fluidization velocity of carbonated and calcined samples of about 3.7 cm s^{-1} can be inferred for more reactive particles, which decreases to about 1.5 cm s^{-1} for less reactive ones. The obtained experimental data were compared with those calculated by the semi-empirical correlation proposed by Grace (Eq. (7)) [72]:

$$\frac{d_p u_{mf} \rho}{\mu} = \left[27.2^2 + 0.0408 \frac{d_p^3 \rho (\rho_p - \rho) g}{\mu^2} \right]^{1/2} - 27.2 \qquad (7)$$

where d_p is the particle diameter, u_{mf} the minimum fluidization velocity, ρ and ρ_p the gas and particle density, respectively, μ the dynamic gas viscosity, and g the gravitational acceleration. Particle size and density data used in Eq. (7) are those reported in Fig. 7–B and 8, respectively. The comparison shows a very satisfactory agreement, confirming the approach proposed with Eq. (4). According to these data, it could be speculated that a solid–solid fluidized bed separation may be feasible at least to some extent, to separate the more reacted particles from the less reacted ones. The exploitation of a fluidized bed classifier, already proposed in literature [70], could be explored for an efficient separation of the investigated granular solids.

5. Discussion

On the whole, the analysis of the experimental results discussed in the present work returns two key findings.

Co-processing of limestone with silica sand reduces the lime reactivity, as inferred from the lower values of mean carbonation degree. Post-process of density data, together with N_2-intrusion porosimetric analysis, and quantitative and qualitative XRD analyses, suggests that this effect is mainly due to a lime/sand mechanical interaction that induces a strong reduction of the total and reactive sorbent porosity. A chemical interaction between CaO and silica sand constituents, not detected by XRD analyses, might only occur at particle surface and to a small extent, and could not justify alone the decay of reactivity observed when coprocessing lime with silica sand. The detrimental effect of this interaction on the CaL performance poses concerns to the use of additives to improve the fluidizability of small particles of limestone and/or to improve its optical performance in terms of absorption of concentrated solar energy. Under the tested conditions, the density of energy storage of limestone co-processed with silica sand becomes lower than that of the molten salts after 7 reaction cycles. However, the stored

energy can be released at higher temperatures, allowing for higher process efficiency in the thermodynamic cycle for energy generation, and is retained in a more stable form, suitable also for seasonal energy storage. Using a bed of only limestone may produce better results, as the density of energy storage is only slightly lower than that of molten salts after 20 cycles. However, this solution might require more efforts in the design of the receiver to reduce the share of reflected or unabsorbed solar energy, by considering for instance "creative" and non-conventional solar particle receivers [8,79,80]. According to these findings, it is advised to consider materials different from sand, if additives need to be used. A good inert material should perform a twofold task. On one side, it should increase the absorption of solar energy, as natural limestone particles have a poor solar optical absorption. On the other side, it should not chemically/physically interact with limestone particles, and possibly shield them from the high concentrated solar radiation. In this way, the performance of the process might reach the higher values obtained in this study with pure limestone and electrical heating. Alternatively, synthetic CaO-based sorbents should be considered. Thanks to the addition of inert stabilizers and/or promoters, these materials are characterized by a lower decay of reactivity over cycling and feature thus higher energy storage densities [27,42]. It is noteworthy that the doping of CaO-based sorbents has been recently targeted to also increase the absorption of solar energy [42,58,59], thus simultaneously counteracting two relevant drawbacks of the CaL cycle for TCES. Finally, it is also recalled that the average life of the sorbent particles in a continuous CaL process is controlled by the fraction of the purge and make-up streams (see Fig. 1). Typically, a purge fraction of 5–10% of the looping streams is considered in literature [67,68] and, in turn, the sorbent particles experience about 20–10 calcination/carbonation cycles, respectively, before they are purged. Thus, in any case, a sudden reactivity decay of sorbent can always be counterbalanced by a further increase of the make-up/purge fraction, which decreases the average life of the sorbent particles and thus increases their energy storage density [41,52]. It is noteworthy that the purge stream of spent sorbent particles does not represent a net energy loss for the process, as it can be reused as raw feedstock in the cement industry [41,73,81,82].

Carbonated and calcined particles are characterized by a different density and porosity, that results into a sufficient difference in their minimum fluidization velocity. This difference may be exploited for the design of a fluidized bed classifier that recycles unreacted or less reacted particles to the carbonator. In this way, it would be possible to maximize the efficiency of the process by ensuring the maximum carbonation degree of sorbent particles, and by avoiding the circulation of streams of unreacted particles through the plant. It is noteworthy that the effective advantage brought by the classifier is strictly related to the material reactivity and resistance to sintering over cycling. When the reactivity of the material abruptly decreases over cycling the efficacy of the classifier is probably lower, as the increase in conversion degree that could be obtained from the material recycling is smaller. However, synthetic sorbents feature a much stronger resistance to sintering, and are able to preserve better their initial reactivity over cycling. In this case, the contribution of the classifier to the overall process efficiency may be much higher.

Further tests will be performed in future works to fully demonstrate the feasibility and efficiency of the FB classifier, and to estimate its contribution to the overall efficiency of the process. Moreover, different inert materials will be tested in mixture with lime, and in different ratio, to scrutinize their potential advantages and drawbacks in the CaL process for TCES.

6. Conclusions

The calcium looping process integrated with TCES has been investigated focusing the attention on the closed loop CO_2 scheme with carbonation/calcination at 850/950 °C under pure CO_2. In particular, the conditions needed for the addition of a solid–solid separation unit

after the carbonator to separate converted and unconverted particles and, consequently, to increase the process efficiency, have been analyzed. The experimental tests, performed in the directly irradiated FB, show that the mean carbonation degree decreases from about 61% (1st cycle) to about 4% (20th cycle), with an average value of 14% over the whole 20 reaction cycles. Similar results are obtained in the electrically heated FB with a bed inventory of limestone and sand. Differently, the tests performed in the same reactor with a bed inventory of limestone show superior performance: the mean carbonation degree decreases indeed from about 62% (1st cycle) to about 14% (20th cycle), with an average value over the whole 20 cycles of about 25% (data were confirmed by evaluation of the deactivation constant, obtained by the application of an initial activity decay equation). It seems that the chemical interaction of CaO with the silica sand constituents at the process temperatures is not the main responsible for the loss of reactive CaO toward CO_2 uptake. Instead, post-process of particle density data, together with N_2-intrusion porosimetric analysis, and quantitative and qualitative XRD analyses, suggests that the sand/lime mechanical interaction induces a strong reduction of the total and reactive sorbent porosity that is the main responsible for the strong decay of reactivity. The detrimental effect of this interaction on the calcium looping performance poses concerns to the use of additives to improve the fluidizability of small particles of limestone and/or to improve its optical performance in terms of absorption of concentrated solar energy. For the tests with a bed inventory of limestone and sand, the average values of energy storage density are quite similar for the two experimental rigs and decrease from about 1550 MJ m^{-3} (1 looping cycle) to 485 MJ m^{-3} (20 looping cycles). Instead, with a bed inventory of limestone, the values decrease from about 1575 MJ m^{-3} (1 looping cycle) to 710 MJ m^{-3} (20 looping cycles). The performance in terms of energy storage density is comparable to that of molten salts when an average sorbent life of 10–20 cycles is considered. However, it should be recalled that, in this CaL process, thermal energy at the carbonator is released at a much higher temperature (i.e., 850 °C), with a consequent higher overall efficiency in the subsequent thermodynamic cycle for energy production. The main properties of calcined and carbonated particles significantly change in terms of particle density, size and porosity, if the limestone is processed with silica sand fluidized particles. Finally, the measurements of minimum fluidization velocity of calcined and carbonated particles upon iterated cycles of calcination and carbonation show that a solid–solid separation based on particle density difference may be conceived by a fluidized bed classifier already proposed in literature [70].

Declaration of Competing Interest

The authors declare that they have no known competing financial interests or personal relationships that could have appeared to influence the work reported in this paper.

Data availability

Data will be made available on request.

References

[1] H. Zhang, H. Benoit, I. Perez-Lopèz, G. Flamant, T. Tan, J. Baeyens, High-efficiency solar power towers using particle suspensions as heat carrier in the receiver and in the thermal energy storage, Renew. Energy. 111 (2017) 438–446, https://doi.org/10.1016/j.renene.2017.03.101.

[2] C. Tregambi, S. Padula, M. Galbusieri, G. Coppola, F. Montagnaro, P. Salatino, M. Troiano, R. Solimene, Directly irradiated fluidized bed reactor for thermochemical energy storage and solar fuels production, Powder Technol. 366 (2020) 460–469, https://doi.org/10.1016/j.powtec.2020.02.045.

[3] C.K. Ho, Advances in central receivers for concentrating solar applications, Sol. Energy. 152 (2017) 38–56, https://doi.org/10.1016/j.solener.2017.03.048.

[4] A. Bayon, A.J. Carrillo, E. Mastronardo, J.M. Coronado, Chapter Six - Thermochemical heat storage at high temperature, in: W. Lipiński (Ed.), Sol. Thermochem., Academic Press, 2021: pp. 247–295. https://doi.org/10.1016/bs.ache.2021.10.004.

[5] A.J. Carrillo, J. González-Aguilar, M. Romero, J.M. Coronado, Solar Energy on Demand: A Review on High Temperature Thermochemical Heat Storage Systems and Materials, Chem. Rev. 119 (2019) 4777–4816, https://doi.org/10.1021/acs.chemrev.8b00315.

[6] W. Lipiński, E. Abbasi-Shavazi, J. Chen, J. Coventry, M. Hangi, S. Iyer, A. Kumar, L. Li, S. Li, J. Pye, J.F. Torres, B. Wang, Y. Wang, V.M. Wheeler, Progress in heat transfer research for high-temperature solar thermal applications, Appl. Therm. Eng. 184 (2021), 116137, https://doi.org/10.1016/j.applthermaleng.2020.116137.

[7] F. Desai, J. Sunku Prasad, P. Muthukumar, M.M. Rahman, Thermochemical energy storage system for cooling and process heating applications: A review, Energy Convers, Manag. 229 (2021) 113617, https://doi.org/10.1016/j.enconman.2020.113617.

[8] C. Tregambi, M. Troiano, F. Montagnaro, R. Solimene, P. Salatino, Fluidized Beds for Concentrated Solar Thermal Technologies – A Review, Front. Energy Res. 9 (2021), 618421, https://doi.org/10.3389/fenrg.2021.618421.

[9] J.A. Almendros-Ibáñez, M. Fernández-Torrijos, M. Díaz-Heras, J.F. Belmonte, C. Sobrino, A review of solar thermal energy storage in beds of particles: Packed and fluidized beds, Sol. Energy. 192 (2019) 193–237, https://doi.org/10.1016/j.solener.2018.05.047.

[10] M.A. Rivero, D. Rodrigues, C.I.C. Pinheiro, J.P. Cardoso, L.F. Mendes, Solid – gas reactors driven by concentrated solar energy with potential application to calcium looping : A comparative review, Renew. Sustain. Energy Rev. 158 (2022), 112048, https://doi.org/10.1016/j.rser.2021.112048.

[11] C. Tregambi, P. Salatino, R. Solimene, F. Montagnaro, An experimental characterization of Calcium Looping integrated with concentrated solar power, Chem. Eng. J. 331 (2018) 794–802, https://doi.org/10.1016/j.cej.2017.08.068.

[12] R. Chirone, P. Salatino, P. Ammendola, R. Solimene, M. Magaldi, R. Sorrenti, G. De Michele, F. Donatini, Development of a Novel Concept of Solar Receiver/Thermal Energy Storage System Based on Compartmented Dense Gas Fluidized Beds, 14th Int, Conf, Fluid, 2013.

[13] G. Flamant, G. Olalde, High temperature solar gas heating comparison between packed and fluidized bed receivers-I, Sol. Energy. 31 (1983) 463–471, https://doi.org/10.1016/0038-092X(83)90050-6.

[14] N. Gokon, T. Izawa, T. Kodama, Steam gasification of coal cokes by internally circulating fluidized-bed reactor by concentrated Xe-light radiation for solar syngas production, Energy. 79 (2015) 264–272, https://doi.org/10.1016/j.energy.2014.11.012.

[15] X. Li, L. Wei, C.W. Lim, J. Chen, P. Chu, W. Lipiński, N. Yan, Y. Dai, C.-H. Wang, Experimental and numerical study on thermal performance of an indirectly irradiated solar reactor with a clapboard-type internally circulating fluidized bed, Appl. Energy. 305 (2022) 117976, https://doi.org/10.1016/j.apenergy.2021.117976.

[16] X. Li, J. Chen, Q. Hu, P. Chu, Y. Dai, C.H. Wang, Solar-driven gasification in an indirectly-irradiated thermochemical reactor with a clapboard-type internally-circulating fluidized bed, Energy Convers. Manag. 248 (2021) 114795, https://doi.org/10.1016/j.enconman.2021.114795.

[17] M. Díaz-Heras, J.F. Belmonte, J.A. Almendros-Ibáñez, Experimental observations on directly irradiated conical spouted and spout-fluid beds, Exp. Therm. Fluid Sci. 130 (2022), 110488, https://doi.org/10.1016/j.expthermflusci.2021.110488.

[18] M. Díaz-Heras, J.F. Belmonte, J.A. Almendros-Ibáñez, Experimental observations on directly irradiated fluidized beds: Even and uneven fluidization, Exp. Therm. Fluid Sci. 120 (2021), 110242, https://doi.org/10.1016/j.expthermflusci.2020.110242.

[19] C. Tregambi, R. Chirone, F. Montagnaro, P. Salatino, R. Solimene, Heat transfer in directly irradiated fluidized beds, Sol. Energy. 129 (2016) 85–100, https://doi.org/10.1016/j.solener.2016.01.057.

[20] S. Migliozzi, A. Paulillo, R. Chirone, P. Salatino, R. Solimene, Hydrodynamics of compartmented fluidized bed for concentrated solar power and thermal energy storage applications, Fluid. XV. (2016), https://doi.org/10.1016/j.powtec.2016.12.052.

[21] T. Esence, E. Guillot, M. Tessonneaud, J.L. Sans, G. Flamant, Solar calcination at pilot scale in a continuous flow multistage horizontal fluidized bed, Sol. Energy. 207 (2020) 367–378, https://doi.org/10.1016/j.solener.2020.06.098.

[22] T. Esence, H. Benoit, D. Poncin, M. Tessonneaud, G. Flamant, A shallow cross-flow fluidized-bed solar reactor for continuous calcination processes, Sol. Energy. 196 (2020) 389–398, https://doi.org/10.1016/j.solener.2019.12.029.

[23] J. Gómez-Hernández, P.A. González-Gómez, J.V. Briongos, D. Santana, Technical feasibility analysis of a linear particle solar receiver, Sol. Energy. 195 (2020) 102–113, https://doi.org/10.1016/j.solener.2019.11.052.

[24] C. Tregambi, C. Bevilacqua, M. Troiano, R. Solimene, P. Salatino, A novel autothermal fluidized bed reactor for concentrated solar thermal applications, Chem. Eng. J. 398 (2020), 125702, https://doi.org/10.1016/j.cej.2020.125702.

[25] S. Padula, C. Tregambi, R. Solimene, R. Chirone, M. Troiano, P. Salatino, A novel fluidized bed "thermochemical battery" for energy storage in concentrated solar thermal technologies, Energy Convers. Manag. 236 (2021), 113994, https://doi.org/10.1016/j.enconman.2021.113994.

[26] T. Uchino, C. Fushimi, Fluidized bed reactor for thermochemical heat storage using Ca(OH)2/CaO to absorb the fluctuations of electric power supplied by variable renewable energy sources: A dynamic model, Chem. Eng. J. 419 (2021), 129571, https://doi.org/10.1016/j.cej.2021.129571.

[27] C. Ortiz, J.M. Valverde, R. Chacartegui, L.A. Perez-Maqueda, P. Giménez, The Calcium-Looping (CaCO3/CaO) process for thermochemical energy storage in Concentrating Solar Power plants, Renew. Sustain. Energy Rev. 113 (2019), 109252, https://doi.org/10.1016/j.rser.2019.109252.

[28] E. Darwish, M. Mansouri, D. Yilmaz, H. Leion, Effect of Mn and Cu substitution on the SrFeO3 perovskite for potential thermochemical energy storage applications, Processes. 9 (10) (2021) 1817, https://doi.org/10.3390/pr9101817.

[29] L. André, S. Abanades, Recent Advances in Thermochemical Energy Storage via Solid – Gas Reversible Reactions at High Temperature, Energies 13 (2020) 5859, https://doi.org/10.3390/en13225859.

[30] SOCRATCES (SOlar Calcium-looping integRAtion for ThermoChemical Energy Storage), https://socratces.eu/. Last accessed: February 2022.

[31] CALyPSOL (CALcium oxide LooPing through SOLar energy), https://www.dlr.de/ff/en/desktopdefault.aspx/tabid-18130/28811_read-71705/. Last accessed: May 2022.

[32] M.T. Dunstan, F. Donat, A.H. Bork, C.P. Grey, C.R. Müller, CO2 Capture at Medium to High Temperature Using Solid Oxide-Based Sorbents: Fundamental Aspects, Mechanistic Insights, and Recent Advances, Chem. Rev. 121 (2021) 12681–12745, https://doi.org/10.1021/acs.chemrev.1c00100.

[33] A. Coppola, O. Senneca, F. Scala, F. Montagnaro, P. Salatino, Looping cycles for low carbon technologies: A survey of recent research activities in Naples, Fuel. 268 (2020), 117371, https://doi.org/10.1016/j.fuel.2020.117371.

[34] C. Tregambi, P. Bareschino, D. Hanak, F. Montagnaro, F. Pepe, E. Mancusi, Modelling of an integrated process for atmospheric carbon dioxide capture and methanation, J. Clean. Prod. 356 (2022), 131827, https://doi.org/10.1016/j.jclepro.2022.131827.

[35] T. Shimizu, T. Hirama, H. Hosoda, K. Kitano, M. Inagaki, K. Tejima, A twin fluid-bed reactor for removal of CO2 from combustion processes, Chem. Eng. Res. Des. 77 (1999) 62–68, https://doi.org/10.1205/026387699525882.

[36] S. Khosravi, S. Hossainpour, H. Farajollahi, N. Abolzadeh, Integration of a coal fired power plant with calcium looping CO2 capture and concentrated solar power generation: Energy, exergy and economic analysis, Energy. 240 (2022), 122466, https://doi.org/10.1016/j.energy.2021.122466.

[37] J.P. Rincon Duarte, D. Kriechbaumer, B. Lachmann, S. Tescari, T. Fend, M. Roeb, C. Sattler, Solar calcium looping cycle for CO2 capturing in a cement plant. Definition of process parameters and reactors selection, Sol. Energy. 238 (2022) 189–202, https://doi.org/10.1016/j.solener.2022.04.031.

[38] U. Tesio, E. Guelpa, V. Verda, Comparison of sCO2 and He Brayton cycles integration in a Calcium-Looping for Concentrated Solar Power, Energy. 247 (2022), 123467, https://doi.org/10.1016/j.energy.2022.123467.

[39] M. Benitez-Guerrero, B. Sarrion, A. Perejon, P.E. Sanchez-Jimenez, L.A. Perez-Maqueda, Manuel Valverde, Large-scale high-temperature solar energy storage using natural minerals, Sol. Energy Mater. Sol. Cells. 168 (2017) 14–21, https://doi.org/10.1016/j.solmat.2017.04.013.

[40] M. Benitez-Guerrero, J.M. Valverde, P.E. Sanchez-Jimenez, A. Perejon, L.A. Perez-Maqueda, Multicycle activity of natural CaCO3 minerals for thermochemical energy storage in Concentrated Solar Power plants, Sol. Energy. 153 (2017) 188–199, https://doi.org/10.1016/j.solener.2017.05.068.

[41] C. Tregambi, F. Di Lauro, F. Montagnaro, P. Salatino, R. Solimene, 110th Anniversary: Calcium Looping Coupled with Concentrated Solar Power for Carbon Capture and Thermochemical Energy Storage, Ind. Eng. Chem. Res. 58 (2019) 21262–21272, https://doi.org/10.1021/acs.iecr.9b03083.

[42] Y. Yang, Y. Li, X. Yan, J. Zhao, C. Zhang, Development of thermochemical heat storage based on CaO/CaCO3 cycles: A review, Energies. 14 (2021) 6847, https://doi.org/10.3390/en14206847.

[43] H. Guo, S. Wang, C. Li, Y. Zhao, Q. Sun, X. Ma, Incorporation of Zr into Calcium Oxide for CO2 Capture by a Simple and Facile Sol-Gel Method, Ind. Eng. Chem. Res. 55 (2016) 7873–7879, https://doi.org/10.1021/acs.iecr.5b04112.

[44] K.T. Møller, T.D. Humphries, A. Berger, M. Paskevicius, C.E. Buckley, Thermochemical energy storage system development utilising limestone, Chem. Eng. J. Adv. 8 (2021), 100168, https://doi.org/10.1016/j.ceja.2021.100168.

[45] A.N. Antzara, A. Arregi, E. Heracleous, A.A. Lemonidou, In-depth evaluation of a ZrO2 promoted CaO-based CO2 sorbent in fluidized bed reactor tests, Chem. Eng. J. 333 (2018) 697–711, https://doi.org/10.1016/j.cej.2017.09.192.

[46] M. Benitez-Guerrero, J.M. Valverde, P.E. Sanchez-Jimenez, A. Perejon, L.A. Perez-Maqueda, Calcium-Looping performance of mechanically modified Al2O3-CaO composites for energy storage and CO2 capture, Chem. Eng. J. 334 (2018) 2343–2355, https://doi.org/10.1016/j.cej.2017.11.183.

[47] A. Antzara, E. Heracleous, A.A. Lemonidou, Improving the stability of synthetic CaO-based CO2 sorbents by structural promoters, Appl. Energy. 156 (2015) 331–343, https://doi.org/10.1016/j.apenergy.2015.07.026.

[48] M. Heidari, M. Tahmasebpoor, A. Antzaras, A.A. Lemonidou, CO2 capture and fluidity performance of CaO-based sorbents: Effect of Zr, Al and Ce additives in tri-, bi- and mono-metallic configurations, Process Saf. Environ. Prot. 144 (2020) 349–365, https://doi.org/10.1016/j.psep.2020.07.041.

[49] D. Choi, A.-H. Alissa Park, Y. Park, Effects of eutectic alkali chloride salts on the carbonation reaction of CaO-based composites for potential application to a thermochemical energy storage system, Chem. Eng. J. 437 (2022), 135481, https://doi.org/10.1016/j.cej.2022.135481.

[50] M. Sayyah, Y. Lu, R.I. Masel, K.S. Suslick, Mechanical Activation of CaO-Based Adsorbents for CO₂ Capture, ChemSusChem. 6 (2013) 193–198, https://doi.org/10.1002/cssc.201200454.

[51] M. Benitez-Guerrero, J.M. Valverde, A. Perejon, P.E. Sanchez-Jimenez, L.A. Perez-Maqueda, Effect of milling mechanism on the CO₂ capture performance of limestone in the Calcium Looping process, Chem. Eng. J. 346 (2018) 549–556, https://doi.org/10.1016/j.cej.2018.03.146.

[52] F. Di Lauro, C. Tregambi, F. Montagnaro, P. Salatino, R. Chirone, R. Solimene, Improving the performance of calcium looping for solar thermochemical energy storage and CO₂ capture, Fuel. 298 (2021) 120791, https://doi.org/10.1016/j.fuel.2021.120791.

[53] J.M. Valverde, M. Barea-López, A. Perejón, P.E. Sánchez-Jiménez, L.A. Pérez-Maqueda, Effect of Thermal Pretreatment and Nanosilica Addition on Limestone Performance at Calcium-Looping Conditions for Thermochemical Energy Storage of Concentrated Solar Power, Energy and Fuels. 31 (2017) 4226–4236, https://doi.org/10.1021/acs.energyfuels.6b03364.

[54] J. Arcenegui-Troya, P.E. Sánchez-Jiménez, A. Perejón, V. Moreno, J.M. Valverde, L.A. Pérez-Maqueda, Kinetics and cyclability of limestone (CaCO₃) in presence of steam during calcination in the CaL scheme for thermochemical energy storage, Chem. Eng. J. 417 (2021) 129194, https://doi.org/10.1016/j.cej.2021.129194.

[55] J. Arcenegui-Troya, P.E. Sánchez-Jiménez, A. Perejón, J.M. Valverde, L.A. Pérez-Maqueda, Steam-enhanced calcium-looping performance of limestone for thermochemical energy storage: The role of particle size, J. Energy Storage. 51 (2022) 104305, https://doi.org/10.1016/j.est.2022.104305.

[56] A. Coppola, A. Esposito, F. Montagnaro, G. De Tommaso, F. Scala, P. Salatino, Effect of exposure to SO₂ and H₂O during the carbonation stage of fluidised bed calcium looping on the performance of sorbents of different nature, Chem. Eng. J. 377 (2019), 120626, https://doi.org/10.1016/j.cej.2018.12.086.

[57] L. Yang, G. Huang, Z. Huang, Optimized design of Ca-based thermochemical heat storage materials for concentrated solar power, J. Energy Storage. 43 (2021), 103236, https://doi.org/10.1016/j.est.2021.103236.

[58] H. Zheng, X. Liu, Y. Xuan, C. Song, D. Liu, Q. Zhu, Z. Zhu, K. Gao, Y. Li, Y. Ding, Thermochemical heat storage performances of fluidized black CaCO₃ pellets under direct concentrated solar irradiation, Renew. Energy. 178 (2021) 1353–1369, https://doi.org/10.1016/j.renene.2021.07.026.

[59] Y. Da, Y. Xuan, L. Teng, K. Zhang, X. Liu, Y. Ding, Calcium-based composites for direct solar-thermal conversion and thermochemical energy storage, Chem. Eng. J. 382 (2020), 122815, https://doi.org/10.1016/j.cej.2019.122815.

[60] V. Moreno, J. Arcenegui-Troya, P. Enrique Sánchez-Jiménez, A. Perejón, R. Chacartegui, J. Manuel Valverde, L. Allan Pérez-Maqueda, Albero: An alternative natural material for solar energy storage by the calcium-looping process, Chem. Eng. J. 440 (2022), 135707, https://doi.org/10.1016/j.cej.2022.135707.

[61] A. Scaltsoyiannes, A. Antzaras, G. Koilaridis, A. Lemonidou, Towards a generalized carbonation kinetic model for CaO-based materials using a modified random pore model, Chem. Eng. J. 407 (2021), 127207, https://doi.org/10.1016/j.cej.2020.127207.

[62] G.M. Castilla, D.C. Guío-Pérez, S. Papadokonstantakis, F. Johnsson, D. Pallarès, Techno-economic assessment of calcium looping for thermochemical energy storage with CO₂ capture, Energies. 14 (2021) 1–17, https://doi.org/10.3390/en14113211.

[63] B. Sarrion, J.M. Valverde, A. Perejon, L. Perez-Maqueda, P.E. Sanchez-Jimenez, On the Multicycle Activity of Natural Limestone/Dolomite for Thermochemical Energy Storage of Concentrated Solar Power, Energy Technol. 4 (2016) 1013–1019, https://doi.org/10.1002/ente.201600068.

[64] B. Sarrión, A. Perejón, P.E. Sánchez-Jiménez, L.A. Pérez-Maqueda, J.M. Valverde, Role of calcium looping conditions on the performance of natural and synthetic Ca-based materials for energy storage, J. CO2 Util. 28 (2018) 374–384, https://doi.org/10.1016/j.jcou.2018.10.018.

[65] S. Pascual, P. Lisbona, M. Bailera, L.M. Romeo, Design and operational performance maps of calcium looping thermochemical energy storage for concentrating solar power plants, Energy. 220 (2021), 119715, https://doi.org/10.1016/j.energy.2020.119715.

[66] S. Pascual, P. Lisbona, L.M. Romeo, Operation maps in calcium looping thermochemical energy storage for concentrating solar power plants, J. Energy Storage. 55 (2022), 105771, https://doi.org/10.1016/j.est.2022.105771.

[67] C. Tregambi, P. Bareschino, E. Mancusi, F. Pepe, F. Montagnaro, R. Solimene, P. Salatino, Modelling of a concentrated solar power – photovoltaics hybrid plant for carbon dioxide capture and utilization via calcium looping and methanation, Energy Convers. Manag. 230 (2021) 113792, https://doi.org/10.1016/j.enconman.2020.113792.

[68] L.M. Romeo, Y. Lara, P. Lisbona, J.M. Escosa, Optimizing make-up flow in a CO₂ capture system using CaO, Chem. Eng. J. 147 (2009) 252–258, https://doi.org/10.1016/j.cej.2008.07.010.

[69] G.S. Grasa, J.C. Abanades, CO₂ Capture Capacity of CaO in Long Series of Carbonation/Calcination Cycles, Ind. Eng. Chem. Res. 45 (2006) 8846–8851, https://doi.org/10.1021/ie0606946.

[70] G. Olivieri, A. Marzocchella, P. Salatino, A fluid-bed continuous classifier of polydisperse granular solids, J. Taiwan Inst. Chem. 40 (2009) 638–644, https://doi.org/10.1016/j.jtice.2009.05.011.

[71] G. Olivieri, A. Marzocchella, P. Salatino, Segregation of fluidized binary mixtures of granular solids, AIChE J. 50 (2004) 3095–3106, https://doi.org/10.1002/aic.10340.

[72] J.R. Grace, Fluidized-bed hydrodynamics, in: G. Hetsroni (Ed.), Handb. Multiph. Syst., Washington: Hemisphere, 1982: pp. 8–1-8–64.

[73] C. Tregambi, R. Solimene, F. Montagnaro, P. Salatino, M. Marroccoli, N. Ibris, A. Telesca, Solar-driven production of lime for ordinary Portland cement formulation, Sol. Energy. 173 (2018) 759–768, https://doi.org/10.1016/j.solener.2018.08.018.

[74] S. Telschow, F. Frandsen, K. Theisen, K. Dam-Johansen, Cement formation-A success story in a black box: High temperature phase formation of portland cement clinker, Ind. Eng. Chem. Res. 51 (2012) 10983–11004, https://doi.org/10.1021/ie300674j.

[75] M. Alonso, Y. Álvarez Criado, J.R. Fernández, C. Abanades, CO₂ Carrying Capacities of Cement Raw Meals in Calcium Looping Systems, Energy and Fuels. 31 (2017) 13955–13962, https://doi.org/10.1021/acs.energyfuels.7b02586.

[76] M. Alonso, J.R. Fernández, J.C. Abanades, Kinetic Study of Belite Formation in Cement Raw Meals Used in the Calcium Looping CO₂ Capture Process, Ind. Eng. Chem. Res. 58 (2019) 5445–5454, https://doi.org/10.1021/acs.iecr.9b00813.

[77] J.M. Valverde, A. Perejon, L.A. Perez-Maqueda, Enhancement of fast CO₂ capture by a nano-SiO₂/CaO composite at Ca-looping conditions, Environ. Sci. Technol. 46 (2012) 6401–6408, https://doi.org/10.1021/es3002426.

[78] R. Barker, The reversibility of the reaction CaCO₃ ⇄ CaO+CO₂, J. Appl. Chem. Biotechnol. 23 (1973) 733–742, https://doi.org/10.1002/jctb.5020231005.

[79] M. Tawfik, A review of directly irradiated solid particle receivers: Technologies and influencing parameters, Renew. Sustain. Energy Rev. 167 (2022), 112682, https://doi.org/10.1016/j.rser.2022.112682.

[80] C.K. Ho, A review of high-temperature particle receivers for concentrating solar power, Appl. Therm. Eng. 109 (2016) 958–969, https://doi.org/10.1016/j.applthermaleng.2016.04.103.

[81] A. Telesca, M. Marroccoli, M. Tomasulo, G.L. Valenti, H. Dieter, F. Montagnaro, Calcium looping spent sorbent as a limestone replacement in the manufacture of portland and calcium sulfoaluminate cements, Environ. Sci. Technol. 49 (2015) 6865–6871, https://doi.org/10.1021/acs.est.5b00394.

[82] A. Telesca, D. Calabrese, M. Marroccoli, M. Tomasulo, G.L. Valenti, G. Duelli (Varela), F. Montagnaro, Spent limestone sorbent from calcium looping cycle as a raw material for the cement industry, Fuel. 118 (2014) 202–205, https://doi.org/10.1016/j.fuel.2013.10.060.

104

Review

Thermal Energy Storage in Concentrating Solar Power Plants: A Review of European and North American R&D Projects

Sara Pascual * [iD], **Pilar Lisbona** [iD] and **Luis M. Romeo** [iD]

Departamento de Ingeniería Mecánica, Escuela de Ingeniería y Arquitectura (EINA), Universidad de Zaragoza, C/María de Luna s/n, 50018 Zaragoza, Spain
* Correspondence: saraps@unizar.es

Abstract: Thermal energy storage (TES) is the most suitable solution found to improve the concentrating solar power (CSP) plant's dispatchability. Molten salts used as sensible heat storage (SHS) are the most widespread TES medium. However, novel and promising TES materials can be implemented into CSP plants within different configurations, minimizing the TES costs and increasing the working temperature to improve the thermal performance of the associated power block. The first objective of this review is to provide an overview of the most widespread CSP technologies, TES technologies and TES-CSP configurations within the currently operational facilities. Once this information has been compiled, the second aim is to collect and present the existing European and North American TES-CSP Research and Development (R&D) projects within the last decade (2011–2021). Data related to these projects such as TES-CSP configuration path, TES and CSP technologies applied, storage capacity, power block associated and the levelized cost of electricity (LCOE) of the commercial up-scaling project are presented. In addition, project information such as location, research period, project leader and budget granted are also extracted. A timeline of the R&D projects launched from 2011 is built, showing the technology readiness level (TRL) achieved by the end of the project.

Keywords: concentrating solar power; thermal energy storage; TES CSP integration paths; TES CSP R&D projects

1. Introduction

One of the most important measures to mitigate greenhouse gases (GHG) emissions is to increase the share of renewable energy sources (RES) in the energy mix, according to the Intergovernmental Panel on Climate Change (IPCC) [1]. At the end of 2021, the renewable energy share in global electricity production was 28.3% with a renewable power capacity exceeding 3000 GW, including hydroelectric power. The annual contribution to renewable power capacity must be multiplied by three to achieve the scenarios of net zero emissions by 2030 and 2050 [2]. Higher daily production of RES could be achieved if those issues related to the variability of electricity production were solved through the storage of energy surplus.

RES which directly supplies electricity to the grid, such as photovoltaic solar power or wind power, may be combined with electromechanical or electrochemical storage systems leading to efficiencies of the load/discharge cycle up to 90% [3]. In contrast, concentrating solar power (CSP) plants which supplies thermal energy to the power cycle, obtain yields close to 100% through their combination with thermal energy storage (TES) systems [3,4]. Furthermore, the capital cost of TES is lower than mechanical or chemical storage systems [5]. The most widespread storage materials used in TES systems are the molten salts which allow for the extension of the operating hours of CSP plants by storing energy as sensible heat during daylight hours. However, thermochemical energy storage (TCES) systems could enable higher conversion efficiencies in CSP plants in the medium–long term [6]. Although the CSP installed capacity in 2021 (6 GW) was significantly lower

than the installed capacity of other RES, the average CSP costs in plants with integrated TES have dropped by 70% in the last decade [2]. The construction of CSP plants in the last decade has grown exponentially throughout the world, indicating an optimistic future for the solar-based RES [7]. Therefore, CSP with TES is emerging as a potential competitor of conventional base load plants, such as fossil fuel power plants [8]. The latest research highlights the importance of techno–economic studies to promote the implementation of TES in CSP. However, the environmental aspect scarcely appears in the literature, even less complete life cycle assessments [9]. Thus, the first objective of this review is to describe the most advantageous integration pathways of TES into CSP plants.

A thorough bibliographic search points out that recent reviews dealing with energy storage technologies coupled with CSP plants may be divided into two categories: (i) latest advances in CSP and TES technologies and (ii) integration concepts. Several studies focus on the most widespread CSP technologies and the future trends in research development [10–13], including an overview of the distribution of CSP facilities by regions [7]. Regarding TES technologies, the reviews were focused on sensible, latent and thermochemical energy storage materials developed since 2000 [14] and the future challenges to be integrated into CSP [15]. The latest research on sensible heat storage was related to (i) the discussion of the best integration of molten salts medium [5], (ii) the potential of solid particles as a heat transfer medium and TES [16] and (iii) the proper future use of cheaper materials such as rocks [17]. The latent heat storage for high temperature operation was investigated to, firstly, overcome challenges of coupling to CSP [18] and to define the phase change materials capable to be used in CSP application [19]. The recent advances on thermochemical reactions as TES for CSP are the most investigated in the last 5 years, given the high operating temperature and long-term durability of solid–gas reversible reactions [20]. Most recent reviews were focused on the most suitable reactors for enhancing heat transfer [21] and chemical reactions efficiency [22]. Secondly, the integration between TES and CSP was defined according to the conventional configurations of first and second generation CSP plants [11,23], requiring new integration concepts for the next generation of CSP plants [24]. In summary, previous reviews focused on TES CSP configurations of currently operational facilities from prototype to commercial scale (first and second generation) and novel trends for TES integration in the next CSP generation. The main gap found among these reviews is the existence of a thorough summary of completed and ongoing research and development (R&D) projects of TES integrated in CSP plants. Thus, the second objective and the main novelty of this revision manuscript is to present a complete international picture of the TES CSP R&D projects from Europe and North America within any technology readiness level (TRL), from lab/pilot to almost commercial scale. Both regions concentrate 65% of the installed capacity of CSP plants currently in operation [25]. Thus, Europe and North America have been the world regions chosen for the review of R&D projects for being at the forefront in the development of CSP technology.

A bibliometric study was performed to search the references for the following sections in the present manuscript (Sections 2 and 3). The Web of Science database was selected for citations belonging to Section 2, focused on CSP and TES technologies, as well as the most spread integrations of TES into CSP plants. In addition, the SolarPACES tool [25] was required to obtain the project profiles of operational CSP facilities around the world. The information about R&D projects in Section 3 was extracted from other databases, such as the Community Research and Development Information Service (CORDIS) [26] and Solar Energy Research Database from the Solar Energy Technologies Office (SETO) [27]. CORDIS provides results from R&D projects funded by the EU's framework programmes, while SETO collects all the active and inactive R&D projects awarded by the U.S. Department of Energy. Table 1 shows the different keyword combinations used to select the scientific references appearing in the present review.

Table 1. Search map to extract information on CSP and TES technologies.

Excluded Phrase	Main Search Phrase	Complementary Search Phrase	Total Papers	Papers in the Last 5 Years (2018–2022)
		Review	381	191
		Review + Technologies	212	112
		Review + Thermal energy storage	137	78
		Review + Sensible heat storage	28	17
Photovoltaic	Concentrated solar power	Review + Latent heat storage	31	18
		Review + Thermochemical energy storage	34	19
		Thermal storage configuration	207	104
		Thermal energy storage + Active system	22	12
		Thermal energy storage + Passive system	15	6

The keywords shown in Table 1 were used to collect the citations related to CSP and TES. The excluded phrase for all searches performed is 'photovoltaic' and the main phrase 'concentrated solar power' is the base word used for all searches. Both main and complementary phrases were searched for as topics in the Web of Science database. The total scientific papers found by each row search are also presented in Table 1. Most of the publications are found by more than one search row, being the sum of all articles higher than the total papers. Moreover, cross references are removed from the present review. At least 88 scientific articles within total papers found have been used to describe the CSP and TES review information, of which 41 were published in the last 5 years from 2018 to 2022.

Table 2 shows the total number of CSP facilities and TES CSP R&D projects found under a proposed keyword map for each research tool: SolarPACES, CORDIS and SETO.

Table 2. Search map to found TES CSP facilities and R&D projects.

Research Tool	Search by	Total TES CSP Facilities	Total TES CSP R&D Projects
SolarPACES	Operational status	119	-
	Operational status + Thermal energy storage	61	-
CORDIS	Concentrated solar power + Energy storage	-	46
SETO	Concentrated solar power + Thermal energy storage + Inactive	-	38
	Concentrated solar power + Thermal energy storage + Active	-	31

The operational CSP plants described in the present review were extracted from the SolarPACES database tool. Most of the information appearing in the profile of each CSP facility has been used throughout this manuscript. Some of the found TES CSP R&D projects: (i) contain duplicate information, or (ii) are out of scope, being related to topics such as photovoltaics or building air-conditioning. Thus, a total of 41 TES CSP R&D projects have been collected from CORDIS and SETO research tools for the present review.

2. Potential Integration of TES in CSP Plants

The typical configuration of an integrated TES CSP plant is illustrated in Figure 1, including the three main blocks of these systems: (i) solar field, (ii) power cycle and (iii) transport media/storage system [28]. This section provides a brief description of the solar collectors and thermal energy storage available technologies and a critical discussion of pros and cons of these technologies and their potential combinations.

Current operation of CSP plants is analogous to conventional thermal power plants, except for the use of solar radiation as a thermal energy source to produce electrical energy through an associated power cycle. A working fluid transfers the thermal energy, circulating between the solar field and the power block. The solar field is composed of concentrators, to improve the use of solar radiation, which is concentrated and projected onto a receiver to heat up at high temperature the working fluid [29]. The typical power block associated

with a CSP plant is the steam Rankine cycle. Most of the existing operational CSP plants use a steam turbine for power generation [25]. However, the trend in recent research is to couple CSP with CO_2-based power cycles: Brayton [30,31] and supercritical (sCO2) [32], improving the overall efficiency of the CSP plant. Besides, the integration of TES in CSP plants will improve their dispatchability when solar radiation is only partially available or during the night [10]. More than half of the total CSP plants which are currently under operation around the world integrate TES systems. Commercial plants represent around 80% of the currently ongoing CSP facilities with TES. The rest of TES CSP facilities are divided among demonstration plants (13%), pilot plants (6%) and prototypes (1%) [9]. Both, the first and second generation of CSP plants have contributed to the development of current commercial CSP facilities, contemplating (i) the direct steam production in the receiver and (ii) higher volumes of molten salt-based storage. The next (third) generation of CSP plants will focus on the research of (i) new non-corrosive TES materials with high heat absorption and high operational durability, (ii) new HTFs with high-temperature and high-degradability resistance and (iii) more efficient power blocks, such as Brayton and supercritical [33].
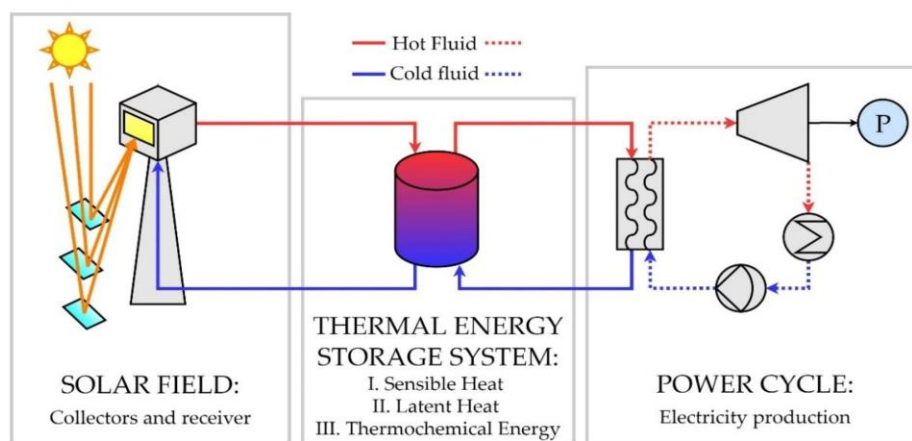
Figure 1. Main elements of an integrated TES CSP plant.

2.1. CSP Technologies

Table 3 shows the main characteristics of the most widespread concentrating solar technologies in CSP plants classified as: (i) parabolic trough collectors (PTC), (ii) linear Fresnel reflectors (LFR), (iii) solar power towers (SPT) and (iv) parabolic dish collectors (PDC), where PTC is the largest developed and established globally [10,24].

PTC and LFR concentrating technologies focus the solar radiation on a linear receiver, while PDC and SPT concentrating solar systems direct solar radiation to a focal point where the receiver is located [11]. The highest solar concentration ratio (up to 3000) is achieved by PDC and SPT [11], reaching high (i) operating temperatures (even above 1000 °C) [24], (ii) thermodynamic efficiencies for the CSP plant [34] and (iii) nominal power capacities (up to 280 and 377 MW, respectively) [9]. The most widespread concentrating solar technology is PTC (62%) followed by SPT (20%) and LFR (7%), within 141 CSP plants currently in operation and under construction. Meanwhile, CSP plants with concentrated solar power PDC technology are currently inoperative [25]. Thus, the development status of PTC and SPT is commercially available, both growing at the same rate in new construction facilities improving their performance, the TES and HTF media [13].

The high thermal efficiency of PDC and SPT, near 30%, and its high-temperature operation makes these emerging technologies very competitive with conventional PTC (18%, 400 °C) and LFR (12%, below 400 °C) applications. However, current TRL

...

of these CSP technologies points out the commercial status of PTC and LFR, while wider experimental feedback, especially at large scale, is required to better know and define the disadvantages of the most efficient technologies. Given their tested characteristics, PTC presents a strong potential to become the leading CSP technology in the mid-term.

Table 3. Specifications and comparison between the main CSP technologies [11,12,24,25,28,34].

CSP Technology	PTC	LFR	SPT	PDC
Solar concentration ratio	70–80	60–100	1000–1500	1300–3000
Operating temperature (°C)	<400	<300	<1000	<1500
Nominal capacity (MW)	10–280	9–125	10–377	<1.5
Average specific cost (€/kW)	7399	5054	6052	-
Average LCOE (€/kWh)	0.24	0.16	0.15	-
Thermodynamic efficiency	↓↓	↓	↑	↑↑
Advantages	• Commercial scale. • Modularity. Good land-use factor	• Readily available. Low manufacturing cost.	• High conversion. High temperature storage. • Optimal for dry cooling.	• Good land-use factor. • With/out heat transfer fluid.
Disadvantages	• Fluid working temperatures up to 400 °C.	• Small plants. Recent entrance in market.	• Low land-use factor. • Larger-scale operation required.	• Further experimental feedback required.

The cost assessment of these technologies shows the highest average specific costs associated to PTC, although other technologies such as LFR or SPT with slightly lower specific costs present values of the same order of magnitude. The higher thermal efficiency of SPT mitigate the investment costs leading to the lowest average levelized cost of electricity (LCOE) among CSP technologies. The average specific cost and the LCOE of the CSP plants with SPT technology is 18% and 40% lower than CSP plants with PTC technology, respectively. The efficiency of PTC is not high enough to reverse the effect of the largest average investment costs and leads to the highest LCOE.

All the CSP plants which are currently under construction contemplate the use of TES instead of the possibility of increasing electricity production with fossil fuels [25]. This trend is driven by the reduction of annual operation and maintenance costs of TES compared to a fossil fuel support system. Moreover, the capacity factor is improved by increasing the electricity production and GHG emissions are minimized. The variability of the TES material annual costs from one year to the next is lower than fossil fuels, whose price trend is less predictable [35].

2.2. TES Technologies/Systems

Regarding the maturity (TRL level, Table 4), the most developed storage technology relies on sensible heat storage (SHS), followed by latent heat storage (LHS) and finally thermochemical energy storage (TCES).

Information on large experimental and industrial-scale plants is available for SHS operation. SHS is based on liquid or solid storage media, liquid medium being the most commonly used in CPS plants, such as water or molten salts [23,25]. LHS technology is still under development for later integration into CPS plants, being mainly at experimental and pilot scale. Although the TRL of LHS systems is somehow lower, LHS are also commercially available for some specific materials [36]. However, TCES is not currently available at commercial scale. Most of the TCES systems are still investigated at laboratory scale for their integration in CSP plants [37].

The energy density of the LHS media is higher than of SHS media, given the higher enthalpy related to the phase change [23]. However, TCES system has the highest energy density compared to other TES [37]. Several TCES materials are currently under development but not commercially available, while SHS materials are widely commercially available. The heat transfer mechanisms are slow for both LHS and TCES, since their materials present low thermal conductivities [24].

Table 4. Summary and comparison of different TES Technologies [23,24,36,37].

TES Technology	SHS	LHS	TCES
TRL	8–9	6–9	4–7
Energy density	Low	Medium	High
Heat transfer	Good	Slow	Slow
Materials costs	Low, except liquid metals and thermal oils	Low	Low, except design and installation of reactors
Required area	High	Medium	Low
Timescale	Hours–Seasonal	Days–Months	Hours–Years
Lifetime	Long	Limited	Depends on reactant
Storage temperature	High	High	Low
Flexibility	Fast switch charge/discharge	Fast switch charge/discharge	Slow switch charge/discharge
Advantages	● Large experimental and industrial feedback. ● Easy implementation.	● Short distance transport. ● Small volumes. ● Constant temperatures for charge/discharge.	● Long distance transport. ● Small volumes. ● Long storage periods without losses.
Disadvantages	● High freezing point for liquid medium. ● Variable and unstable discharging temperature. ● Large volumes.	● Corrosivity of materials. ● Large heat losses. ● Formation of solid deposits on the heat exchange area.	● Complex technology. ● High capital costs. ● Technical issues: melting, incomplete reversibility, low reaction kinetics, sintering. ● Storage of gases. ● Required improvement of heat and mass transfer. ● Low charging rate.

The lifetime of SHS materials (which can reach 20 years) is four times higher than that of LHS materials and even ten times higher than TCES materials [38]. The storage time of TCES materials exceeds that of LHS and SHS materials, even reaching a temporary scale of years.

Based on the information gathered in Table 4, strong R&D efforts in the development of TCES (TRL 4–7) must be conducted to overcome those drawbacks identified for this technology, since its potential to gain the leadership among TES-CSP technologies is extremely high. The accumulation of key advantages when compared to SHS and LHS technologies, such as the higher energy density, the smaller required volumes or the dramatic increase of the storage period without significant energy losses, makes TCES the most promising technology to couple with CSP plants in the long-term. However, efforts must be carried out to find materials with a long lifetime (avoiding melting/sintering issues, achieving complete reversibility, enhancing reaction kinetics) able to be in stored at low temperature. The improvement of heat and mass transfer mechanisms, together with the simplification of TCES operation, will also lead to a needed reduction of capital costs to become economically competitive.

TES systems can be classified by the materials and technology used, such as storage medium [39,40]. Figure 2 shows the main storage materials used by each TES technology: SHS, LHS and TCES.

2.2.1. Sensible Heat Storage (SHS)

Sensible heat storage (SHS) is the simplest method, based on the storage of thermal energy by raising the temperature of a liquid or solid storage medium (e.g., water, sand, molten salts, or rocks), without undergoing phase change over the temperature range of the storage process. SHS systems are cheap, commercial, simple and easy to control, but they present low energy density compared with LHS systems [37].

SHS systems use the heat capacity and the temperature variation of the storage medium during the process of charging and discharging. The amount of heat stored

depends on (i) the specific heat of the medium, (ii) the temperature variation and (iii) the amount of storage material option [41,42] (Equation (1)).

$$Q_s = \int_{T_i}^{T_f} m \cdot c_p \, dT \cong m \cdot c_p \cdot (T_f - T_i) \tag{1}$$

where Q_s is the quantity of heat stored (J), m is the mass of heat storage medium (kg), c_p is the specific heat (J/(kg·K)), T_i is the initial temperature (°C) and T_f is the final temperature (°C).
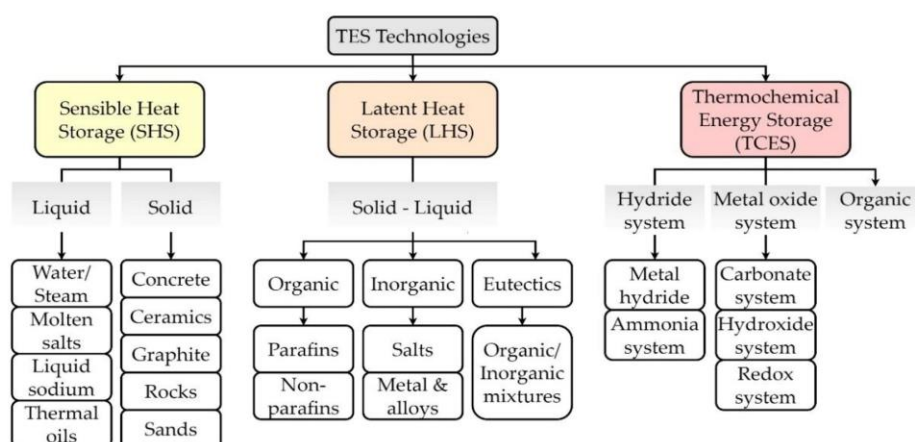
Figure 2. Main TES technologies classified according to the storage medium.

The most popular SHS materials withstand high temperatures (>500 °C), such as concrete, ceramics, graphite, rocks or sands [24,43]. Storage temperatures up to 1000 °C are mainly standby regenerator-type storage systems which transfer heat from gas directly to the solid material. Ceramics and concrete materials are being used in CSP operational facilities in demonstration, such as in the Jülich Solar Tower plant [44], or in CSP under development plants, such as in Huaqiang TeraSolar 15 MW Fresnel plant [25], given their good thermal and mechanical properties and low cost [45]. Among high temperature resilient materials, graphite is a suitable SHS candidate, given its high thermal diffusivity [46], whereas concrete and high alumina cement concrete blocks are identified as a potential SHS medium, given their low cost [43]. Furthermore, rocks are used as a SHS medium at the operational pilot plant Airlight Energy Ait-Baha, also given their low cost [25]. Natural rocks can be a sustainable option to improve energy dispatch in CSP plants located in regions with earth-abundant resources [47]. However, waste materials and byproducts are available as a SHS medium, entailing an environmental and economic benefit [48,49]. Experimental results show similar performances comparing a 100% recycled material and an alumina-based medium as SHS (i.e., net exergy considering thermal losses and pressure drop losses) [50].

The liquid materials used as SHS, such as molten salts, water, thermal oils and liquid sodium have already been tested in existing CSP plants [43]. Molten salts are the most widespread, since their thermal stability in the presence of air up to 500 °C [51,52], and other advantageous characteristics such as low vapor pressure, low freezing temperature for ternary mixed, low viscosity, high thermal conductivity and specific heat [53]. Almost 78% of the CSP plants currently under commercial operation or under construction use molten salts as a thermal storage medium [25]. Moreover, molten salts are also used as heat transfer fluid (HTF) in a large number of CSP commercial plants from Gemasolar CSP plant in Spain (2011) to the last operational CSP plant in China Qinghai Gonghe—50 MW Tower (2019), all of them using power tower technology [25,54]. Once the corrosion issue is

solved, the next generation of molten salts will be based on chloride materials, given their resistance to high temperatures and low cost [55], keeping similar thermophysical properties as currently commercial molten salts [56]. Moreover, the inclusion of nanoparticles in molten salts will improve their thermophysical properties, enabling their use as HTF and TES [57].

Beyond molten salts, water is also commercially used as a thermal storage medium. The main advantages of water as TES are: its easy availability, non-toxicity, non-flammability and that it is completely harmless [23]. Water can be stored as saturated steam or pressurized water in a pressurized tank. When superheated steam is fed to the storage tank, the temperature and pressure increase, changing the saturation state. If saturated water enters the tank, the mass of water increases, keeping constant the pressure and temperature. During the discharge process, saturated steam is extracted from the storage tank as its pressure drops [36]. The main issue associated with water use in CSP plants is the scarcity if the plant is located in desert areas [58]. In addition, water can be use as a HTF and thermal storage medium, as in Puerto Errado 2 Thermosolar Power (PE2) [54] and Khi Solar One CSP plant [59,60].

Liquid metals used as thermal storage media, such as liquid sodium, are currently under development. They present safety problems related to its high combustibility in contact with water, in addition to discouraging higher costs than some molten salts. Currently, the Jemalong Solar Thermal Station pilot CSP plant in Australia, under operation from 2017, uses liquid sodium as HTF and as a thermal storage medium.

Other liquid media used for thermal storage by sensible heat are the thermal oils, although their usage is currently restricted to HTF in most CPS plants in operation [25]. The main advantage of thermal oils over water is their permanence in the liquid phase at temperatures higher than those of water, up to 250 °C at atmospheric pressure. Thus, thermal oils have a lower vapor pressure and, unlike molten salts, they do not need protection against freezing. However, thermal oils degrade and produce acids at temperatures above their operating range, accelerating the corrosion of containers and pipes [23,61]. Therefore, the possibility of using non-edible vegetable oils such as HTF and TES is being developed [61]. On the other hand, thermal oils at an experimental level are being used as a storage medium together with solid materials [62,63].

In summary, molten salt SHS TES have reached high commercial TRLs for high temperature applications, becoming the standard solution for dispatching solar thermal electricity at full load. However, their potential has not been fully developed in industrial applications (TRL 4–6). SHS TES solids regenerator-type storage systems are also commercially deployed in steel and glass industries for waste heat recovery, while their application in power plants is still being developed (TRL 6–7). Despite their TRLs, low cost and widely available natural rocks are very promising storage materials for large scale CSP plants when air is used as heat transfer fluid [11].

The cost of storage unit per high-temperature SHS systems is estimated to range between €20–70/kWh for liquid storage and between €15–40/kWh for solids storage [64]. Regarding the future economic feasibility of high-temperature SHS liquid storage, novel molten salts mixtures must be developed to expand the operating temperature range, together with the exploration of fully new materials with long-term reliability. Future efforts must focus on cost reductions of regenerator-type storage systems through (i) the development of low-cost materials from industry wastes or the use of natural rocks, (ii) less expensive pressurised vessels and (iii) the scale-up of regenerator-type storage technology.

For CSP application, the demonstration of novel SHS TES technologies at a relevant scale is still pending. Hence, pre-commercial small-scale demonstrations and pilot plants should be funded with a strong focus on increased flexibility through heat storage integration.

2.2.2. Latent Heat Storage (LHS)

Latent heat storage (LHS) materials are known as phase change materials (PCMs) with regard to the energy released or absorbed during a change in physical state. The

heat is mainly stored in the phase-change process (at a quite constant temperature) and it is directly connected to the latent heat of the substance. Thus, charging and discharging phenomena occur during the phase change either from solid to liquid, liquid to gaseous, solid to gaseous or solid to solid [30]. However, since the storage of gaseous products is difficult, LHS technologies usually make use of solid to liquid phase transition rather than liquid to gas phase change [37] and they are considered to be an efficient alternative to SHS systems [45]. The use of a LHS system using PCMs is an effective way of storing thermal energy and has the advantages of medium energy storage density and the isothermal nature of the storage process [41].

The main advantage of using LHS over SHS is its capacity of storing heat at an almost similar temperature range. Initially, these materials act like SHS materials, in that the temperature rises linearly with the system enthalpy; however, later, heat is absorbed or released at almost constant temperature with a change in physical state [41] (Equation (2)).

$$Q_s = \int_{T_i}^{T_m} m \cdot c_{ps}\, dT \; + \; m \cdot f \cdot \Delta q \; + \; \int_{T_m}^{T_f} m \cdot c_{pl}\, dT$$
$$Q_s \cong m \cdot \left[c_{ps} \cdot (T_m - T_i) + f \cdot \Delta q \; + \; c_{pl} \cdot (T_f - T_m) \right] \tag{2}$$

where Q_s is the storage capacity (J), T_m is the melting temperature (°C), m is the mass of PCM medium (kg), c_{ps} is the average specific heat of the solid phase between T_i and T_m (J/(kg·K)), c_{pl} is the average specific heat of the liquid phase between T_m and T_f (kJ/(kg·K)), f is the melted fraction and Δq is the latent heat of fusion (J/kg).

LHS is a nearly isothermal process, providing significantly enhanced storage quantities when compared to SHS systems of the same temperature range. Isothermal storage is an important characteristic because the solar field inlet and exit temperatures are limited due to (i) constraints in the HTF (ii) solar field equipment and (ii) the power cycle [36]. However, LHS systems present low thermal conductivity [37,65] and solid deposits may form on the heat transfer surfaces [38,45]. The latest research on PCMs focuses on the development of mechanisms to enhance their thermal conductivity, using metal foam, fins, heat pipes, mixtures of PCMs or embedded nanoparticles [66].

Generally, solid–liquid PCMs are the most interesting to be applied in a thermal storage and are classified into organic and inorganic materials [45].

Organic PCMs can melt and solidify many times without phase separation, so they have a high chemical and thermal stability, crystallize with little or no supercooling and are generally non-corrosive [41,67]. They also show some limitations such as a low enthalpy of phase change, low thermal conductivity and better thermal stability than inorganic PCMs [68]. Organic PCMs also can be classified into paraffins or non-paraffins compounds. Paraffins compounds are by-products of oil refinery [69,70], cheaper than other PCMs and compatible with all metal containers. However, they also have some disadvantages, such as large volume change with phase change [71]. On the other hand, non-paraffin compounds are the largest category for potential use as latent heat storage materials. However, they have different features based on each material [72], since this category is divided into fatty acids, alcohols, esters and glycols. Within the non-paraffin category, fatty acids have similar properties to paraffin compounds [71,72], but they are non-cost effective [73].

Inorganic PCMs show higher thermal conductivities compared to organic PMCs [74] but, in contrast, their maintenance is one of the most reported challenges due to their lack of thermal stability. They are frozen at low temperatures and they are difficult to handle at high temperatures, and they can be corrosive [41,67]. There are two large groups of materials within the inorganic PMCs: salts and metals and metal alloys. Salts, in general, have low heat conductivity, a relatively high degree of supercooling and cause degradation at high temperatures [75], while metals and metal alloys have high thermal conductivity and small volume change, therefore they could potentially be a good material, although they have low heat of fusion per unit weight [76].

Moreover, mixtures of different organic and inorganic materials can be generated [71], giving rise to eutectic materials with phase change almost always without segregation,

high conductivities and thermal densities [41]. The lower melting temperature of eutectic mixtures than their constituents allows crystallization into a single crystal [77]. Thus, eutectic materials have the ability to melt and solidify consistently without appreciable phase segregation [73]. Depending on the mass fraction of each material, it is possible to vary the melting point of the resulting eutectic mixture [78]. They present low latent and specific heat capacities [79]. The development of high temperature eutectic materials above 500 °C grows in interest as stable thermal energy storage in CSP plants [18].

The main applications of PCMs have been developed for air-conditioning [67], heating and cooling [69,70] in buildings. Nevertheless, there is a potential use of PCMs as TES in CSP plants [68,80]. Up until now, only numerical and experimental research have been carried out, such as cascaded latent heat storage with alkali nitrate salts [81], the combination of SHS with LHS using stearic acid [82], the use of a eutectic mixture such as PCM [83], the use of pure $NaNO_3$ as PCM [84] for direct steam generation (DSG) in a CSP plant or the use of embedded nanomaterials in PCMs to improve the thermal stability during storage and the heat transfer [85].

In summary, latent heat energy density of storage unit ranges between 90–100 kWh/m^3 for high-temperature LHS systems for feasible sizes 10 kWh–10 MWh. High temperature LHS with variable phase-change temperatures between 140–300 °C have been constructed and demonstrated in the operational environment, while, high power systems are still under development with some demonstration projects (TRL 5–6) and high capacity storage systems are TRL 5–9 [64].

The cost of a storage unit per high-temperature LHS systems is estimated to range between €20–70/kWh [64]. These costs need to be reduced to be able to exploit the technological advantages of LHS in the market. This reduction should be mainly focused on the enhancement of heat transfer mechanisms and the development of low-cost PCM systems able to operate at 400–500 °C.

2.2.3. Thermochemical Energy Storage (TCES)

Thermochemical energy storage (TCES) systems are based on reversible chemical reactions [37]. In this way, the endothermic reaction generates the charging process, causing a reagent "A" to separate into two parts, giving rise to products "B" and "C", Equation (3), which can be stored independently and at ambient temperature until the discharge process is required, so that heat losses are practically non-existent [23]. The discharge process takes place with the exothermic reaction and therefore energy is released through the mixture of products "B" and "C" at the required pressure and temperature conditions [41].

$$\text{Charging (Endothermic reaction): } A + \text{Heat} \rightarrow B + C$$
$$\text{Discharging (Exothermic reaction): } B + C \rightarrow A + \text{Heat} \tag{3}$$
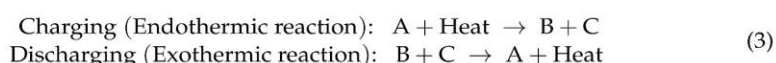
The TCES system is the least investigated storage technology though it can potentially store higher amounts of energy than SHS or LHS systems due to (i) its high energy density [36] (almost 10 times higher than SHS and 5 times than LHS [86]) and (ii) its indefinitely long storage duration at ambient temperature [24]. The amount of heat stored (Q_s) in a chemical reaction depends on the heat of reaction and the extent of conversion given by Equation (4).

$$Q_s = m \cdot a_r \cdot \Delta H_r + \int_{T_i}^{T_f} m \cdot c_p \, dT$$
$$Q_s \cong m \cdot \left[a_r \cdot \Delta H_r + c_p \cdot (T_f - T_i) \right] \tag{4}$$

where, a_r is the mass fraction reacted, ΔH is the heat of reaction (J/kg) and m is the amount of mass of the storage medium (kg), T_i is the initial temperature (°C), T_f is the final temperature (°C) and c_p is the average specific heat between T_i and T_f (J/(kg·K)).

TCES technology must overcome some challenges, due to limitations in heat transfer, cycling stability, reversibility and cost [36]. TCES technology is still in an immature stage and remains at the research level (TRL 3–4) [87,88].

The main technologies that are being studied as possible TCES medium are classified in hydride systems, metal oxide systems and organic systems. These systems are capable of working at high temperatures between 400 and 1000 °C [40,86]. Therefore, TCES technology use materials with higher operation temperature levels than those of the materials used for SHS, such as molten salts (500 °C). Therefore, heat recovery efficiency is greater due to larger operating time, i.e., it is possible to produce more power for the same operating time lapse as SHS.

Hydride systems are classified as metal hydride and ammonia systems. Among metallic hydrides, the most developed is the magnesium hydride (MgH_2) system, which does not generate byproducts. The products of the reaction are solid–gas, so they can be easily separated and have high cycles of reversibility. The ammonia system has important experimental feedback. However, their reaction kinetic is slow and requires high operating pressure, presenting also high costs [40,86].

Metal oxide systems are classified as hydroxide systems, carbonate systems and redox systems. Among hydroxide systems, there are materials with high energy density, good reversibility of the reaction operating at atmospheric pressure, but with low thermal conductivity. Carbonate systems are low cost and use very high energy density materials. The reaction products can be easily separated, but they show sintering problems and poor reactivity. Redox systems do not need a catalyst, they use oxygen as a reactant and the reaction products can be separated, but there are few experiment feedbacks and the systems produce an environmental impact [40].

Finally, organic systems, such as methane reforming, present high reaction enthalpy, but produce side reactions and have low reversibility [86].

Both hydride and carbonate systems are the most promising TCES systems, given their high energy storage density and low cost. Nevertheless, the cyclic degradability and storage requirement of the gas make the redox system the most suitable TCES option [89].

Around 95% of installed TCES systems based on chemical reactions are under research and development and reach TRL 4. In addition to the research on materials, the main challenge for TCES is this technology is related to global system issues such as reaction control, reactor design or process integration. A large room for research is found to increase the TRL of the reactive systems of TCES technology in very different aspects: (i) design of improved reactor concepts, (ii) better integration of gaseous reactants, (iii) material improvement (kinetics, stability) and (iv) optimisation of full reversibility.

Due to the advantages of TCES over LHS and SHS, new advances in research are focused on reducing costs of TCES systems while improving the stability of the cycles in the reversible reactions that occur, developing the design of reactors in which the reaction takes place, through charging/discharging rate, and its integration in the CSP plants [40].

A key aspect to boost their integration in CSP plants will be the enhancement of heat and mass transfers inside the reactor. Furthermore, attention should be paid to the capability of hybrid storage combining 2–3 TES technologies [11].

Current costs are not competitive, given the low TRL of this technology, but the target of cost of storage for TCES with chemical reaction ranges between €10–90/kWh [64]. Cost reduction will include the increase of reactor lifetime and the decrease of the cost of reactants.

2.3. TES CSP Integrated Configurations

Once the main characteristics of CSP and TES has been detailed in Sections 2.1 and 2.2; a revision of the best suited combinations of both technologies is elaborated in this section. As known, electricity production in conventional CSP plants is concentrated during the daily period with solar energy availability. The integration of a thermal energy storage system which makes the electricity production more flexible improves the economic feasibility of CSP plants. More than half of the CSP facilities (51%) currently operating in the world include TES systems [25], storing the energy surplus to be used during high demand periods. Moreover, conventional fossil fuel-based support systems are commonly

associated with CSP plants becoming operational when the renewable alternative or the retrieval of stored energy is not enough [90]. However, the use of fossil fuels to satisfy the demand induces an increase in the cost and CO_2 emissions, further contributing to global warming [23].

Therefore, the use of TES in CSP plants implies an environmental and economic benefit, avoiding the loss of thermal energy by storing the excess heat produced to be used when required. The selection of the best TES system to each CSP technology must consider the following characteristics with regard to storage [14,41]:

- The heat storage capacity, which defines the thermal energy which can be stored in the system for a given process, medium and size of the storage system. The larger energy density of the storage medium (MJ/m^3), the smaller storage volume required.
- The storage/discharge rates related to the speed and time elapsed in each charge or discharge process.
- The period of time during which energy can be stored. It will depend on the storage medium, from hours to months.
- The chemical compatibility of the storage medium with the CSP plant. The storage medium must be mechanically and chemically stable, minimizing its degradation after each charge/discharge cycle.
- The energy storage efficiency which relates the energy retrieved from the storage medium and the energy required in the storage process, accounting for the energy losses between each charge/discharge cycle. Thus, excellent heat transfer must occur between the HTF and the storage medium to improve the energy efficiency above 95%. Besides, there must be high chemical compatibility between HTF, heat exchanger and storage medium, with minimum thermal losses.
- The compatibility with the power block associated to the CSP plant. The higher operating temperature of the storage medium, the greater overall efficiency of the CSP plant. Up until now, the Rankine power cycles have been the most widespread in CSP plants using molten salts as the storage medium. However, novel storage materials currently under development withstand operating temperatures above 700 °C and can improve the efficiency of the CSP system by coupling to Brayton cycles.
- The cost of the storage medium including capital and operation and maintenance costs. The longer lifetime and the lower cost of a storage medium, the better the economic and commercial feasibility.
- The storage medium must be safe and environmentally-friendly, considering its lifetime.

Despite the characteristics required to choose the thermal storage medium that best suits the CSP plant, the main configurations to integrate the TES system to the CSP plant must be accounted. The TES system can be classified as active or passive, considering the movement of the storage medium during its charging and discharging, as shown in Figure 3.

The advantages and limitations of the main TES CSP integrated configurations are shown in Table 5.

In active storage systems, the storage medium is a fluid capable of absorbing or emitting thermal energy through forced convection. If the storage medium is the HTF, the storage system is active–direct and no heat transfer mechanism is required. Solid particles will be a potential TES and HTF for the third generation of CSP plants, allowing operating temperatures above 800 °C to improve the thermal conversion efficiency of the associated power cycle [91]. However, if the storage medium is not the same as the HTF, a heat exchanger between both fluids is required. In addition, in the TES active systems, two separate tanks or a single tank can be used. When 2-tanks are used, one of them contains the storage medium charged with thermal energy, while the other contains the discharged material. When conventional molten salts are the storage medium in the 2-tank format, freezing is possible at high temperature (120–220 °C). The use of a single tank reduces the cost and the required volume for the storage tank. In this case, the stored heat may be stratified, creating a thermal gradient, but it is difficult to maintain the thermal stratification.

Another option is the accumulation of water as saturated steam or saturated liquid in a single pressurized tank, which does not require a heat exchanger if it is an active-direct system. Despite its low energy density and the high cost of pressurized tanks [24], the extensive use of water as steam in different applications makes it possible to store water in different saturation states, discarding the rest of the gases as storage media for sensible heat.
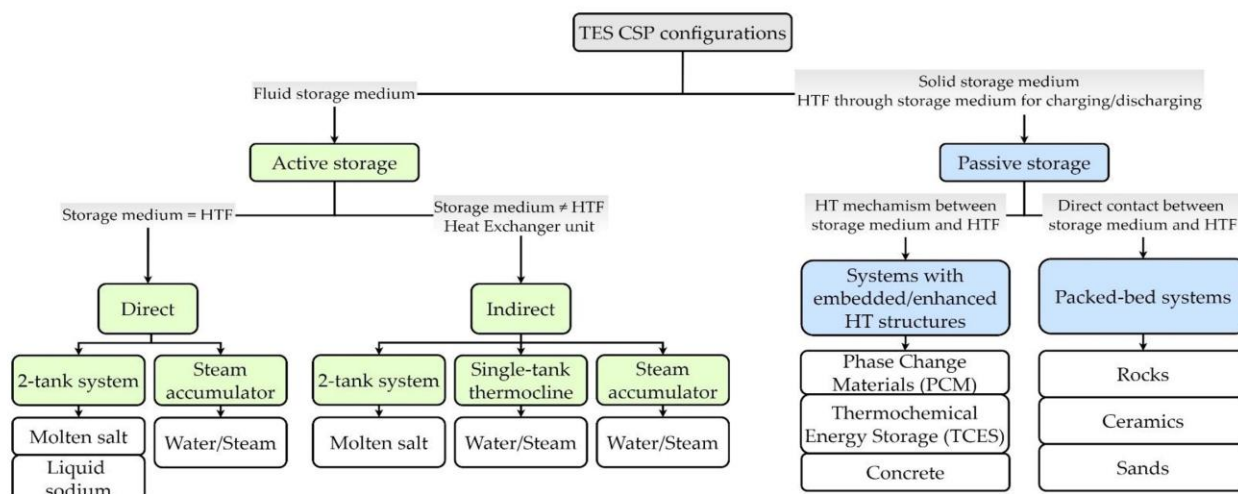
Figure 3. Main TES configurations implemented into CSP plants, according to the concept active/passive storage.

Contrarily, in passive storage systems, the storage medium is normally a low-cost solid material—simple and compact storage unit—and the HTF circulates through it stimulating the charging/discharging of thermal energy stored. Moreover, a heat exchange mechanism between the storage medium and the HTF may be necessary, although if direct contact between the medium storage and HTF is possible, the heat transfer may be better. The temperature during the discharge step is unstable under packed-bed systems. Nevertheless, the heat exchangers required under the embedded heat transfer structures raise the investment cost [24,36]. Among the passive storage systems, the packed-bed system is a promising alternative, given its wide operating temperature range [92].

The most widespread TES system in currently operative CSP plants is the 2-tank format within the active–indirect system (71%). The CSP technology associated with the 2-tank active–indirect TES system is PTC, using molten salts as storage medium and a thermal oil as HTF. The HTF, such as thermal oil, limits the maximum solar-field outlet temperature at 393 °C. The expected electricity production of this type of plants ranges from 158 to 944 GWh/year for CSP plants whose size is 50 MW and 250 MW, respectively. The plant capacity factor as the ratio between the expected production and the maximum possible production within a year is between 26 and 57%, considering a storage size from 3 to 10 h [25].

Additionally, the commercial CSP plant Puerto Errado 2 uses LFR CSP technology in conjunction with a single thermocline tank active–indirect TES system. The water is used as HTF, which reaches a solar-field outlet temperature of 270 °C. The storage size is 0.5 h with a capacity factor of 19% and a net power at nominal conditions of 30 MW [93]. Previously to the Puerto Errado 2 CSP plant, a prototype named Puerto Errado 1 evaluated the single tank thermocline system, with a 1.4 MW DSG power block [25].

Table 5. Main advantages and limitations of each possible TES configuration into a CSP plant [24,36].

TES CSP Integrated Configurations		Advantages	Limitations
Active Direct Storage	2-tank	• Separate hot/cold storage tanks • No heat exchanger required • (HTF = Storage medium)	• Suitable materials as HTF and storage medium required • Larger stored volume required • High cost and freezing point (<220°) for molten salts
	Steam accumulator	• Direct Steam Generation (DSG) • No heat exchanger required • (HTF = Storage medium)	• Low volumetric storage capacity • Expensive pressurized storage tanks
Active Indirect Storage	2-tank	• Commercial maturity • Separate hot/cold storage tanks	• Larger stored volume required • High cost and freezing point (<220°) for molten salts
	Single tank	• Smaller stored volume required • 35% cheaper than 2-tank system	• Complex filler material configuration to keep stratification
	Steam accumulator	• Direct use of stored steam in Rankine power cycle	• HTF such as synthetic oil is required • Low volumetric storage capacity • Expensive pressurized storage tanks
Passive Storage	Embedded HT structures	• Cheap solids may be used • High volumetric storage capacity • (PCMs and TCES)	• Low heat transfer rates • High investment cost for heat exchangers
	Packed-bed systems	• Cheap solids may be used • High heat transfer rates	• Discharge temperature may vary

The characteristics of the most widespread TES CSP configurations under currently operational commercial CSP facilities are listed in Table 6.

The second most commonly integrated TES system is the active–direct (24%) in both modalities: 2-tanks and steam accumulator [25]. Under each modality, the storage medium and the HTF is the same substance and the heat transfer is produced by forced convection [24]. The active–direct TES system is commonly integrated as SHS technology in SPT plants [25]. However, the CSP technology implemented in some operational demonstration plants is PTC, such as Archimede and ASE Demo Plant [94], or LFR (Lanzhou Dacheng Dunhuang (DCTC Dunhuang)—10 MW and 50 MW Fresnel CSP Plant [95]). The 2-tanks format use molten salts as storage medium and HTF, reaching a solar-field outlet temperature up to 565 °C [25]. Nevertheless, the Jemalong Solar Thermal Station operational pilot plant uses liquid sodium as HTF and storage medium [96], while the SUPCON Delingha 10 MW Tower CSP Plant operational demonstration facility adopts double heat transfer fluid as water and molten salt [97]. The expected electricity production ranges from 110 to 500 GWh/year for commercial CSP plants with a 2-tank direct system whose size is 20 MW and 150 MW, respectively. The storage size (6–15 h) improves the plant capacity factor up to 33–36%. Moreover, steam has been used as a storage medium and HTF since 2009, reaching a solar-field outlet temperature up to 530 °C, when the steam is stored as saturated steam, and between 250–300 °C for pressurized water. The expected electricity production ranges from 23.4 to 180 GWh/year for commercial CSP plants whose size is 11 MW and 50 MW, respectively. The plant capacity factor is between 24 and 41% considering a storage size up to 2 h [25].

Regarding passive storage TES CSP configuration, the Huaqiang TeraSolar 15 MW Fresnel CSP Plant uses concrete as TES and water as HTF [98]. The steam turbine net capacity is 14 MW, reaching an electrical production of 75 GWh/year. The storage capacity of 14 h allows a high plant capacity factor of 57% [25].

Table 6. Main characteristics of TES CSP configuration currently operating under commercial scale [25].

TES CSP Configuration	Active Storage				Passive Storage
	Direct		Indirect		Embedded HT Structures
	2-Tank	Steam Accumulator	2-Tank	Single-Tank	
CSP technology	SPT	SPT	PTC	LFR	LFR
TES medium	Molten salts	Water	Molten salts	Ruths tank	Concrete
HTF medium	Molten salts	Water	Thermal oil	Water	Water
T_{out} solar field (°C)	565	250–530	393	270	450–550
Expected production (GWh/year)	110–500	23–180	158–944	49	75
Nominal capacity (MWe)	20–150	11 to 50	50–250	30	15
Storage size (h)	6 to 15	1 to 2	3 to 10	0.5	14
Power block	Steam Rankine	Steam Rankine	Steam Rankine	Steam Rankine	Steam Rankine
Number of commercial TES CSP plants	8	3	32	1	1

The rest of the TES CSP facilities currently in operation use combinations of the previous ones, such as in the case of Dahan Power Plant [99] in which the steam accumulator system is combined with two indirect tanks; or passive storage systems, such as packed-bed systems in Jülich Solar Tower Plant [44], all of these being demonstration or pilot plants.

3. European and North American TES CSP R&D Projects Review

In the present section, a review of the completed and ongoing TES CSP R&D projects launched in the last decade (2011–2022) from Europe and North America, which analyze the full integration between CSP, TES and the associated power block, are detailed. Other R&D projects launched in the last decade and not focused on the integration of the full TES CSP system at large scale are not included in this review. These projects oriented to the development of new materials or components required for TES systems, whose application is at small scale or for building and district heating systems, are beyond the scope of the present review.

Before 2011, the CSP-based R&D projects were focused on the integration of SHS and LHS as TES [27]. Molten salts were the most developed storage medium within SHS system, even used as HTF in active direct storage systems configuration [100,101]. Furthermore, research based on molten salts was focused on strategies to minimize its main drawbacks: (i) increasing the storage temperature over 650 °C [102] and (ii) improving the specific heat with embedded ceramic particles [103]. Regarding the CSP TES passive storage configuration, SHS and LHS storage mediums were also investigated. Within SHS the most developed passive storage configurations were: (i) packed-bed system of sand [104] or concrete [105], and (ii) solid graphite modular blocks to achieve operating temperatures up to 1650 °C [106]. Additionally, since 2008, the development of PCMs as LHS increased, transferring the thermal energy by heat exchangers [107,108] or embedded thermosyphon heat pipes [109], even integrating nanoparticles into the PCM to improve the heat transfer efficiency [27].

3.1. Summary of R&D Projects (2011–2022): Timeline and TRL

This section summarizes and compares all the European and North American R&D projects, completed and ongoing, launched in the last decade. Table 7 gathers general information about these TES CSP R&D projects whose technical and economic data will be provided in the following subsections.

119

Table 7. TES CSP R&D projects from 2011 to the present.

| TES	Project Name *	Location	Period	Coordinator *	Budget (M€)	Ref.
LHS	DDI-TES	Florida (USA)	2011–2012	USFl	0.7	[110]
TCES	TCS-Power	Germany	2011–2015	DRL	4.4	[111]
TCES	RESTRUCTURE	Greece	2011–2016	CERTH	3	[112]
TCES	STORRE	France	2012–2016	CEA	2.9	[113]
TCES	LCMH-TES	South Carolina (USA)	2012–2016	SRNL	2.5	[114]
LHS	HELH-TES	Illinois (USA)	2012–2018	ArNL	1	[115]
TCES	SC-TES	Florida (USA)	2014–2015	UFl	0.4	[116]
TCES	RC-TES	Alabama (USA)	2014–2016	SRI	0.8	[117]
TCES	ELEM-TES	Colorado (USA)	2014–2017	CSM	1	[118]
TCES	ISR-TES	New Hampshire (USA)	2015–2018	BE	2.6	[119]
TCES	BMC-TES	New Mexico (USA)	2015–2018	AlNL	3.4	[120]
TCES	CaL-TES	Alabama (USA)	2015–2018	SRI	2.8	[121]
SHS	NEXT-CSP	France	2016–2020	CNRS	4.9	[122–127]
Other	SOLSTORE	Spain	2017–2019	CIC	0.1	[128,129]
LHS	NPMSSES	United Kingdom	2017–2019	ULe	0.2	[130]
LHS	AMADEUS	Spain	2017–2019	UPM	3.2	[131]
TCES	SesPER	Spain	2017–2020	CSIC	0.2	[132]
SHS	NEXTOWER	Italy	2017–2021	ENEA	6.2	[133]
SHS + LHS	IN-POWER	Spain	2017–2021	LEITAT	5.8	[134]
SHS + LHS	NewSOL	Portugal	2017–2021	UEv	5.6	[135]
TCES	SOCRATCES	Spain	2018–2021	USe	4.9	[136,137]
LHS	THERMES	United Kingdom	2019–2021	UBir	0.2	[138]
SHS	LPP-SS	Colorado (USA)	2018-	NREL	8	[139]
LHS	TES-HE	New Hampshire (USA)	2018-	BE	1.1	[140]
SHS	CSP-ERANET (Newcline)	Spain	2019–2024	AGENEX	13.8	[141]
TCES	SS-TES	Michigan (USA)	2020-	MiSU	2	[27]
TCES	EWSCh-TES	Arizona (USA)	2020-	ArSU	2.9	[27]
TCES	EC-TES	South Carolina (USA)	2020-	SRNL	0.2	[27]
SHS	HTMS-TES	Tennessee (USA)	2020-	ORNL	0.1	[142]
SHS	FULL-TES	California (USA)	2020-	EDISUN	39	[27]
SHS	PB	Montana (USA)	2021-	MoSU	0.1	[27]

* Abbreviation of project's name and main coordinator. Full name appears in Appendix A.

The United States of America (USA) is the country with greatest development of TES CSP R&D projects, mainly focused on TCES technology. Meanwhile, Spain has launched the second highest number of TES CSP R&D projects in the last decade (Table 7). Both countries have a long record of developing CSP technology, concentrating the largest number of currently operating CSP facilities deployed in the world with and without TES (i.e., 17 in the USA [25] and 51 in Spain [7]). Figure 4 illustrates the distribution by countries and TES technology of the number of TES CSP R&D projects.

Figure 5 represents a timeline built with the TES CSP R&D projects within the scope of the present study. The upper part comprehends the ongoing TES CSP R&D projects, while the bottom part shows the TES CSP R&D projects already completed since 2011. In addition, the TRL of all the TES CSP R&D projects is shown through a colour scale from low (dark red—TRL 1) to high (dark green—TRL 9) technological readiness level by the end of the project.

The most widespread TES technology among the research projects (almost 55%) between 2011 and 2018 involve the integration of TCES with a CSP plant, reaching a TRL by the end of the project between four and eight; from experimental demonstration to near commercial scale. Within ongoing TES CSP R&D projects, SHS and TCES systems are the most extended with lower TRLs which range from two to six, except for a project which reaches a TRL of eight. Regarding research projects which include LHS as TES, the development level oscillates within lab and pilot scale (TRL 3–5). However, R&D projects

120

involving SHS and LHS TES reached a development level at demonstration scale in the relevant environment (TRL 6).
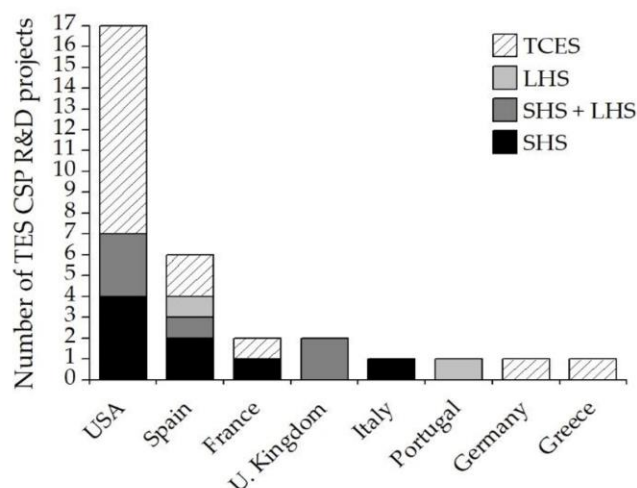
Figure 4. TES CSP R&D projects from 2011 distributed by country and TES technology.

3.2. TES CSP R&D Projects Completed between 2011–2022

This section gathers the technical and economic information of those TES CSP R&D projects finished from 2011 onwards within Europe and North America. Most of the analyzed projects focus on the complete TES CSP configuration. However, few research projects aim to only develop a specific block of the TES CSP system: storage medium, required equipment for the heat transfer between CSP-TES and TES-power cycle, or new storage concepts. Table 8 summarizes economic and technical data of the TES CSP R&D projects which assess the full integration of the TES with the CSP plant and the power block.

3.2.1. TCS-Power

The overall objective of the Thermochemical Energy Storage for Concentrated Solar Power Plants (TCS-Power) research project was to develop a new, efficient and economically viable TCES for CSP plants, minimizing electricity production costs. Two low-cost and long-term stable TCES systems were proposed within the TCS-Power project: redox and hydroxide. Manganese oxide is the storage medium selected as redox TCES to be integrated into SPT CSP plants, given the high operating temperature (>700 °C). The air is the fluid used as HTF and oxygen carrier for the redox reaction, while calcium oxide is the storage material used as hydroxide TCES integrated into PTC CSP plants, achieving a working temperature between 400 and 600 °C. Molten salts were selected as HTF within hydroxide TCES. However, the hydroxide TCES medium could be used as HTF and TES, given the possibility of the material conveying. Both TCES systems use charge/discharge reactors for the heat transfer between HTF and TES as passive storage TES CSP configuration. The power block associated with both TES systems was the steam Rankine, given its technological maturity. Both TCES systems were evaluated at lab and pilot scale to 10 kW (TRL 4–5). Furthermore, a techno–economic assessment evaluated the TCES up-scaling to commercial scale, being the obtained LCOE of €0.14 and €0.21/kWh under hydroxide and redox TCES systems, respectively. This European R&D project launched in 2011 was coordinated by Deutsches Zentrum für Luft—und Raumfahrt e.V. (DRL) from Germany [111].
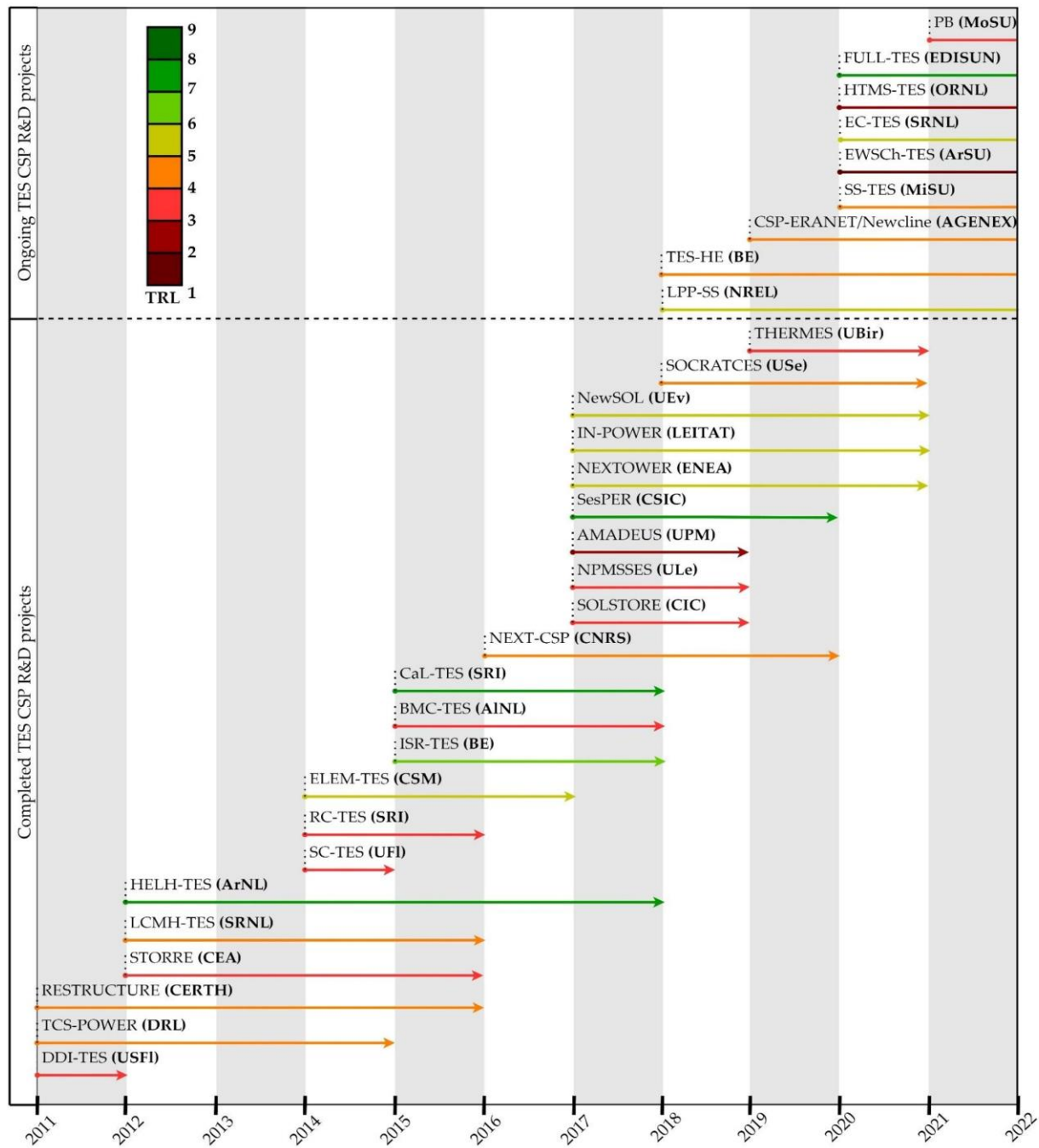
Figure 5. Timeline of TES CSP R&D projects from 2011 to the present.

Table 8. Technical and economical parameters of completed TES CSP R&D projects from 2011.

Project Name Abbreviation	TES CSP Configuration	TES Technology	Storage Size (h)	CSP Technology	HTF	T_{max} [¥] (°C)	Power Block	TRL [§]	LCOE * (€/kWh)	Ref.
TCS-Power	Passive storage	Redox TCES Hydroxide TCES	up to 12	SPT / PTC	Air Molten salts	400–600	Steam Rankine	4–5	0.14 / 0.21	[111]
RESTRUCTURE	Passive storage	Redox TCES	6 to 13	SPT	Air	up to 1000	Air Brayton CC	4–5	<0.15	[112]
STORRE	Active storage direct/indirect 2-tank	Hydroxide TCES	6 to 13	PTC, LFR	HTF = TES or HTF ≠ TES	300–550	Steam Rankine	3–4	-	[113]
CaL-TES	Passive storage	Carbonate TCES	-	SPT	sCO_2	720	Closed loop CO_2	7–8	0.06	[121]
NEXT-CSP	Active storage direct 2-tank	Solid particles SHS	up to 12	SPT	HTF = TES	650–750	Gas turbine, Subcritical steam, Air Brayton	5	0.1	[122–127]
NEXTOWER	Active storage indirect single-tank	Liquid metal SHS	-	SPT	Air	800	Gas turbine	6	-	[133]
IN-POWER	Active storage single-tank & Passive storage	Molten salts SHS & PCM LHS	-	LFR, PTC	Molten salts	600	DSG	6	0.1	[134]
NewSOL	Passive storage / Active storage single-tank & Passive storage	Concrete module / Molten salts SHS & PCM LHS	- / 8	PTC	Ca-ternary molten salt mixture	up to 550	Steam Rankine	5–6	0.1–0.12	[135]
SOCRATCES	Passive storage	Carbonate TCES	days/ months	SPT	HTF = TES	600–1000	Closed-loop CO_2 Brayton	5	0.07	[137]

* Expected LCOE under commercial up-scaling. [§] Expected TRL when project ends. [¥] Maximum temperature achieved in the process from TES to power block.

3.2.2. RESTRUCTURE

The Redox Materials-based Structured Reactors/Heat Exchangers for Thermo-Chemical Heat Storage Systems in Concentrated Solar Power Plants (RESTRUCTURE) research project aimed to develop a new heat transfer mechanism for the redox TCES systems based on monolithic structures, such as honeycombs or foams partially or totally made of redox materials. The STP CSP technology was selected to integrate the redox TCES system, reaching working temperatures of 1000 °C. The associated power block was a Brayton combined cycle (CC) using air as HTF. The projected storage period was between 6 to 13 h, considering an assessment of up-scaling to commercial scale (70.5 MWe). A LCOE below €0.15/kWhth was estimated through a commercial scale analysis. Before the up-scaling assessment, the redox TCES system was tested under pilot scale at Solar Tower Jülich/STJ research platform in Germany (TRL 4–5). The European R&D project launched in 2011 was coordinated by Ethniko Kentro Erevnas kai Technologikis Anaptyxis (CERTH) from Greece [112].

3.2.3. STORRE

The high temperature thermal energy storage by reversible thermochemical reaction (STORRE) research project aimed to develop the integration of a high-density TCES system in LFR and PTC CSP plants. The calcium hydroxide is the TES material, allowing high-working temperatures up to 550 °C and storage capacities of days. The TES CSP configuration selected is 2-tank active storage, being indirect if there is a HTF between the solar field and the TES or direct if the solid particles are heated into a solar receiver. The reactors required to perform de gas–solid reversible reaction of calcium hydroxide were tested at pilot scale (TRL 3–4). The power block for the up-scaling assessment up to commercial scale (85 MWe) was a steam Rankine with a storage capacity of 6 and 13 h. The European R&D project launched in 2012 was coordinated by Commissariat a l'Energie Atomique et aux Energies Alternatives (CEA) from France [113].

3.2.4. CaL-TES

The Demonstration of High-Temperature Calcium-Based Thermochemical Energy Storage System for Use with Concentrating Solar Power Facilities (CaL-TES) research project aimed to develop a low cost TCES system to couple with sCO$_2$ power cycles integrated into SPT CSP plants. A carbonate TCES system based on calcium oxide was selected to achieve high operating temperatures for the power block up to 720 °C. The same packed-bed reactor is used to perform the reversible reaction. Under the endothermic reaction, the HTF transfers heat to the reactor to decompose limestone into CaO and CO$_2$, diverting the gas to storage. The exothermic reaction occurs when CO$_2$ from storage reacts with CaO in the reactor to retrieve the stored energy and to be transferred to the HTF. Thus, the TES cSP configuration is a passive storage, considering (i) molten salts or liquid metal as HTF between the packed-bed reactor and an intermediate heat exchanger and (ii) sCO$_2$ as HTF between the intermediate heat exchanger and the power block. A demonstration up-scaling of 100 MWh will be expected beyond the project (TRL 7–8). The American R&D project launched in 2015 was coordinated by the Southern Research Institute (SRI) [121].

3.2.5. NEXT-CSP

The NEXT-CSP research project (High temperature concentrated solar thermal power plan with particle receiver and direct thermal storage) aimed to validate an industrial pilot plant (TRL5) tested at Thémis SPT experimental facility (France) for integrating new technology in CSP plants. The Centre National de la Recherche Scientifique (CNRS) in France coordinated the European R&D project launched in 2016 [122].

A fluidized particle in-tube concept, first published in 1980, was developed to design the solar receiver (scaling up to 50 MWth per single unit) to heat the TES up to 650–750 °C [123]. The solar receiver with fluidized particle recirculation was previously demonstrated at 150 KW in the CSP2 (Concentrated Solar Power in Particles) research project [124]. Silicon carbide solid particles were used as TES medium and HTF, as two-tank active direct TES CSP configuration. The cold and hot particles tanks were interconnected through a particle-pressurized air fluidized bed heat exchanger [123]. This novel storage configuration was coupled to a gas turbine reaching a power block efficiency of 46% [125]. However, the integration of subcritical steam or air Brayton power cycles also achieved good efficiencies (up to 41% [126] and 39% [127], respectively) with lower energy penalties. Additionally, the integration of supercritical steam or CO$_2$ cycles could minimize energy penalties and cost of the TES CSP plant. For future work, the large-scale facility (>100 MWe) using multiples SPTs will be developed and demonstrated [123].

3.2.6. NEXTOWER

The NEXTOWER research project (Advanced materials solutions for next generation high efficiency concentrated solar power (CSP) tower system) aimed to demonstrate the durability over 20 years of ceramic materials for large CSP air-based SPT (>5 MWe). The air is heated up to 800 °C in the solar receiver and the thermal energy is transferred to an innovative single tank thermocline with liquid metal as TES medium by an air–lead heat exchanger. The TES CSP configuration is an indirect active system using air as HTF. The liquid metal storage material is based on liquid lead stored in new non-corrosive alumina forming steels, which has been transferred from nuclear fission technology. The liquid lead as TES was installed and proved at demo scale TRL 6 (SOLEAD) in *Plataforma Solar de Almería* (Spain). The high temperature achieved by the storage medium extends the thermal applications of CSP plants. Regarding the association of high-temperature power blocks to the CSP plant, the easiest integration would be achieved with working fluids such as compressed gases or supercritical fluids. The European R&D project launched in 2017 was coordinated by Italian National Agency for New Technologies, Energy and Sustainable Economic Development (ENEA) [133].

3.2.7. IN-POWER

The Advanced Materials technologies to QUADRUPLE the Concentrated Solar Thermal current POWER GENERATION (IN-POWER) European R&D project aimed to develop new technology solutions for LFR and PTC CSP plants to improve the efficiency and to minimize the costs. Regarding energy storage, a combination of SHS and LHS media is investigated. The TES CSP configuration is a molten salt (60% $NaNO_3$ and 40% KNO_3) single-tank thermocline active storage with encapsulated PCM (Aluminium silicon). The molten salts act as HTF to the PCM as passive storage TES CSP configuration. This new SHS-LHS hybrid TES system (i) minimizes the charge/discharge cyclical degradation and (ii) maximizes the storage capacity compared to the same volume of a classic molten salts single-tank thermocline system. Thus, the TES system could be reduced and also its cost (LCOE beyond 2020 €0.10/kWh), testing in LFR and PTC pilot plants (TRL 6) for DSG. The European R&D project launched in 2017 was coordinated by Acondicionamiento Tarrasense Asociación (LEITAT) from Spain [134].

3.2.8. NewSOL

The main objective of New StOrage Latent and sensible concept for high efficient CSP Plants (NewSOL) research project is to develop new materials for energy storage in (CSP) plants. Two innovative concrete storage media were investigated for integration into existing or new PTC CSP plants, reaching storage temperatures up to 550 °C. A concrete module tank is proposed as SHS medium for existing CSP plants, using a new Ca-ternary molten salt mixture as HTF circulating inside the embedded pipes (passive storage TES CSP configuration with a storage capacity of 1600 kWh_{th}). Under new CSP plants, a Ca-ternary molten salt single-tank thermocline with concrete walls and encapsulated PCMs is implemented as a SHS and LHS system within an active storage TES CSP configuration, using the new molten salt mixture as HTF for the PCM passive storage medium. Thus, the new thermocline system replaces classic steel walls with cement (i) to minimize cyclic thermocline degradation and (ii) to improve the storage performance. The new SHS-LHS TES system was implemented as a prototype at demo scale (TRL 5–6) in Évora Molten Salts Platform (Portugal), producing 8 additional hours of steam to the associated power block. The NewSOL European R&D project launched in 2017, led by Universidade de Évora (UEv) from Portugal [135].

3.2.9. SOCRATCES

The SOlar Calcium-looping integRAtion for Thermo-Chemical Energy Storage (SOCRATCES) research project focused on reducing the intermittency in electricity production of SPT CSP plants, using the advantages of calcium looping (CaL) compared to other types of technologies used as TCES, such as the low price of $CaCO_3$ (€10/ton) and its wide availability. In addition, the equipment used in the CaL system was previously developed as CO_2 capture technology. Solar energy decomposes limestone into CO_2 and CaO at calciner receiver to be later independently stored, even at ambient temperature. When electric demand is high, the stored products are fed to the carbonator reactor, retrieving thermal energy to the power block. The TES CSP configuration can be considered as passive storage, with heat exchangers needed between the storage tanks and the main reactors. The high working temperatures achieved (600 and 1000 °C) could improve the power block efficiency associated to a SPT CSP plant. Among the power cycles assessed, the best promising option for upscaling the CaL TCES system is the closed-loop CO_2 Brayton cycle, reaching overall efficiencies up to 45%. The CaL TCES system has been tested in the relevant environment at pilot scale (TRL 5). The LCOE expected will be lower than 0.07€/kWh at commercial scale [136]. The European R&D project launched in 2018 was led by University of Seville (USe) from Spain [137].

3.2.10. Other TES CSP R&D Projects (Materials, Concepts, Technology)

Since 2011, TES research projects focused on the development of concepts, materials or heat transfer technologies have also been investigated as an application to CSP plants. Regarding LHS TES systems, different structures to store PCM were researched. The University of South Florida (USFl) from the USA validated at lab scale encapsulated PCM into a packed-bed system as passive storage [110]. Furthermore, Argonne National Laboratory (ArNL) from the USA developed a 2-phase project from lab to demonstration scale to validate PCM using graphite foam to improve its thermal efficiency, infiltrating $MgCl_2$ into the graphite pores [115]. Moreover, the European NPMSSES research project (United Kingdom) researched the introduction of nanoparticles into a PCM (solar salt) to improve its thermo–physical properties at lab scale [130]. Another European R&D project (AMADEUS from Spain) developed synthetic PCM, demonstrating at proof of concept the thermal energy retrieval through a hybrid thermionic–photovoltaic converter to produce electricity [131]. Regarding the application of LHS TES system to low temperature solar fields, the European THERMES R&D project (United Kingdom) developed a microemulsion of PCM to act as HTF and TES at lab scale [138].

Additionally, the main developed TCES technologies were based on two systems: hydride and metal oxides. The Savannah River National Laboratory (SRNL) and Brayton Energy (BE) institutions (USA) validated a metal hydride TCES at bench scale to be integrated into a CSP with an associated high temperature sCO_2 power block [114,119]. Binary metal chalcogenide as TCES system in a modular reactor was developed by Los Alamos National Laboratory (AlNL) from the USA to achieve working temperatures up to 750 °C [120]. Regarding metal oxide systems, the carbonate one was developed at lab and bench scale by University of Florida (UFl) and Southern Research Institute (SRI) from the USA, respectively. The strontium carbonate TCES system reached temperature up to 1000 °C (UFl) [116], while the regenerative carbonate system developed by SRI operated at medium temperature (650–850 °C) [117]. Besides, new TCES materials as perovskites researched by Colorado School of Mines (CSM) from the USA [118] and SesPER R&D project (Spain) [132], achieving high storage temperatures (up to 1200 °C) at advanced TRL 6 to 8. However, new TES similar to SHS system have been developed by SOL-STORE R&D project (Spain), providing extra thermal energy by the enthalpy of a solid-state reaction [128,129].

3.3. Ongoing TES CSP R&D Projects Lauched between 2011–2022

This section gathers the ongoing TES CSP R&D projects launched from 2011 within the European and North American regions. The currently active TES CSP R&D projects focuses on (i) new SHS materials and (ii) the growing use of TCES technology. Table 9 summarized the main relevant data of the current active TES CSP R&D projects since 2011.

The National Renewable Energy Laboratory (NREL), from the USA, promotes a demonstration scale research project (TRL 6) with 2-tank indirect active storage TES CSP configuration, using new molten chloride salts as SHS medium (up to 12 h of storage capacity) and liquid-metal sodium as HTF to achieve a high temperature (740 °C) for the associated power block (sCO_2) to the SPT CSP plant [139]. The new molten chloride salts are also developed by Oak Ridge National Laboratory (ORNL), from the USA, in a single-tank thermocline TES CSP configuration to reduce costs [142]. The thermocline concept will be developed by NEWCLINE (CSP-ERANET) R&D project, using PCM at pilot scale (TRL 5) [141]. The integration of a sCO_2 power cycle is developed in other R&D projects, using as TES (i) composite PCM (Brayton Energy (BE), USA) [140], (ii) multiple TCES to suitably dispatch electricity (Arizona State University (ArSU), USA) [27] or (iii) solid material to be demonstrated at full scale (5 MW), such as packed-bed of rocks (EDISUN (USA)) [27]. Regarding the BE research project, the main objective is to test a new heat exchanger design, given as TES the graphite foam-based PCM developed by ArNL from 2012 to 2018. The development of TCES research projects continues to expand, increasing the working temperature up to 1300 °C with redox reactions (Michigan State

University (MiSU), USA) [27] or improving the storage capacity at ambient temperature of a new molten carbonate mixture (Savannah River National Laboratory (SRNL), USA) [27]. Finally, research on improving the heat transfer efficiency of packed-bed passive storage systems is developed by Montana State University (MoSU), from the USA [27].

Table 9. Technical and economical parameters of active TES CSP R&D projects from 2011.

Project Name Abbreviation	TES CSP Configuration	TES Technology	CSP Technology	T_{max} [¥] (°C)	Power Block	TRL [§]	LCOE * (€/kWh)	Ref.
LPP-SS	Active storage (2-tank indirect)	Molten chloride salts SHS	SPT	740	sCO$_2$	6	0.06	[139]
TES-HE	Passive storage	PCM LHS	SPT	>700	sCO$_2$	5	-	[140]
CSP-ERANET (Newcline)	Active storage indirect single-tank & Passive storage	Ceramics/PCM LHS	PTC, SPT	-	-	5	-	[141]
SS-TES	Passive storage	Redox TCES	-	up to 1300	-	5	-	[27]
EWSCh-TES	Passive storage	Multiple TCES	-	-	sCO$_2$	1–2	-	[27]
EC-TES	Passive storage	Carbonate TCES	-	-	-	5–6	-	[27]
HTMS-TES	Active storage indirect single-tank	Chloride salts SHS	-	-	More-efficient	3	-	[142]
FULL-TES	Passive storage packed-bed	Rocks SHS	SPT	600	sCO$_2$	7–8	<0.05	[27]
PB	Passive storage packed-bed	SHS	-	-	-	3–4	-	[27]

* Expected LCOE under commercial up-scaling. [§] Expected TRL when project ends. [¥] Maximum temperature achieved in the process from TES to power block.

4. Discussion and Conclusions

The problem of intermittency in energy production associated to the CSP facilities will only be solved by increasing the use of TES. More than a half of the currently operating CSP facilities have a TES system, mainly based on molten salts SHS medium. Despite molten salts having a high TRL for high-temperature applications, natural rocks will be a promising SHS medium given their low storage cost. Within LHS systems, high-temperature PCM has been tested in the operational environment, being one of the potential TES systems when its heat transfer ratio and storage cost are improved. Regarding the TCES system, issues such as the reactor design and the reaction control are being investigated at TRL 4. When a greater development of the chemical reactions involving TCES is reached, a lower storage cost is expected even below SHS and LHS materials.

Almost all of the European and North American TES CSP R&D projects completed before 2011 implemented the conventional configuration related to the first and second generation of CSP plants associated with a steam Rankine power block, including (i) molten salts as TES, (ii) thermal oil as HTF and (iii) PTC technology in solar fields. Firstly, even though LCOE of PTC technology is one of the highest, its advantageous properties proven on a commercial scale will boost its leadership in the CSP market. Secondly, despite the 2-tank indirect active storage system being the most commercially extended, the steam accumulator format within the active direct storage system allows direct use of steam generated in the solar field for storage and production of electrical energy through the steam power cycle. Moreover, savings of 35% of the cost of the TES system can be achieved by using a single tank. The major issue of the active storage systems are the limitations associated with the media currently used in commercial CSP plants, such as the high freezing point of common molten salts, the low thermal conductivity of water, as well as the high costs of conventional molten salts and pressurized water storage tanks. Thus, the R&D projects launched after 2011 in Europe and North America developed new TES, using TES CSP configurations based on passive storage and single tank thermocline active storage to minimize the LCOE of the CSP facilities, being able to use low-cost materials and achieving better heat transfer. Furthermore, one of the most important advantages is the inclusion of a thermocline system in the passive storage using molten salts and PCM, leading to a new storage configuration with lower LCOE. Regarding HTF, the use of TES as HTF or even air is advantageous over the use of conventional molten salts, minimizing the costs of electricity production. Nevertheless, since there is a high number of R&D projects with

high-temperature TCES storage systems, the associated CSP technologies are mainly based on SPT and PTC. One of the limitations of high-temperature TCES storage systems focuses on the development of materials that can withstand these working temperatures. The USA and Spain are the leading countries in the implementation of research projects related to the integration of TES in CSP facilities with an associated power cycle for large-scale electricity production. Their great track record of technology development in CSP plants endorses both countries, accounting for almost 60% of the currently operating CSP plants.

Regarding SHS media, new molten salts allow to achieve operating temperatures up to 740 °C. In addition, novel storage media based on liquid metal or solids (i.e., particles or rocks) begin to develop from pilot to sub-commercial scale at the STP CSP plants. Similarly, the combination of SHS and LHS within LFR and PTC CSP facilities are under development at demo scale. The LHS system using different PCMs could increase the thermal energy that could be stored. Furthermore, new lab-scale research based on introducing nanoparticles improves the thermophysical properties of the PCM. The TCES-based R&D projects extended are related to hydroxide, carbonate and redox TCES systems, reaching working temperatures up to 1000 °C and a level of development from demo to sub-commercial scale.

The TCES systems have been the most investigated TES technologies in the last decade, given the low cost of the storage medium and the high temperatures achieved when retrieving the stored thermal energy. Thus, new high-temperature power blocks can be implemented into the TES CSP facilities to improve the overall plant efficiency, such as Brayton or supercritical CO_2 cycles. The main objective of the largest budget allocated to an ongoing TES CSP R&D project is to develop the sCO_2 power cycle associated with CSP plants on a commercial scale.

5. Future Directions

The next steps of research in TES CSP integration in the near future will be focused on the upscaling, from demo to commercial stage, the SPT and PTC CSP facilities, using (i) high energy density, low-cost TES materials for larger storage time with minimal energy losses (i.e., solid SHS as passive storage, combination of liquid SHS and PCM as LHS medium, carbonate or redox TCES systems) and (ii) high efficiency power blocks (i.e., supercritical or Brayton) to even minimize the LCOE of the CSP facility below 0.05 €/kWh. Solid particles or packed-beds of rocks, with SHS as passive storage, may be able to reduce the investment cost of the CSP facility. Among LHS systems, the newly developed PCMs together with the use of new low-freezing point molten salts will set a new configuration between the passive and active system, minimizing the storage size and therefore associated costs. Notably, the TCES systems will grow exponentially, leading the conversion of CSP facilities to base-load plants with safe and uninterrupted electricity production.

Nomenclature

Symbols

a	fraction reacted, -
c	specific heat, J/kg·K
f	melt fraction, -
m	mass of storage medium, kg
Q	heat, J
T	temperature, °C
ΔH	heat of reaction, J/kg
Δq	latent heat of fusion, J/kg

Subscripts and superscripts

f	final
I	initial
m	melting
max	maximum
out	outlet
p	constant pressure
pl	liquid phase
ps	solid phase
r	reaction
s	storage/stored

Acronyms and abbreviations

CC	Combined Cycle
CORDIS	Community Research and Development Information Service
CSP	Concentrating Solar Power
GHG	Greenhouse Gases
HT	Heat Transfer
HTF	Heat Transfer Fluid
IPCC	Intergovernmental Panel on Climate Change
LCOE	Levelized Cost Of Electricity
LFR	Linear Fresnel Reflectors
LHS	Latent Heat Storage
PDC	Parabolic Dish Collectors
PMCs	Phase Change Materials
PTC	Parabolic Trough Collectors
RES	Renewable Energy Sources
R&D	Research and Development
sCO_2	Supercritical CO_2
SETO	Solar Energy Technologies Office
SHS	Sensible Heat Storage
SPT	Solar Power Towers
TCES	Thermochemical Energy Storage
TES	Thermal Energy Storage
TRL	Technology Readiness Level
USA	United States of America

Appendix A. List of R&D Projects, Co-Ordinators and Abbreviations

Table A1. List of R&D projects name and abbreviations.

Abbreviation	Project Name
AMADEUS	Next GenerAtion MateriAls and Solid State DevicEs for Ultra High Temperature Energy Storage and Conversion
BMC-TES	Binary Metal Chalcogenides for High Temperature Thermal Storage
CaL-TES	Demonstration of High-Temperature Calcium-Based Thermochemical Energy Storage System for Use with Concentrating Solar Power Facilities

Table A1. *Cont.*

Abbreviation	Project Name
CSP-ERANET (Newcline)	Advanced thermocline concepts for thermal energy storage for CSP
DDI-TES	Development and Demonstration of an Innovative Thermal Energy Storage System for Baseload Power Generation
EC-TES	Eutectic Carbonates for Low Cost-Efficient Thermochemical Heat Storage System
ELEM-TES	Efficiently Leveraging Equilibrium Mechanisms for Engineering New Thermochemical Storage
EWSCh-TES	Economic Weekly and Seasonal Thermochemical and Chemical Energy Storage for Advanced Power Cycles
FULL-TES	Development, Build and Operation of a Full-Scale, Nominally 5MWe, Supercritical Carbon Dioxide Power Cycle Coupled with Solid Media Energy Storage
HELH-TES	High Efficiency Latent Heat Based Thermal Energy Storage System Compatible with Supercritical Carbon Dioxide Power Cycle
HTMS-TES	Simplified High-Temperature Molten Salt Concentrating Solar Power Plant Preconceptual Design
IN-POWER	Advanced Materials technologies to QUADRUPLE the Concentrated Solar Thermal current POWER GENERATION
ISR-TES	Integrated Solar Receiver with Thermal Storage for an sCO_2 Power Cycle
LMMH-TES	Low-Cost Metal Hydride Thermal Energy Storage System for Concentrating Solar-Thermal Power Systems
LPP-SS	Liquid-Phase Pathway to SunShot
NewSOL	New StOrage Latent and sensible concept for high efficient CSP Plants
NEXT-CSP	High Temparature concentrated solar thermal power plan with particle receiver and direct thermal storage
NEXTOWER	Advanced materials solutions for next generation high efficiency concentrated solar power (CSP) tower systems
NPMSSES	Nanoparticle Enhanced Molten Salts for Solar Energy Storage
PB	Efficient Thermal Energy Storage with Radial Flow in Packed Beds
RC-TES	Regenerative Carbonate-Based Thermochemical Energy Storage System for Concentrating Solar Power
RESTRUCTURE	Redox Materials-based Structured Reactors/Heat Exchangers for Thermo-Chemical Heat Storage Systems in Concentrated Solar Power Plants
SC-TES	Carbon Dioxide Shuttling Thermochemical Storage Using Strontium Carbonate
SesPER	Solar Energy Storage PERovskites
SOCRATCES	SOlar Calcium-looping integRAtion for Thermo-Chemical Energy Storage
SOLSTORE	Solid-state reactions for thermal energy storage
SS-TES	Solid State Solar Thermochemical Fuel for Long-Duration Storage
STORRE	High temperature thermal energy Storage by Reversible thermochemical Reaction
TCS-Power	Thermochemical Energy Storage for Concentrated Solar Power Plants
TES-HE	Integrated Thermal Energy Storage Heat Exchanger for Concentrating Solar Power Applications
THERMES	A new generation high temperature phase change microemulsion for latent thermal energy storage in dual loop solar field

Table A2. List of R&D project coordinators and abbreviations.

Abbreviation	Project Coordinator
AGENEX	Agencia Extremeña de la Energía
AlNL	Los Alamos National Laboratory
ArNL	Argonne National Laboratory
ArSU	Arizona State University
BE	Brayton Energy
CEA	Commissariat a l'Energie Atomique et aux Energies Alternatives
CERTH	Ethniko Kentro Erevnas kai Technologikis Anaptyxis
CIC	Centro de Investigación Cooperativa de Energías Alternativas
CNRS	Centre National de la Recherche Scientifique
CSIC	Agencia Estatal Consejo Superior de Investigaciones Científicas
CSM	Colorado School of Mines
DRL	Deutsches Zentrum für Luft-und Raumfahrt e.V.
EDISUN	Edisun

Table A2. *Cont.*

Abbreviation	Project Coordinator
ENEA	Italian National Agency for New Technologies, Energy and Sustainable Economic Development
LEITAT	Acondicionamiento Tarrasense Asociación
MiSU	Michigan State University
MoSU	Montana State University
NREL	National Renewable Energy Laboratory
ORNL	Oak Ridge National Laboratory
SRI	Southern Research Institute
SRNL	Savannah River National Laboratory
UBir	University of Birmingham
UEv	Universidade de Évora
UFl	University of Florida
ULe	Univertisty of Leeds
UPM	Universidad Politécnica de Madrid
USe	Universidad de Sevilla
USFl	University of South Florida

References

1. IPCC. *Climate Change 2022: Mitigation of Climate Change. Contribution of Working Group III to the Sixth Assessment Report of the Intergovernmental Panel on Climate Change*; Shukla, P.R., Skea, J., Slade, R., Al Khourdajie, A., van Diemen, R., McCollum, D., Pathak, M., Some, S., Vyas, P., Fradera, R., et al., Eds.; Cambridge University Press: Cambridge UK; New York, NY, USA, 2022.
2. Renewables 2022. *Global Status Report*; Zervos, A., Adib, R., Eds.; REN21 Secretariat: Paris, France, 2022; ISBN 978-3-948393-04-5.
3. Morante, J.R. *El Almacenamiento de Electricidad—Fundación Gas Natural Fenosa*; Fundación Gas Natural Fenosa, Ed.; Fundación Gas Natural Fenosa: Barcelona, Spain, 2014; ISBN 9788469598979.
4. Peón Menendez, R. *Optimización del Control del Sistema de Almacenamiento Térmico en Centrales Solares Termoeléctricas*; Universidad de Oviedo: Oviedo, Spain, 2012.
5. Kunwer, R.; Pandey, S.; Pandey, G. Technical Challenges and Their Solutions for Integration of Sensible Thermal Energy Storage with Concentrated Solar Power Applications—A Review. *Process Integr. Optim. Sustain.* **2022**, *6*, 559–585. [CrossRef]
6. International Renewable Energy Agency (IRENA). *Innovation Outlook: Thermal Energy Storage*; International Renewable Energy Agency (IRENA): Abu Dhabi, United Arab Emirates, 2020; ISBN 978-92-9260-279-6.
7. Goyal, N.; Aggarwal, A.; Kumar, A. Concentrated solar power plants: A critical review of regional dynamics and operational parameters. *Energy Res. Soc. Sci.* **2022**, *83*, 102331. [CrossRef]
8. Kraemer, S. CSP Doesn't Compete with PV—It Competes with Gas. Available online: Solarpaces.org/csp-competes-with-natural-gas-not-pv/ (accessed on 1 July 2022).
9. Cabeza, L.F.; de Gracia, A.; Zsembinszki, G.; Borri, E. Perspectives on thermal energy storage research. *Energy* **2021**, *231*, 120943. [CrossRef]
10. Islam, T.; Huda, N.; Abdullah, A.B.; Saidur, R. A comprehensive review of state-of-the-art concentrating solar power (CSP) technologies: Current status and research trends. *Renew. Sustain. Energy Rev.* **2018**, *91*, 987–1018. [CrossRef]
11. Achkari, O.; El Fadar, A. Latest developments on TES and CSP technologies—Energy and environmental issues, applications and research trends. *Appl. Therm. Eng.* **2020**, *167*, 114806. [CrossRef]
12. Shahabuddin, M.; Alim, M.A.; Alam, T.; Mofijur, M.; Ahmed, S.F.; Perkins, G. A critical review on the development and challenges of concentrated solar power technologies. *Sustain. Energy Technol. Assess.* **2021**, *47*, 101434. [CrossRef]
13. Calderón, A.; Barreneche, C.; Prieto, C.; Segarra, M.; Fernández, A.I. Concentrating Solar Power Technologies: A Bibliometric Study of Past, Present and Future Trends in Concentrating Solar Power Research. *Front. Mech. Eng.* **2021**, *7*, 682592. [CrossRef]
14. Palacios, A.; Barreneche, C.; Navarro, M.E.; Ding, Y. Thermal energy storage technologies for concentrated solar power—A review from a materials perspective. *Renew. Energy* **2020**, *156*, 1244–1265. [CrossRef]
15. Alnaimat, F.; Rashid, Y. Thermal energy storage in solar power plants: A review of the materials, associated limitations, and proposed solutions. *Energies* **2019**, *12*, 4164. [CrossRef]
16. Calderón, A.; Palacios, A.; Barreneche, C.; Segarra, M.; Prieto, C.; Rodriguez-Sanchez, A.; Fernández, A.I. High temperature systems using solid particles as TES and HTF material: A review. *Appl. Energy* **2018**, *213*, 100–111. [CrossRef]
17. El Alami, K.; Asbik, M.; Agalit, H. Identification of natural rocks as storage materials in thermal energy storage (TES) system of concentrated solar power (CSP) plants—A review. *Sol. Energy Mater. Sol. Cells* **2020**, *217*, 110599. [CrossRef]
18. Opolot, M.; Zhao, C.; Liu, M.; Mancin, S.; Bruno, F. A review of high temperature ($\geq$ 500 °C) latent heat thermal energy storage. *Renew. Sustain. Energy Rev.* **2022**, *160*, 112293. [CrossRef]

19. Liu, M.; Omaraa, E.S.; Qi, J.; Haseli, P.; Ibrahim, J.; Sergeev, D.; Müller, M.; Bruno, F.; Majewski, P. Review and characterisation of high-temperature phase change material candidates between 500 C and 700 °C. *Renew. Sustain. Energy Rev.* **2021**, *150*, 111528. [CrossRef]

20. André, L.; Abanades, S. Recent Advances in Thermochemical Energy Storage via Solid–Gas Reversible Reactions at High Temperature. *Energies* **2020**, *13*, 5859. [CrossRef]

21. Carrillo, A.J.; González-Aguilar, J.; Romero, M.; Coronado, J.M. Solar Energy on Demand: A Review on High Temperature Thermochemical Heat Storage Systems and Materials. *Chem. Rev.* **2019**, *119*, 4777–4816. [CrossRef] [PubMed]

22. Zsembinszki, G.; Solé, A.; Barreneche, C.; Prieto, C.; Fernández, A.; Cabeza, L. Review of Reactors with Potential Use in Thermochemical Energy Storage in Concentrated Solar Power Plants. *Energies* **2018**, *11*, 2358. [CrossRef]

23. Alva, G.; Lin, Y.; Fang, G. An overview of thermal energy storage systems. *Energy* **2018**, *144*, 341–378. [CrossRef]

24. Pelay, U.; Luo, L.; Fan, Y.; Stitou, D.; Rood, M. Thermal energy storage systems for concentrated solar power plants. *Renew. Sustain. Energy Rev.* **2017**, *79*, 82–100. [CrossRef]

25. Concentrating Solar Power Projects. National Renewable Energy Laboratory. Available online: https://solarpaces.nrel.gov/projects (accessed on 1 July 2022).

26. CORDIS. EU Research Results. European Commission. Available online: https://cordis.europa.eu/projects/en (accessed on 15 July 2022).

27. Solar Energy Research Database. Solar Energy Technologies Office. U.S. Department of Energy. Available online: https://www.energy.gov/eere/solar/solar-energy-research-database (accessed on 15 July 2022).

28. Teske, S.; Leung, J. *Solar Thermal Electricity—Global Outlook 2016*; Rochon, E., Ed.; Greenpeace International: Amsterdam, The Netherlands; European Solar Thermal Electricity Association (ESTELA): Bruxelles, Belgium; SolarPACES Secretariate: Almeria, Spain, 2016.

29. Pavlovic, T.; Radonjic, I. A review of concentrating solar power plants in the world and their potential use in Serbia. *Renew. Sustain. Energy Rev.* **2012**, *16*, 12. [CrossRef]

30. Chacartegui, R.; Alovisio, A.; Ortiz, C.; Valverde, J.M.; Verda, V.; Becerra, J.A. Thermochemical energy storage of concentrated solar power by integration of the calcium looping process and a CO_2 power cycle. *Appl. Energy* **2016**, *173*, 589–605. [CrossRef]

31. Ortiz, C.; Chacartegui, R.; Valverde, J.M.; Alovisio, A.; Becerra, J.A. Power cycles integration in concentrated solar power plants with energy storage based on calcium looping. *Energy Convers. Manag.* **2017**, *149*, 815–829. [CrossRef]

32. Tesio, U.; Guelpa, E.; Verda, V. Integration of thermochemical energy storage in concentrated solar power. Part 2: Comprehensive optimization of supercritical CO_2 power block. *Energy Convers. Manag.* **2020**, *6*, 100038. [CrossRef]

33. Arias, I.; Cardemil, J.; Zarza, E.; Valenzuela, L.; Escobar, R. Latest developments, assessments and research trends for next generation of concentrated solar power plants using liquid heat transfer fluids. *Renew. Sustain. Energy Rev.* **2022**, *168*, 112844. [CrossRef]

34. Barlev, D.; Vidu, R.; Stroeve, P. Innovation in concentrated solar power. *Sol. Energy Mater. Sol. Cells* **2011**, *95*, 2703–2725. [CrossRef]

35. Wagner, S.J.; Rubin, E.S. Economic implications of thermal energy storage for concentrated solar thermal power. *Renew. Energy* **2014**, *61*, 81–95. [CrossRef]

36. Kuravi, S.; Trahan, J.; Goswami, D.Y.; Rahman, M.M.; Stefanakos, E.K. Thermal energy storage technologies and systems for concentrating solar power plants. *Prog. Energy Combust. Sci.* **2013**, *39*, 285–319. [CrossRef]

37. Dizaji, H.B.; Hosseini, H. A review of material screening in pure and mixed-metal oxide thermochemical energy storage (TCES) systems for concentrated solar power (CSP) applications. *Renew. Sustain. Energy Rev.* **2018**, *98*, 9–26. [CrossRef]

38. Nazir, H.; Batool, M.; Bolivar, F.J.; Isaza-ruiz, M.; Xu, X.; Vignarooban, K.; Phelan, P.; Kannan, A.M. Recent developments in phase change materials for energy storage applications: A review. *Int. J. Heat Mass Transf.* **2019**, *129*, 491–523. [CrossRef]

39. Liu, C.; Rao, Z. Challenges in various thermal energy storage technologies. *Sci. Bull.* **2017**, *62*, 231–233. [CrossRef]

40. Chen, X.; Zhang, Z.; Qi, C.; Ling, X.; Peng, H. State of the art on the high-temperature thermochemical energy storage systems. *Energy Convers. Manag.* **2018**, *177*, 792–815. [CrossRef]

41. Sarbu, I.; Sebarchievici, C. A Comprehensive Review of Thermal Energy Storage. *Sustainability* **2018**, *10*, 191. [CrossRef]

42. Kumar, A.; Shukla, S.K. A Review on Thermal Energy Storage Unit for Solar Thermal Power Plant Application. *Energy Procedia* **2015**, *74*, 462–469. [CrossRef]

43. Khare, S.; Dell'Amico, M.; Knight, C.; McGarry, S. Selection of materials for high temperature sensible energy storage. *Sol. Energy Mater. Sol. Cells* **2013**, *115*, 114–122. [CrossRef]

44. Tiddens, A.; Röger, M.; Stadler, H.; Hoffschmidt, B. Air return ratio measurements at the solar tower Jülich using a tracer gas method. *Sol. Energy* **2017**, *146*, 351–358. [CrossRef]

45. Gil, A.; Medrano, M.; Martorell, I.; Lázaro, A.; Dolado, P.; Zalba, B.; Cabeza, L.F. State of the art on high temperature thermal energy storage for power generation. Part 1-Concepts, materials and modellization. *Renew. Sustain. Energy Rev.* **2010**, *14*, 31–55. [CrossRef]

46. Aggarwal, A.; Goyal, N.; Kumar, A. Thermal characteristics of sensible heat storage materials applicable for concentrated solar power systems. *Mater. Today Proc.* **2021**, *47*, 5812–5817. [CrossRef]

47. El Alami, K.; Asbik, M.; Boualou, R.; Ouchani, F.-Z.; Agalit, H.; Bennouna, E.G.; Rachidi, S. A critical overview of the suitability of natural Moroccan rocks for high temperature thermal energy storage applications: Towards an effective dispatching of concentrated solar power plants. *J. Energy Storage* **2022**, *50*, 104295. [CrossRef]

48. Gutierrez, A.; Miró, L.; Gil, A.; Rodríguez-Aseguinolaza, J.; Barreneche, C.; Calvet, N.; Py, X.; Inés Fernández, A.; Grágeda, M.; Ushak, S.; et al. Advances in the valorization of waste and by-product materials as thermal energy storage (TES) materials. *Renew. Sustain. Energy Rev.* **2016**, *59*, 763–783. [CrossRef]

49. Ortega-Fernández, I.; Calvet, N.; Gil, A.; Rodríguez-Aseguinolaza, J.; Faik, A.; D'Aguanno, B. Thermophysical characterization of a by-product from the steel industry to be used as a sustainable and low-cost thermal energy storage material. *Energy* **2015**, *89*, 601–609. [CrossRef]

50. Al-Azawii, M.M.S.; Alhamdi, S.F.H.; Braun, S.; Hoffmann, J.F.; Calvet, N.; Anderson, R. Experimental study on packed-bed thermal energy storage using recycled ceramic as filler materials. *J. Energy Storage* **2021**, *44*, 103375. [CrossRef]

51. Bradshaw, R.W.; Siegel, N.P. Molten nitrate salt development for thermal energy storage in parabolic trough solar power systems. In Proceedings of the ASME 2008 2nd International Conference on Energy Sustainability, Jacksonville, FL, USA, 10–14 August 2008; Volume 2, pp. 631–637.

52. Peng, Q.; Wei, X.; Ding, J.; Yang, J.; Yang, X. High-temperature thermal stability of molten salt materials. *Int. J. Energy Res.* **2008**, *32*, 1164–1174. [CrossRef]

53. Zhao, C.Y.; Wu, Z.G. Thermal property characterization of a low melting-temperature ternary nitrate salt mixture for thermal energy storage systems. *Sol. Energy Mater. Sol. Cells* **2011**, *95*, 3341–3346. [CrossRef]

54. Vignarooban, K.; Xu, X.; Arvay, A.; Hsu, K.; Kannan, A.M. Heat transfer fluids for concentrating solar power systems—A review. *Appl. Energy* **2015**, *146*, 383–396. [CrossRef]

55. Caraballo, A.; Galán-Casado, S.; Caballero, Á.; Serena, S. Molten salts for sensible thermal energy storage: A review and an energy performance analysis. *Energies* **2021**, *14*, 1197. [CrossRef]

56. Ding, W.; Bauer, T. Progress in Research and Development of Molten Chloride Salt Technology for Next Generation Concentrated Solar Power Plants. *Engineering* **2021**, *7*, 334–347. [CrossRef]

57. Aljaerani, H.A.; Samykano, M.; Saidur, R.; Pandey, A.K.; Kadirgama, K. Nanoparticles as molten salts thermophysical properties enhancer for concentrated solar power: A critical review. *J. Energy Storage* **2021**, *44*, 103280. [CrossRef]

58. Pistocchini, L.; Size, P.M.; Plant, P.; Motta, M.; Lambruschini, V. Feasibility Study of an Innovative Dry-Cooling System With Phase-Change Material Storage for Concentrated Solar. *Sol. Energy Eng.* **2011**, *133*, 031010. [CrossRef]

59. González-Roubaud, E.; Pérez-Osorio, D.; Prieto, C. Review of commercial thermal energy storage in concentrated solar power plants: Steam vs. molten salts. *Renew. Sustain. Energy Rev.* **2017**, *80*, 133–148. [CrossRef]

60. CMI Solar. *Khi Solar One South Africa 50 MW CMI 's First Thermo Solar Receiver*; CMI-Abengoa Solar, Ed.; CMI Solar: Seraing, Belgium, 2016.

61. Serge, E.; Edem, K.; Tsoukpoe, N.; Ouédraogo, I.W.K.; Coulibaly, Y.; Py, X.; Marie, F.; Ouédraogo, A.W. Energy for Sustainable Development Jatropha curcas crude oil as heat transfer fl uid or thermal energy storage material for concentrating solar power plants. *Energy Sustain. Dev.* **2017**, *40*, 59–67. [CrossRef]

62. Molina, S.; Haillot, D.; Deydier, A.; Bedecarrats, J. Material screening and compatibility for thermocline storage systems using thermal oil. *Appl. Therm. Eng.* **2018**, *146*, 252–259. [CrossRef]

63. Bruch, A.; Molina, S.; Esence, T.; Couturier, R.; Molina, S.; Esence, T.; Couturier, R. Experimental investigation of cycling behaviour of pilot-scale thermal oil packed-bed thermal storage system. *Renew. Energy* **2016**, *103*, 277–285. [CrossRef]

64. EASE/EERA. European Energy Storage Technology Development Roadmap towards 2030. 2017. Available online: https://eera-es.eu/wp-content/uploads/2016/03/EASE-EERA-Storage-Technology-Development-Roadmap-2017-HR.pdf (accessed on 11 September 2022).

65. Jodeiri, A.M.; Orozco, C. *Thermal Energy Storage in CSP Technologies: From Commercialized to Innovative Solutions*; Technical Report; French National Centre for Scientific Research: Paris, France, 2018. [CrossRef]

66. Tofani, K.; Tiari, S. Nano-enhanced phase change materials in latent heat thermal energy storage systems: A review. *Energies* **2021**, *14*, 3821. [CrossRef]

67. Kasaeian, A.; Pourfayaz, F.; Khodabandeh, E. Experimental studies on the applications of PCMs and nano-PCMs in buildings: A critical review. *Energy Build.* **2017**, *154*, 96–112. [CrossRef]

68. Xu, B.; Li, P.; Chan, C. Application of phase change materials for thermal energy storage in concentrated solar thermal power plants: A review to recent developments. *Appl. Energy* **2015**, *160*, 286–307. [CrossRef]

69. Konuklu, Y.; Şahan, N.; Paksoy, H. 2.14 Latent Heat Storage Systems. In *Comprehensive Energy Systems*; Elsevier: Amsterdam, The Netherlands, 2018; Volume 2, pp. 396–434. ISBN 9780128095973.

70. Reddy, K.S.; Mudgal, V.; Mallick, T.K. Review of latent heat thermal energy storage for improved material stability and effective load management. *J. Energy Storage* **2018**, *15*, 205–227. [CrossRef]

71. Crespo, A.; Barreneche, C.; Ibarra, M.; Platzer, W. Latent thermal energy storage for solar process heat applications at medium-high temperatures—A review. *Sol. Energy* **2018**, *192*, 3–34. [CrossRef]

72. Sharma, S.D. Latent heat storage materials and systems: A review. *Int. J. Green Energy* **2005**, *2*, 1–56. [CrossRef]

73. Saha, S.; Ruslan, A.R.M.; Monjur Morshed, A.K.M.; Hasanuzzaman, M. Global prospects and challenges of latent heat thermal energy storage: A review. *Clean Technol. Environ. Policy* **2021**, *23*, 531–559. [CrossRef]

74. Mumtaz, M.; Khan, A.; Saidur, R.; Al-sulaiman, F.A. A review for phase change materials (PCMs) in solar absorption refrigeration systems. *Renew. Sustain. Energy Rev.* **2017**, *76*, 105–137. [CrossRef]

75. Kenisarin, M.M. High-temperature phase change materials for thermal energy storage. *Renew. Sustain. Energy Rev.* **2010**, *14*, 955–970. [CrossRef]
76. Ge, H.; Li, H.; Mei, S.; Liu, J. Low melting point liquid metal as a new class of phase change material: An emerging frontier in energy area. *Renew. Sustain. Energy Rev.* **2013**, *21*, 331–346. [CrossRef]
77. Luo, L.; Le Pierrès, N. Chapter 3—Innovative Systems for Storage of Thermal Solar Energy in Buildings. In *Solar Energy Storage*; Academic Press: Cambridge, MA, USA; Elsevier: Amsterdam, The Netherlands, 2015; pp. 27–62. ISBN 9780124095403.
78. Sharma, A.; Tyagi, V.V.; Chen, C.R.; Buddhi, D. Review on thermal energy storage with phase change materials and applications. *Renew. Sustain. Energy Rev.* **2009**, *13*, 318–345. [CrossRef]
79. Su, W.; Darkwa, J.; Kokogiannakis, G. Review of solid—Liquid phase change materials and their encapsulation technologies. *Renew. Sustain. Energy Rev.* **2015**, *48*, 373–391. [CrossRef]
80. Nomura, T.; Akiyama, T. High-temperature latent heat storage technology to utilize exergy of solar heat and industrial exhaust heat. *Int. J. Energy Res.* **2016**, *41*, 240–251. [CrossRef]
81. Michels, H.; Pitz-paal, R. Cascaded latent heat storage for parabolic trough solar power plants. *Sol. Energy* **2007**, *81*, 829–837. [CrossRef]
82. Bhale, P.V.; Rathod, M.K.; Sahoo, L. Thermal analysis of a solar concentrating system integrated with sensible and latent heat storage. *Energy Procedia* **2015**, *75*, 2157–2162. [CrossRef]
83. Bayón, R.; Rojas, E.; Valenzuela, L.; Zarza, E.; León, J. Analysis of the experimental behaviour of a 100 kW th latent heat storage system for direct steam generation in solar thermal power plants. *Appl. Therm. Eng.* **2010**, *30*, 2643–2651. [CrossRef]
84. Garcia, P.; Olcese, M.; Rougé, S. Experimental and numerical investigation of a pilot scale latent heat thermal energy storage for CSP power plant. *Energy Procedia* **2015**, *69*, 842–849. [CrossRef]
85. Alhuyi Nazari, M.; Maleki, A.; Assad, M.E.H.; Rosen, M.A.; Haghighi, A.; Sharabaty, H.; Chen, L. A review of nanomaterial incorporated phase change materials for solar thermal energy storage. *Sol. Energy* **2021**, *228*, 725–743. [CrossRef]
86. Pardo, P.; Deydier, A.; Anxionnaz-minvielle, Z.; Rougé, S.; Cabassud, M.; Cognet, P. A review on high temperature thermochemical heat energy storage. *Renew. Sustain. Energy Rev.* **2014**, *32*, 591–610. [CrossRef]
87. Liu, D. Progress in thermochemical energy storage for concentrated solar power: A review. *Int. J. Energy Res.* **2018**, *42*, 4546–4561. [CrossRef]
88. Estado de las Tecnologías de Almacenamiento. *Resumen Ejecutivo*; Grupo Interplataformas de Almacenamiento (GIA), Ed.; International Telecommunication Union: Geneva, Switzerland, 2016.
89. Bellan, S.; Kodama, T.; Gokon, N.; Matsubara, K. A review on high-temperature thermochemical heat storage: Particle reactors and materials based on solid–gas reactions. *WIREs Energy Environ.* **2022**, *11*, e440. [CrossRef]
90. Alvarez Barcia, L. *Optimizacion del Control del Sistema de Aceite Termico en Centrales Solares Termoeletricas*; Universidad de Oviedo: Oviedo, Spain, 2015.
91. Nie, F.; Bai, F.; Wang, Z.; Li, X.; Yang, R. Solid particle solar receivers in the next-generation concentrated solar power plant. *EcoMat* **2022**, *4*, e12207. [CrossRef]
92. Ortega-Fernández, I.; Hernández, A.B.; Wang, Y.; Bielsa, D. Performance assessment of an oil-based packed bed thermal energy storage unit in a demonstration concentrated solar power plant. *Energy* **2021**, *217*, 119378. [CrossRef]
93. Basildo Garcia, J.A. Balance de explotación de la Planta Termosolar Puerto Errado 2. Conferencia y ponencias invitadas. In Proceedings of the III Encuentro de Ingeniería de la Energía del Campus Mare Nostrum, Murcia, Spain, 27 September 2016.
94. Maccari, A.; Bissi, D.; Casubolo, G.; Guerrini, F.; Lucatello, L.; Luna, G.; Rivaben, A.; Savoldi, E.; Tamano, S.; Zuanella, M. Archimede Solar Energy molten salt parabolic trough demo plant: A step ahead towards the new frontiers of CSP. *Energy Procedia* **2015**, *69*, 1643–1651. [CrossRef]
95. Kong, L.; Chen, X.; Gong, J.; Fan, D.; Wang, B.; Li, S. Optimization of the hybrid solar power plants comprising photovoltaic and concentrating solar power using the butterfly algorithm. *Energy Convers. Manag.* **2022**, *257*, 115310. [CrossRef]
96. Romero, M.; González-Aguilar, J. 7—Next generation of liquid metal and other high-performance receiver designs for concentrating solar thermal (CST) central tower systems. In *Advances in Concentrating Solar Thermal Research and Technology*; Blanco, M.J., Santigosa, L.R., Eds.; Woodhead Publishing Series in Energy; Elsevier: Amsterdam, The Netherlands, 2017; pp. 129–154. ISBN 9780081005163.
97. Zhu, Z.; Zhang, D.; Mischke, P.; Zhang, X. Electricity generation costs of concentrated solar power technologies in China based on operational plants. *Energy* **2015**, *89*, 65–74. [CrossRef]
98. Platzer, W.J.; Mills, D.; Gardner, W. Chapter 6—Linear Fresnel Collector (LFC) solar thermal technology. In *Concentrating Solar Power Technology*, 2nd ed.; Lovegrove, K., Stein, W., Eds.; Woodhead Publishing Series in Energy; Elsevier: Amsterdam, The Netherlands, 2021; pp. 165–217. ISBN 9780128199701.
99. Xu, E.; Yu, Q.; Wang, Z.; Yang, C. Modeling and simulation of 1 MW DAHAN solar thermal power tower plant. *Renew. Energy* **2011**, *36*, 848–857. [CrossRef]
100. Grogan, D.C.P. *Development of Molten-Salt Heat Transfer Fluid Technology for Parabolic Trough Solar Power Plants—Public Final Technical Report*; Abengoa Solar, LLC: Lakewood, CO, USA, 2013; pp. 303–323. [CrossRef]
101. Tilley, D.; Kelly, B.; Burkholder, F. *Baseload Nitrate Salt Central Receiver Power Plant Design*; Final Report; Abengoa Solar LLC: Lakewood, CO, USA, 2014. [CrossRef]

134

102. Wang, T.; Mantha, D.; Reddy, R.G. High Thermal Energy Storage Density LiNO₃-NaNO₃-KNO₃-KNO₂ Quaternary Molten Salts for Parabolic Trough Solar Power Generation. In *Energy Technology 2012*; John Wiley & Sons, Inc.: Hoboken, NJ, USA, 2012; pp. 73–84.

103. Shin, D.; Banerjee, D. Experimental Investigation of Molten Salt Nanofluid for Solar Thermal Energy Application. In Proceedings of the ASME/JSME 2011 8th Thermal Engineering Joint Conference, Honolulu, HI, USA, 13–17 March 2011.

104. Li, P.W.; Lew, J.V.; Karaki, W.; Chan, C.L.; Stephens, J.; O'Brien, J.E. Transient Heat Transfer and Energy Transport in Packed Bed Thermal Storage Systems. In *Developments in Heat Transfer*; InTech: Bolton, UK, 2011.

105. John, E.E.; Hale, W.M.; Selvam, R.P. Development of a High-Performance Concrete to Store Thermal Energy for Concentrating Solar Power Plants. In Proceedings of the ASME 2011 5th International Conference on Energy Sustainability, Parts A, B, and C, Washington, DC, USA, 7–10 August 2011; pp. 523–529.

106. Villarroel, E.; Fernandez-Pello, C.; Lenartz, J.; Parysek, K. *High Efficiency Thermal Storage System for Solar Plants (HELSOLAR)*; Final Report; SENER Engineering and Systems, Inc.: San Francisco, CA, USA, 2013. [CrossRef]

107. Newmarker, M.; Campbell, M. *Indirect, Dual-Media, Phase Changing Material Modular Thermal Energy Storage System*; Final Technical Report; ACCIONA SOLAR POWER, INC.: Washington, DC, USA, 2012. [CrossRef]

108. Mathur, A. *Heat Transfer and Latent Heat Storage in Inorganic Molten Salts for Concentrating Solar Power Plants*; Final Report; Terrafore Inc.: Riverside, CA, USA, 2013. [CrossRef]

109. Robak, C.W.; Bergman, T.L.; Faghri, A. Enhancement of latent heat energy storage using embedded heat pipes. *Int. J. Heat Mass Transf.* **2011**, *54*, 3476–3484. [CrossRef]

110. Goswami, D.Y. *Development and Demonstration of an Innovative Thermal Energy Storage System for Baseload Power Generation*; Final Report; University of South Florida: Tampa, FL, USA, 2012. [CrossRef]

111. Linder, M. Thermochemical Energy Storage for Concentrated Solar Power Plants (TCSPower). Final Report. Available online: https://cordis.europa.eu/project/id/282889/reporting/es (accessed on 22 July 2022).

112. Karagiannakis, G. Redox Materials-based Structured Reactors/Heat Exchangers for Thermo-Chemical Heat Storage Systems in Concentrated Solar Power Plants (RESTRUCTURE). Final Report. Available online: https://cordis.europa.eu/project/id/283015/reporting (accessed on 22 July 2022).

113. STORRE High Temperature Thermal Energy Storage by Reversible Thermochemical Reaction (STORRE). Final Report. Available online: https://cordis.europa.eu/project/id/282677/reporting (accessed on 22 July 2022).

114. Project Profile: Low-Cost Metal Hydride Thermal Energy Storage System. United States. Available online: https://www.energy.gov/eere/solar/project-profile-low-cost-metal-hydride-thermal-energy-storage-system (accessed on 22 July 2022).

115. Singh, D.; Yu, W.; France, D.M. *High Efficiency Latent Heat Based Thermal Energy Storage System Compatible with Supercritical CO2 Power Cycle*; Final Report; Argonne National Lab. (ANL): Argonne, IL, USA, 2019. [CrossRef]

116. Mei, R. *Carbon Dioxide Shuttling Thermochemical Storage Using Strontium Carbonate*; Final Report; Argonne National Lab. (ANL): Argonne, IL, USA, 2015. [CrossRef]

117. Gangwal, S.; Muto, A. *Regenerative Carbonate-Based Thermochemical Energy Storage System for Concentrating Solar Power*; Final Report; Southern Research Inst.: Durham, NC, USA, 2017. [CrossRef]

118. Project Profile: High-Temperature Thermochemical Storage with Redox-Stable Perovskites for Concentrating Solar Power. United States. Available online: https://www.energy.gov/eere/solar/project-profile-high-temperature-thermochemical-storage-redox-stable-perovskites (accessed on 22 July 2022).

119. Project Profile: Integrated Solar Receiver with Thermal Storage for an sCO₂ Power Cycle. United States. Available online: https://www.energy.gov/eere/solar/project-profile-brayton-energy (accessed on 22 July 2022).

120. Project Profile: Binary Metal Chalcogenides for High Temperature Thermal Storage. United States. Available online: https://www.energy.gov/eere/solar/project-profile-binary-metal-chalcogenides-high-temperature-thermal-storage-sunlamp (accessed on 22 July 2022).

121. Muto, A.; Hansen, T.A. *Demonstration of High-Temperature Calcium-Based Thermochemical Energy Storage System for Use with Concentrating Solar Power Facilities*; Final Technical Report; Southern Research Inst.: Birmingham, AL, USA, 2019. [CrossRef]

122. Baeyens, J. *High Temperature Concentrated Solar Thermal Power Plant with Particle Receiver and Direct Thermal Storage (NEXT-CSP)*; Centre National De La Recherche Scientifique CNRS: Paris, France, 2017. [CrossRef]

123. Baeyens, J.; Siros, F.; Valentin, B.; Brau, J.-F. Report on Particle Handling Solutions for Large-Scale Facilities. Next-CSP Project. Available online: http://next-csp.eu/ (accessed on 22 July 2022).

124. Concentrated Solar Power in Particles European Project (CSP2). Final Project Report. Available online: http://www.csp2-project.eu/ (accessed on 22 July 2022).

125. Behar, O.; Grange, B.; Flamant, G. Design and performance of a modular combined cycle solar power plant using the fluidized particle solar receiver technology. *Energy Convers. Manag.* **2020**, *220*, 113108. [CrossRef]

126. Reyes-Belmonte, M.A.; Sebastián, A.; Spelling, J.; Romero, M.; González-Aguilar, J. Annual performance of subcritical Rankine cycle coupled to an innovative particle receiver solar power plant. *Renew. Energy* **2019**, *130*, 786–795. [CrossRef]

127. Rovense, F.; Reyes-Belmonte, M.A.; González-Aguilar, J.; Amelio, M.; Bova, S.; Romero, M. Flexible electricity dispatch for CSP plant using un-fired closed air Brayton cycle with particles based thermal energy storage system. *Energy* **2019**, *173*, 971–984. [CrossRef]

128. Periodic Reporting for Period 1—SOLSTORE (Solid-State Reactions for Thermal Energy Storage). Available online: https://cordis.europa.eu/project/id/752520/reporting (accessed on 22 July 2022).
129. Doppiu, S.; Dauvergne, J.-L.; Palomo del Barrio, E. Solid-State Reactions for the Storage of Thermal Energy. *Nanomaterials* **2019**, *9*, 226. [CrossRef] [PubMed]
130. Periodic Reporting for Period 1—NPMSSES (Nanoparticle Enhanced Molten Salts for Solar Energy Storage). Available online: https://cordis.europa.eu/project/id/706788/reporting (accessed on 22 July 2022).
131. Periodic Reporting for Period 2—AMADEUS (Next GenerAtion MateriAls and Solid State DevicEs for Ultra High Temperature Energy Storage and Conversion). Available online: https://www.amadeus-project.eu/news (accessed on 22 July 2022).
132. Periodic Reporting for Period 2—SESPer (Solar Energy Storage PERovskites). Available online: https://cordis.europa.eu/project/id/746167/reporting (accessed on 22 July 2022).
133. Advanced Materials Solutions for Next Generation High Efficiency Concentrated Solar Power (CSP) Tower Systems (NEXTOWER). Final Results. Available online: https://www.h2020-nextower.eu/ (accessed on 22 July 2022).
134. Garcia, P.; Pouvreau, J. High temperature combined sensible-latent thermal energy storage. In Proceedings of the AIP Conference Proceedings 2126, Casablanca, Morocco, 2–5 October 2019; p. 200020.
135. Gálvez, A.; Cubillo, J.J.; Guerreiro, L.; Azevedo, P.; Diamantino, T.; Alonso, M.C.; Bonk, A.; Bauer, T.; Franke, W.; Haselbacher, A.; et al. NEW StOrage Latent and Sensible Concept for High Efficient CSP Plants Preliminary Selection of Materials Compositions and TES System Predesign (NewSOL). Available online: http://www.newsol.uevora.pt/ (accessed on 22 July 2022).
136. SOlar Calcium-looping IntegRAtion for ThermoChemical Energy Storage. Final Innovation. Evaluation Report. Available online: https://cordis.europa.eu/project/id/727348/results (accessed on 22 July 2022).
137. Periodic Reporting for Period 1—SOCRATCES (SOlar Calcium-looping IntegRAtion for Thermo-Chemical Energy Storage). Available online: https://socratces.eu/ (accessed on 22 July 2022).
138. A New Generation High Temperature Phase Change Microemulsion for Latent Thermal Energy Storage in Dual Loop Solar Field (THERMES). Fact Sheet. Available online: https://cordis.europa.eu/project/id/831756 (accessed on 22 July 2022).
139. Turchi, C.; Gage, S.; Martinek, J.; Jape, S.; Armijo, K.; Coventry, J.; Pye, J.; Asselineau, C.-A.; Venn, F.; Logie, W.; et al. *CSP Gen3: Liquid-Phase Pathway to SunShot*; National Renewable Energy Lab. (NREL): Golden, CO, USA, 2021. [CrossRef]
140. Project Profile: Brayton Energy 2 (Gen3 CSP). United States. Available online: https://www.energy.gov/eere/solar/project-profile-brayton-energy-2-gen3-csp (accessed on 22 July 2022).
141. NEWCLINE Project CSP ERANET: 1st Cofund Joint Call. Available online: http://www.newcline.eu/ (accessed on 22 July 2022).
142. Robb, K. *Simplified High-Temperature Molten Salt CSP Plant Preconceptual Design*; Oak Ridge National Lab. (ORNL): Oak Ridge, TN, USA, 2022. [CrossRef]

3. Summary

The present PhD Thesis proposes the development of the Calcium Looping process as thermochemical energy storage system integrated into the next generation of concentrated solar power plants, considering higher operating temperatures to improve the energy performance. The aim of this research is (i) to propose novel methodologies and systems for the CaL process as TCES and (ii) to enhance the energy efficiency and minimize the energy costs of the conventional CaL TCES configuration proposed in literature under dynamic mode. The inclusion of a novel equipment to enhance the energy efficiency subjected to solids management has been proposed and assessed. Moreover, the operation under dynamic state of the CaL TCES system has been defined, adjusting to the hourly variability of the solar resource and the energy demand.

3.1. Objective

Up to now, an operational methodology based on the hourly load variability of a non-oversized CaL TCES system without any support is not contemplated in literature. Most of the research in literature propose an oversizing of the storage tanks or the support from other renewable energy sources to adequately manage availability of solar resource and power generation. Regardless of energy demand, the energy stored during the sunlight hours is proportionally retrieved when solar resource is not fully available. The present PhD thesis addresses the influence of the solar resource availability and the solids circulation management on the CaL TCES plant equipment sizing. Energy savings and size reductions could be reached for the CaL TCES system, minimizing the circulation of unreacted solids and assessing the real dynamic operation influenced by the offer (solar resource) and the demand (electricity prices). Both the novel configuration and the defined methodology are the PhD Thesis proposals to achieve the core objectives related to the CaL TCES system: (i) the efficiency improvement and (ii) the dynamic operation study.

The **first main contribution** of this PhD Thesis is to demonstrate the potential efficiency improvement of the conventional CaL process as TCES. Thus, the starting point of this work is focused on the energy assessment of the large-scale CaL process as TCES under a conventional configuration proposed in literature. The conventional CaL TCES configuration could improve its energy savings based on solids management. Thus, the second step of this PhD Thesis in devoted to the proposal and assessment of a novel CaL TCES configuration. The inclusion of an ideal solid-solid fluidized bed classifier minimizes the amount of inert solids conveying between reactors, recirculating into carbonator the unreacted material after separating from carbonated material. The energy savings and the performance enhancement of the CaL TCES system after implementing the solid-solid classifier have been quantified by simulation and experimental tests. An energy assessment was performed through simulation to evaluate the effect of the SSU on the CaL TCES size and efficiency. The experimental campaign addressed the technical feasibility of the SSU.

The **second main contribution** of the present PhD Thesis is to define an economically optimized dynamic operation of the CaL TCES system under real conditions. The energy production from the CSP plants is linked to the availability of the solar resource (offer) and the electricity prices (demand). The CaL TCES system provides stability to the operation of the CSP plant, being able to supply energy maximizing the economic profit. The final stage of this PhD Thesis develops a methodology to define the dynamic operation of the novel CaL TCES configuration integrated into CSP plants, enhancing the energy and economic savings. The methodology takes into account the different energy loads of offer and demand, maximizing the daily income of the CSP plant. Moreover, optimized operating maps have been defined with the operation points which maximize the efficiency of the system under each pair of carbonator/calciner loads while meeting technical, design and energy criteria. Thus, the energy storage has been designed to balance the availability of solar resource with the periods of greatest demand with the highest prices.

3.2. Methodology

The CaL process has been widely assessed as a carbon capture technology through computer simulation and experimental test. Recent research works pointed out the potential use of CaL process as a TCES system integrated into CSP plants. Thus, the level of knowledge of the CaL process and the involve equipment, the most suitable methodology is computer simulation supported by experimental works to validate simulation results.

The Engineering Equation Solver (EES) software was used (i) to model the carbonation reaction, (ii) to define the operation maps and (iii) to code and implement the methodology to determine the dynamic operation and the energy modelling of the CaL TCES system. The mass and energy balances of the CaL TCES system under conventional and novel configuration were performed by gas properties extracted from the EES extensive database and solids properties (lime [115] and limestone [116]) belonging to external data. The experimental campaign was carried out to validate (i) the sorbent deactivation during carbonation step and (ii) the technical feasibility of the carbonated solid separation proposed under the novel CaL TCES configuration.

The first carbonator was design as an entrained flow reactor to suitably evacuate the thermal energy during carbonation at large scale. The carbonation kinetics was based on the literature model developed by Ortiz et al. [56], assuming a sorbent conversion of 13.54% at the end of the reaction controlled phase. Since kinetic models of the CaL process such as TCES are

scarce, reasonable parts of the existing carbonator models in literature have been extracted. Experimentation under operating conditions of the novel CaL TCES system is non-existent, being on the frontier of knowledge. Within the following research stages of this PhD Thesis, a fluidized bed reactor was assumed to perform the carbonation reaction. The average sorbent activity was computed by a sorbent deactivation model, considering a conservative estimation of the particle population age in the carbonator proposed by Abanades for carbon capture [111]. The decay of sorbent conversion was firstly tuned adjusting to Grasa et el. carbonator kinetic model developed under carbon capture conditions [104]. Once the first lab scale experimental determination of carbonation degree was performed under CaL TCES conditions on an electrically heated fluidized bed with limestone and sand as inventory bed, the sorbent deactivation results were tuned adjusting to Valverde et al. carbonator kinetic model developed for the CaL process as TCES [126,127]. The last sorbent deactivation experimental results on an EHFB with inventory only composed by limestone were better adjusted to an initial activity decay model. Secondly, a sorbent purge in the calciner was considered to improve the average sorption capacity. Parametrical analyses were done to select the most suitable CaO purge percentage, considering a carbon capture efficiency over 90% and a proper Ca/C molar ratio entering the carbonator.

The operation maps which maximize the efficiency of the CaL TCES system have been selected applying design and technical criteria. The energy storage efficiency was maximized under energy storage operation mode (ESOM) and the thermal energy availability efficiency was maximized under energy retrieval operation mode (EROM). A single operating point was selected under each pair of carbonator/calciner loads, also complying with behaviour and load restrictions of the plant equipment involve in the CaL TCES system. The EE heat exchangers always released thermal energy and those named ER had to behave as energy demanders. Regarding load thresholds, a minimum load for energy-releasing equipment with a nominal size greater than 15 MW and a maximum load for the heat exchanger which preheats carbonate solids discharged from storage were imposed to ensure energy supply and minimize energy consumption. The operating map is defined by storage and discharge fractions of CaO and carbonated material under ESOM and EROM, respectively.

The methodology was coded and implemented using the EES software. A genetic method [131] was applied to maximize the daily incomes for the CSP plant. The variable inputs were the direct normal irradiation and the electricity prices for the selected for eight representative days within a standard year in a specific location. The daily incomes are influenced by the energy retrieval from the CaL TCES system. The applied constraints were the operating maps and the conservation of stored energy at the beginning and end of the day. An operating pattern resulting for each representative day was obtained, including the daily distribution of the energy recovery and the stored energy.

Regarding the experimental campaign, the sorbent carbonation degree, bulk density and the minimum fluidization velocity for carbonated and calcined particles were measured. The CaO deactivation was firstly measured under CaL TCES conditions in two fluidized bed facilities with and without simulation of solar radiation using as bed inventory a mixture of sand and limestone. The second measurement of the sorbent conversion was only performed with limestone in an EHFB without solar radiation simulation. The objective of these experimental tests was to assess the effect of the solar radiation and the presence of sand on the sorbent activity. The measure of the bulk density promoted the development of a novel data characterization for sorbent conversion in large scale CaL TCES facilities. Moreover, the bulk density test validated the effect of the sand in the bed inventory on the sorbent activity, given an increase in the particle density due to the porosity minimization. The last experimental research was led to estimate the technical feasibility of solids after carbonation step. The minimum fluidization velocity was measured for carbonated

and calcined particles thought the pressure drop vs. the superficial gas velocity curves, using limestone as bed inventory in an EHFB. The difference range of minimum fluidization velocities between carbonated and calcined particles would reveal the potential separation of unreacted particles from the most reactive ones due to density difference. As expected, the experimental minimum fluidization velocity trend coincided with the particle density variation within the analyzed carbonation/calcination cycles. Thus, the fluidized bed could be a potential technology to partially separate the carbonated solids by density difference, given sufficient difference between the minimum fluidization velocities of partially carbonated and calcined particles.

3.3. Contributions

The present PhD Thesis is framed in the field of engineering, specifically in the development of energy storage coupled with renewable energy sources. Main contributions explore novel technical proposals, being able to help improve the technological development of the energy storage system based on the Calcium Looping (CaL) process. This PhD Thesis addresses the efficiency improvement and the dynamic operation of the CaL process as thermochemical energy storage. A summary of the main contributions is shown below:

- The development of a novel CaL TCES configuration to enhance energy efficiency subjected to solids management in a CaL process for TCES integrated into a CSP plant. A simulation model verified the energy and size benefits generated by avoiding the circulation of unreacted solids between reactors.

- The proposal for the integration of a new equipment to separate the non-reactive particles from the carbonated ones after carbonation reaction, minimizing the energy cost of the CaL TCES system. The solid-solid classifier is based on a fluidized bed to separate by density difference between less and more carbonated particles.

- The technical assessment by experimental tests of the solid-solid separation unit. The difference between calcined and carbonated particles of the experimental minimum fluidization velocity under CaL TCES conditions was measured. The experimental results indicate a potential partial separation of the less reactive particles from the more reactive ones. A fluidized bed could be the most appropriate technology to classify granular solids by means of density difference.

- The definition of the most suitable operating maps for the CaL TCES system. The energy performance of all potential operating points under each pair of calciner/carbonator load was quantified. A proper operating point was selected under each pair of reactor loads, maximizing (i) the energy storage efficiency under storage operation mode (ESOM) and (ii) the thermal energy availability efficiency under retrieval operation mode (EROM). Moreover, the selected operating maps comply with technical and design criteria, enhancing the operation of the CaL TCES system.

- The development of a methodology to determine the operation patter which maximizes the daily economic profit CSP plant, operating the CaL TCES system under the selected operation maps to maximize the energy performance. The CaL TCES dynamic operation was assessed, comprising the variability of solar resource and the

energy demand. Operating pattern of the CaL TCES was extracted, discovering the real operational behaviour of the CaL TCES system under transient mode.

- The energy and economic performance of the CaL TCES system was enhanced by the novel CaL TCES configuration. Equipment size reductions up to 4% and energy savings between 11% and 28% for energy storage and thermal energy availability, respectively, was achieved when the solid-solid classifier integrated into the CaL TCES system.

The contributions to international conferences done during the development of the present PhD Thesis are:

2019   Bailera M., Lisbona P., Pascual S., Díez L.I. and Romeo L.M. *On the modelling of a lime carbonator operating in a concentrated solar power plant for energy storage*. 32nd International Conference on Efficiency, Cost, Optimization, Simulation and Environmental Impact of Energy Systems, 23rd-28th June 2019, Wroclaw, Poland.

2019   Pascual S., Bailera M., Lisbona P., Díez L.I. and Romeo L.M. *Calcium Looping como uso directo del CO_2 para el almacenamiento de energía solar*. 3ª Conferencia Aportando valor CO_2, 2nd-3rd October 2019, Madrid, Spain. Proceedings pp. 102-103.

2020   Pascual S., Bailera M., Lisbona P., Díez L.I. and Romeo L.M. *Solar Calcium Looping energy storage: Preliminary comparison between pilot and large scale*. 33rd International Conference on Efficiency, Cost, Optimization, Simulation and Environmental Impact of Energy Systems, 29th June - 3rd July 2020, Osaka, Japan. Proceedings pp. 1511-1522.

2021   Pascual S., Di Lauro F., Lisbona P., Romeo L.M., Tregambi C., Montagnaro F., Solimene R., Salatino P. *Improvement of performance of fluidized bed Calcium Looping for thermochemical solar energy storage: Modelling and experiments*. 10th European Combustion Meeting, 14th-15th April 2021, Naples, Italy. Proceedings pp. 1430-1435.

2022   Pascual S., Lisbona P., Romeo L.M. *New strategies for solids management in a Ca-looping based TCES System*. 24th International Conference on Fluidized Bed Conversion, 8th-11th May 2022, Gothenburg, Sweden.

Additional contributions have been done through an online webinar within the SOCRATCES project and a doctoral seminar led by the Ph.D. Program in Renewable Energy and Energy Efficiency of the University of Zaragoza (Spain):

2021   Romeo L.M., Pascual S., Lisbona P., Díez L.I., Bailera M. *Operational Performance of CSP and Ca-L*. SOCRATCES Webinar, 10th June 2021, online.

2022   Pascual S. *Gestión de sólidos en el sistema de almacenamiento termoquímico basado en ciclo de calcio: Una herramienta para la mejora de la eficiencia energética*. 2ª Jornada de doctorandos del Programa de doctorado en Energías Renovables y Eficiencia Energética de la Universidad de Zaragoza, 5th May 2022, Zaragoza, Spain.

Other previous contributions related to the Calcium Looping technology coupled with other types of processes have been also produced. Transversal and specific training in the Calcium Looping technology have been received during the PhD Thesis development:

2019   Scholarship to attend the "7th Sotacarbo International Summer School on CCUS and low carbon technologies", 10th - 14th June 2019, Carbonia, Italy.

2019   Scholarship to attend the "13th IEAGHG International Summer School on CCUS", 7th - 12th July 2019, Regina, Canada.

Additionally, the Calcium Looping process has been explored, simulated and modelled within the field of carbon capture to reach negative emissions in bioenergy systems or to upgrade the biogas from anaerobic digestion. The contributions were presented in international journal papers and conferences:

2021   Lisbona P., Pascual S., Pérez V., Romeo L.M. *Technical feasibility analysis of a negative emissions BECCS system for a livestock waste treatment plant*. 15th International Conference on Greenhouse Gas Control Technologies, 15th - 18th March 2021, Abu Dhabi, UAE.

2021   Lisbona P., Pascual S., Pérez V. *Evaluation of Synergies of a Biomass Power Plant and a Biogas Station with a Carbon Capture System*. Energies 2021, 14, 908.

2022   Godos I., Pascual S., Lisbona P. *Novel biogas upgrading technology by means of Calcium Looping process*. 16th International Conference on Greenhouse Gas Control Technologies, 23rd - 27th October 2022, Lyon, France.

The dissemination of the contributions in carbon capture field through the Calcium Looping process were also carried out within different seminars and workshops:

2018   Pascual S. *CCUS technologies: an opportunity in the mitigation of climate change technical conference*. CO_2 capture technical day: technologies for large-scale capture - CO_2 Spanish Technological Platform, 15th June 2018, Soria, Spain.

2018   Pascual S. *Techno-economic feasibility analysis of an innovative renewable energy system with negative emissions integrated into a livestock waste treatment plant in the province of Soria*. 16th Science Week in Castilla y León, 12th - 18th November 2018, Soria, Spain.

2020   Pascual S. *Technical feasibility analysis of a BECCS system of negative emissions for a livestock waste management plant*. Quality, Production and Sustainability working group meeting of the Food for Life-Spain technological platform, 23rd January 2020, Madrid, Spain.

2021   Pascual S. *Calcium Looping systems for CO_2 capture, integration in biogas plants*. 1st Summer course of LIFE Smart Agromobility - Biogas production on farms and use in sustainable mobility, 16th July 2021, Soria, Spain.

3.4. Challenges and further work

A roadmap directs the next research steps to develop future work based on the main conclusions derived from this PhD Thesis. The CaL TCES system has been approached from two possible thresholds from the energetic point of view. The major challenge for the future is to define

the actual configuration and real operation of a CaL TCES system integrated into a CSP plant, enhancing the energy efficiency subjected to unreacted solids convey. As further work, three main blocks must be developed: (i) the kinetic and partial separation of solids models from the results of the experimental campaign, (ii) the real design of the solid-solid classifier, (iii) the economic assessment of the real CaL TCES configuration.

Experimental results provided information related to the sorbent deactivation with the number of carbonation/calcination cycles under CaL TCES conditions (850 ºC carbonation and 950 ºC calcination, both under pure CO_2 atmosphere) in lab-scale facilities. Both reactions were performed into fluidized bed reactors, whose behaviour is close to large-scale. Carbonator kinetic models have been developed using data from thermogravimetric analysis. The next step for carbonation reaction is to develop a kinetic model based on the experimental results provided by the electrically heated fluidized bed (EHFB) using limestone as bed inventory. The kinetic model to be developed must be validated for the carbonation and calcination conditions with a greater number of cycles experimentally analysed.

The experimental minimum fluidization velocity results could be essential to estimate a partial separation degree of less reactive material. After carbonation step the partial carbonated material is fed into a solid-solid separation unit to obtain two streams: (i) one with a higher percentage of fully carbonated particles and (ii) another with a higher concentration of unreacted CaO in the particles. The solid material with higher concentration of unreacted CaO could be recirculated into the carbonator and the most carbonated material could be directed to the calciner or the storage tank ST1. The solid-solid separation could be based on a fluidized bed classifier by density difference. A complete design of the solid-solid classifier, already proposed in literature [123], could be developed to partially separate the particles from the less reactive ones. The operation of the solid-solid classifier could be assessed performing new experimental tests to address its efficiency and feasibility. The partial separation of solids model to be developed must be validated for newly and highly cycled particles under carbonation conditions.

Once the carbonator kinetic model and the solid-solid separation degree for partially carbonated material are developed, the energy assessment of the partial separation CaL TCES configuration under large-scale could be performed. The energy and size results of this configuration could be between the conventional and novel configuration assessed during the present PhD Thesis. The operation maps which maximize the performance of the partial separation CaL TCES configuration could be defined. The real economic profit of the CSP plant could be provided by applying the operating methodology to the large-scale CaL TCES system including a partial separation of carbonated material.

3.5. Concluding remarks

The results of the present PhD Thesis contribute to the development of more energy efficient TCES systems based on CaL technology, promoting energy and economic savings under real operation. The TCES based on gas-solid reactions, such as CaL process, is attracting a great deal of attention and constitutes one of the most mid-term promising candidates for thermal energy storage integrated into the next generation of CSP plants coupled with high-temperature power blocks. Progress is undoubtedly still required on the development and economic assessment of the real CaL TCES configuration, considering partial separation of carbonated material.

Nevertheless, the inclusion of the solid-solid separation unit into the CaL TCES system generates potential expectations of efficiency improvement and cost reduction, being able to increase the interest of CaL as TCES and enabling its large-scale deployment in third generation CSP plants.

Nomenclature

Symbols

E	thermal energy, MWh
f	fraction, -
h	hour, h
In	incomes, €
k	CaO deactivation constant, -
L	load, -
m	weight, mg
$\dot{m}$	mass flow rate, kg/s
N	number of carbonation-calcination cycles
Q	heat flow rate, MW
R	molar ratio CaO/CO_2, -
V	volume, m^3
x	content, -
X	conversion, -

Greek symbols

ΔH_R^0	enthalpy of carbonation, kJ/mol
ε	void fraction, -
η	efficiency, -
ρ	density, -

Subscripts and superscripts

av	thermal energy availability
AV	available
$carb$	carbonated

calc	calcined
CR	carbonator
CL	calciner
dch	discharge
disc	discarded
g	gas
max	maximum
min	minimum
N	number of carbonation-calcination cycles
nom	nominal
p	purge or particle
part	partial load
s	solid
st	storage

Acronyms and abbreviations

CaL	Calcium-looping
CCT	Compressor-Cooling Train
CSP	Concentrating Solar Power
DE	Discharging Expansion
DIFB	Directly Irradiated Fluidized Bed
DNI	Direct Normal Irradiation
EC	European Commission
EE	Energy Emitted
EES	Engineering Equation Solver
EHFB	Electrically Heated Fluidized Bed
EP	Electricity Price
ER	Energy Required
EROM	Energy Retrieval Operation Mode
ESOM	Energy Storage Operation Mode
FB	Fluidized Bed
GHG	Greenhouse Gases
HE	Heat Exchanger
HTF	Heat Transfer Fluid
IEA	International Energy Agency
IPCC	Intergovernmental Panel on Climate Change

LHS	Latent Heat Storage
MW	Molecular Weight
NCAR	National Center for Atmospheric Research
PCMs	Phase Change Materials
PVGIS	Photovoltaic Geographical Information System
R&D	Research and Development
RES	Renewable Energy Sources
SC1	Conventional CaL TCEs configuration (scenario 1)
SC2	Novel CaL TCES configuration (scenario 2)
SHS	Sensible Heat Storage
SSC	Specific Storage ConsumptionSSU
SSU	Solid-solid Separation Unit
ST	Storage Tank
TCES	Thermochemical Energy Storage
TES	Thermal Energy Storage

List of figures

List of tables

Bibliography

[1]   P.R. Shukla, J. Skea, R. Slade, A. Al Khourdajie, R. van Diemen, D. McCollum, M. Pathak, S. Some, P. Vyas, R. Fradera, M. Belkacemi, A. Hasija, G. Lisboa, S. Luz, J. Malley, eds., "IPCC, 2022: Climate Change 2022: Mitigation of Climate Change. Contribution of Working Group III to the Sixth Assessment Report of the Intergovernmental Panel on Climate Change", Cambridge University Press, Cambridge, UK and New York, NY, USA, 2022.

[2]   IEA, "World Energy Outlook 2022. Technical report", International Energy Agency, 2022.

[3]   IEA, "Status of Power System Transformation 2019. Power system flexibility", International Energy Agency, 2019.

[4]   A. Zervos, R. Adib, eds., "Renewables 2022. Global Status Report", REN21 Secretariat, 2022.

[5]   IEA, "Net Zero by 2050: A Roadmap for the Global Energy Sector", International Energy Agency, 2021.

[6]   EC, "Report from the Commision to the European Parliament, the European Council, the Council, the European Economic and Social Committee and the Committee of the Regions. The European Green Deal", European Commission, 2019.

[7]   N. Goyal, A. Aggarwal, A. Kumar, "Concentrated solar power plants: A critical review of regional dynamics and operational parameters", *Energy Res. Soc. Sci.*, vol. 83, pp. 102331, 2022.

[8]   EC, "Commission staff working document: Energy storage – the role of electricity", European Commission, 2017.

[9]   R. Kunwer, S. Pandey, G. Pandey, "Technical Challenges and Their Solutions for Integration of Sensible Thermal Energy Storage with Concentrated Solar Power Applications—a Review", *Process Integr. Optim. Sustain.*, vol. 6, pp. 559–585, 2022.

[10]   S.J. Wagner, E.S. Rubin, "Economic implications of thermal energy storage for concentrated solar thermal power", *Renew. Energy*, vol. 61, pp. 81–95, 2014.

[11]   S. Teske, J. Leung, "Solar Thermal Electricity - Global Outlook 2016", Greenpeace International, European Solar Thermal Electricity Association (ESTELA), SolarPACES Secretariate, 2016.

[12]   T. Pavlovic, I. Radonjic, "A review of concentrating solar power plants in the world and their potential use in Serbia", *Renew. Sustain. Energy Rev.*, vol. 16, pp. 12, 2012.

[13]   T. Islam, N. Huda, A.B. Abdullah, R. Saidur, "A comprehensive review of state-of-the-art concentrating solar power (CSP) technologies : Current status and research trends", *Renew. Sustain. Energy Rev.*, vol. 91, pp. 987–1018, 2018.

[14]   A. Kumar, S.K. Shukla, "A Review on Thermal Energy Storage Unit for Solar Thermal Power Plant Application", *Energy Procedia*, vol. 74, pp. 462–469, 2015.

[15]   E. González-Roubaud, D. Pérez-Osorio, C. Prieto, "Review of commercial thermal energy storage in concentrated solar power plants: Steam vs. molten salts", *Renew. Sustain. Energy Rev.*, vol. 80, pp. 133–148, 2017.

[16]   O. Achkari, A. El Fadar, "Latest developments on TES and CSP technologies – Energy and environmental issues, applications and research trends", *Appl. Therm. Eng.*, vol. 167, pp. 114806, 2020.

[17]   J.A. Noël, S. Kahwaji, L. Desgrosseilliers, D. Groulx, M.A. White, "Phase Change Materials", in: T.M. Letcher (Ed.), *Storing Energy*, Elsevier, 2016: pp. 249–272.

[18]   A. Mohammad, J. Khoshbaf, H. Groningen, C. Orozco, "Thermal energy storage in CSP technologies: from commercialized to innovative solutions", French National Centre for Scientific Research, 2018.

[19]   B. Xu, P. Li, C. Chan, "Application of phase change materials for thermal energy storage in concentrated solar thermal power plants : A review to recent developments", *Appl. Energy*, vol. 160, pp. 286–307, 2015.

[20]   J.A. Almendros-Ibáñez, M. Fernández-Torrijos, M. Díaz-Heras, J.F. Belmonte, C. Sobrino, "A review of solar thermal energy storage in beds of particles: Packed and fluidized beds", *Sol. Energy*, vol. 192, pp. 193–237, 2019.

[21]   C. Prieto, L.F. Cabeza, "Thermal energy storage (TES) with phase change materials (PCM) in solar power plants (CSP). Concept and plant performance", *Appl. Energy*, vol. 254, pp. 113646, 2019.

[22]   X. Chen, Z. Zhang, C. Qi, X. Ling, H. Peng, "State of the art on the high-temperature thermochemical energy storage systems", *Energy Convers. Manag.*, vol. 177, pp. 792–815, 2018.

[23]   P. Pardo, A. Deydier, Z. Anxionnaz-minvielle, S. Rougé, M. Cabassud, P. Cognet, "A review on high temperature thermochemical heat energy storage", *Renew. Sustain. Energy Rev.*, vol. 32, pp. 591–610, 2014.

[24]   National Renewable Energy Laboratory, "Concentrating Solar Power Projects.", 2022. [Online]. Available: https://solarpaces.nrel.gov/projects [accessed July 1, 2022].

[25]   E. Commission, "CORDIS. EU research results", 2022. [Online]. Available: https://cordis.europa.eu/projects/en [accessed July 15, 2022].

[26]   U.S. Department of Energy, "Solar Energy Research Database. Solar Energy Technologies Office", 2022. [Online]. Available: https://www.energy.gov/eere/solar/solar-energy-research-database [accessed July 15, 2022].

[27]   S. Pascual, P. Lisbona, L.M. Romeo, "Thermal Energy Storage in Concentrating Solar Power Plants : A Review of European and North American R&D Projects", *Energies*, vol. 15, pp. 8570, 2022.

[28]   K. Vignarooban, X. Xu, A. Arvay, K. Hsu, A.M. Kannan, "Heat transfer fluids for concentrating solar power systems – A review", *Appl. Energy*, vol. 146, pp. 383–396, 2015.

[29]   U. Pelay, L. Luo, Y. Fan, D. Stitou, M. Rood, "Thermal energy storage systems for concentrated solar power plants", *Renew. Sustain. Energy Rev.*, vol. 79, pp. 82–100, 2017.

[30]   S. Kuravi, J. Trahan, D.Y. Goswami, M.M. Rahman, E.K. Stefanakos, "Thermal energy storage technologies and systems for concentrating solar power plants", *Prog. Energy Combust. Sci.*, vol. 39, pp. 285–319, 2013.

[31]   K. El Alami, M. Asbik, R. Boualou, F. zahra Ouchani, H. Agalit, E.G. Bennouna, S. Rachidi, "A critical overview of the suitability of natural Moroccan rocks for high temperature thermal energy storage applications: Towards an effective dispatching of concentrated solar power plants", *J. Energy Storage*, vol. 50, pp. 104295, 2022.

[32]   A. Calderón, A. Palacios, C. Barreneche, M. Segarra, C. Prieto, A. Rodriguez-Sanchez, A.I. Fernández, "High temperature systems using solid particles as TES and HTF material: A review", *Appl. Energy*, vol. 213, pp. 100–111, 2018.

[33]   F. Nie, F. Bai, Z. Wang, X. Li, R. Yang, "Solid particle solar receivers in the next-generation concentrated solar power plant", *EcoMat*, vol. 4, pp. e12207, 2022.

[34]   M. Romero, J. González-Aguilar, "Next generation of liquid metal and other high-performance receiver designs for concentrating solar thermal (CST) central tower systems", in: M.J. Blanco, L.R. Santigosa, In Woodhead Publishing Series in Energy, Advances in Concentrating Solar Thermal Research and Technology, Woodhead Publishing (Eds.), *Adv. Conc. Sol. Therm. Res. Technol.*, Elsevier, 2017: pp. 129–154.

[35]   A. Caraballo, S. Galán-Casado, Á. Caballero, S. Serena, "Molten salts for sensible thermal energy storage: A review and an energy performance analysis", *Energies*, vol. 14, pp. 1–15, 2021.

[36]   W. Ding, T. Bauer, "Progress in Research and Development of Molten Chloride Salt Technology for Next Generation Concentrated Solar Power Plants", *Engineering*, vol. 7, pp. 334–347, 2021.

[37]   M. Opolot, C. Zhao, M. Liu, S. Mancin, F. Bruno, "A review of high temperature (≥ 500 ºC) latent heat thermal energy storage", *Renew. Sustain. Energy Rev.*, vol. 160, pp. 112293, 2022.

[38]   K. Tofani, S. Tiari, "Nano-enhanced phase change materials in latent heat thermal energy storage systems: A review", *Energies*, vol. 14, pp. 18–31, 2021.

[39]   EASE/EERA, "European energy Storage Technology Development Roadmap Towards 2030", European Association for Storage of Energy, 2012.

[40]   I. Arias, J. Cardemil, E. Zarza, L. Valenzuela, R. Escobar, "Latest developments, assessments and research trends for next generation of concentrated solar power plants using liquid heat transfer fluids", *Renew. Sustain. Energy Rev.*, vol. 168, pp. 112844, 2022.

[41]   C. Prieto, P. Cooper, A.I. Fernández, L.F. Cabeza, "Review of technology : Thermochemical energy storage for concentrated solar power plants", *Renew. Sustain. Energy Rev.*, vol. 60, pp. 909–929, 2016.

[42]   IRENA, "Innovation Outlook: Thermal Energy Storage", International Renewable Energy Agency, Abu Dhabi., 2020.

[43]   J.C. Abanades, G. Grasa, M. Alonso, N. Rodriguez, E.J. Anthony, L.M. Romeo, "Cost structure of a postcombustion CO2 capture system using CaO", *Environ. Sci. Technol.*, vol. 41, pp. 5523–5527, 2007.

[44]   L.M. Romeo, D. Catalina, P. Lisbona, Y. Lara, A. Martínez, "Reduction of greenhouse gas emissions by integration of cement plants, power plants, and CO2 capture systems", *Greenh. Gases Sci. Technol.*, vol. 1, pp. 72–82, 2011.

[45]   D.P. Hanak, E.J. Anthony, V. Manovic, "A review of developments in pilot-plant testing and modelling of calcium looping process for CO 2 capture from power generation systems", *Energy Environ. Sci.*, vol. 8, pp. 2199–2249, 2015.

[46]   S. Michalski, D.P. Hanak, V. Manovic, "Advanced power cycles for coal-fired power plants based on calcium looping combustion: A techno-economic feasibility assessment", *Appl. Energy*, vol. 269, pp. 114954, 2020.

[47]   D.P. Hanak, V. Manovic, "Calcium looping combustion for high-efficiency low-emission power generation", *J. Clean. Prod.*, vol. 161, pp. 245–255, 2017.

[48]   M. Haaf, R. Anantharaman, S. Roussanaly, J. Ströhle, B. Epple, "CO2 capture from waste-to-energy plants: Techno-economic assessment of novel integration concepts of calcium looping technology", *Resour. Conserv. Recycl.*, vol. 162, pp. 104973, 2020.

[49]   M.E. Diego, M. Alonso, "Operational feasibility of biomass combustion with in situ CO2 capture by CaO during 360 h in a 300 kWth calcium looping facility", *Fuel*, vol. 181, pp. 325–329, 2016.

[50]   R. Barker, "The Reactivity of Calcium Oxide Towards Carbon Dioxide and Its Use for Energy Storage", *Appl. Chem. Biotechnol.*, vol. 24, pp. 221–227, 1974.

[51]   A.A. Khosa, T. Xu, B.Q. Xia, J. Yan, C.Y. Zhao, "Technological challenges and industrial applications of CaCO3/CaO based thermal energy storage system – A review", *Sol. Energy*, vol. 193, pp. 618–636, 2019.

[52]   X. Chen, X. Jin, X. Ling, Y. Wang, "Exergy Analysis of Concentrated Solar Power Plants with Thermochemical Energy Storage Based on Calcium Looping", *ACS Sustain. Chem. Eng.*, vol. 8, pp. 7928–7941, 2020.

[53]   J.C. Abanades, E.S. Rubin, E.J. Anthony, "Sorbent Cost and Performance in CO2 Capture Systems", *Ind. Eng. Chem. Res.*, vol. 43, pp. 3462–3466, 2004.

[54]   P. Lisbona, M. Bailera, T. Hills, M. Sceats, L.I. Díez, L.M. Romeo, "Energy consumption minimization for a solar lime calciner operating in a concentrated solar power plant for thermal energy storage", *Renew. Energy*, vol. 156, pp. 1019–1027, 2020.

[55]   F. Di Lauro, C. Tregambi, F. Montagnaro, P. Salatino, R. Chirone, R. Solimene, "Improving the performance of calcium looping for solar thermochemical energy storage and CO2 capture", *Fuel*, vol. 298, pp. 120791, 2021.

[56]   C. Ortiz, J.M. Valverde, R. Chacartegui, L.A. Perez-Maqueda, "Carbonation of Limestone Derived CaO for Thermochemical Energy Storage: From Kinetics to Process Integration in Concentrating Solar Plants", *ACS Sustain. Chem. Eng.*, vol. 6, pp. 6404–6417, 2018.

[57]   I. Sarbu, C. Sebarchievici, "A Comprehensive Review of Thermal Energy Storage", *MDPI Sustain.*, vol. 10, pp. 1–32, 2018.

[58]   D. Liu, L. Xin-Feng, L. Bo, Z. Si-quan, X. Yan, "Progress in thermochemical energy storage for concentrated solar power: A review", *Int. J. Energy Res.*, vol. 42, pp. 4546–4561, 2018.

[59]   G. Alva, Y. Lin, G. Fang, "An overview of thermal energy storage systems", *Energy*, vol. 144, pp. 341–378, 2018.

[60]   M. Benitez-guerrero, B. Sarrion, A. Perejon, P.E. Sanchez-jimenez, L.A. Perez-maqueda, J. Manuel, "Large-scale high-temperature solar energy storage using natural minerals", *Sol. Energy Mater. Sol. Cells*, vol. 168, pp. 14–21, 2017.

[61]   M. Benitez-guerrero, J. Manuel, P.E. Sanchez-jimenez, A. Perejon, L.A. Perez-maqueda, "Multicycle activity of natural CaCO 3 minerals for thermochemical energy storage in Concentrated Solar Power plants", *Sol. Energy*, vol. 153, pp. 188–199, 2017.

[62]   C. Tregambi, F. Di Lauro, F. Montagnaro, P. Salatino, R. Solimene, "110th anniversary: Calcium looping coupled with concentrated solar power for carbon capture and thermochemical energy storage", *Ind. Eng. Chem. Res.*, vol. 58, pp. 21262–21272, 2019.

[63]   U. Tesio, E. Guelpa, V. Verda, "Comparison of sCO2 and He Brayton cycles integration in a Calcium-Looping for Concentrated Solar Power", *Energy*, vol. 247, pp. 123467, 2022.

[64]   C. Tregambi, P. Salatino, R. Solimene, F. Montagnaro, "An Experimental Characterization of Calcium Looping Integrated with Concentrated Solar Power", *Chem. Eng. J.*, vol. 331, pp. 794–802, 2017.

[65]   M. Sayyah, Y. Lu, R.I. Masel, K.S. Suslick, "Mechanical Activation of CaO-Based Adsorbents for CO2 Capture", *ChemSusChem*, vol. 6, pp. 193–198, 2013.

[66]   M. Benitez-Guerrero, J.M. Valverde, A. Perejon, P.E. Sanchez-Jimenez, L.A. Perez-Maqueda, "Effect of milling mechanism on the CO2 capture performance of limestone in the Calcium Looping process", *Chem. Eng. J.*, vol. 346, pp. 549–556, 2018.

[67]   J.M. Valverde, M. Barea-López, A. Perejón, P.E. Sánchez-Jiménez, L.A. Pérez-Maqueda, "Effect of Thermal Pretreatment and Nanosilica Addition on Limestone Performance at Calcium-Looping Conditions for Thermochemical Energy Storage of Concentrated Solar Power", *Energy and Fuels*, vol. 31, pp. 4226–4236, 2017.

[68]   J. Arcenegui-Troya, P.E. Sánchez-Jiménez, A. Perejón, V. Moreno, J.M. Valverde, L.A. Pérez-Maqueda, "Kinetics and cyclability of limestone (CaCO3) in presence of steam during calcination in the CaL scheme for thermochemical energy storage", *Chem. Eng. J.*, vol. 417, pp. 129194, 2021.

[69]   J. Arcenegui-Troya, P.E. Sánchez-Jiménez, A. Perejón, J.M. Valverde, L.A. Pérez-Maqueda, "Steam-enhanced calcium-looping performance of limestone for thermochemical energy storage: The role of particle size", *J. Energy Storage*, vol. 51, pp. 104305, 2022.

[70]   A. Coppola, A. Esposito, F. Montagnaro, G. De Tommaso, F. Scala, P. Salatino, "Effect of exposure to SO2 and H2O during the carbonation stage of fluidised bed calcium looping on the performance of sorbents of different nature", *Chem. Eng. J.*, vol. 377, pp. 120626, 2019.

[71]   Y. Da, Y. Xuan, L. Teng, K. Zhang, X. Liu, Y. Ding, "Calcium-based composites for direct solar-thermal conversion and thermochemical energy storage", *Chem. Eng. J.*, vol. 382, pp. 122815, 2020.

[72]   L. André, S. Abanades, "Evaluation and performances comparison of calcium, strontium and barium carbonates during calcination/carbonation reactions for solar thermochemical energy storage", *J. Energy Storage*, vol. 13, pp. 193–205, 2017.

[73]   Y. Yang, Y. Li, X. Yan, J. Zhao, C. Zhang, "Development of thermochemical heat storage based on CaO/CaCO3 cycles: A review", *Energies*, vol. 14, pp. 6847, 2021.

[74]   H. Guo, S. Wang, C. Li, Y. Zhao, Q. Sun, X. Ma, "Incorporation of Zr into Calcium Oxide for CO2 Capture by a Simple and Facile Sol-Gel Method", *Ind. Eng. Chem. Res.*, vol. 55, pp. 7873–7879, 2016.

[75]   K.T. Møller, T.D. Humphries, A. Berger, M. Paskevicius, C.E. Buckley, "Thermochemical energy storage system development utilising limestone", *Chem. Eng. J. Adv.*, vol. 8, pp. 100168, 2021.

[76]   A. Antzara, E. Heracleous, A.A. Lemonidou, "Improving the stability of synthetic CaO-based CO2 sorbents by structural promoters", *Appl. Energy*, vol. 156, pp. 331–343, 2015.

[77]   M. Benitez-Guerrero, J.M. Valverde, P.E. Sanchez-Jimenez, A. Perejon, L.A. Perez-Maqueda, "Calcium-Looping performance of mechanically modified Al2O3-CaO composites for energy storage and CO2 capture", *Chem. Eng. J.*, vol. 334, pp. 2343–2355, 2018.

[78]   D. Choi, A.-H. Alissa Park, Y. Park, "Effects of eutectic alkali chloride salts on the carbonation reaction of CaO-based composites for potential application to a thermochemical energy storage system", *Chem. Eng. J.*, vol. 437, pp. 135481, 2022.

[79]   B. Sarrión, A. Perejón, P.E. Sánchez-Jiménez, L.A. Pérez-Maqueda, J.M. Valverde, "Role of calcium looping conditions on the performance of natural and synthetic Ca-based materials for energy storage", *J. CO2 Util.*, vol. 28, pp. 374–384, 2018.

[80]   L. Yang, G. Huang, Z. Huang, "Optimized design of Ca-based thermochemical heat storage materials for concentrated solar power", *J. Energy Storage*, vol. 43, pp. 103236, 2021.

[81]   H. Zheng, X. Liu, Y. Xuan, C. Song, D. Liu, Q. Zhu, Z. Zhu, K. Gao, Y. Li, Y. Ding, "Thermochemical heat storage performances of fluidized black CaCO3 pellets under direct concentrated solar irradiation", *Renew. Energy*, vol. 178, pp. 1353–1369, 2021.

[82]   C. Ortiz, A. Carro, R. Chacartegui, J.M. Valverde, "Low-pressure calcination to enhance the calcium looping process for thermochemical energy storage", *J. Clean. Prod.*, vol. 363, pp. 132295, 2022.

[83]   F. Martinez Castilla, G.; Guío-Pérez, D.C.; Papadokonstantakis, S.; Pallarès, D.; Johnsson, "Techno-Economic Assessment of Calcium Looping for Thermochemical Techno-Economic Assessment of Calcium Looping for Thermochemical Energy Storage with CO2 Capture", *Energies*, vol. 14, pp. 0–17, 2021.

[84]   C. Ortiz, J.M. Valverde, R. Chacartegui, L.A. Perez-Maqueda, P. Giménez, "The Calcium-Looping (CaCO3/CaO) process for thermochemical energy storage in Concentrating Solar Power plants", *Renew. Sustain. Energy Rev.*, vol. 113, pp. 109252, 2019.

[85]   G. Zsembinszki, A. Sole, C. Barreneche, C. Prieto, A.I. Fernández, L.F. Cabeza, "Review of reactors with potential use in thermochemical energy storage in concentrated solar power plants", *Energies*, vol. 11, pp. 2358, 2018.

[86]   C. Tregambi, M. Troiano, F. Montagnaro, R. Solimene, P. Salatino, "Fluidized Beds for Concentrated Solar Thermal Technologies—A Review", *Front. Energy Res.*, vol. 9, pp. 1–26, 2021.

[87]   E. Koepf, I. Alxneit, C. Wieckert, A. Meier, "A review of high temperature solar driven reactor technology: 25 years of experience in research and development at the Paul Scherrer Institute", *Appl. Energy*, vol. 188, pp. 620–651, 2017.

[88]   S. Padula, C. Tregambi, R. Solimene, R. Chirone, M. Troiano, P. Salatino, "A novel fluidized bed "thermochemical battery" for energy storage in concentrated solar thermal technologies", *Energy Convers. Manag.*, vol. 236, pp. 113994, 2021.

[89]   M. Alvarez Rivero, D. Rodrigues, C.I.C. Pinheiro, J.P. Cardoso, L.F. Mendes, "Solid–gas reactors driven by concentrated solar energy with potential application to calcium looping: A comparative review", *Renew. Sustain. Energy Rev.*, vol. 158, pp. 112048, 2022.

[90]   SOCRATCES Project, "SOlar Calcium-looping integRAtion for ThermoChemical Energy Storage", 2022. [Online]. Available: https://socratces.eu/ [accessed February 1, 2022].

[91]   E. Karasavvas, K.D. Panopoulos, S. Papadopoulou, S. Voutetakis, "Study of a drop-tube carbonator reactor for CSP-calcium looping based on a heterogeneous reaction model", *Chem. Eng. Trans.*, vol. 76, pp. 877–882, 2019.

[92]   M. Bailera, P. Lisbona, L.M. Romeo, L.I. Díez, "Calcium looping as chemical energy storage in concentrated solar power plants: Carbonator modelling and configuration assessment", *Appl. Therm. Eng.*, vol. 172, pp. 115186, 2020.

[93]   Y. Yan, K. Wang, P.T. Clough, E.J. Anthony, "Developments in calcium/chemical looping and metal oxide redox cycles for high-temperature thermochemical energy storage: A review", *Fuel Process. Technol.*, vol. 199, pp. 106280, 2020.

[94]   R. Bravo, C. Ortiz, R. Chacartegui, D. Friedrich, "Multi-objective optimisation and guidelines for the design of dispatchable hybrid solar power plants with thermochemical energy storage", *Appl. Energy*, vol. 282, pp. 116257, 2021.

[95]   R. Bravo, C. Ortiz, R. Chacartegui, D. Friedrich, "Hybrid solar power plant with thermochemical energy storage: A multi-objective operational optimisation", *Energy Convers. Manag.*, vol. 205, pp. 112421, 2020.

[96]   C. Tregambi, P. Bareschino, E. Mancusi, F. Pepe, F. Montagnaro, R. Solimene, P. Salatino, "Modelling of a concentrated solar power – photovoltaics hybrid plant for carbon dioxide capture and utilization via calcium looping and methanation", *Energy Convers. Manag.*, vol. 230, pp. 113792, 2021.

[97]   C. Ortiz, R. Chacartegui, J.M. Valverde, A. Carro, C. Tejada, J. Valverde, "Increasing the solar share in combined cycles through thermochemical energy storage", *Energy Convers. Manag.*, vol. 229, pp. 113730, 2021.

[98]   C. Ortiz, C. Tejada, R. Chacartegui, R. Bravo, A. Carro, J.M. Valverde, J. Valverde, "Solar combined cycle with high-temperature thermochemical energy storage", *Energy Convers. Manag.*, vol. 241, pp. 114274, 2021.

[99]   C. Ortiz, R. Chacartegui, J.M. Valverde, A. Alovisio, J.A. Becerra, "Power cycles integration in concentrated solar power plants with energy storage based on calcium looping", *Energy Convers. Manag.*, vol. 149, pp. 815–829, 2017.

[100]   U. Tesio, E. Guelpa, V. Verda, "Integration of thermochemical energy storage in concentrated solar power. Part 2: Comprehensive optimization of supercritical CO2 power block", *Energy Convers. Manag.*, vol. 6, pp. 100038, 2020.

[101]   C. Ortiz, M.C. Romano, J.M. Valverde, M. Binotti, R. Chacartegui, "Process integration of Calcium-Looping thermochemical energy storage system in concentrating solar power plants", *Energy*, vol. 155, pp. 535–551, 2018.

[102]   R. Chacartegui, A. Alovisio, C. Ortiz, J.M. Valverde, V. Verda, J.A. Becerra, "Thermochemical energy storage of concentrated solar power by integration of the calcium looping process and a CO2 power cycle", *Appl. Energy*, vol. 173, pp. 589–605, 2016.

[103]   E. Karasavvas, K.D. Panopoulos, S. Papadopoulou, S. Voutetakis, "Energy and exergy analysis of the integration of concentrated solar power with calcium looping for power production and thermochemical energy storage", *Renew. Energy*, vol. 154, pp. 743–753, 2020.

[104]   F-Chart, "Engineering Equation Solver (EES) Software", 2022. [Online]. Available: https://www.fchartsoftware.com/ees/.

[105]   C.Y. Wen, T.Z. Chaung, "Entrainment Coal Gasification Modeling", *Ind. Eng. Chem. Process Des. Dev.*, vol. 18, pp. 684–695, 1979.

[106]   M. Zlokarnik, "Scale-Up in Chemical Engineering", Wiley, 2006.

[107]   J. Taler, W. Zima, P. Ocłoń, S. Grądziel, D. Taler, A. Cebula, M. Jaremkiewicz, A. Korzeń, P. Cisek, K. Kaczmarski, K. Majewski, "Mathematical model of a supercritical power boiler for simulating rapid changes in boiler thermal loading", *Energy*, vol. 175, pp. 580–592, 2019.

[108]   M. Bailera, S. Pascual, P. Lisbona, L.M. Romeo, "Modelling calcium looping at industrial scale for energy storage in concentrating solar power plants", *Energy*, vol. 225, pp. 120306, 2021.

[109]   C. Song, P. Wang, H.A. Makse, "A phase diagram for jammed matter", *Nature*, vol. 453, pp. 629–632, 2008.

[110]   G.S. Grasa, J.C. Abanades, "CO2 Capture Capacity of CaO in Long Series of Carbonation/Calcination Cycles", *Ind. Eng. Chem. Res.*, vol. 45, pp. 8846–8851, 2006.

[111]   J.C. Abanades, "The maximum capture efficiency of CO2 using a carbonation/calcination cycle of CaO/CaCO3", *Chem. Eng. J.*, vol. 90, pp. 303–306, 2002.

[112]   S. Pascual, P. Lisbona, M. Bailera, L.M. Romeo, "Design and operational performance maps of calcium looping thermochemical energy storage for concentrating solar power plants", *Energy*, vol. 220, pp. 119715, 2021.

[113]   V. Manovic, J.P. Charland, J. Blamey, P.S. Fennell, D.Y. Lu, E.J. Anthony, "Influence of calcination conditions on carrying capacity of CaO-based sorbent in CO2 looping cycles", *Fuel*, vol. 88, pp. 1893–1900, 2009.

[114]   C. Ortiz, M.C. Romano, J.M. Valverde, M. Binotti, R. Chacartegui, "Process integration of Calcium-Looping thermochemical energy storage system in concentrating solar power plants", *Energy*, vol. 155, pp. 535–551, 2018.

[115]   M.W. Chase Jr., "NIST-JANAF Themochemical Tables", in: *J. Phys. Chem. Ref. Data, Monogr. 9*, Fourth Edi, 1998: pp. 1–1951.

[116]   G.K. Jacobs, D.M. Kerrick, K.M. Krupka, "The high-temperature heat capacity of natural calcite (CaCO3)", *Phys. Chem. Miner.*, vol. 7, pp. 55–59, 1981.

[117]   S. Pascual, P. Lisbona, L.M. Romeo, "Operation maps in calcium looping thermochemical energy storage for concentrating solar power plants", *J. Energy Storage*, vol. 55, pp. 105771, 2022.

[118]   C. Tregambi, F. Montagnaro, P. Salatino, R. Solimene, "Solar-Driven Torrefaction of a Lignin-Rich Biomass Residue in a Directly Irradiated Fluidized Bed Reactor", *Combust. Sci. Technol.*, vol. 191, pp. 1609–1627, 2019.

[119] S. Pascual, F. Di Lauro, P. Lisbona, L.M. Romeo, C. Tregambi, F. Montagnaro, R. Solimene, P. Salatino, "Improvement of Performance of Fluidized Bed Calcium Looping for Thermochemical Solar Energy Storage : Modelling and Experiments", *Proc. 10th Eur. Combust. Meet.*, pp. 1430–1435, 2021.

[120] C. Tregambi, F. Di Lauro, S. Pascual, P. Lisbona, L.M. Romeo, R. Solimene, P. Salatino, F. Montagnaro, "Solar-driven calcium looping in fluidized beds for thermochemical energy storage", *Chem. Eng. J.*, vol. 466, pp. 142708, 2023.

[121] J.M. Valverde, A. Perejon, L.A. Perez-Maqueda, "Enhancement of fast CO_2 capture by a nano-SiO_2/CaO composite at Ca-looping conditions", *Environ. Sci. Technol.*, vol. 46, pp. 6401–6408, 2012.

[122] J.R. Grace, "Fluidized-bed hydrodynamics", in: G. Hetsroni (Ed.), *Handb. Multiph. Syst.*, Washington: Hemisphere, 1982: pp. 8-1-8–64.

[123] G. Olivieri, A. Marzocchella, P. Salatino, "A fluid-bed continuous classifier of polydisperse granular solids", *J. Taiwan Inst. Chem. Eng.*, vol. 40, pp. 638–644, 2009.

[124] B. Sarrion, J.M. Valverde, A. Perejon, L. Perez-maqueda, P.E. Sanchez-jimenez, "On the Multicycle Activity of Natural Limestone / Dolomite for Thermochemical Energy Storage of Concentrated Solar Power", *Energy Technol.*, vol. 4, pp. 1013–1019, 2016.

[125] F. Rinaldi, M. Binotti, A. Giostri, G. Manzolini, "Comparison of linear and point focus collectors in solar power plants", *Energy Procedia*, vol. 49, pp. 1491–1500, 2013.

[126] J.M. Valverde, P.E. Sanchez-Jimenez, A. Perejon, L.A. Perez-Maqueda, "Role of looping-calcination conditions on self-reactivation of thermally pretreated CO_2 sorbents based on CaO", *Energy and Fuels*, vol. 27, pp. 3373–3384, 2013.

[127] J.M. Valverde, "A model on the CaO multicyclic conversion in the Ca-looping process", *Chem. Eng. J.*, vol. 228, pp. 1195–1206, 2013.

[128] European Commission, "PVGIS - Photovoltaic geographical information system", 2021. [Online]. Available: https://ec.europa.eu/jrc/en/pvgis [accessed October 4, 2021].

[129] Red Eléctrica de España, "PVPC | ESIOS electricidad·datos·transparencia", 2021. [Online]. Available: https://www.esios.ree.es/es/pvpc [accessed October 4, 2021].

[130] F-Chart, "Genetic Method. Engineering Equation Solver (EES) Software", 2021. [Online]. Available: https://fchartsoftware.com/ees/ [accessed October 4, 2021].

[131] P. Charbonneau, B. Knapp, "PIKAIA. High Altitude Observatory. National Center for Atmospheric Research", 2021. [Online]. Available: http://www.hao.ucar.edu/modeling/pikaia/pikaia.php#sec1 [accessed October 4, 2021].

Apéndice A. Carta aceptación *Journal of Energy Storage*

29-Abril-2023

Manuscript Number: EST-D-23-00518R1
Optimized Ca-looping Thermochemical Energy Storage under Dynamic Operation for Concentrated Solar Power

Dear Professor Romeo,

Thank you for submitting your manuscript to Journal of Energy Storage.

I am pleased to inform you that your manuscript has been **accepted** for publication.

Your accepted manuscript will now be transferred to our production department. We will create a proof which you will be asked to check, and you will also be asked to complete a number of online forms required for publication. If we need additional information from you during the production process, we will contact you directly.

What happens next?
1. Our production department will create a proof of your article, which will be shared with you for approval.
2. We will send you a link to your post-acceptance online author forms. These forms include the publishing agreement for you to complete as well as confirming whether your article is to be published open access or subscription. We kindly request you complete the forms as soon as possible upon receipt of the link.

If we need any further information from you during the typesetting process, we will let you know.

We appreciate and value your contribution to Journal of Energy Storage.

Kind regards,
Luisa F. Cabeza
Editor-in-Chief
Journal of Energy Storage

Apéndice B. Factor de impacto y área temática de las publicaciones

A continuación, se indica el factor de impacto, cuartil y área temática de las revistas en las que han sido publicados los manuscritos que conforman esta Tesis Doctoral. La información ha sido tomada del Journal of Citations Reports (JCR), cuyos datos más actuales pertenecen al año 2021.

Tabla A1. Revistas en las que se han publicado el compendio de artículos que conforman la presente Tesis Doctoral.

Artículos	Revista	Factor Impacto 2021	Factor Impacto (5 últimos años)	Área temática 1	Área temática 2
i, ii	Energy	8.857	8.234	Energy & Fuels (Q1, 24th/119th)	Thermodynamics (Q1, 3rd/63rd)
iii, vi	Journal of Energy Storage	8.907	8.140	Energy & Fuels (Q1, 23rd/119th)	-
iv	Proceedings 10th ECM	No indexada (Congreso)		-	-
v	Chemical Engineering Journal	16.744	14.610	Engineering, chemical (Q1, 4th/143rd)	Engineering, environmental (Q1, 2nd/54th)
vii	Energies	3.252	3.333	Energy & Fuels (Q3, 80th/119th)	-

Apéndice C. Contribución a las publicaciones

D. Luis Miguel Romeo Giménez y Dña. María Pilar Lisbona Martín, Profesores titulares del Área de Máquinas y Motores Térmicos del Departamento de Ingeniería Mecánica de la Universidad de Zaragoza:

Certifican que la contribución de Dña. Sara Pascual Sevilla ha sido esencial en las tareas de concepción y diseño de las ideas, realización de los modelos y simulaciones, análisis de los resultados y redacción de los manuscritos de las siguientes publicaciones:

i) Bailera M, Pascual S, Lisbona P, Romeo LM. *Modelling Calcium Looping at industrial scale for energy storage in concentrating solar power plants*. Energy (2021), 225, 120306.

ii) Pascual S, Lisbona P, Bailera M, Romeo LM. *Design and operational performance maps of Calcium Looping thermochemical energy storage for concentrating solar power plants*. Energy (2021), 220, 119715.

iii) Pascual S, Lisbona P, Romeo LM. *Operation maps in Calcium Looping thermochemical energy storage for concentrating solar power plants*. Journal of Energy Storage (2022), 55, 105771.

iv) Pascual S, Di Lauro F, Lisbona P, Romeo LM, Tregambi C, Montagnaro F, Solimene R, Salatino P. *Improvement of performance of fluidized bed Calcium Looping for thermochemical solar energy storage: Modelling and experiments*. Proceedings of 10th European Combustion Meeting (2021).

v) Tregambi C, Di Lauro F, Pascual S, Lisbona P, Romeo LM, Solimene R, Salatino P, Montagnaro F. *Solar-driven Calcium Looping in fluidized beds for thermochemical energy storage*. Chemical Engineering Journal (2023), 466, 142708.

vi) Pascual S, Lisbona P, Romeo LM. *Optimized Ca-looping thermochemical energy storage under dynamic operation for concentrated solar power*. Journal of Energy Storage (2023). Accepted for publication.

vii) Pascual S, Lisbona P, Romeo LM. *Thermal energy storage in concentrating solar power plants: A review of European and North American R&D projects*. Energies (2022), 15, 8570.

Zaragoza, Mayo de 2023

María Pilar Lisbona Martín   Luis Miguel Romeo Giménez